Model-Based Traffic Control for Sustainable Mobility

Solomon Kidane Zegeye

(ሰለሞን ኪዳነ ዘገዬ)

Model-Based Traffic Control for Sustainable Mobility

Proefschrift

ter verkrijging van de graad van doctor
aan de Technische Universiteit Delft,
op gezag van de Rector Magnificus prof. ir. K.C.A.M. Luyben,
voorzitter van het College voor Promoties,
in het openbaar te verdedigen op dinsdag 11 oktober 2011 om 15.00 uur

door

Solomon Kidane ZEGEYE (ሰለሞን ኪዳነ ዘገዬ),

Master of Science in Systems and Control,
geboren te Tigray, Ethiopië.

Dit proefschrift is goedgekeurd door de promotoren:
Prof. dr. ir. B. De Schutter
Prof. dr. ir. J. Hellendoorn

Samenstelling promotiecommissie:

Rector Magnificus	voorzitter
Prof. dr. ir. B. De Schutter	Technische Universiteit Delft, promotor
Prof. dr. ir. J. Hellendoorn	Technische Universiteit Delft, promotor
Prof. Dr. -Ing. M. Papageorgiou	Technical University of Crete, Griekenland
Prof. J. Polak	Imperial College London, Verenigd Koninkrijk
Prof. dr. ir. E. van Berkum	Universiteit Twente
Prof. dr. ir. B. van Arem	Technische Universiteit Delft
Dr. E.A. Breunesse	Shell Nederland B.V.
Prof. ir. L.H. Immers	Technische Universiteit Delft, reservelid

This thesis has been completed in partial fulfillment of the requirements of the Dutch Institute of Systems and Control (DISC) and the Netherlands Research School on Transport, Infrastructure and Logistics (TRAIL) for graduate studies. The research described in this thesis was financially supported by the Shell/TU Delft Sustainable Mobility Program.

TRAIL Thesis Series T2011/12, the Netherlands TRAIL Research School

Published and distributed by: Solomon Kidane Zegeye
E-mail: s.k.zegeye@gmail.com

ISBN 978-90-5584-150-9

Keywords: Model-based control, receding-horizon parametrized control, emissions.

Printed in the Netherlands

. . . to my parents and my wife.

Preface

It has not been an easy start. However, in hindsight, doing a PhD was the right choice that I have made. Indeed the "tour" has demanded me perseverance and hard work, as it has offered me unforgettable joyful moments. Yet, the end is not easy, as it leaves me with—what is next?

Although it is true that a PhD project is an independent research work, it is hard to imagine what it could be without the right and timely supervision, or without the support I have gotten from and the cooperation and discussions I have had with many people. When I see this thesis, first and foremost, I think of my promotors Bart De Schutter and Hans Hellendoorn for their continuous and tireless support and guidance they have provided me, and for the kind of research questions they have though me to ask. If it was not for their dedicated and always available supervision, and for their critical remarks and planned approaches, I would not be able to finish my thesis with the same quality. Dear Bart and dear Hans, I owe you a lot of thanks and appreciations (ባለዉለታዮ ናቹ).

I would also like to thank and express my appreciation for Ewald Breunesse. The discussions we have had, and his practical insights and ability to assess the global picture of the project, have been of great value.

I have greatly appreciated and benefited from the cooperation and discussions I have had with several people, viz. I thank Andreas Hegyi, Balazs Kulcsár, Tamás Luspay, Lakshmi Baskar, Shu Lin, and Noortje Groot. I would also like to acknowledge Rudy Negenborn, for his time and patience to answer my silly questions, for the valuable discussions we had, and for his support. I am greatly indebted for Jan Willem Zwarteveen, Johan 't Hart, Sander van der Horst, and Yinyi Ma for doing their M.Sc. projects with me. It has been a pleasure to supervise and to work with them.

I thank my PhD committee members Prof. John Polak, Prof. Markos Papageorgiou, Prof. Eric van Berkum, Prof. Bart van Arem, Prof. Ben Emmers, Dr. Ewald Breunesse, Prof. Hans Hellendoorn, and Prof. Bart De Schutter for their valuable time and suggestions provided to improvise my thesis.

It was a delight for me to work among my colleagues at the Delft Center for Systems and Control (DCSC). I feel greatly indebted to my colleagues, in one way or another, for their support and friendly interactions during my stay at the DCSC. I also thank my friends Alemgena, Anteneh, Eyasu, and Million for the good times we have had.

I would like to use this opportunity to thank my parents Kidane Zegeye and Meakelesh Ezgi-haye, and my brothers and sisters. Last but not least, my special thanks to my beloved wife Liya Markos, for the unreserved love and care she nurture me.

Solomon Kidane Zegeye (ሰለሞን ኪዳኔ ዘገዬ),
Delft, October 2011.

Contents

Preface **vii**

1 Introduction **1**
1.1 Traffic systems and their challenges . . . 1
1.1.1 Economic concerns . . . 2
1.1.2 Environmental concerns . . . 3
1.1.3 Conflicting interests . . . 4
1.2 Possible traffic solutions . . . 6
1.2.1 Extension of existing infrastructures and construction of new infrastructures . . . 7
1.2.2 Enhancing vehicle and fuel technology . . . 7
1.2.3 Use of intelligent transportation systems . . . 8
1.3 Problem statement . . . 10
1.3.1 Objectives . . . 10
1.3.2 Approaches . . . 10
1.3.3 Scope of the thesis . . . 11
1.4 Contribution of the thesis . . . 11
1.4.1 Modeling . . . 12
1.4.2 Control design . . . 12
1.5 Thesis overview . . . 13

I TRAFFIC MODELS **15**

2 Traffic Flow Modeling **17**
2.1 Overview of traffic flow models . . . 17
2.1.1 Applications of traffic flow models . . . 18
2.1.2 Classification of traffic flow models . . . 18
2.2 Car-following models . . . 22
2.2.1 Overview of car-following models . . . 22
2.2.2 The GHR model . . . 24
2.2.3 The IDM model . . . 26
2.3 The METANET model and its extensions . . . 27
2.3.1 Link equations . . . 28
2.3.2 Node equations . . . 31
2.3.3 Origins . . . 32
2.3.4 Boundary conditions . . . 34
2.4 Summary . . . 34

3 Traffic Emissions and Fuel Consumption Modeling 37
3.1 Overview of emissions and fuel consumption models . . . 38
3.1.1 Application of traffic emissions and fuel consumption models . . . 38
3.1.2 Classification of traffic emissions and fuel consumption models . . 39
3.2 The VT-micro model . . . 43
3.3 The COPERT model . . . 44
3.4 The VT-macro model . . . 46
3.4.1 Integration of models . . . 46
3.4.2 Segmental acceleration . . . 48
3.4.3 Cross-segmental acceleration . . . 49
3.4.4 VT-macro emissions and fuel consumption equations . . . 51
3.4.5 Analysis of VT-macro . . . 53
3.4.6 Empirical verification . . . 54
3.5 Conclusions . . . 61

4 Traffic Emissions Dispersion Modeling 63
4.1 Overview of dispersion models . . . 63
4.1.1 Dispersion models . . . 64
4.1.2 Applications of dispersion models . . . 68
4.2 Point source dispersion modeling . . . 69
4.2.1 Basic dispersion model . . . 69
4.2.2 Variable-wind dispersion model . . . 70
4.3 Grid-based dispersion modeling . . . 73
4.3.1 Extended grid-based dispersion model . . . 73
4.3.2 Expanding grid-based dispersion model . . . 76
4.3.3 Comparison of grid-based dispersion models . . . 78
4.4 Conclusions . . . 79

II TRAFFIC CONTROL DESIGN 81

5 Model Predictive Traffic Control 83
5.1 Philosophy of model predictive control . . . 83
5.2 Conventional MPC for traffic systems . . . 86
5.3 Traffic performance criteria . . . 88
5.3.1 Flow performance criteria . . . 88
5.3.2 Emissions and fuel consumption performance criteria . . . 89
5.3.3 Variation in traffic control measures . . . 91
5.4 Multi-criteria optimization . . . 92
5.4.1 Weighted sum . . . 93
5.4.2 Normalization . . . 93
5.4.3 Optimization method . . . 94
5.5 Case studies . . . 94
5.5.1 Balanced reduction of travel times, emissions, and fuel consumption 94
5.5.2 Reduction of area-wide emissions . . . 105
5.6 Conclusions . . . 114

6 Receding-Horizon Parametrized Control **115**
6.1 Parametrized MPC . . . 115
6.2 Basic concepts of RHPC . . . 117
6.2.1 Philosophy of RHPC traffic controller . . . 117
6.2.2 General formulation of RHPC for traffic systems . . . 120
6.3 RHPC for variable speed limits and ramp metering . . . 122
6.3.1 RHPC for variable speed limits . . . 122
6.3.2 RHPC for ramp metering control . . . 125
6.4 Reduction of area-wide emissions . . . 126
6.4.1 Case study E: Using a point source model . . . 127
6.4.2 Case study F: Using extended grid-based dispersion model . . . 133
6.5 Conclusions . . . 136

7 Conventional MPC versus RHPC **139**
7.1 Qualitative comparison of controllers . . . 139
7.2 Case study G: Reduction of travel times and emissions . . . 142
7.2.1 Set-up of the case study . . . 142
7.2.2 Control objective . . . 143
7.2.3 Results and discussion . . . 145
7.3 Case study H: Reduction of dispersion of emissions . . . 150
7.3.1 Set-up of the case study . . . 150
7.3.2 Control objective . . . 152
7.3.3 Results and discussion . . . 152
7.4 Conclusions . . . 155

8 Conclusions and Open Issues **159**
8.1 Conclusions . . . 159
8.2 Open issues . . . 163

A Model Parameters **167**
A.1 VT-macro (VT-micro) parameters . . . 167
A.2 Parameters of part of the A12 Dutch freeway . . . 168

B Derivation of The Intersection Formulas **169**

Bibliography **173**

Glossary **191**

TRAIL Thesis Series publications **201**

Summary **203**

Samenvatting **207**

Curriculum Vitae **211**

Chapter 1

Introduction

Since the invention of vehicles, the volume, frequency, and speed of the transportation of people and goods have increased significantly. The capacity and quality of vehicular transportation systems, in particular in developed countries, have increased substantially. However, due to the unmatched increase in demand for transportation, road transport is frequently impeded by recurrent and non-recurrent traffic jams and incidents. The increasing number of traffic jams, the rise in the health and environmental effects of the vehicular emissions, and the increasing fuel prices are other dimensions of the challenges of vehicular mobility in most developed countries.

As a result, it has become apparent that multi-objective transportation control and management systems should be developed to address the multifaceted traffic problems. One of the well accepted and promising solutions is the use of intelligent transportation systems. In this regard, this thesis contributes its share to improve the freeway traffic mobility by considering both environmental (emissions and dispersion of emissions) and economic concerns (travel time and energy consumption) of different stakeholders. The contribution of the thesis is delivered in eight chapters. This chapter introduces the general freeway traffic challenges and the specific problems investigated in this thesis. It starts with discussing the traffic systems and challenges that have motivated the commencement of this thesis in Section 1.1. The possible traffic solutions advocated in literature are in general elaborated and discussed in Section 1.2. Next the problem statement and the contribution of the thesis to the state-of-the-art are provided in Sections 1.3 and 1.4 respectively. Finally, the outline of the thesis is presented in Section 1.5.

1.1 Traffic systems and their challenges

The increasing public awareness and the more stringent environmental policies regarding the emission of exhaust gases and particulate matter, in combination with the ever increasing demand for transportation and the related traffic jams, have an increasing impact on the further evolution of our mobility. Either directly or indirectly the recurrent and non-recurrent traffic problems are affecting our daily life.

For example, freeway traffic systems encounter frequent traffic congestion, incidents, and increasing and varying traffic demands. Freeway traffic systems operate below-capacity during the rush hours due to inefficient driving behavior of drivers and non-optimal traffic

management systems and during the off-rush hours as there is limited traffic demand. Moreover, the emissions released and the fuel consumed by vehicles are other issues that require due attention in the introduction of any transportation solution.

The low efficiency of freeway traffic flow can be improved either by shifting the traffic demand through changes in the mode of transportation systems, by the introduction of incentives to shift the departure and arrival time of commuters, or by improving the traffic control and management systems such that the traffic systems are operated optimally. However, improving the traffic flow may have a negative impact on the fuel consumption, emissions, and safety. This means that every transport solution must be scrutinized from different directions so that a (sub-)optimal solution can be obtained to the multifaceted traffic challenges.

In order to provide a background understanding of the specific problem statement of this thesis, in the sequel, the main challenges of freeway traffic systems are briefly discussed by broadly classifying them into three categories as economic concerns, environmental concerns, and conflicting interests.

1.1.1 Economic concerns

In general, freeway traffic flows vary over space and time. Thus, the effects of the traffic flows are also distributed spatially and temporally. However, all traffic flows share some common behavior and have common effects. This common behavior basically originates from the desire of each driver to reach an intended destination as fast as and as safely as possible. This desire also bears some negative effects (such as traffic jams and accidents due to the conflict of interest between drivers). On the other hand, faster and more reliable transportation systems are necessary for sustained and faster economic prosperity of a country. Freeway traffic systems are one of the main economic blood vessels that link cities, towns, and villages with each other and with other economic hubs (such as ports and industrial zones). As such, every minute or second spent in the freeway traffic system amounts to economic costs. Moreover, the amount of fuel consumed and the depreciation costs of inefficiently exploited transportation facilities are other important economic concerns.

These transport costs are not static and they vary with the world economy, the traffic demand, and the efficiency of the traffic transport systems. Due to the increasing demand for mobility, and hence the increase in the number of vehicles, the traffic networks are more often jammed. Increased travel time due to continuous and frequent traffic jams creates additional losses in the productive hours of both people and goods. The long time spent stranded in the traffic networks is also most often observed to increase the stress level of drivers or passengers [84, 181]. This increases the health risk level of drives, which in turn affects the economy of drivers (or in general the economy of a country).

On the one hand, the increased traffic jams are causing increased fuel consumption. On the other hand, world wide fuel cost is on average increasing [54]. Altogether the economic losses due to the wasted fuel caused by traffic congestion are increasing. In addition, the frequent traffic jams lead to an increase of accidents, which subsequently affects the economy in many aspects. Every time an incident happens, additional time and resources are allocated to clear the incident and to reopen the traffic network for traffic. Above all, incidents that cost lives are not avoidable and the subsequent socio-economic disturbances are harsh. By and large, directly or indirectly the ever increasing traffic jams have severe consequences on the economy of a country.

1.1.2 Environmental concerns

In addition to the unproductive hours drivers spend in congested traffic flows and the increased number of accidents and volume of fuel consumption drivers face, motor vehicle emissions are one main sources of atmospheric pollution [127, 165, 193]. In fact road transportation is one of the major contributors to man-made polluting emissions. In European cities it has been estimated that more than 40% of the hydrocarbon, more than 70% of the nitrogen oxides, and over 90% of the carbon monoxide are accounted for by road transport [175]. Approximately 15% of the world's emissions of carbon dioxide[1], the principal global warming gas, is generated by motor vehicles [131]. Moreover, transportation is responsible for approximately 50% of the emissions of nitrogen oxide and 90% of the carbon monoxide emission world wide [131]. The emissions of road traffic have also highly adverse effects on the health of the society [86, 197].

The principal pollutants emitted from typical motor engines are carbon monoxide (CO), hydrocarbon (HC), oxides of nitrogen (NO_x), and particulate matter (PM) [193]. Carbon monoxide, which is a product of inefficient fuel combustion of engines, is a poisonous gas. Carbon monoxide reduces the flow of oxygen in the bloodstream of a human body and it can be fatal. Hydrocarbon emissions result from fuel that does not burn completely and that is chemically transformed in (and outside of) the engine [193]. Hydrocarbons released by vehicle exhaust systems are also toxic and are known to cause cancer in the long term. Hydrocarbons react with oxides of nitrogen to form ozone (O_3), which is the major component of smog. Ozone causes irritations of the eyes and damages the respiratory system. Oxides of nitrogen (NO_x) are formed by the chemical reaction that occurs during the combustion in the engine of vehicles. Oxides of nitrogen, in particular NO_2, cause short and long term health effects [193]. Particulate matters, a complex mixture of solid and liquid particles in the air, are emitted mainly by diesel and poorly maintained petrol vehicles [30, 193]. Vehicles (such as cars, trucks, and buses) are major sources of fine particles [30]. Particulate matter with an aerodynamic diameter[2] below $10\,\mu$m (PM_{10}) and especially the finer fraction with aerodynamic diameter below $2.5\,\mu$m ($PM_{2.5}$) was found to be associated with increased daily mortality and asthma [59, 73, 191].

In line with these facts, traffic conditions have significant impacts on the concentration of emissions released by vehicles. Depending on the traffic conditions, the emission levels can be reduced or even get worse. Since the air-to-fuel ratio consumed by an engine is a major determinant factor for the efficiency of engines, the highest CO and HC levels are produced under fuel-rich conditions, and the highest NO_x level is emitted under fuel-lean conditions [89]. Generally, since fuel-rich operations occur during cold-start conditions, or under heavy engine loads such as during rapid accelerations at high speeds and on steep grades, high levels of CO and HC are generated on congested highways and in other areas with high traffic density. Moreover, the frequent stop-and-go motion of vehicles in traffic networks does not only impact the travel time, but also the fuel consumption of the vehicles, which also severely increases the emission levels. Thus, increased traffic congestion or improved traffic flows have severe consequences on the emission level, which in turn affects the environment and the health of drivers in the traffic networks and neighborhoods near to

[1] The CO_2 emissions is affinely related to the fuel consumption [141]. See also (3.4).

[2] The aerodynamic diameter is a measure to express the size of a particle. The aerodynamic diameter is defined as the diameter of a unit-density sphere that has the same settling velocity as the particle in question [59]. The settling velocity is the maximum velocity a particle can have for a given force and a drag force dependent on its velocity. Thus, at the settling velocity the drag force is equal to the applied force.

the traffic networks.

1.1.3 Conflicting interests

Road traffic flow is different from other transportation systems (such as railway systems and airlines) in various ways. The main difference emanates from the fact that the trips in road transport, in general, are not centrally controlled and planned well ahead as in other transportation systems. The road traffic demand is stochastic and the traffic control and management strategies of road transport have to deal with uncertain predictions. One main challenge in traffic control and management systems is designing a traffic controller or management strategy in such a way that the traffic jams are reduced to the minimum possible, while still keeping the required safety level. Another challenge is the desire to reduce emissions and fuel consumption of the vehicles in a traffic network through policy and traffic control and management measures.

The multifaceted nature of the desired control objectives of traffic systems makes traffic control and management challenging [187]. The traffic control objectives can vary both spatially and temporally. The objective of a controller can be reduction of travel times, increasing safety, or reduction of emissions and fuel consumption at different times or locations. Moreover, the objectives of traffic control and management systems may be conflicting or concurring depending on the traffic conditions [1]. Likewise, the transport authorities and drivers can have conflicting or concurring objectives. In the following sections, the conflicting and concurring objectives of transport authorities with respect to drivers and with respect to the environment are discussed.

Drivers versus transport authorities

In general, people would like to have short trips and short travel times any time they are in the traffic network. However, it is hardly possible for the transport authorities to offer short and fast routes to each individual driver without compromising the mobility of the other drivers. Moreover, what could be user equilibrium may not necessarily be system optimal [155, 198]. This means that if the travel cost (such as the travel distance, amount of fuel consumed, comfort level, and the like) of every driver is the same regardless of the route or departure time the driver chose—with no unused route-departure time choices having a lower cost, then the state is at user (drivers) equilibrium [4, 65, 199]. However, there are cases where the travel cost of some drivers should be compromised so that the system's total travel cost can be lower. In this sense, since the interest of transport authorities is, by and large, to improve the total travel cost of the transport systems as a whole, the interest of the drivers and the transport authorities may sometimes be conflicting.

To illustrate a possible conflict of interest between transport authorities and drivers, let us first discuss the effect of driving behavior on travel time using Fig. 1.1. The figure shows possible trajectories of two vehicles (one that moves at a suggested speed and hence called managed vehicle and one that moves at the maximum speed limit called unmanaged vehicle) that have the same origin and destination. Suppose that at the initial time and position there is a traffic jam downstream of the vehicles. The unmanaged vehicle will arrive at the downstream jam at a time instant $t_{\mathrm{jam,unmanaged}}$. However, since the time required by vehicles to decelerate is smaller than the time required to accelerate [58], the unmanaged vehicle will accelerate slower to the maximum speed than it decelerates to the

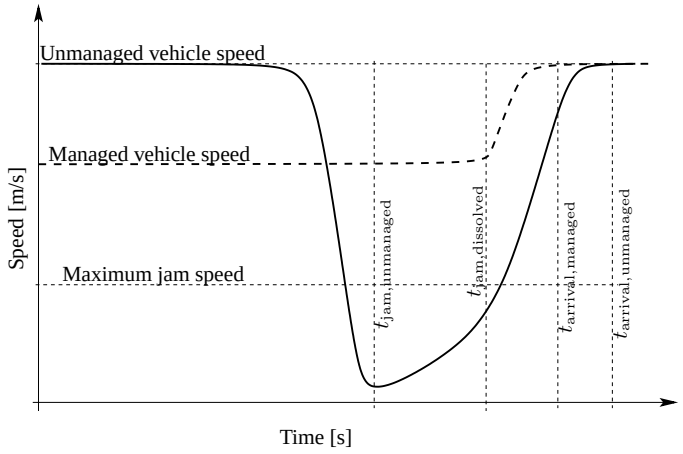

Figure 1.1: Schematic illustration of capacity drop caused due to the difference in acceleration and deceleration of a vehicle.

jam speed. Finally, it arrives at its destination at the arrival time instant $t_{\text{arrival,unmanaged}}$. On the contrary, the managed vehicle does not drive at the maximum speed down to the traffic jam. It is assigned a lower speed limit such that by the time it arrives the location of the downstream traffic jam, the jam has been dissolved, i.e., the vehicle arrives at the location where the jam was at the time instant $t_{\text{jam,dissolved}}$. This means that the managed vehicle does not get the traffic jam (depending on the length of the jam and the distance between the location of the jam and the managed vehicle). Hence, the managed vehicle takes smaller time to accelerate to the maximum speed after the jam location. Finally, the managed vehicle arrives its destination faster than the unmanaged vehicle (at time instant $t_{\text{arrival,managed}} < t_{\text{arrival,unmanaged}}$). This means that the traffic jam is dissolved and will not propagate upstream in the managed case, while the jam will propagate upstream until the demand decreases under the unmanaged case.

This simple scenario conveys two important messages. First, it shows that the difference in acceleration and deceleration behavior of vehicles (more specifically drivers) can lead to increased travel time. Second, it demonstrates that transport managers and operators can set driving strategies that can dissolve traffic jams to provide better traffic flow for the continuing demand. Such solutions can also be in the interest of every driver if there are no off-ramps upstream of the traffic jam location. Otherwise, drivers that have to drive to the off-ramp before the traffic jam location will be forced to slow down for the benefit of other drivers that are going to drive through the traffic jam. This means that the transport authorities will improve the overall system travel time at the expense of the travel time of the drivers going through the off-ramps.

On-ramp metering is also one of the control measures that creates conflicting interests between drivers and transport authorities. In general, drivers like to enter the freeway directly after their arrival at an on-ramp, because, by and large, a continuous on-ramp inflow into the freeway reduces the travel times of the vehicles at the on-ramp. However, it can create a traffic jam just upstream of the on-ramp location that can impact the upstream traffic. In this sense, the transport authorities would like to regulate the on-ramp flow so that the

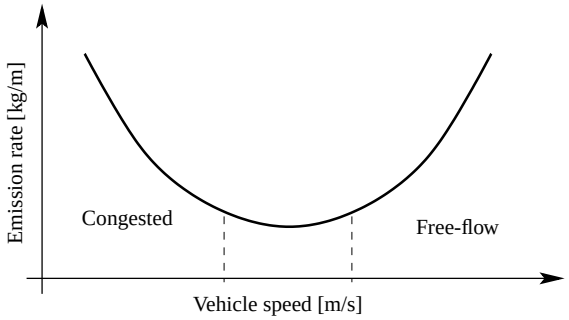

Figure 1.2: General evolution of vehicular emission rates.

overall performance of the freeway is improved. In other words, the transport authorities have to compromise the travel times of the drivers at the on-ramp (by regulating the inflow) in order to avoid a possible traffic jam just upstream of the on-ramp, thereby they improve the traffic network performance.

Transport authorities versus the environment

In general, higher speeds favor the traffic flow but increases the amount of emissions released [1]. This means that the desire to improve the mobility of people and goods by the transport authorities can affect the emission levels severely. To improve the emission level, the speed of vehicles should not exceed a certain threshold (e.g., 30 to 70 km/h). This is illustrated with the general emission (or fuel consumption) model in Fig. 1.2. The emissions rate per unit distance of a vehicle is minimum only at speeds between the congested and the free-flow regions shown in Fig. 1.2. Under congested traffic conditions, improvement of the traffic flow also improves the fuel consumption and emissions provided that the improved speed is such that fuel consumption or emissions at that speed are lower than the ones at the congested speed.

In order to improve the traffic flow, transport authorities may want to construct new and expand existing transport infrastructures. However, environmentalists are also concerned with the loss of green areas due to the new infrastructures and the additional emissions that can be generated due to the improved traffic flow and newly added vehicles (the increased demand due to the induced effect of improved traffic flow).

So, finding a solution that balances these conflict of interests is one of the challenges that hampers road traffic control and management. Some of the possible solutions to reduce these and other road traffic problems are the subject of next section.

1.2 Possible traffic solutions

As traffic problems are multi-dimensional and intricate, the solutions to address the requirements of different stakeholders have to pass through rigorous and all-round examinations. As the literature suggests, there are several possible approaches to improve the day-to-day traffic jams, the increased traffic emissions and fuel consumption, and the number of traffic incidents. The span of possible traffic solutions ranges from the extension of existing infras-

tructures and construction of new infrastructures, over large-scale substitution of fossil oil by alternative environmentally safe fuel, and enhancing vehicle technology, to the utilization of efficient traffic control and management strategies (i.e., introduction of intelligent transportation systems). These solutions are briefly discussed in the ensuing sections.

1.2.1 Extension of existing infrastructures and construction of new infrastructures

One of the easiest and most straightforward solutions to improve the traffic flow is to increase the capacity of the traffic networks. This would mean to either extend the existing infrastructures (such as increasing the number of lanes and improving the slope and quality of the road networks) or to build new alternative routes wherever there is traffic bottleneck. However, this solution is often not feasible for several reasons. One and the most obvious reason is that in many cases there is limited available land that can be used for the construction of new roads or for extension of existing road networks. Sometimes, construction of new or extension of existing road networks also requires the relocation of established socio-economic structures (such as residential areas, schools, shops, and farming facilities).

Secondly, even if it is found that there is enough land for the construction of road networks, construction of new roads or extension of existing road networks is very expensive. In addition, it may also be heavily time consuming.

Thirdly, the construction of new roads or extension of existing road networks have severe environmental consequences. The land that would have been green area has to be used for transportation facilities, the traffic that uses the road will release emissions, and the fine particles emitted during and after construction have severe consequences on the human health. Moreover, improvement in traffic flow due to improved traffic facilities would mean increased emissions not only in the areas where the new road networks are built, but also in the areas where the traffic flow is improved due the diversion of part of the traffic to the newly constructed alternative traffic road.

Finally, improved traffic flow can also have an induced effect on the traffic demand [137, 142]. The newly constructed roads or the extended road networks will first reduce the traffic jams and make road transport more reliable in the sense that the variations in the travel times will be reduced. However, the increased reliability and reduced traffic jams can motivate people to switch from public transportation to driving a car or to increase driving frequency. Consequently, the traffic demand increases, which in turn negatively impacts the traffic flow and the environment.

1.2.2 Enhancing vehicle and fuel technology

Another important solution that can address some of the traffic challenges outlined above is the advancement of vehicle technology. For example, by improving the engine technology of vehicles, it is possible to reduce the energy consumption and emissions of vehicles [156, 184]. As the efficiency of the engines improves, the fuel consumption of vehicles at lower speeds is reduced and thereby the emission rate in that speed range is reduced. This means that the emission rate curve will be changed as shown in Fig. 1.3(a). Moreover, if the aerodynamic shape of vehicles is designed in such a way that the drag force—which is significant at high vehicle speeds—is reduced, then the fuel consumption at high vehicle

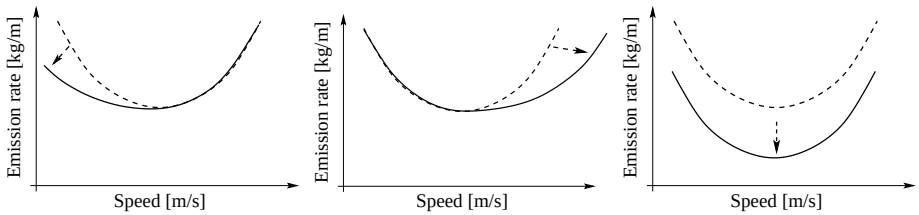

(a) Efficient engine (b) Reduced drag force (c) Cleaner fuel

Figure 1.3: Alternative approaches to reduce the emission rates of vehicles. For each case, the emission rate changes from the dashed curve to the solid curve.

speeds can be reduced. Subsequently, the emissions of the vehicles at high speeds are reduced as shown in Fig. 1.3(b).

Another alternative approach is the complete substitution of fossil fuels with environmentally friendly fuel sources or a shift to electric vehicles. An efficient fuel source with less pollutants would mean reducing the emission rate of vehicles as shown in Fig. 1.3(c) [93, 200].

These technological improvements of vehicles can contribute towards creating environmentally friendly vehicles, and hence the traffic managers and traffic controllers will have a wider range of speeds corresponding to low emission rates of vehicles, where they could focus only on the improvement of traffic flow. Moreover, if vehicles would have been made intelligent enough to communicate to each other and to the road-side infrastructure, the capacity drop that is caused due to the driver's behavior can be reduced to the level where the infrastructure is used efficiently. Moreover, incidents can be easily detected and vehicles can be used as means of sensors and information channels to and from the infrastructures. Intelligent vehicles can be equipped with decision support systems to assist drivers. The intelligence of vehicles can be used to form platoons so that the drag force of following vehicles can be reduced, which in turn reduces the fuel consumption and emissions of the vehicles [6, 17].

However, the achievement of such vehicles and clean fuels is thought not to be realizable in the short to medium term (e.g., 10 years) and vehicle improvements seem to be approaching their limits [97] . Hence, in the short term, other means have to be sought to address the traffic challenges. Moreover, even if vehicles are made intelligent, the release of particulate matter and hydrocarbons (due to the oils and grease used in the vehicle parts) would still continue (but at lower levels) due to the mechanical motion of the parts of the vehicles and due to the friction between the tire and the road.

1.2.3 Use of intelligent transportation systems

An alternative and promising solution is the implementation of Intelligent Transportation Systems (ITS). ITS adds information and communication systems to transport infrastructures and vehicles. This means that ITS uses the in-vehicle and the road-side information and communication systems to improve the traffic flow in such a way that the existing infrastructure is utilized as efficiently as possible. ITS can make decisions based on the prevailing and predicted traffic conditions and based on the interests and constraints of traffic authorities, environmentalists, and policy makers. In addition, ITS can integrate, coordinate,

and optimize different traffic flow control measures (such as traffic signals, ramp metering, speed limits, route guidance, etc.) to minimize the impact of traffic jams (such as long travel times and high emission levels).

ITS includes intelligent vehicles (e.g., vehicles that communicate to each other and to the infrastructure) and intelligent infrastructures (intelligent sensor systems, communication systems, control systems, and the like) that allow all stakeholders to interact in a productive and efficient way so that the traffic system is operated close to optimal.

For example, if vehicles are made intelligent (e.g., vehicles with automatic cruise control and vehicle-to-vehicle and vehicle-to-infrastructure communication systems), the capacity drop caused due to the difference in the reaction time of drivers and the difference in the reaction time of a driver under free-flow and congestion conditions can be minimized. Moreover, vehicles can be platooned at small inter-vehicle distances, which increases the operational capacity of freeways, because the density of vehicles on a freeway can be increased while maintaining high speed at small inter-vehicle distances. Since the vehicles in a platoon communicate continuously, all vehicles can brake or accelerate at the same time (if the vehicles are fully automated), which means that the size of the distance between each vehicle does not matter. Moreover, as has been discussed in Section 1.2.2, the use of ITS to platoon vehicles can reduce the fuel consumption and emissions, as a result of reduced drag force.

Since ITS includes intelligent vehicles and infrastructures, ITS in its full potential is not realizable in the short to medium term. However, it is possible to increase the intelligence of current traffic control and management decision systems with the available road-side information and control systems. For example, the variable speed limits, ramp metering, and route guidance systems of freeway traffic can be optimally and dynamically coordinated and integrated to address travel time, safety, fuel consumption, emissions, and dispersion of emissions. This is also the main focus of the thesis.

In traditional traffic control and management systems, transport authorities often set focus on the reduction of the total emission levels of freeways in order to reduce the emissions that affect some protected areas (such as schools, hospitals, and residences). Reduced total emission levels of vehicles on freeways are attained at low traffic speeds (between 30 and 70 km/h). Imposing such speed limits to reduce the total emissions heavily restricts the traffic flow. However, using ITS, it is possible to only consider the dispersion of emissions to a protected target zone. ITS can predict the dispersion of emissions to a given target zone based on the predicted wind speed and wind direction. Then, instead of reducing the total emissions in the entire network (which has negative impact on the travel time), ITS can dynamically focus only on the part of the freeway that affects the emission levels of the given protected zone. In this way ITS can reduce the emission levels in the target zone while at the same time improving the traffic flow at the parts of the freeway that do not have effect on the emission level of the target zone.

With integrated vehicle-road communication systems in place, the ITS-based traffic control and management systems can guide vehicles based on the emission rate of each vehicle dynamically. The greener vehicles can be allowed to move through protected areas while environmentally unfriendly vehicles can be routed through industrial (or unprotected) areas. Therefore, by and large, ITS can be used to provide a balanced trade-off between different conflicting interests of stakeholders.

1.3 Problem statement

Out of the three possible traffic solutions highlighted above, the focus of this thesis is the utilization of ITS-based traffic control and management systems. In general, ITS represents an extensive and broad traffic management approach. As such, the focus of this thesis is limited to infrastructure-based ITS. This thesis designs road-side intelligent (dynamic) controllers that provide a balanced trade-off between the travel times, fuel consumption, emissions, and dispersion of emissions to a target zone. In view of this, the scope of the ITS-based solution and the traffic challenges on which this thesis focuses are elaborated below.

1.3.1 Objectives

As has been indicated in the previous sections, the traffic challenges in general have both economic and environmental dimensions and there are conflicting interests. The economic concerns include travel times, fuel consumption, and safety. Emissions and the dispersion of emissions are two of the environmental issues. The question is then, can an ITS-based traffic control and management approach reconcile or provide trade-off between these concerns that are sometimes conflicting and sometimes concurring? To answer this research question, this thesis sets as an objective to design a road-side-based traffic control strategy to reduce the economic concerns (specifically, the travel time of vehicles in a traffic network and the fuel consumption) and environmental concerns (in particular, emissions and the dispersion of emissions to a given target zone) in a balanced way for a given freeway traffic network with a predictable traffic demand and traffic states.

Therefore, the core research problem of this thesis is defined as to:

> *Design a dynamic traffic controller such that a balanced trade-off is obtained between the total time spent, the total emissions released, the total fuel consumed, and the targeted-dispersion of emissions released by vehicles in given traffic network.*

1.3.2 Approaches

In order to realize the research objective set above, several choices have to be made. Since traffic systems are relatively slow and since current traffic solutions can have negative impact on the future traffic conditions, the outcome of each control decision on the future of the traffic conditions have to be predicted before the implementation of any control action. This can be done using predictive control approaches. But, in order to make predictions, traffic models are required. Hence, a model-based predictive traffic control approach is chosen. Furthermore, since models cannot describe the traffic phenomena exactly, predictions can be erroneous. Thus, the selected control approach should be able to take the model mismatch into account. To this end, the model-based predictive approach is used in a receding-horizon feedback fashion, where the prediction is shifted and repeated every time a new value for the control measure is determined so that the errors in the prediction can be adapted to the measured values. In this sense, the following are the important conditions considered for the realization of the envisaged model-based traffic controller:

- The traffic flow, emission, fuel consumption, and dispersion of emission models used have to be fast enough for on-line control applications and have to be accurate enough

to give good predictions of the traffic states (such as flow, density, speed, emissions, fuel consumption, and dispersion of emissions) so that the control decisions based on these states can have a positive impact on the traffic system.

- Since traffic systems are highly non-linear and since traffic problems are multifaceted, the receding-horizon model-based predictive controller should be able to handle non-linear models, multi-objective traffic control criteria, several constraints, and model mismatches.

In the light of the above criteria, a model-predictive control approach is selected. This control approach is able to accommodate non-linearity, handle constraints, multi-objective criteria, and model mismatch, and it can be operated in a receding-horizon fashion.

1.3.3 Scope of the thesis

The research objective defined above can be attained using different ITS-based traffic control and management systems. Moreover, since the research objective is a wide and complicated subject, the scope of the thesis is limited to a manageable level and its focus is much more specific as follows:

- This thesis focuses only on freeway traffic flow to examine and provide a potential solution under conflicting and concurring situations of traffic control objectives. This is because, unlike the urban traffic, the need to reduce emissions and travel times of freeway traffic systems can be conflicting and concurring [1, 110]. Moreover, to narrow the focus of the research, throughout the thesis, a homogeneous vehicle composition is assumed. So, all the vehicles in the freeway traffic are assumed to exhibit the same flow and emission characteristics.

- Due to the limited time and facilities, none of the traffic models or control approaches are tested on real systems. The research is illustrated using only simulations.

- The emissions considered in this thesis are CO, CO_2, HC, and NO_x. Other road-based traffic emissions such as SO_x and particulate matter (PM_x, where x is the aerodynamic diameter) are not considered, because there is abundant literature on the models of CO, CO_2, HC, and NO_x and the proposed control approaches can quite easily be extended to those emissions not considered in this thesis.

- As an illustration of the control approaches, the thesis exploits only two traffic control measures: variable speed limits and ramp metering. This is because these control measures have been extensively used in many papers to reduce travel time and avoid or reduce traffic shock waves [7, 19, 22, 75, 77, 79]. Moreover, these control measures can be easily modeled in most of the existing traffic flow models. Note, however, that the approaches can also be extended to other control measures.

1.4 Contribution of the thesis

In addition to the demonstration of the potential of existing models and control approaches for a sustainable mobility, the major contributions of this thesis are development of traffic models and design of traffic controllers.

1.4.1 Modeling

Since the main goal of the thesis is to design a traffic control strategy that provides a balanced trade-off between the travel times, the fuel consumption, the emissions, and the dispersion of emissions to a given target zone in a predictive fashion, the approach requires models to make accurate and reliable predictions of the traffic flow, emissions, and the dispersion of emissions. On the other hand, these models are required to be fast enough, so that they can be used for on-line based control applications. Therefore, it is imperative to select or develop appropriate models, i.e., models that are fast and that provide accurate predictions.

Following a literature study on the available traffic flow models, the METANET model [103, 124, 185] and its extensions [75, 78] have been selected to be used for the prediction of the traffic flow. The METANET model is a macroscopic model that uses aggregate variables to describe the traffic flow. But, macroscopic emission and fuel consumption models are not accurate enough to provide the prediction of emissions and fuel consumption. As a result, a way to integrate the macroscopic METANET traffic flow model with a more accurate and dynamic emission and fuel consumption model is necessary. Therefore, a strategy is developed to integrate macroscopic traffic flow models with microscopic emission and fuel consumption models, in particular the VT-micro [2] emission and fuel consumption model. This results in a macroscopic, but dynamic, emission and fuel consumption model that has relatively better accuracy.

In order to predict the dispersion of emissions to neighborhoods of freeway traffic networks, dispersion models are required. As papers in literature suggest, the existing dispersion models are computationally very slow and are not suitable for on-line control applications. So, this thesis also develops new dispersion models that are computationally efficient. Note, however, that these models are not compared to the already existing dispersion models and are neither calibrated to real-life data.

1.4.2 Control design

The second contribution of the thesis is the design of model-based traffic controllers. Initially, this thesis uses the already established control approaches—model predictive control—to assess the possibility to address some of the traffic challenges. A model predictive control approach with multi-objective performance criteria is designed for several cases to demonstrate that it can indeed reduce the emissions, fuel consumption, and the dispersion of the emissions while still reducing the total time spent by the vehicles in the traffic network. In doing so, two traffic control measures are used: variable speed limits and on-ramp metering.

However, as model predictive control is slow and intractable in practice—despite its capability to provide a balanced trade-off between the conflicting control objectives, another version of the control approach is designed. This thesis presents a parametrized model predictive control, specifically called the receding-horizon predictive traffic controller that is very fast and that (at least for the case studies considered in the thesis) has a performance that is almost the same as that of the conventional model predictive controller. The thesis also compares the two control approaches and shows that the receding-horizon predictive traffic control approach can be used in practice. The receding-horizon predictive traffic controller is able to reduce the emissions and fuel consumption as well as the dispersion of the emissions and travel time to almost the same levels as the conventional predictive traffic

controller, but with faster computation time, which makes it suitable for practical on-line control applications.

1.5 Thesis overview

This thesis contains eight chapters, including this chapter, and is presented in two parts, Part I (traffic models) and Part II (traffic control design). Part I contains Chapters 2, 3, and 4 and Part II consists of Chapters 5, 6, and 7. This chapter (Chapter 1) gives the general overview of the thesis, the problem statement, the approach employed in this thesis, and the contribution of the thesis to the state-of-the-art.

Part I of the thesis deals with the modeling of traffic flow in Chapter 2, traffic emissions in Chapter 3, and the dispersion of traffic emissions into neighborhood of freeways in Chapter 4. The models presented in this part are used for the prediction and simulation of the control strategies presented in Part II. Therefore, for better understanding of the thesis, it is suggested to first read Part I and proceed to the next chapters as indicated in the structure of the thesis in Fig. 1.4.

Part II of the thesis presents two traffic control strategies and compares them using simulation-based experiments. This part first discusses conventional model predictive control for traffic in Chapter 5. The control strategy is used in several case studies using the models developed in Part I. Chapter 6, presents a version of the model predictive control approach, called the receding-horizon predictive control for traffic. In Chapter 7, the performance of the receding-horizon predictive controller is assessed and compared with the conventional model predictive controller both in terms of computation time and traffic control performance criteria.

Finally, the thesis is concluded in Chapter 8, in which both parts of the thesis are summarized and several recommendations for future work are presented.

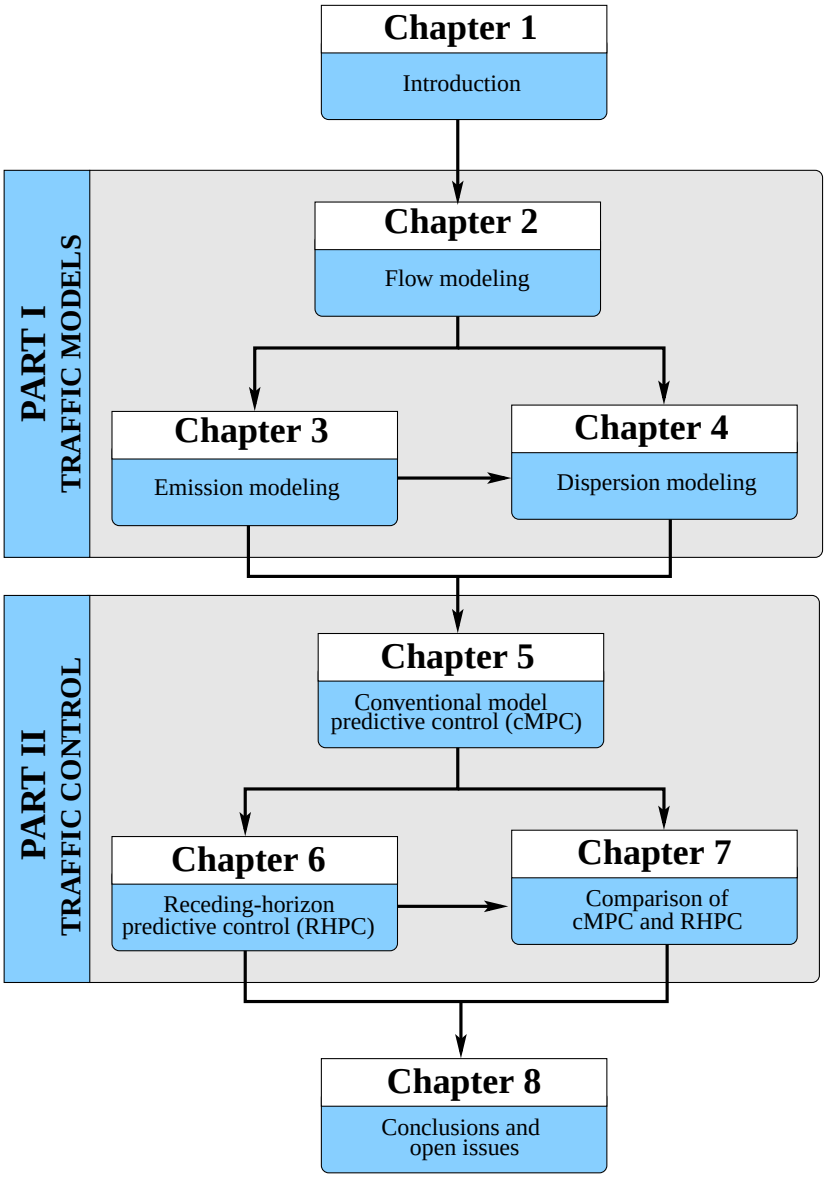

Figure 1.4: Structure of the thesis.

Part I

TRAFFIC MODELS

Chapter 2

Traffic Flow Modeling

As has been introduced in Chapter 1, model-based traffic control approaches utilize traffic models to design the traffic control measures in such a way that the desired control objectives are attained. Therefore, it is imperative to make a selection of (or to develop) models that are suitable for the envisaged traffic control approaches. The traffic models can be models of traffic flow, traffic emissions and fuel consumption, and dispersion of traffic emissions. In this chapter the traffic flow models that are used throughout this thesis are discussed. The models that describe the traffic emissions, fuel consumption, and dispersion of emissions will be the subject of the subsequent chapters.

In order to build the basic understanding of traffic flow models, this chapter begins with first providing a brief overview of traffic flow models in Section 2.1, where it discusses the application of traffic flow models and the different groups of traffic flow models. Next in Section 2.2 car-following (or follow-the-leader) traffic flow models are further examined with special emphasis on the Gazis-Herman-Rothery [67] and Intelligent Driver Model [186] models. Section 2.3 presents the METANET [124] model and its extensions [78]. Finally, a summary of the chapter is provided in Section 2.4

2.1 Overview of traffic flow models

Traffic flow models seek to describe the interaction of vehicles with their drivers and the infrastructure. Almost all the models—directly or indirectly—characterize the relationship among the traffic variables: the position, the speed, the flow, and the density of vehicles. These relationships can be based on either the behavior of individual vehicles in a traffic network in relation to the dynamics of other vehicles, the overall characteristics of the flow of vehicles in a traffic network, or a combination of the behavior of individual vehicles in a traffic network and the overall traffic flow characteristics. Almost every traffic flow modeling technique follows the same principle, i.e., first a first-principles model based on the physics governing the system or other analogy system is developed. Next, the parameters that determine the characteristics of the infrastructure, the behavior of drivers, and the characteristics of vehicles are estimated from data. This is the general procedure in most traffic modeling approaches [29, 87, 158, 164]. However, there are also some traffic flow models or relations between traffic variables that are solely determined from data (e.g., the

non-parameter modeling approaches) [41, 87].

In the sequel, the application of traffic flow models and the classification of traffic models based on their level of detail are elaborated. The discussion will provide a clear picture for the motivation of the selection of the traffic flow models used in this thesis.

2.1.1 Applications of traffic flow models

Many traffic flow models can be used for different applications. They can be used for the assessment of traffic control strategies, for the design of model-based traffic controllers, for the design of new transportation facilities, and for the training of traffic operators and traffic managers [75, 87].

Appropriate traffic solutions to reduce the recurrent and non-recurrent traffic challenges can be obtained through thorough understanding of the system and through conduction of in-depth research. However, field research and experiments are expensive, because they disturb the prevailing traffic and require heavy investments. Moreover, due to unpredictable disturbances and traffic demands, real traffic flow does not guarantee repeatability of experiments and it is thus difficult to assess the performance of a dynamic traffic control or a dynamic traffic assignment strategy. However, operations and experiments with models are cheaper and faster. If necessary, experiments can be repeated and different traffic control and assignment strategies can be compared under the same conditions [75, 87].

Traffic flow models are also used for model-based traffic control or state estimation. Some traffic control strategies require the model of the traffic system for either prediction of the traffic state over a time horizon or for an estimation of unobservable (or unmeasured) traffic state. Traffic flow models enable traffic operators and managers to forecast the traffic conditions (such as high demands, or travel times) that will occur in a traffic network over a predetermined future time horizon [147].

New transportation facilities such as new roads may not have the desired effect after they are constructed. For example, new on-ramps to freeways from urban roads may increase the access of the freeway for urban drivers, and this may increase the possibility of more traffic jams on the freeways [75]. Traffic flow models can be used to simulate different designs under different traffic scenarios and thus new transportation facilities can be evaluated before they are constructed [75, 87, 147].

Traffic flow models are also used to provide desired training and skills for traffic operators and traffic managers [75, 87]. They help in providing support for traffic operators to understand the consequences of different traffic control and management actions. Moreover, decision support systems can be built based on models to assist or support traffic operators and traffic managers in their traffic control or assignment operations.

2.1.2 Classification of traffic flow models

Traffic flow models can be studied by grouping them in several ways. The nature of traffic flow models can be different in terms of their application area, in terms of their level of detail, in terms of the time domain used to describe them (as discrete-time or continuous-time models), and in terms of their stochastic or deterministic nature in the description of the traffic variables [87]. Based on their level of detail, they can be categorized as microscopic, macroscopic, and mesoscopic traffic flow models [87]. Traffic flow models that treat and model the behavior of individual vehicles in a traffic network fall in the category

of *microscopic* traffic flow models. *Macroscopic* traffic models describe the collective vehicle dynamics in terms of the spatial vehicle density, the average flow, and average speed. *Mesoscopic* models describe the behavior of small groups of vehicles of a specific user-class classified by their position, velocity, and desired velocity at an instant of time [87].

Microscopic traffic flow models

Microscopic traffic flow models describe the physics of individual vehicles as they interact with the driver and the infrastructure. In such modeling techniques lane changes, the inter-vehicle distance, and the effect of neighboring vehicles to a vehicle are described. The main advantage of microscopic traffic flow models is that the behavior of the drivers and vehicles are described in detail. Therefore, they can provide relatively more information regarding the characteristics of the traffic flow (e.g., headway time or distance; position, speed, and acceleration of individual vehicles; heterogeneity of vehicles; and the like) than other types of models. The main limitation of microscopic models is that they require a large memory size and they are very slow when used for large traffic networks [117, 130]. Moreover, microscopic models most often require large number of parameters, which are most often difficult to calibrate. So microscopic traffic flow models are not feasible for on-line prediction and optimization of traffic control systems. These models are mostly useful for local traffic studies.

Microscopic traffic flow models can also be categorized into different groups based on their conceptual approaches [87], these are: car-following, microscopic simulation, submicroscopic simulation, cellular automaton, and particle models.

The car-following models, also called follow-the-leader models, were pioneered by Pipes [158]. These models describe the dynamics of a vehicle (along with its driver and the infrastructure) in relation to its predecessor [29, 87, 158]. Car-following models are very widely used in traffic flow analysis, design, and simulation [164].

Microscopic simulation traffic flow models are computer models where the driver behavior is modeled with extensive production (if-then) rules. These models describe both car-following and lane-changing behavior of individual vehicles [87]. AIMSUN2 and FOSIM [192] are two examples of microsimulation traffic models.

Submicroscopic simulation models are similar to the microscopic simulation models except that they have additional non time-space features [87]. These include functioning of specific parts of vehicles, dynamics of vehicles, and driving tasks of the driver. For instance they describe how a driver applies the breaks, his reaction time, and the like.

The cellular automaton model describes the traffic system as a lattice of cells of equal size [128, 129]. A cellular automaton model describes the movement of vehicles from cell to cell in a discrete way. Moreover, the vehicles assume only a limited number of discrete speed values [87].

The particle traffic flow models trace and distinguish individual vehicles in a traffic network. But these models use aggregate equations (e.g., macroscopic traffic flow equations) of motion to describe the behavior of the individual vehicles [87]. The INTEGRATION [83] traffic flow model is an example of such a particle models.

Macroscopic traffic flow models

Since in the microscopic traffic models each car is described by its own equations of motion, the computer time and memory requirements of corresponding traffic simulations grow as

the number of simulated cars increases [81, 87]. Therefore, these kinds of models are mainly suitable for off-line traffic simulations, detailed studies (such as on-ramps or lane merging), or numerical evaluation of collective quantities [8] like the density-dependent velocity distribution, the distribution of headway distances, etc., and other quantities that are difficult to determine empirically [81]. For these reasons, coarse fast microsimulation models have been developed for the simulation of large freeways or freeway networks [48, 130]. However, although they reproduce the main effects of traffic flow, they are not very suitable for detailed predictions because of their coarse-grained description [81]. Therefore, many authors prefer macroscopic traffic flow models to microscopic flow models [80, 94, 95, 108, 144].

Macroscopic traffic flow models deal with traffic flow in terms of aggregate variables (such as average speed, flow, and density). These aggregate variables, which describe the behavior of the drivers or vehicles, are assumed to depend on the traffic conditions in the drivers' (or vehicles') direct environments [87]. Macroscopic traffic models do not distinguish the behavior of individual vehicles in a traffic stream. So, in macroscopic models the simulation time and memory requirements mainly depend on the size of spatio-temporal discretization, but not on the number of cars [48, 81, 87]. Therefore, macroscopic traffic flow models are suitable for faster than *real-time* traffic simulations [81, 87]. Another advantage of macroscopic traffic flow models is that they allow to simulate the traffic dynamics in several lanes by effective one lane models [82].

Most often macroscopic models are derived from the analogy between vehicular flow and flow of continuous media (e.g., fluids or gases) [103], resulting in traffic flow models with a limited number of equations that are relatively easy to handle [87]. The first macroscopic traffic models were reported in [108] and [169]. These models established the theory for the development of the more finer and accurate traffic flow models presented in [124, 145, 146, 154, 185].

The independent variables of a continuous macroscopic traffic flow model are location x, and time instant t. Most macroscopic traffic flow models describe the dynamics of the density $\rho = \rho(x,t)$, the average speed $v = v(x,t)$, and the flow $q = q(x,t)$; and the relationship of these variables. Virtually all macroscopic traffic models are based on the continuity equation [82]

$$\frac{\partial \rho(x,t)}{\partial t} + \frac{\partial\big(\rho(x,t)v(x,t)\big)}{\partial x} = \nu(x,t) \tag{2.1}$$

for the source term $\nu(x,t)$ denoting the rate of vehicles entering the freeway at on-ramp section or the rate of vehicles leaving the freeway at off-ramp section.

Moreover, in addition to (2.1) most macroscopic models define the relation between the density $\rho(x,t)$, the flow $q(x,t)$, and the average speed $v(x,t)$ as

$$q(x,t) = \rho(x,t)v(x,t) \tag{2.2}$$

where the density $\rho(x,t)$ is per single lane.

However, equations (2.1) and (2.2) do not completely describe the traffic dynamics, because the number of unknown variables is more than the number of equations. Consequently to get a complete description of the traffic dynamics, other equations are needed. If no on-ramp and off-ramp is considered on a section of a freeway, the source term $\nu(x,t) = 0$. As a third equation, most first-order macroscopic traffic flow models assume a static

speed-density relation [52, 53, 108, 134, 169], which leads to $v(x,t) = V(\rho(x,t))$, where $V(\rho(x,t))$ is the equilibrium speed. But for the description of emergent traffic jams and stop-and-go traffic, one needs a dynamic speed equation [82]. Then, for most higher-order macroscopic models, the third equation that describes the dynamics of the average speed $v(x,t)$ can be written in general [82, 204]

$$\frac{\partial v(x,t)}{\partial t} + v(x,t)\frac{\partial v(x,t)}{\partial x} = \\ -\frac{1}{\rho(x,t)}\frac{\partial \mathcal{P}(\rho(x,t)v(x,t))}{\partial x} + \frac{1}{\tau}\big(V(\rho(x,t) - v(x,t))\big) \tag{2.3}$$

where $V(\rho(x,t))$ is the generalized equilibrium speed given by the fundamental diagram[1] relationship between $v(x,t)$ and $\rho(x,t)$, τ is the relaxation time, and $\mathcal{P}(\rho(x,t), v(x,t))$ is the traffic pressure. The traffic pressure is a quantity that describes the degree to which drivers must interact with each other [157].

The third dynamic equation (2.3) results in a second-order traffic flow model. The difference between the various existing macroscopic traffic flow models mainly concern the traffic pressure $\mathcal{P}(\rho(x,t), v(x,t))$, the relaxation time τ, and the generalized equilibrium speed $V(\rho(x,t))$ [204] that results in different equations for the average speed $v(x,t)$. However, [81] introduced a fourth equation that describes the dynamics of the variance of the average speed. Many papers [49, 103, 124, 145, 171, 185] show that in practice the second-order macroscopic models, in particular the METANET [124] traffic flow model, can accurately describe the average traffic dynamics of freeway traffic. So, in this thesis, a second-order traffic flow model, more specifically the METANET model and some of its extensions [78], are presented in details in Section 2.3 and it is extensively used in the subsequent chapters.

Mesoscopic traffic flow models

The mesoscopic traffic flow models describe the traffic flow in lesser detail than the microscopic models and in greater detail than the macroscopic models. In such models the vehicle or the driver behavior is not described individually, but in more aggregate terms. For example the same probability distribution functions can be used to categorize or describe the behavior of a vehicle or a driver [87] in some range of time or distance.

So mesoscopic traffic flow models describe the dynamics of individual or small groups of vehicles using aggregate variables, such as the velocity distribution at a specific location and time instant. For example, in a gas-kinetic mesoscopic traffic model the phase-space density $\hat{\rho}(x,v,t)$ is defined as the *mean* number of vehicles that are at a place between $x - \Delta x/2$ and $x + \Delta x/2$ and driving with a velocity between $v - \Delta v/2$ and $v + \Delta v/2$ during the time range $[t - \Delta t/2,\ t + \Delta t/2]$ [81].

The mesoscopic traffic flow models can be grouped into three categories [87]: headway distribution models (such as [31, 33]), cluster models, and the gas-kinetic continuum models (such as [153, 159]). Since the mesoscopic models combine some of the microscopic characteristics to macroscopic models or the other way around, these models become more complicated to simulate and calibrate than their corresponding microscopic or macroscopic versions. So these models are not used in this thesis and hence are not discussed in details. An interested reader is referred to [31, 33, 87, 153, 159].

[1] See Fig. 2.2 for specific fundamental diagram.

2.2 Car-following models

2.2.1 Overview of car-following models

The car-following models, which are also called follow-the-leader models, describe the interaction of a vehicle with its predecessor. Most generally, car-following refers to a situation in which a vehicle's speed and longitudinal position are influenced by the vehicle immediately ahead of it in the same lane. Car–following is characterized by the headway (time or distance between vehicles) and the degree to which the following vehicle tracks the velocity changes of the leading vehicle. Car-following behavior is influenced by the driving goals, road curvature, relative velocity, stream speed, whether car-following is chosen or imposed, and the duration in the interaction (or coupled) state [164]. Car-following is one of the main processes in all microscopic simulation models and in modern traffic flow theory. It attempts to explain the interplay between the phenomena at the individual driver level and global behavior on a more macroscopic scale [29].

Car-following models have a wide range of applications. By using car-following models, one can deduct the behavior of a single-lane traffic stream by examining the manner in which individual vehicles follow one another and from the joint behavior of pairs of vehicles [164]. Moreover, traffic stability is a logical extension of car-following theory, where local stability refers to the response of a following vehicle in a single pair of vehicles and asymptotic stability refers to the manner in which the fluctuations of the leading vehicle are propagated through an entire stream of vehicles in the same lane [119]. Microscopic models of individual car-following behavior form the building blocks for microsimulation models of traffic flow, which are used to assess the effects of interventions such as changes in roadway geometry, traffic signal timing, delineation, signing, etc. [164]. In recent years the importance of car-following models has increased further in forming the basis of the functional definitions of advanced vehicle control and safety systems [29]. Other systems, such as autonomous cruise control, seek to replicate human driving behavior through partial control of the accelerator, while removing potential hazards that may occur through driver misperception and reaction time [29].

In this thesis stimulus-response car-following models are discussed and they are used in the subsequent chapters. To present the motivation for the choice of these models a short account on safe-distance car-following models is also presented. It is also important to note that in this thesis only the longitudinal kinematic behavior of vehicles and drivers is considered. Since these models are used to demonstrate the potential of the proposed control approaches as a "proof of concept," detailed modeling such as lane changing and overtaking are not considered. However, the traffic control approaches to be presented and illustrated in the second part of this thesis are generic and are also valid for other more complex models that also include lane changing and other traffic behavior.

The general longitudinal kinematic motion of vehicles is described by

$$x_\alpha(k_\mathrm{m}+1) = x_\alpha(k_\mathrm{m}) + v_\alpha(k_\mathrm{m})T_\mathrm{m} + 0.5a_\alpha(k_\mathrm{m})T_\mathrm{m}^2 \tag{2.4}$$

$$v_\alpha(k_\mathrm{m}+1) = v_\alpha(k_\mathrm{m}) + a_\alpha(k_\mathrm{m})T_\mathrm{m} \tag{2.5}$$

where $x_\alpha(k_\mathrm{m})$, $v_\alpha(k_\mathrm{m})$, and $a_\alpha(k_\mathrm{m})$ are respectively the position, speed, and acceleration of vehicle α in the network at time $t = k_\mathrm{m}T_\mathrm{m}$, where k_m is the microscopic simulation time step counter, while T_m (e.g., $T_\mathrm{m} = 1$ s) is the microscopic simulation time step of the discretized model. The acceleration in (2.4) and (2.5) is determined from the longitudinal

driver model described in the sequel.

Safe-distance models

The safe-distance car-following modeling approach has been pioneered by Pipes [158]. He developed a very simple mathematical model based on his postulate that 'the movements of several vehicles are controlled by an idealized "law of separation"'. The law considered in the analysis specifies that each vehicle must maintain a certain prescribed "following distance" from the preceding vehicle. This distance is the sum of a distance proportional to the velocity of the following vehicle and a given certain minimum distance of separation when the vehicles are at rest. After discretization, the longitudinal position $x_\alpha(k_\mathrm{m})$ of the following vehicle α relative to the leading vehicle is given by

$$x_\alpha(k_\mathrm{m}) = s_{0,\alpha} + l_\alpha + T_{\mathrm{d},\alpha} v_\alpha(k_\mathrm{m}) \tag{2.6}$$

where $s_{0,\alpha}$ denotes the minimum stand-still inter-vehicle distance, l_α denotes the length of the following vehicle, $v_\alpha(k_\mathrm{m})$ is the velocity of the following vehicle, and $T_{\mathrm{d},\alpha}$ is the overall reaction time of vehicle α, where the overall reaction time $T_{\mathrm{d},\alpha}$ is defined as the total time a driver requires to take an action from the time he/she perceives a stimulus (a change in the driving behavior of a neighboring vehicle).

The equation shows a linear relationship between the safe distance and the velocity of the following vehicle. However, the reaction time can also be considered as having three components: perception time, decision time, and braking time [87]. The braking distance is defined as the distance needed by a vehicle to come to a full stop, incorporating the reaction time of the driver and the maximum deceleration. The maximum deceleration term is a function of the friction coefficient $\mu_{\mathrm{f},\alpha}$ between the tire and the road, and the acceleration due to gravity g. Hence, the total safe distance is

$$x_\alpha(k_\mathrm{m}) = s_{0,\alpha} + l_\alpha + T_{\mathrm{d},\alpha} v_\alpha(k_\mathrm{m}) + \frac{v_\alpha^2(k_\mathrm{m})}{2\mu_{\mathrm{f},\alpha} g}. \tag{2.7}$$

The model implies that if the first vehicle stops, the second vehicle needs the distance it can cover during the overall reaction time $T_{\mathrm{d},\alpha}$ with unreduced speed and the distance it can move due to its inertia as full break is applied in order to stop safely.

Stimulus-response models

The main principle behind the stimulus-response car-following modeling is that the driver reacts to the changes in the kinematic dynamics (stimulus) of a leading vehicle. The reaction of a following vehicle can be modeled as a function of the changes in the position, speed, etc. of the leading vehicle. In general such car-following models are given by the form

$$\mathrm{Response}_\alpha = f_\alpha\big(\mathrm{Sensitivity}_\alpha, \mathrm{Stimulus}_\alpha\big) \tag{2.8}$$

where f_α is the function that describes the influence of the stimulus and sensitivity on the response of vehicle α.

In general, in most stimulus-response models the response is the acceleration or deceleration a_α of the following vehicle α responding to a stimulus observed $T_{\mathrm{d},\alpha}$ overall reaction time ahead. In most stimulus-response models the stimulus is assumed to depend on the

relative position $x_\alpha - x_{\alpha-1}$ and the relative velocity $v_\alpha - v_{\alpha-1}$ of the leading vehicle $\alpha-1$ and following vehicle α. Then, in general the stimulus-response car-following models can be described as

$$a_\alpha(k_\mathrm{m}) = f_\alpha\big(x_\alpha(k_\mathrm{m}, T_{\mathrm{d},\alpha}), x_{\alpha-1}(k_\mathrm{m}, T_{\mathrm{d},\alpha}), v_\alpha(k_\mathrm{m}, T_{\mathrm{d},\alpha}), v_{\alpha-1}(k_\mathrm{m}, T_{\mathrm{d},\alpha})\big) \tag{2.9}$$

where the sensitivity, the stimulus, and the response of the driver are determined according to the function f_α.

The Gazis-Herman-Rothery (GHR) [67], the car-following model of Newell [133], the Optimal Velocity Model (OVM) [15], and the Intelligent Driver Model (IDM) [186] fall into stimulus-response car-following models. Two of these models are presented below: the GHR and IDM models. These models are also used in the simulation studies of the subsequent chapters.

2.2.2 The GHR model

The microscopic Gazis-Herman-Rothery (GHR) [67] traffic flow model is the most well-known stimulus-response based car-following model. This model is developed based on the intuitive assumption that each driver reacts in some specific fashion to stimuli from the cars ahead of or behind him. But, since the follow-the-leader theory applies to fairly dense traffic, some car-following models cannot be used for all traffic conditions. The theory of the GHR model in its simple form is one of such models, and it should not be extrapolated to the range of very low vehicle concentrations [67]. Therefore, in order to use the car-following models (and so the GHR model) for fairly dense traffic, a threshold variable is introduced to determine whether a vehicle is in the state of car-following or free-flow traffic conditions [19, 203]. Since the speed and the nature of the reaction of drivers is dependent on their time (or distance) headway, the threshold is defined based on the time headway. The time headway is defined as the time difference between two consecutive vehicles that pass a certain location. This can be described as the time needed by the following vehicle to reach the current position of the leading vehicle with its current speed. This reads as

$$t_\mathrm{h}(k_\mathrm{m}) = \frac{x_{\alpha-1}(k_\mathrm{m}) - x_\alpha(k_\mathrm{m})}{v_\alpha(k_\mathrm{m})} \tag{2.10}$$

where $x_{\alpha-1}(k_\mathrm{m})$, $x_\alpha(k_\mathrm{m})$ are respectively the positions of the leading and the following vehicles at time $t = k_\mathrm{m}T_\mathrm{m}$, and $v_\alpha(k_\mathrm{m})$ is the speed of the following vehicle at time $t = k_\mathrm{m}T_\mathrm{m}$.

Depending on the time headway a vehicle can be either in car-following or in free-flow mode. When the time headway is larger than the threshold time headway t_tr (e.g, $t_\mathrm{tr} = 10\,\mathrm{s}$), then the vehicle is said to be in free-flow mode, whereas if the time headway is smaller than the threshold time headway, then the vehicle is in a car-following mode.

When a vehicle is in a car-following mode, the GHR model describes the follow-the-leader traffic behavior following the stimulus-response law in (2.8) with

$$f_\alpha\big(\mathrm{Sensitivity}_\alpha, \mathrm{Stimulus}_\alpha\big) = \mathrm{Sensitivity}_\alpha \times \mathrm{Stimulus}_\alpha \tag{2.11}$$

where $\mathrm{Stimulus}_\alpha$ is the relative speed of the following vehicle α with respect to the leading vehicle $\alpha-1$ and the $\mathrm{Sensitivity}_\alpha$ is a function of the position and speed of the following

vehicle α and the relative position of the following vehicle α to the leader vehicle $\alpha - 1$.

In the GHR model the reaction of the driver has been taken as the acceleration of the vehicle, because a driver has direct control of the acceleration through the gas and brake pedals. The acceleration is assumed as to be a function of the variation of its current speed, and the relative speed and position of the vehicle with respect to its predecessor vehicle [67]. The model also takes the delay in the reaction of the driver into account in the relative speed and position of the vehicle. This is given as

$$a_\alpha(k_\mathrm{m}) = c_\alpha v_\alpha^{\imath_\alpha}(k_\mathrm{m}) \frac{\big(v_{\alpha-1}(k_\mathrm{m} - T_{\mathrm{d},\alpha}) - v_\alpha(k_\mathrm{m} - T_{\mathrm{d},\alpha})\big)}{\big(x_{\alpha-1}(k_\mathrm{m} - T_{\mathrm{d},\alpha}) - x_\alpha(k_\mathrm{m} - T_{\mathrm{d},\alpha})\big)^{\jmath_\alpha}} \tag{2.12}$$

where c_α, $\imath_\alpha$, and $\jmath_\alpha$ are model parameters, and $T_{\mathrm{d},\alpha}$ is the overall reaction time of the driver. Note that since we are using discrete-time models, for computational issues it is assumed that the overall reaction time $T_{\mathrm{d},\alpha}$ is a positive integer.

However, when the time headway is larger than the threshold time headway t_tr, the interactions between vehicles vanish. Hence, as there is no car-following behavior the GHR model cannot describe the traffic flow under such situations [67]. Under the free-flow cases, drivers intend to relax their speed to their desired speed $v_{0,\alpha}(k_\mathrm{m})$. So, the stimulus of the drivers is changed to the relative speed between the vehicle and the desired speed or speed limit, whichever is smallest. The sensitivity is considered to be a constant [19]. This is taken to be

$$a_\alpha(k_\mathrm{m}) = \sigma_\alpha \left(\min\big\{v_{\mathrm{vsl},\alpha}(k_\mathrm{m} - T_{\mathrm{d},\alpha}), v_{0,\alpha}(k_\mathrm{m} - T_{\mathrm{d},\alpha})\big\} - v_\alpha(k_\mathrm{m} - T_{\mathrm{d},\alpha})\right) \tag{2.13}$$

where σ_α is the sensitivity of vehicle α (typically 0.01–0.4), $v_{\mathrm{vsl},\alpha}(k_\mathrm{m} - T_{\mathrm{d},\alpha})$ is the speed limit observed $T_{\mathrm{d},\alpha}$ ahead.

Under the car-following conditions the GHR model in (2.12) is supposed to use a single set of parameters $p_\mathrm{GHR} = \{c_\alpha, \imath_\alpha, \jmath_\alpha, T_{\mathrm{d},\alpha}\}$. However, as the real-world experiences indicate the acceleration of a vehicle is smaller than its deceleration. Vehicles require larger time to achieve a certain high speed than to decelerate back to the original low speed, which is related to the slow-to-start phenomena introduced in [16]. The larger time required to accelerate than to decelerate is one of the reasons for the reduction in the operational capacity of a freeway network, which is most often referred to as the capacity drop [38, 72, 75]. Therefore, to capture the difference in the magnitude of the acceleration and deceleration, the GHR model requires the use of different parameter sets for each case. In literature [19, 203] it is suggested to use two parameter sets except for $T_{\mathrm{d},\alpha}$, one set during the accelerating mode of the vehicles and the second set during the decelerating mode of the vehicles.

Similarly, under free-flow traffic conditions in which the dynamics of a vehicle is described by (2.13), the parameter σ_α is also set differently for vehicles accelerating or decelerating towards the desired speed [19, 203].

The main problem in the GHR model is that when the speed difference between the leading and following vehicles is zero, the response (or acceleration) disappears regardless of the inter–vehicle distance. This problem is solved by the car-following model of Newell [133] and the Optimal-Velocity-Model [15]. However, these new models lead to very high accelerations of order $v_{0,\alpha}(k_\mathrm{m})/T_{\mathrm{d},\alpha}$ [186]. The IDM [186] solves the problems encountered in [15, 67, 133].

2.2.3 The IDM model

The intelligent driver traffic flow model [186] is a simple model that has only a few intuitive parameters. Unlike the GHR [67] model, which describes only the congested traffic state, the IDM model can describe both free-flow and congested traffic states. Although in many of the stimulus-response based models the acceleration of the vehicles is modeled by introducing a delay related to the overall reaction time, the IDM model does not use the driver reaction time (or any) as a delay parameter for the determination of the acceleration of the following vehicle, which makes it computationally suitable. In [173] the IDM model is improved in order to also model high traffic capacity (e.g., 1900 veh/h/lane and above) of freeways.

In the IDM model the acceleration of a vehicle α following another preceding vehicle $\alpha - 1$ is described as

$$a_\alpha = a_{\max,\alpha}\left[1 - \left(\frac{v_\alpha}{v_{0,\alpha}}\right)^\delta - \left(\frac{s^*(v_\alpha, \Delta v_\alpha)}{s_\alpha}\right)^2\right] \tag{2.14}$$

where v_α denotes the speed of vehicle α, $s_\alpha = x_{\alpha-1} - x_\alpha - l_\alpha$ denotes the inter-vehicle (or actual) gap of vehicle α from the leading vehicle $\alpha-1$, $\Delta v_\alpha = v_\alpha - v_{\alpha-1}$ denotes the speed difference (approach rate) between the following vehicle α and the leading vehicle $\alpha - 1$, $a_{\max,\alpha}$ denotes the maximum comfortable acceleration of vehicle α, δ denotes the free-flow acceleration exponent, $v_{0,\alpha}$ denotes the desired speed of vehicle α, and $s^*(v_\alpha, \Delta v_\alpha)$ denotes the minimum desired gap given by

$$s^*_\alpha(v_\alpha, \Delta v_\alpha) = s_{0,\alpha} + \max\left\{T_{\mathrm{d},\alpha} v_\alpha + \frac{v_\alpha \Delta v_\alpha}{2\sqrt{a_{\max,\alpha} b_{\max,\alpha}}},\ 0\right\} \tag{2.15}$$

with $s_{0,\alpha}$ denoting the minimum inter-vehicle distance at stand still, $b_{\max,\alpha}$ denoting the maximum comfortable deceleration of vehicle α.

The acceleration expression in (2.14) is a superposition of two acceleration terms. These are the free-flow acceleration and the car-following acceleration. Under free-flow traffic conditions, the actual gap $s_\alpha \gg 0$ and thus the influence of the last term in (2.14) becomes negligible to result in

$$a_\alpha \approx a_{\max,\alpha}\left[1 - \left(\frac{v_\alpha}{v_{0,\alpha}}\right)^\delta\right]$$

which describes the driver behavior under free-flow traffic conditions. This shows that as the speed of vehicle α reaches the desired speed $v_{0,\alpha}$ the acceleration approaches zero. When the speed of vehicle α is greater (or less) than the desired speed $v_{0,\alpha}$, the acceleration becomes negative (or positive).

As the traffic behavior almost gets congested, the actual speed v_α, the desired speed $v_{0,\alpha}$ and the actual gap s_α of vehicle α decrease. Hence, the acceleration in (2.14) describes the driver behavior under car-following traffic conditions with the last term becoming significant. Then, the car-following acceleration reads as

$$a_\alpha \approx a_{\max,\alpha}\left[1 - \left(\frac{s^*(v_\alpha, \Delta v_\alpha)}{s_\alpha}\right)^2\right].$$

This expression indicates that as the actual gap s_α of a vehicle α approaches the minimum desired gap s^*_α (i.e., $s_{0,\alpha}$) in a congested (or in car-following) situations, the acceleration a_α of vehicle α decreases to zero. If the actual gap continued decreasing below the minimum desired gap, the last term of (2.14) dominates and the vehicle decelerates.

In the IDM model, according to the sign of the approach rate Δv_α, the desired gap in (2.15) determines the magnitude of the acceleration and deceleration of a vehicle in a congested traffic state. The magnitude of the acceleration or deceleration under free-flow conditions is determined by the ratio of the actual and desired speed (the second term in (2.14)). Thus, unlike the GHR model, the IDM model describes the dynamics of the traffic equation with a single parameter set $p_{\mathrm{IDM}} = \{\delta, s_{0,\alpha}, v_{0,\alpha}, T_{\mathrm{d},\alpha}, a_{\max}, b_{\max}, l_\alpha\}$.

2.3 The METANET model and its extensions

METANET [124] is a deterministic modeling tool for simulating traffic flow phenomena in freeway networks of arbitrary topology and characteristics including freeway stretches, bifurcations, on-ramps, and off-ramps [103, 124, 185]. It is a discrete-time, discrete-space second-order macroscopic traffic flow model that treats the traffic flow as a compressible fluid. The modeling approach allows for the simulation of all kinds of traffic conditions (free, dense, congested) and of capacity-reducing events (incidents) with prescribed characteristics (location, intensity, duration). Furthermore, METANET along with its extensions allows for taking into account control actions such as variable speed limits, ramp metering, and route guidance [78, 103, 124].

The dimension of the state space of the model depends on the size of the spatial discretization. Since the number of the vehicles does increase neither the number of the variables nor the number of the states, the computation speed of the model is only affected by two factors: the temporal and the spatial discretization step sizes. But, since the discretization in space ($500\,\mathrm{m}$–$1000\,\mathrm{m}$) and the discretization in time ($10\,\mathrm{s}$–$15\,\mathrm{s}$) are coarse, the computation time of the model is low.

The METANET model uses aggregate variables to describe the behavior of the vehicles on a freeway. These variables are the density ρ [veh/km/lane] that is defined as the number of vehicles occupying a length of freeway per lane, the flow q [veh/h] that is also defined as the number of vehicles passing a point in a given time [119], and the space-mean speed v [km/h] that describes the average of the instantaneous speed of vehicles occupying a section of a freeway.

In the METANET model a graphical representation of the traffic network is used in such a way that a node is placed wherever there is a change in the geometry of a freeway (such as a lane drop, on-ramp, off-ramp, or a bifurcation). A homogeneous freeway stretch that connects such nodes is designated as a link indexed by m and it is described by a single set of parameters (see Fig. 2.1). Thus, the traffic network is divided into links with homogeneous traffic characteristics and each link is subdivided into N_{m} segments of equal length L_m (typically 500-1000 m).

In the METANET traffic flow model five different links are defined. These are:

Freeway links represent homogeneous freeways, and are described by the freeway average density, speed, and the average outflow.

Origin links are parts of the freeway that receive the traffic demand from outside the network and forward it into the network. They are described by their flow capacity and

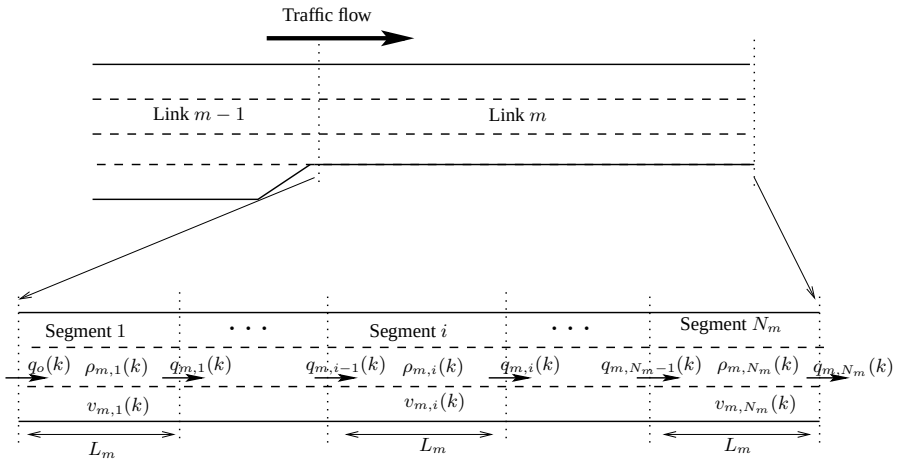

Figure 2.1: A link m of a freeway sectioned into N_m segments.

their queue.

Destination links receive traffic flow from inside the network and push it to the outside. They are influenced by the downstream traffic conditions.

Store-and-forward links are characterized by their queue length, flow capacity, their constant travel time. These links are used to store the inflow traffic and forward it to the outflow with some time delay.

Dummy links are links with zero length. They are used in order to decompose complex network nodes.

As such the dynamic equations that describe the evolution of the traffic state are grouped as link equations and node equations. In the sequel the link equations, the node equations, the origins, and the boundary conditions along with some of the extensions of the METANET model are discussed.

2.3.1 Link equations

As mentioned above, the METANET model uses aggregate variables to describe the behavior of the vehicles on a freeway. The traffic dynamics in a link m are formulated by first sectioning the link m into N_m segments of equal length L_m as in Fig. 2.1, and next the traffic dynamics in each segment are described in relation to the traffic conditions in the neighboring segments. Three aggregate variables are used to model the traffic behavior in each segment i of link m. These variables are the density $\rho_{m,i}(k)$ [veh/km/lane] of segment i of link m at time step k, the outflow $q_{m,i}(k)$ [veh/h] of segment i of link m during the time period $[kT, (k+1)T)$, and the space-mean speed $v_{m,i}(k)$ [km/h] of segment i of link m at time step k (see also Fig. 2.1).

Note that in order to make a distinction between the microscopic time step counter and the macroscopic time step counter, a time step counter k is introduced as macroscopic time step counter as opposed to the microscopic time counter k_{m} and a time step T is used as the

macroscopic time step size (typically $T = 10$ s) as opposed to the microscopic time step T_{m} (typically $T_{\mathrm{m}} =$1 s–2 s). Related to the CFL criterion encountered in [47], for computational stability reasons the relation between the length of the segment L_m and the simulation time step T must satisfy the condition

$$L_m > v_{\mathrm{free},m} T \tag{2.16}$$

where $v_{\mathrm{free},m}$ is the free-flow speed of the link m.

The outflow $q_{m,i}(k)$ of segment i of link m during the time period $[kT, (k+1)T)$ is the discrete-time domain version of the relation given in (2.2). This is described by

$$q_{m,i}(k) = \lambda_m \rho_{m,i}(k) v_{m,i}(k) \tag{2.17}$$

where λ_m is the number of lanes in link m.

The dynamics of the density $\rho_{m,i}(k)$ of segment i of link m is derived from the conservation of vehicles law in (2.1), which states that the number of vehicles in a segment is the sum of the number of vehicles in the segment and the difference between the number of inflowing and outflowing vehicles. For a segment i of link m without an on-ramp and off-ramp, the dynamics of the density $\rho_{m,i}(k)$ is described as

$$\rho_{m,i}(k+1) = \rho_{m,i}(k) + \frac{T}{L_m \lambda_m} \left[q_{m,i-1}(k) - q_{m,i}(k) \right] \tag{2.18}$$

where $q_{m,i-1}(k)$ is the inflow of segment i (or outflow of segment $i-1$) of link m during the time period $[kT, (k+1)T)$ and $q_{m,i}(k)$ is the outflow of segment i of link m during the time period $[kT, (k+1)T)$.

The discrete-time link equations described by (2.17) and (2.18) are based on physical principles that are exact. These two equations constitute a system of two independent equations and three unknown variables. Consequently, to get a complete description of traffic dynamics, a third independent model equation is needed [87]. This is the general case for macroscopic models as has been discussed in Section 2.1. In the METANET model the evolution of the space-mean speed in relation to the density is modeled heuristically following the continuous space-mean speed dynamics in (2.3). The update equation of the space-mean speed $v_{m,i}(k)$ of segment i of link m at time step k is given by the sum of the space-mean speed at time step k, the *relaxation* term that represents the desire of the drivers to reach a desired speed $V(\rho)$, a *convection* term describing the change in the space-mean speed of a segment caused by the vehicles inflowing from upstream segments, and an *anticipation* term that reflects the change in space-mean speed of a segment due to the difference in density level of a segment with the downstream segment. This is expressed as

$$\begin{aligned} v_{m,i}(k+1) =& v_{m,i}(k) + \frac{T}{\tau} \left[V\big(\rho_{m,i}(k)\big) - v_{m,i}(k) \right] \\ &+ \frac{T v_{m,i}(k) \left[v_{m,i-1}(k) - v_{m,i}(k) \right]}{L_m} \\ &- \frac{T \eta \left[\rho_{m,i+1}(k) - \rho_{m,i}(k) \right]}{\tau L_m \left(\rho_{m,i}(k) + \kappa \right)} \end{aligned} \tag{2.19}$$

where τ and η respectively denote a time constant and the anticipation constant, κ is model

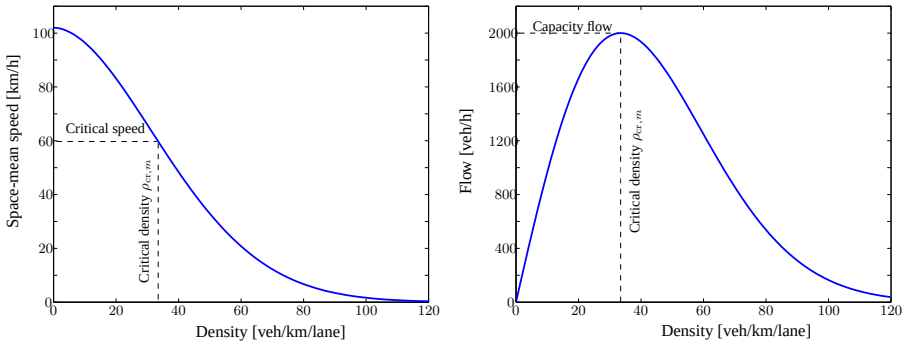

(a) Speed-density curve (b) Flow-density curve

Figure 2.2: Fundamental diagram of a freeway characterized by the relation (2.20) and (2.17) with $v_{\text{free},m} = 102$ km/hr, $\rho_{\text{cr},m} = 33.5$ veh/km/lane, and $b_m = 1.867$.

parameter, and $V\big(\rho_{m,i}(k)\big)$ is the desired speed drivers would like to achieve and it is given by

$$V\big([\rho_{m,i}(k)\big) = v_{\text{free},m} \exp\left[-\frac{1}{b_m}\left(\frac{\rho_{m,i}(k)}{\rho_{\text{cr},m}}\right)^{b_m}\right] \tag{2.20}$$

with $\rho_{\text{cr},m}$ being the critical density and b_m being the parameter[2] of the fundamental diagram. An illustration of the fundamental diagram is depicted in Fig. 2.2. The diagram is generated for a freeway characterized by the relation (2.20) and (2.17) with $v_{\text{free},m} = 102$ km/h, $\rho_{\text{cr},m} = 33.5$ veh/km/lane, and $b_m = 1.867$ [75].

Remark 2.1 The anticipation parameter in (2.19) captures the reaction of drivers to different traffic densities in the downstream segment. In the original METANET model a single parameter value is used regardless of the sign of the difference in density between the segments, i.e., the model does not distinguish between accelerating or decelerating behavior as a result of density difference between the actual segment and the downstream segment. However, as has been also discussed in the car-following models in Sections 2.2.2 and 2.2.3, drivers tend to decelerate faster than to accelerate [19, 58, 203]. Thus different parameter values are required when the downstream density of a segment is higher or lower than the density of the actual segment. In [75, 78] it has been suggested to use a time and segment-dependent η such that

$$\eta = \begin{cases} \eta_{\text{h}} & \text{if } \rho_{m,i+1}(k) \geq \rho_{m,i}(k) \\ \eta_{\text{l}} & \text{otherwise} \end{cases} \tag{2.21}$$

where η_{h} and η_{l} are anticipation model parameters for the two different cases. In this way the value of the anticipation constant η models the operational capacity drop. □

[2] In the original METANET model the parameter b_m is denoted by a_m. However, in order to avoid confusion with the acceleration (which will be indicated with $a_{(\cdot)}$ in this thesis) b_m is used instead.

Remark 2.2 Although it is indicated that the METANET model allows to model controlled speed limits by varying the parameters $\rho_{\mathrm{cr},m}$, $v_{\mathrm{free},m}$, and b_m in the METANET manual [185], in [75] it has been suggested to use different expressions. For controlled speed limits Hegyi [75] suggested that the desired speed in (2.20) be replaced by the following expression

$$V\big(\rho_{m,i}(k)\big) = \min\left\{ v_{\mathrm{free},m} \exp\left[-\frac{1}{b_m} \left(\frac{\rho_{m,i}(k)}{\rho_{\mathrm{cr},m}} \right)^{b_m} \right], (1+\varrho) u_{\mathrm{vsl},m,i}(k) \right\} \tag{2.22}$$

where $u_{\mathrm{vsl}}(k)$ is the speed limit imposed on segment i of link m at simulation time k, and ϱ is the drivers non-compliance factor[3]. If $0 < \varrho < 1$, it expresses that the drivers' target speed is higher than the displayed speed limit, and if $-1 < \varrho < 0$, then the drivers' target speed is less than the displayed speed limit. □

2.3.2 Node equations

Two or more links can merge or leave from a node of a traffic network as in Fig. 2.3. The coupling of the traffic variables of the merging links to or the leaving links from the node is modeled using node equations. Consider Fig. 2.3, where n_1 links (numbered $m_1, m_2, \ldots, m_{n_1}$), enter and n_2 links (numbered $\mu_1, \mu_2, \ldots, \mu_{n_2}$) leave node n. The total flow $Q_n(k)$ that enters node n is computed as the sum of outflow of all incoming links, i.e.,

$$Q_n(k) = \sum_{i=1}^{n_1} q_{m_i,N_{m_i}}(k). \tag{2.23}$$

The total flow $Q_n(k)$ entering node n is distributed among the leaving n_2 links according to

$$q_{\mu_i,0}(k) = \beta_{n,\mu_i}(k) Q_n(k) \tag{2.24}$$

where $i = 1, 2, \ldots, n_2$, $\beta_{n,\mu_i}(k)$ are the turning rates (i.e., the fraction of the total flow through node n that leaves via link μ_i), and $q_{\mu_i,0}(k)$ is the flow that leaves node n via link μ_i.

A node provides a (virtual) downstream density to incoming (or merging) links and a (virtual) upstream speed to leaving links, which are needed in (2.19). Thus, the virtual upstream speed $v_{\mu_i,0}(k)$ of leaving link μ_i is obtained as the weighted average of all the space-mean speeds of the incoming links, which is given by

$$v_{\mu_i,0}(k) = \frac{\sum_{i=1}^{n_1} v_{m_i,N_{m_i}}(k) q_{m_i,N_{m_i}}(k)}{\sum_{i=1}^{n_1} q_{m_i,N_{m_i}}(k)}. \tag{2.25}$$

Moreover, the virtual downstream density $\rho_{m_i,N_{m_i}+1}(k)$ of a link m_i entering node n is given by

$$\rho_{m_i,N_{m_i}+1}(k) = \frac{\sum_{i=1}^{n_2} \rho_{\mu_i,1}^2(k)}{\sum_{i=1}^{n_2} \rho_{\mu_i,1}(k)}. \tag{2.26}$$

[3] In [75, 78] the non-compliance factor is denoted by α. Here, we use ϱ since α is used to designate a vehicle in the microscopic modeling approaches discussed in Section 2.2.

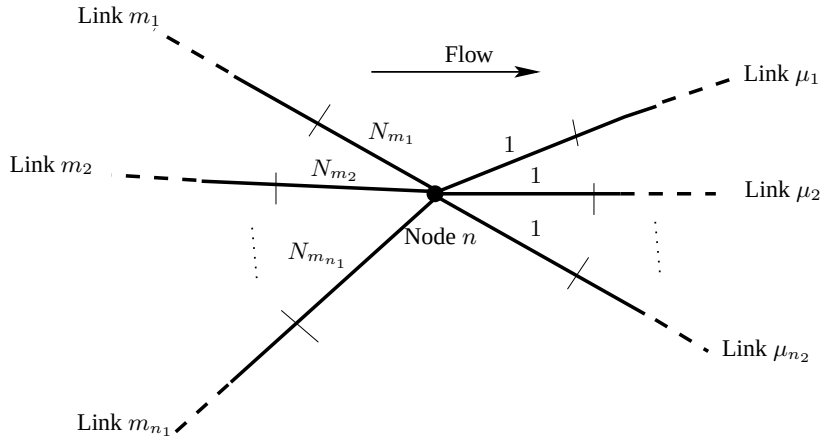

Figure 2.3: General interconnection of road links at a node n.

In case the number of lanes changes, a node n is placed in the METANET model. Let m and $m+1$ be the indices of respectively the ingoing link and the outgoing link of node n. Then, the space-mean speed of the last segment N_m of link m is either reduced or increased by adding the weaving phenomena term

$$-\frac{\phi T \Delta\lambda_m \rho_{m,N_m}(k) v^2_{m,N_m}(k)}{L_m \lambda_m \rho_{\mathrm{cr},m}} \tag{2.27}$$

to (2.19), where ϕ is a model parameter and $\Delta\lambda_m = \lambda_m - \lambda_{m+1}$ denotes the number of lanes dropped or increased.

2.3.3 Origins

For origins (such as on-ramps and mainstream entry points) a simple queue model is used. The dynamics of the queue length $w_o(k)$ at the origin o is modeled as

$$w_o(k+1) = w_o(k) + T(d_o(k) - q_o(k)) \tag{2.28}$$

where $d_o(k)$ and $q_o(k)$ denote respectively the demand and outflow of the origin o during the time period $[kT, (k+1)T)$.

The outflow $q_o(k)$ of the origin depends on the nature of the origin o. The equations describing on-ramp origins and mainstream origins are different, and these are presented below.

On-ramp origins

An on-ramp origin is a small road that provides an access to a traffic freeway network. The on-ramp origins can be both metered (in other words controlled) or unmetered. Ramp metering is one of the freeway traffic control measures used to regulate the traffic flow on the freeways by controlling the inflow of vehicles from on-ramp origins to prevent the

occurrence of traffic breakdown (or congestion) and to reduce the traffic jams [20, 75, 100, 103, 149, 219].

The outflow of metered on-ramp origin depends on the traffic conditions: the available traffic at the on-ramp that is expressed as the sum of the traffic demand and the queue length per unit time step, the maximal flow allowed by the metering rate expressed as a fraction of the origin capacity, and the maximum space available in the freeway to accommodate the incoming traffic expressed as the fraction of the capacity of the on-ramp origin. This is given by [101, 102]

$$q_o(k) = \min\left\{ d_o(k) + \frac{w_o(k)}{T},\ r_o(k)C_o,\ C_o\left(\frac{\rho_{\mathrm{jam},m} - \rho_{m,1}(k)}{\rho_{\mathrm{jam},m} - \rho_{\mathrm{cr},m}}\right)\right\}, \tag{2.29}$$

where C_o is the capacity [veh/h] of the on-ramp o under free-flow conditions and $\rho_{\mathrm{jam},m}$ is the jam density (or the maximum density of a segment under jammed conditions) of the link m connected to origin o, and $r_o(k) \in [0, 1]$ is the ramp metering rate at time step k.

For an unmetered on-ramp (where $r_o(k) \equiv 1$) the outflow $q_o(k)$ in (2.29) is recast as

$$q_o(k) = \min\left\{ d_o(k) + \frac{w_o(k)}{T},\ C_o,\ C_o\left(\frac{\rho_{\mathrm{jam},m} - \rho_{m,1}(k)}{\rho_{\mathrm{jam},m} - \rho_{\mathrm{cr},m}}\right)\right\}. \tag{2.30}$$

If m is the link out of a node to which an on-ramp o is connected, then for the first segment of link m the term

$$-\frac{\delta T q_o(k) v_{m,1}(k)}{L_m \lambda_m (\rho_{m,1}(k) + \kappa)} \tag{2.31}$$

is added to the speed update equation (2.19) in order to account for the speed drop caused by the merging phenomena, where δ is model parameter.

Main-stream origins

The main-stream origin link o is suggested to be modeled different from the on-ramp origins in [75]. It is argued that the inflow of a segment can be limited by an active speed limit or by the actual speed of the segment. Then, [75] assumes that the maximal inflow equals the flow that follows from the speed-flow relationship that can be derived from (2.17) and (2.20) with the speed equal to the speed limit or the actual speed on the first segment, whichever is smaller. So, the limiting speed of the first segment of link μ is given by

$$v_{\mathrm{lim},\mu,1}(k) = \min\left\{ u_{\mathrm{vsl},\mu,1}(k),\ v_{\mu,1}(k)\right\}. \tag{2.32}$$

Moreover, the outflow of the main-stream origin o of link μ that is required for queue model given in (2.28) cannot exceed

$$q_o(k) = \min\left\{ d_o(k) + \frac{w_o(k)}{T},\ q_{\max,\mu,1}(k)\right\} \tag{2.33}$$

where

$$q_{\max,\mu,1}(k) = \begin{cases} \lambda_\mu v_{\lim,\mu,1}(k)\rho_{\mathrm{cr},\mu}\left[-b_\mu \ln\left(\frac{v_{\lim,\mu,1}(k)}{v_{\mathrm{free},\mu}}\right)\right]^{\frac{1}{b_\mu}} & \text{if } v_{\lim,\mu,1}(k) < V(\rho_{\mathrm{cr},\mu}) \\ \lambda_\mu V(\rho_{\mathrm{cr},\mu})\rho_{\mathrm{cr},\mu} & \text{otherwise.} \end{cases}$$

2.3.4 Boundary conditions

Since the dynamic equations that describe the evolution of the traffic states in each segment are interdependent, i.e., the traffic situation downstream and upstream of a segment influences the traffic in the actual segment, then at the entry and exit points of the traffic network boundary conditions have to be defined. In particular, in the METANET model the states of a segment depend on the upstream speed, the upstream flow, and the downstream density. Hence, we need to describe the upstream speed and upstream flow for the entries of the network and downstream densities for the exit networks.

Let the virtual speed of a main-stream origin o entering node n be denoted by $v_o(k)$. The virtual speed can be user-defined, but if it is not specified it is set to be equal to the speed of the first segment of the link leaving node n, i.e.,

$$v_o(k) = v_{\mu,0}(k) = v_{\mu,1}(k)$$

The boundary conditions for the upstream flow are described by the flow equations discussed in 2.3.3.

Remark 2.3 The only downstream boundary condition required is the virtual density. In the standard METANET model, it is assumed that the destination is congestion-free, but it is also possible to consider user-defined density scenario [75]. When the destination is assumed to be congestion free, the virtual downstream density $\rho_{m_i,N_{m_i}+1}(k)$ of link m is always considered to be the smallest of the critical density $\rho_{\mathrm{cr},m_i}(k)$ of link m_i and the density of the last segment N_{m_i} of link m_i. This can be rewritten as [75]

$$\rho_{m_i,N_{m_i}+1}(k) = \min\{\rho_{m_i,N_{m_i}}(k),\ \rho_{\mathrm{cr},m_i}\}. \tag{2.34}$$

But, if the destination demand scenario $\rho_d(k)$ is defined, the virtual downstream density in (2.34) is recast as

$$\rho_{m_i,N_{m_i}+1}(k) = \rho_d(k).$$

□

2.4 Summary

As the phrase “model-based traffic control” indicates, the control approach presented in Part II of this thesis requires models of the traffic system. So, in this chapter an overview of the traffic flow models in general and the specific traffic models to be used have been discussed. The chapter has provided the general overview of the traffic models by exploring the general applications of these models and the way they can be classified. Based on the level of details, the classification of traffic models as microscopic, macroscopic, and

mesoscopic has been discussed with a special emphasis on microscopic and macroscopic models. The general modeling concepts underling the microscopic and macroscopic models have been in particular discussed.

Among the microscopic models, a brief account has been given for the car-following models, because the car-following models are the building blocks of most traffic flow models. Two of the car-following models, the GHR model and the IDM model have been discussed in detail. Since the GHR model is unable to model the traffic flow under free-flow conditions, it has been suggested to use a separate expression to model the free-flow traffic conditions if one opts to use the GHR model for the car-following situations under high to medium traffic densities. Therefore, the GHR model and the additional free-flow expression can be used to model free-flow and congested traffic conditions for both accelerating and decelerating cases of individual vehicles. The IDM model, however, is a full-fledged model that can capture the traffic scenarios the GHR model, without the additional free-flow expression, cannot. The IDM model does not require different parameters for different traffic conditions as the GHR model does.

This chapter has also presented the METANET model and some of its extensions. It has been pointed out that, unlike the microscopic models, the computation time of the macroscopic METANET model does not depend on the number of vehicles in a traffic network. Therefore, it can be used for the simulation of large networks. Moreover, in addition to the ramp metering control, it has been also shown how the extended METANET model is able to include variable speed limits explicitly.

Despite the fact that specific models (GHR, IDM, and METANET) have been chosen for the model-based strategies in the subsequent chapters, the strategies and approaches to be presented next in this thesis are general and can be used with more complex and fast models that are suitable for on-line control applications.

Chapter 3

Traffic Emissions and Fuel Consumption Modeling

Traffic control approaches based on on-line optimization require fast and accurate integrated traffic flow, emissions, and fuel consumption models. On the one hand, one may use macroscopic traffic flow models to reduce the computation time. But in principle such models dictate the use of macroscopic emissions and fuel consumption models that provide coarse estimates. On the other hand, relatively accurate estimates of emissions and fuel consumption can be obtained using microscopic emissions and fuel consumption models. However, such models are used with microscopic traffic flow models that require intensive computation times.

Thus, one may want to integrate macroscopic traffic flow models with microscopic emissions and fuel consumption models, which can result in fast computation speeds with fairly accurate estimates of the emissions and fuel consumption. In general, however, macroscopic traffic flow models and microscopic emissions and fuel consumption models cannot be integrated with each other because the inputs required by microscopic emissions and fuel consumption models describe the dynamics of *individual* vehicles, while macroscopic traffic flow models characterize the *average* traffic flow. So how can these different models be integrated? If they can be integrated, can the error be quantified?

This chapter provides answers to these and other questions. In answering the questions, this chapter begins with an overview of emissions and fuel consumption models in Section 3.1. It briefly discusses the applications and classifications of the models. Next, in Sections 3.2 and 3.3 the established microscopic VT-micro [2] and macroscopic COPERT [139] models are respectively discussed. Their advantages and disadvantages are presented. Section 3.4 first presents a general framework for integrating microscopic emissions and fuel consumption models with macroscopic traffic flow models. Next, the section illustrates the integration strategy using the VT-micro and METANET models, resulting in the VT-macro emissions and fuel consumption model. The error that can be introduced due to the use of macroscopic traffic flow variables with microscopic emissions and fuel consumption models is analyzed and quantified both mathematically and empirically. The chapter ends with conclusions in Section 3.5.

Parts of this chapter are published in [114, 212, 218].

3.1 Overview of emissions and fuel consumption models

Traffic emissions and fuel consumption models are models of any form (graphs, tables, mathematical expressions, computer algorithms, etc.), that calculate (or provide information about) emissions and fuel consumption rates for different traffic conditions. In other words, these models provide the emissions released or fuel consumed by a vehicle or a group of vehicles based on the operating conditions and status of the vehicle(s). The operating conditions refer to variables such as speed, acceleration, engine speed, engine power demand, air-to-fuel ratio, and so on. The status of a vehicle refers to its physical conditions related to its age, technology, and maintenance level.

In a broader sense, emissions and fuel consumption models can be either technology-based engineering emissions and fuel consumption models or traffic emissions and fuel consumption models. The main difference between these modeling approaches is their level of detail and their intended applications. Technology-based engineering models are models for a specific engine type and size. The main inputs for such models are the speed, acceleration, engine load, and the specification of the vehicle (or engine). Therefore, technology-based engineering models are primarily meant to be used by car-manufacturing companies for the assessment of new technological developments and by government agencies for regulation purposes [36]. Since these models are very specific and very detailed, they can neither generalize the emissions and fuel consumption rate of other vehicles in the fleet nor be used for on-line estimation and prediction, and thus they are not of interest for this thesis.

Traffic emissions and fuel consumption models are developed for diverse collections of vehicles grouped in homogeneous categories. These models are simpler and have relatively less details than the technology-based engineering models. Traffic emissions and fuel consumption models mainly consider the inter-relationship of the different traffic flow variables (speed, acceleration, flow, density) with the emissions and fuel consumption of the vehicles in the fleet. Since these models generally try to relate the traffic flow variable with the fleet emissions and fuel consumption, these models are more suited for the study of the effects of traffic flow control and management strategies. Moreover, these models are more suited for on-line estimation and predictions than the technology-based engineering models. Therefore, traffic emissions and fuel consumption models are the center of attention of this chapter and thesis. In the sequel, the possible applications and classifications of traffic emissions and fuel consumption models are elaborated.

3.1.1 Application of traffic emissions and fuel consumption models

Road transport has a significant impact upon the environment locally and globally. In developed countries, road transport is one of the major sources of CO_2 emissions, which contributes to climate change which in turn has perilous domestic and global consequences [107, 143, 162]. This means that the ability to estimate and predict the air pollution will be essential for local transport plans focusing on the reduction of traffic emissions. Real-time environmental data and accurately predicted emissions and fuel consumption rates will be needed to be integrated with existing traffic control and traveler information systems. Real-time environmental data can be provided with a grid of sensors. However, models are required to predict the emission or fuel consumption levels of a transport network.

Traffic emissions and fuel consumption data can be used to determine the most important parameters that influence the emissions and fuel consumption of road vehicles [91]. These

important parameters are the building blocks of emissions and fuel consumption models. With these models, the impact of Intelligent Transportation Systems (ITS) alternatives on the emissions and fuel consumption can be assessed [1, 44, 45, 131, 163]. Generally, air quality problems as well as the effectiveness of potential solutions are assessed on the basis of emissions and fuel consumption models rather than on the basis of measurements, because experimentation of ITS solutions in real-time is expensive and cannot guarantee repeatability.

Emissions and fuel consumption models can also be used for the evaluation and assessment of construction of new roads and other transport networks. For example, a newly constructed road network can reduce the traffic jams of a traffic network, but it can have severe consequences for the neighborhoods and the environment. An assessment of the impact level could help in the redesign, provision of solutions, or the decision making process of such projects. Emissions and fuel consumption models can also be used in the design and evaluation of local emission control strategies [46]. For example, to evaluate traffic measures that influence driving behavior (like signal coordination or speed limits) accurate models are needed that can produce reliable predictions about the magnitude and direction of relatively small changes in emission levels [44, 45, 131, 177]. With the aid of traffic flow models and traffic emissions and fuel consumption models, it becomes possible to consider both congestion and emissions in the problem of policies development, assessment, and optimization [177].

Often during the development, assessment, and optimization process of environmental policies the decision process are characterized by a high degree of complexity, uncertainty, and subjectivity [46]. Therefore, models can be used in the context of decision support systems to provide the analysts and the decision makers with quantitative estimates, trends, and insights on the policies simulated.

3.1.2 Classification of traffic emissions and fuel consumption models

There are several types of traffic emissions and fuel consumption models. Based on their applications, level of detail, modeling strategies, and the like, traffic emissions and fuel consumption models can be grouped into different categories. In general, traffic emissions and fuel consumption models can be categorized as either static or dynamic models. Static emission and fuel consumption models calculate the emissions and fuel consumption of vehicles based on static traffic behavior (e.g., average speed), while dynamic models consider the dynamic behavior of the traffic flow (e.g., instantaneous speeds and accelerations). Static models are generally fed with output of macroscopic traffic models or with forecasts of total vehicle kilometer traveled. On the other hand, dynamic models allow both instantaneous and modal analysis based on instantaneous traffic kinematic variables, such as instantaneous speed and instantaneous acceleration, or on more aggregated modal variables, such as time spent in acceleration mode, in cruise mode, and in idle mode.

Based on the level of detail, emissions and fuel consumption models can be classified into three groups viz. microscopic, macroscopic, and mesoscopic emissions and fuel consumption models. Microscopic models use instantaneous speed and acceleration data to estimate the emissions and fuel consumption of an individual vehicle. Macroscopic models use aggregate network or link-based data to estimate network-wide or link-based emissions and fuel consumption. Mesoscopic models use scales that lie between the macroscopic scale and microscopic scale. The ensuing sections provide an overview of these model groups.

Microscopic models

In order to predict traffic emissions and fuel consumption more accurately and with high spatial and temporal detail, models that include the variation of vehicle dynamics over time and space are necessary. Such models are called microscopic emissions and fuel consumption models. Microscopic emissions and fuel consumption models are derived from the relationship between the second-by-second emissions and fuel consumption rates and vehicle characteristics and road conditions. The vehicle characteristics include the second-by-second speed, acceleration, and in some cases the vehicle jerk, power, and so on. These models take the instantaneous vehicle kinematic variables (speed, acceleration, or aggregate modal variables such as time spent in acceleration mode, in cruise mode, idle mode, and so on) into account [36, 182]. In general, microscopic emissions and fuel consumption models can be described as

$$J_{\bar{y}}(k_{\mathrm{m}}) = f_{\bar{y}}(v(k_{\mathrm{m}}), a(k_{\mathrm{m}}), \cdots) \tag{3.1}$$

where the subscript $\bar{y}$ denotes the emission or fuel consumption $\bar{y} \in \bar{\mathcal{Y}} = \{\mathrm{CO}, \mathrm{CO}_2, \mathrm{HC}, \mathrm{NO}_x, \text{fuel}\}$ and $f_{\bar{y}}(\cdot)$ denotes the function that relates the microscopic-instantaneous speed $v(k_{\mathrm{m}})$, the microscopic-instantaneous acceleration $a(k_{\mathrm{m}})$, etc. to the emissions or fuel consumption rate $J_{\bar{y}}(k_{\mathrm{m}})$ at time step k_{m}.

Due to the disaggregate characteristics of the emissions and fuel consumption data, these models are usually used to evaluate individual transportation projects and individual vehicles. These models are also used in microscopic traffic simulation models; however, they are costly and time consuming [206]. The POLY [162], CMEM [9], and VT-Micro [2, 3] models are some examples of microscopic emissions and fuel consumption models.

Microscopic emissions and fuel consumption models can be *emissions and fuel consumption maps*, *regression-based*, or *load-based* models.

Emissions and fuel consumption maps are a two-dimensional array of emissions and fuel consumption quantities for different operational conditions of the vehicles. These models, also called velocity-acceleration look-up tables, have the form of a matrix, where one dimension represents speed ranges, and the other acceleration or specific power ranges. For each emission type (CO, CO_2, HC, and NO_x) and fuel consumption and for each vehicle category, the instantaneous emissions and fuel consumption measurements are assigned to one cell of the emissions and fuel consumption matrix, according to vehicle speed and acceleration measured at that time instant.

Although these models are easy to generate and to use, they can be sparse and sensitive to the driving cycle used to generate them; in addition, they are not flexible enough to account factors such as road grade, accessory use, or history effects [182].

Regression-based models are usually linear regression functions of instantaneous speed and acceleration or modal variables [2, 163]. These models can overcome the sparseness and discretization problems of the emission map models. However, these models lack a clear physical interpretation, and can also over-fit the calibration data when using a large number of explanatory variables.

Load-based models represent the physical and chemical phenomena that generate emissions. The primary variable of these models is the fuel consumption rate. The fuel consumption rate is mainly dependent on the engine speed, the engine power, and air-to-fuel ratio [36]. In principle, load-based models are adequate to describe the emissions and fuel consumption of any vehicle with similar technology and any vehicle operating conditions by adjusting their parameters. However, these models require detailed specification of vehicles' engine (such as the engine speed, the engine power, and air-to-fuel ratio) and they are relatively complicated models. Thus, since such data is not available from the traffic flow models, the load-based models are not suitable for model-based traffic control approaches.

Macroscopic models

Macroscopic emissions and fuel consumption models estimate or predict the emissions or fuel consumption of a group (or class) of vehicles over a period of time or over a road segment. These models use the average aggregate network variables (such as average speed, average density, and road grade) to estimate the network-wide emissions and fuel consumption rates of the traffic flow. Macroscopic emissions models are important tools in an area-wide emission assessment, which are typically used to calculate and develop national or regional emission inventory. In the emission regulatory process, macroscopic emissions models are required for estimating the quantity of pollutants discharged from vehicles.

Macroscopic emissions and fuel consumption models can in general be also studied by grouping them into three classes as: *average-speed-based models*, *traffic-situation-based models*, and *traffic-variance-based models*.

Average-speed-based emissions and fuel consumption models are the simplest emissions and fuel consumption models. These models use the trip-based average speed of the traffic fleet as an input to estimate or predict the average emissions or fuel consumptions of vehicles in a traffic network [28, 63, 139]. Since the average-speed-based models do not capture the emissions and fuel consumption due to the variation of the speed of the traffic [1, 28], the average-speed-based models are more coarse than microscopic emissions and fuel consumption models and thus provide less accurate estimates or predictions of the emissions and fuel consumption than the microscopic models. But they result in fast computation times. Although, in principle, the average-speed-based emissions and fuel consumption models use the trip-based average speed, in practice it is also common to use local speed measurements (in other words the average speed over short time periods) at discrete locations as input to the models [28]. In this way, the variation of the speeds can partly be considered and thereby the estimation accuracy of the models can increase.

For example, the average-speed-based MOBILE [138] emissions model and COPERT [139] emissions and fuel consumption model estimate the average emissions and fuel consumption based on the average speed of vehicles. The MOBILE model is not sensitive to a vehicle's modal events such as idling, cruising, acceleration, and deceleration [205]. The MOBILE model requires the average speed as the sole descriptor of a vehicle's modal events and driving conditions. Moreover, MOBILE requires inputs of detailed vehicle information such as the vehicle technology, the vehicle age, vehicle mileage, the ambient temperature, fuel parameters, and the vehicle operating mode are also considered in MOBILE [138]. For a better discussion of the COPERT emissions and fuel consumption model the reader is referred to Section 3.3.

The macroscopic fuel consumption models *Elemental* [40, 63] and *Watson* [196] use the space-mean speed as input to estimate or predict fuel consumption of a traffic flow. The Elemental model is an urban fuel consumption model. In the Elemental model, the fuel consumption is linearly related to the average trip time for a unit distance. Hence, the model is easy to use in macroscopic traffic models. However, it does not incorporate the effect of speed variations in the trip. Hence, this may introduce more prediction errors. The Watson fuel consumption model, however, also incorporates the changes in the positive kinetic energy during acceleration as a predictor variable. This partially introduces the effect of speed variations in a trip. But the effects of speed changes during the deceleration phase are not included. Moreover, at higher average speeds the effect of aerodynamic drag on fuel consumption becomes significant (this occurs at average speeds over 55 km/h [63]) and in this case both models do not give good estimates of the fuel consumption. Thus, these models can only be used for average speeds less than 50 km/h [206]. This implies that such models are not suitable to model fuel consumption of freeway traffic.

Traffic-situation-based models use emissions and fuel consumption factors grouped by traffic situations described by the average speed, vehicle composition, or volume-to-capacity ratio to provide the estimate of the emissions or fuel consumption of the traffic flow. In these models, different emissions and fuel consumption factors are designated for the different traffic conditions. Then, accordingly, the total emissions and fuel consumption of the traffic flow are computed by integrating the emissions and fuel consumption contributed by each traffic situation and the corresponding traffic intensity. The models VERSIT+$^{\mathrm{macro}}$ [178], HBEFA [74], and ARTEMIS [92] are examples of traffic-situation-based models. The VERSIT+$^{\mathrm{macro}}$ grids the average speed, and volume-to-capacity ratio of traffic flow and assigns them emissions and fuel consumption factors to each cell. The HBEFA emissions model describes road traffic emissions based on several classifications such as vehicle category, fuel type, and driving conditions (such as freeway driving at different mean velocities, urban driving, stop-and-go traffic etc. for different road gradients). The ARTEMIS emissions model has different sub-models for urban, rural, and freeways driving conditions and for cold-start and hot-start conditions.

Traffic-variance-based models are other macroscopic models that take the variation of the average traffic variables into account. In such models, the emissions and fuel consumption are modeled based on the average traffic variables (such as the average speed, flow, and density) and an additional correction factor to account for the effect of the variation of the variables from their average. In doing so, first the models generate driving patterns using the traffic variables (average speed, flow, and density) and infrastructure variables (e.g. link length, number of lanes, and type of intersection) [132]. Next, the correction factors that represent the variation of the speed, flow, or density along the link are introduced. The models in [118, 132] are examples of such models.

Mesoscopic models

One common variable of macroscopic emissions and fuel consumption models is the average speed. This leads to one common weakness of macroscopic models, because of the fact that the average speed of a trip may be constructed in a number of different ways, with differing number of transient vehicle operation. Clearly, all the types of operations associated

with a given average speed cannot be accounted for by the use of a single emission factor [143]. This is normally not a problem at higher average speeds, as these are associated with relatively little variation in operation, but at the low average speeds associated with congestion the range of possible operational conditions associated with a given average speed tends to be much greater [28]. The marked variability of vehicle operation at low average speeds is partly responsible for the poor reliability of the corresponding emission factors [28]. On the other hand, microscopic models are very detailed and thus are costly and consume much computation time. This implies that they are not feasible for on-line estimation or prediction applications.

Mesoscopic emissions and fuel consumption models have some characteristics of microscopic models and some characteristics of macroscopic models. The inputs to mesoscopic models are more aggregate than microscopic models and more disaggregate than macroscopic models. Generally, mesoscopic models use few explanatory variables to estimate vehicle emissions and fuel consumption [206]. For instance, the VT-meso model [206] estimates the average emissions and fuel consumption rates of light-duty vehicle on a link-by-link basis using three independent variables, viz. average travel speed, average number of stops per unit distance, and average stop duration. In general, mesoscopic models (such as the model of Akçelik [5, 170], MEASURE [11, 12], and VT-meso [206]) estimate the emissions during cruising, idling, and acceleration-deceleration driving behavior separately.

However, mesoscopic models are relatively complicated models as compared to their counterpart microscopic and macroscopic models. For example, the mesoscopic VT-meso model (see [206]) requires the average travel speed, average number of stops per unit distance, and average stop duration to compute the emissions and fuel consumption of vehicles within a link using relatively complicated equations, whereas its microscopic version the VT-micro model (see Section 3.2) requires the instantaneous speed and acceleration of vehicles to compute the emissions and fuel consumptions with simpler expressions. Thus, as the input variables for the mesoscopic models are not easily obtained from traffic flow models, integration of the mesoscopic models with the traffic models is not simple. In view of this, a new and simple macroscopic emissions and fuel consumption model that takes the dynamics of the traffic flow into account is developed in Section 3.4. This model provides accurate estimates relative to the macroscopic models and has fast computation times. But first the microscopic VT-micro traffic emissions and fuel consumption model is discussed in the next section, because this model is the basis for the development of the macroscopic model discussed in Section 3.4.

3.2 The VT-micro model

VT-micro [2] is a microscopic emissions and fuel consumption model that yields the instantaneous emissions and fuel consumption rate of an individual vehicle α using the second-by-second speed and acceleration of the vehicle. Since the speed and acceleration variation of vehicles have significant impacts on the emissions and fuel consumption, the VT-micro model captures the effects of these two important factors. Moreover, this model is very simple and can be easily integrated with microscopic traffic flow models. The VT-micro model has been evaluated and used in different traffic applications [1–3, 163, 206].

The VT-micro model describes the emissions and fuel consumption $\bar{y} \in \bar{\mathcal{Y}}/\{CO_2\}$ of

an individual vehicle α at time step k_m as

$$J_{\alpha,\bar{y}}(k_\mathrm{m}) = \exp\left(\tilde{v}_\alpha^\top(k_\mathrm{m}) P_{\bar{y}} \tilde{a}_\alpha(k_\mathrm{m})\right) \tag{3.2}$$

where $J_{\alpha,\bar{y}}(k_\mathrm{m})$ is the estimate or prediction of the variable $\bar{y}$ per unit time at every microscopic simulation time step k_m, the operator $\tilde{\cdot}$ defines the vectors of the speed v_α and the acceleration a_α as

$$\begin{aligned} \tilde{v}_\alpha(k_\mathrm{m}) &= [1\ v_\alpha(k_\mathrm{m})\ v_\alpha^2(k_\mathrm{m})\ v_\alpha^3(k_\mathrm{m})]^\top \\ \tilde{a}_\alpha(k_\mathrm{m}) &= [1\ a_\alpha(k_\mathrm{m})\ a_\alpha^2(k_\mathrm{m})\ a_\alpha^3(k_\mathrm{m})]^\top \end{aligned} \tag{3.3}$$

for time step k_m, and $P_{\bar{y}}$ denotes the model parameter matrix for the variable $\bar{y} \in \bar{\mathcal{Y}}/\{\mathrm{CO}_2\}$. The values of the entries of $P_{\bar{y}}$ are given in Appendix A.

The operating region of the VT-micro emissions and fuel consumption model is described in [163] to be from 0 km/h to 120 km/h for the speed[1] and from 0 m/s^2 to 2.75 m/s^2 for the acceleration, where the maximum value of the acceleration $a_{\max,\alpha}(k_\mathrm{m})$ is given by

$$a_{\max,\alpha}(k_\mathrm{m}) = \begin{cases} 2.75 & \text{if } \ v_\alpha(k_\mathrm{m}) \leq 35\,\text{km/h} \\ 2.75 - 2.75\frac{v_\alpha(k_\mathrm{m})-35}{85} & \text{if } \ 35\,\text{km/h} < v_\alpha(k_\mathrm{m}) \leq 120\,\text{km/h}. \end{cases}$$

Moreover, the VT-micro emissions and fuel consumption model does not yield estimates of the CO_2 emission rate. However, in [141] it is shown that there is an almost affine relationship between fuel consumption and CO_2 emission. Then the CO_2 emission can be computed using the relation

$$J_{\alpha,\mathrm{CO}_2}(k_\mathrm{m}) = \delta_1 v_\alpha(k_\mathrm{m}) + \delta_2 J_{\alpha,\mathrm{fuel}}(k_\mathrm{m}) \tag{3.4}$$

where $J_{\alpha,\mathrm{CO}_2}(k_\mathrm{m})$ denotes the CO_2 [kg/s] emission rate of vehicle α for time step k_m, $J_{\alpha,\mathrm{fuel}}(k_\mathrm{m})$ denotes the fuel consumption rate in l/s for time step k_m, with the model parameters $(\delta_1, \delta_2) = (1.17 \cdot 10^{-6}\,\mathrm{kg/m}, 2.65\,\mathrm{kg/l})$ for a diesel car and $(\delta_1, \delta_2) = (3.5 \cdot 10^{-8}\,\mathrm{kg/m}, 2.39\,\mathrm{kg/l})$ for a gasoline car.

3.3 The COPERT model

One of the most commonly used average-speed-based macroscopic emission and fuel consumption models is the COPERT [139] model. In this model, the emissions (CO, CO_2, HC, and NO_x) or fuel consumption of a group (or class) of vehicles are described as a function of their trip-based average speed in the traffic network. The model provides the estimation or prediction of the emissions or fuel consumption $\bar{y} \in \bar{\mathcal{Y}}$ based on simple second-order polynomial functions of the trip-based average-speed v_av. This is given by

$$J_{\bar{y}} = c_0 v_\mathrm{av}^2 + c_1 v_\mathrm{av} + c_2 \tag{3.5}$$

where c_0, c_1, and c_2 are model parameters.

For instance, the COPERT emissions model for light-duty EURO I vehicles with 1.4 l

[1] The unit km/h is used as the unit for vehicles (traffic) speed because it is most commonly used in The Netherlands.

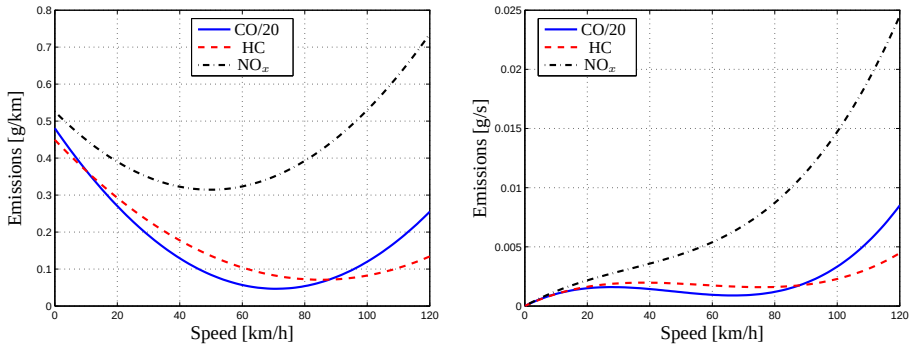

(a) COPERT (b) Transformed COPERT

Figure 3.1: COPERT model for a 1.4 l to 2.0 l light-duty EURO I passenger car.

to 2.0 l is given by [139]

$$J_{\mathrm{CO}} = (0.001785v_{\mathrm{av}}^2 - 0.245v_{\mathrm{av}} + 9.617)\,[\mathrm{g/km}]$$
$$J_{\mathrm{HC}} = (0.0000521v_{\mathrm{av}}^2 - 0.00888v_{\mathrm{av}} + 0.4494)\,[\mathrm{g/km}]$$
$$J_{\mathrm{NO}_x} = (0.0000854v_{\mathrm{av}}^2 - 0.0085v_{\mathrm{av}} + 0.526)\,[\mathrm{g/km}]$$

where the trip-based average speed v_{av} is in km/h.

Although in principle the input of COPERT emissions and fuel consumption model is the trip-based average speed, it is also used with the speed measurements taken at discrete locations [28]. For such approaches, the discretization can be made fine enough by considering the distance the vehicles travelled in a single sampling period. This is equivalent to using the model on second-by-second basis. Thus, in order to use the model in such approaches, the emissions and fuel consumption rate is needed to be converted from emissions per unit distance to emissions per unit time, because the distance traveled every simulation time step can be different. So the model should be transformed to emissions and fuel consumption rates in terms of grams per unit time, which can be done by multiplying the expression in (3.5) by the average speed v_{av}. This transformation provides a way to use the average-speed models to calculate the emissions released or fuel consumed at every macroscopic simulation time step k.

Now, since the input for the transformed model is the speed at each sampling time, the model considers the variation of the speed in computing the emissions and fuel consumption of the traffic flow. Fig. 3.1(a) and Fig. 3.1(b) show the trip average-speed-based and 'instantaneous' average-speed-based COPERT model for a light-duty EURO I vehicle. Fig. 3.1(a) depicts the COPERT model used as a trip-based average-speed-based model, where the emissions rate are provided in g/km, whereas Fig. 3.1(b) depicts the emissions curves of the COPERT model used with an instantaneous average-speeds, resulting emissions rate in g/s.

3.4 The VT-macro model

Since the inputs for microscopic emissions and fuel consumption models are the operating conditions of individual vehicles, the computation time required is proportional to the number of vehicles. But the inputs for macroscopic emissions and fuel consumption models are the average operating conditions of a group of vehicles. Hence, the computation time of the macroscopic models is reduced as compared to the microscopic models. On the other hand, relatively accurate estimates of emissions and fuel consumption can in general only be obtained using microscopic emissions and fuel consumption models.

Macroscopic emissions and fuel consumption models are in principle used with macroscopic traffic flow models, and the microscopic emissions and fuel consumption models are used with microscopic traffic flow models. For example in [163], an integrated microscopic traffic flow model and emissions model has been used for quantifying the environmental impacts of ITS alternatives. Moreover, a study in [88] shows the integration of a microscopic emissions and fuel consumption model with a microscopic traffic flow model using a distributed framework to tackle the computation time. In both [88] and [163] the integration is based on microscopic traffic flow models and microscopic emissions and fuel consumption models. In general, the output of the macroscopic traffic flow models can be easily fed to macroscopic emissions and fuel consumption models and the output of microscopic traffic flow models can be easily fed to microscopic emissions and fuel consumption models. This means that the choice made on the traffic flow models also affects the choice of the emissions and fuel consumption models. Hence, the accuracy of the estimates of the emissions released and fuel consumed cannot be enhanced if one uses macroscopic models unless the macroscopic emissions and fuel consumption models themselves are accurate. But as studies show the available macroscopic emissions and fuel consumption models do not provide accurate estimations relative to microscopic emissions and fuel consumption models [1, 28].

So, to get a balanced trade-off between computational complexity and accuracy, one may want to combine macroscopic traffic flow modes with microscopic emissions and fuel consumption models. However, this is not straightforward. The macroscopic outputs of the macroscopic traffic flow models should be transformed into microscopic variables. Moreover, the error that can be introduced due to such approximations is unknown. Therefore, this section presents an approach to integrate these two types of models so that the macroscopic variables can be used to produce relatively accurate estimates of the emissions and the fuel consumption of the traffic flow.

3.4.1 Integration of models

In the sequel, a general approach to integrate macroscopic traffic flow models with microscopic emissions and fuel consumption models is presented. This approach is generic and it can be adopted to most combinations of a macroscopic traffic flow model and a microscopic emissions and fuel consumption model such as POLY [162], CMEM [18], and the microscopic models in [91, 143].

In order to integrate macroscopic traffic flow models with microscopic emissions and fuel consumption models, the average acceleration, average speed, and the number of vehicles subject to these variables at each simulation time step have to be generated from the macroscopic traffic variables. This idea is illustrated in Fig. 3.2. The macroscopic traf-

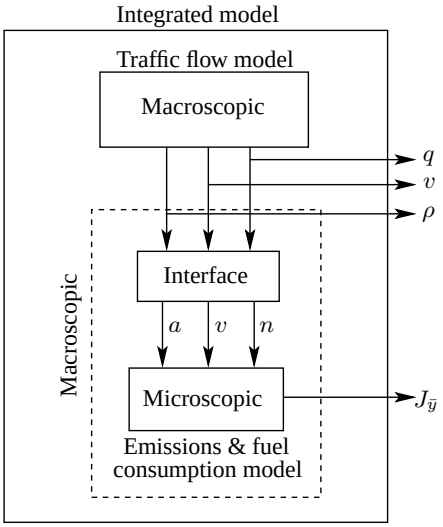

Figure 3.2: Model integration block diagram. The output variables of the macroscopic traffic model are the average flow q, the average space-mean speed v, and the average density ρ. These variables are fed to the interface block. The interface block generates the acceleration a, the speed v, and the corresponding number of vehicles n, which are inputs to the microscopic emissions and fuel consumption model. The microscopic emissions and fuel consumption model yields the emissions and the fuel consumption $J_{\bar{y}}$ of the traffic flow. Then, both the interface block and microscopic emissions and fuel consumption model block form the macroscopic emissions and fuel consumption model.

fic variables (the average density, average space-mean speed, and average flow) are fed to the interface block. The interface block transforms these variables into variables that describe the average behavior of individual vehicles, i.e., it produces average speed, average acceleration, and the number of vehicles that are subject to the average speed and average acceleration. Note that the macroscopic speed does not contain enough information to fully reconstruct the individual vehicle trajectories that would be needed to exactly calculate the microscopic emissions and fuel consumptions. The error that can be introduced by considering the average speed over a group of vehicles will be analyzed in Section 3.4.5.

Now the general integration approach is illustrated using the METANET traffic flow model discussed in Section 2.3 and the VT-micro emissions and fuel consumption model presented in Section 3.2, which will result in a new dynamic macroscopic emissions and fuel consumption model VT-macro, specifically derived for the METANET traffic flow model.

Since the METANET model is discrete in both space and time there are two acceleration components involved in the model. The first is the "*segmental*" acceleration of the vehicles moving within a given segment. The second component is the "*cross-segmental*" acceleration of the vehicles going from one segment to another within one simulation time step (see Fig. 3.3). The segmental and cross-segmental accelerations describe the average dynamics of a group of vehicles. Therefore, the number of vehicles that are subject to the corresponding accelerations are also determined. Hence, triples of the form (a, v, n),

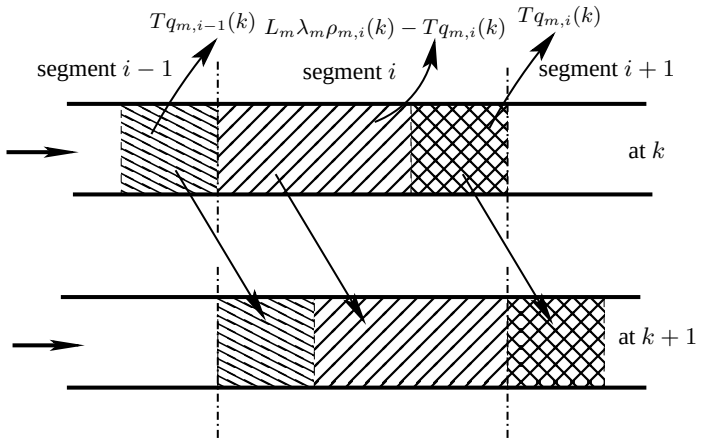

Figure 3.3: Illustration of segmental and cross-segmental traffic flow in METANET.

where a represents the acceleration, v the speed, and n the number of vehicles involved are generated.

3.4.2 Segmental acceleration

Recall that in the METANET model, the space and time discretization has to be done in such a way that $L_m > Tv_{\text{free},m}$ is satisfied (cf. (2.16)). This condition assures that a vehicle cannot cross a segment of a link without at least staying there for one full simulation time step. This means that vehicles can experience speed changes within a segment in one simulation time step. Therefore, the term segmental acceleration refers to the acceleration of the vehicles due to the change in space-mean speed within a segment in one time step. This acceleration is only experienced by the vehicles that stay within the segment from one time step to the next. The segmental acceleration of the vehicles in the segment i of link m at time step[2] k is thus given by

$$a_{\text{seg},m,i}(k) = \frac{v_{m,i}(k+1) - v_{m,i}(k)}{T} \tag{3.6}$$

where the subscript 'seg' is shorthand for 'segmental'.

Now let us determine the number of vehicles that are subject to this segmental acceleration from time step k to $k+1$. At time step k the number of vehicles in segment i is equal to $L_m\lambda_m\rho_{m,i}(k)$ and from time step k to $k+1$ the number of vehicles leaving segment i is $Tq_{m,i}(k)$ (see Fig. 3.3). Hence,

$$n_{\text{seg},m,i}(k) = L_m\lambda_m\rho_{m,i}(k) - Tq_{m,i}(k) \tag{3.7}$$

is the number of vehicles that stayed in segment i and that are subject to the segmental acceleration given in (3.6).

[2]Since the METANET model uses the simulation time step k, the acceleration, speed, and the corresponding number of vehicles subject to the acceleration and speed are determined at the simulation time step k.

3.4.3 Cross-segmental acceleration

The cross-segmental acceleration is the change in speed experienced by vehicles moving from one segment of a link to another segment of the same link or of a different link. Depending on the geometry of the traffic network, there are several possible scenarios for vehicles moving from one segment to another. In particular, the cross-segmental acceleration from one segment to another segment is different for vehicles staying in a link and for vehicles crossing a node (an on-ramp, an off-ramp, merging links, and splitting links). In the sequel the cross-segmental acceleration for each case is discussed.

Vehicles moving between consecutive segments within the same link

At the time step k the space-mean speed of the vehicles in segment i of link m is $v_{m,i}(k)$. In the next time step $k+1$ and in the next segment $i+1$, the speed will be $v_{m,i+1}(k+1)$. Thus, for time step k the cross-segmental acceleration of the vehicles leaving segment i to segment $i+1$ of a link m is

$$a_{\text{cross},m,i,i+1}(k) = \frac{v_{m,i+1}(k+1) - v_{m,i}(k)}{T} \tag{3.8}$$

where the subscript 'cross' is shorthand for 'cross-segmental'.

The number of vehicles that are subject to the cross-segmental acceleration in (3.8) is obtained as

$$n_{\text{cross},m,i,i+1}(k) = T q_{m,i}(k). \tag{3.9}$$

Vehicles crossing a node

Here, first the cross-segmental acceleration and the number of vehicles subject to the acceleration for a general case are presented. Next, these are explained for specific cases.

General case: Let us consider the general case, where several incoming and outgoing links are connected to a node n as in Fig. 2.3. In the figure, there are n_1 incoming links and n_2 outgoing links. The cross-segmental acceleration of vehicles moving from incoming link m_i to outgoing link μ_j is given by

$$a_{\text{cross},m_i,\mu_j}(k) = \frac{v_{1,\mu_j}(k+1) - v_{m_i,N_{m_i}}(k)}{T} \tag{3.10}$$

The corresponding number of vehicles subject to the cross-segmental acceleration in (3.10) is given by

$$n_{\text{cross},m_i,\mu_j}(k) = T\beta_{m_i,n,\mu_j}(k) q_{m_i,N_{m_i}}(k) \tag{3.11}$$

where $\beta_{m_i,n,\mu_j}(k)$ is the turning rate from link m_i to the link μ_j (the fraction of the total outflow of link m_i that leaves via n to link μ_j).

Specific cases: Here the general case for vehicles crossing a node is explained for the specific cases, viz. for an on-ramp, an off-ramp, and a lane drop/increase.

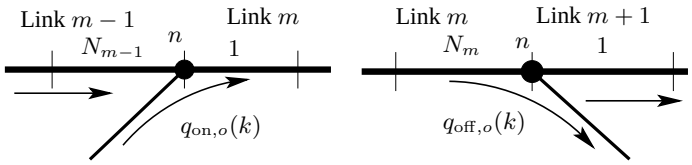

(a) on-ramp (b) off-ramp

Figure 3.4: On-ramp and off-ramp.

- *On-ramp:* In METANET the speed of an on-ramp is not defined. But to determine the cross-segmental acceleration of the vehicles moving from the on-ramp to the freeway, we need to assign the speed of the on-ramp. This speed is assumed to be based on measured or historic data in case no on-line measurements are available. Hence, we use the on-ramp speed $v_{\mathrm{on},o}(k)$ for the on-ramp o. In particular, for a situation like the one sketched in Fig. 3.4(a), the cross-segmental acceleration and the number of vehicles subject to the acceleration are respectively

$$a_{\mathrm{cross,on},o}(k) = \frac{v_{m,1}(k+1) - v_{\mathrm{on},o}(k)}{T} \tag{3.12}$$

$$n_{\mathrm{cross,on},o}(k) = T q_{\mathrm{on},o}(k). \tag{3.13}$$

  where $q_{\mathrm{on},o}(k)$ is the on-ramp flow given by the equations of the form (2.29) or (2.30).

- *Off-ramp:* In general, the vehicles in the freeway can leave to an off-ramp o with an off-ramp speed $v_{\mathrm{off},o}(k)$, where $v_{\mathrm{off},o}(k)$ can be determined in a similar way as the on-ramp speed discussed above. In particular, in Fig. 3.4(b) the flow of the vehicles from segment N_m of link m to the off-ramp o is given by

$$q_{\mathrm{off},o}(k) = \beta_{n,o}(k) q_{m,N_m}(k) \tag{3.14}$$

  where $\beta_{n,o}(k)$ is the turning rate (i.e., the fraction of the total flow through node n that leaves via the off-ramp o).

  Now the cross-segmental acceleration and the number of vehicles flowing from the segment N_m of link m to the off-ramp o can be computed as

$$a_{\mathrm{cross,off},o}(k) = \frac{v_{\mathrm{off},o}(k+1) - v_{m,N_m}(k)}{T} \tag{3.15}$$

$$n_{\mathrm{cross,off},o}(k) = T q_{\mathrm{off},o}(k). \tag{3.16}$$

- *Lane drop/increase:* The cross-segmental acceleration of vehicles moving from the last segment (with index N_m) of the first link m with λ_m lanes to the first segment of the second link $m+1$ with λ_{m+1} lanes is computed using the relation

$$a_{\mathrm{cross},m,m+1}(k) = \frac{v_{m+1,1}(k+1) - v_{m,N_m}(k)}{T}. \tag{3.17}$$

Moreover, the number of vehicles experiencing the acceleration is computed as

$$n_{\text{cross},m,m+1}(k) = T q_{m,N_m}(k). \tag{3.18}$$

The accelerations derived in the above sections have been based on physical interpretation of the METANET model. In [114] a pure mathematical derivation is given to express the accelerations in their original continuous-time domain descriptions. The accelerations are discretized and these accelerations and the accelerations derived in the above sections are found to be not identical but consistent and convergent approximations of the original continuous-time equations.

3.4.4 VT-macro emissions and fuel consumption equations

Unlike in the microscopic case where the speed-acceleration pair is for a single vehicle, the speed-acceleration pairs generated in Sections 3.4.2 and 3.4.3 hold for groups of vehicles. Therefore, the emissions and fuel consumption obtained for the given speed-acceleration pair have to be multiplied by the corresponding number of vehicles in order to obtain the total emissions and fuel consumption. The emissions and fuel consumption of each case is provided next.

Vehicles moving within a segment

In Section 3.4.2 we have derived the segmental acceleration and the corresponding number of vehicles within a segment of a link at simulation step k. Using these variables as an input to the VT-micro model in (3.2), a new macroscopic emissions and fuel consumption model for the vehicles moving within a segment is obtained as

$$\bar{J}_{\text{seg},\bar{y},m,i}(k) = n_{\text{seg},m,i}(k) \exp\left(\tilde{v}_{m,i}^{\top}(k) P_{\bar{y}} \tilde{a}_{\text{seg},m,i}(k)\right) \tag{3.19}$$

where $\bar{J}_{\text{seg},\bar{y},m,i}(k)$ denotes the values of the variable $\bar{y} \in \bar{\mathcal{Y}}/\{\text{CO}_2\}$ at simulation step k and $\bar{\mathcal{Y}} = \{\text{CO, CO}_2\text{, HC, NO}_x\text{, fuel}\}$, the average acceleration vector $\tilde{a}_{\text{seg},m,i}(k)$ and the average space-mean speed vector $\tilde{v}_{m,i}(k)$ are respectively obtained from $a_{\text{seg},m,i}(k)$ and $v_{m,i}(k)$ by using the operator $\tilde{\cdot}$ defined in (3.3), while $a_{\text{seg},m,i}(k)$ and $n_{\text{seg},m,i}(k)$ are respectively given by (3.6) and (3.7), and $v_{m,i}(k)$ is the average space-mean speed of the vehicles in segment i of link m at simulation step k.

The emissions model in (3.19) can also be extended to model the CO_2 emission using the expression in (3.4) as

$$\bar{J}_{\text{seg},\text{CO}_2,m,i,i+1}(k) = n_{\text{seg},m,i}(k)\big(\delta_1 v_{m,i}(k) + \delta_2 \exp(\tilde{v}_{m,i}^{\top}(k) P_{\text{fuel}} \tilde{a}_{\text{seg},m,i}(k))\big) \tag{3.20}$$

where the δ_1 and δ_2 are model parameters as given in (3.4).

Vehicles moving from segment to segment within a link

For vehicles moving from one segment of a link to another segment of the same link, the macroscopic emissions and fuel consumption model is given by

$$\bar{J}_{\text{cross},\bar{y},m,i,i+1}(k) = n_{\text{cross},m,i,i+1}(k) \exp\left(\tilde{v}_{m,i}^{\top}(k) P_{\bar{y}} \tilde{a}_{\text{cross},m,i,i+1}(k)\right) \tag{3.21}$$

$$\bar{J}_{\text{cross},\text{CO}_2,m,i,i+1}(k) = n_{\text{cross},m,i,i+1}(k)\big(\delta_1 v_{m,i}(k) + \delta_2 \exp(\tilde{v}_{m,i}^{\top}(k) P_{\text{fuel}} \tilde{a}_{\text{cross},m,i,i+1}(k))\big) \tag{3.22}$$

where $\bar{J}_{\text{cross},\bar{y},m,i,i+1}(k)$ denotes the value of the variable $\bar{y} \in \bar{\mathcal{Y}}/\{\text{CO}_2\}$ of vehicles moving from segment i to segment $i+1$ of link m at simulation step k, $\bar{J}_{\text{cross},\text{CO}_2,m,i,i+1}(k)$ denotes the value of the CO_2 emission released by vehicles moving from segment i to segment $i+1$ of link m at simulation step k, the average acceleration vector $\tilde{a}_{\text{cross},m,i,i+1}(k)$ and the average space-mean speed vector $\tilde{v}_{m,i}(k)$ are respectively obtained by applying the vector operation $\tilde{\cdot}$ (cf. (3.3)) on $a_{\text{cross},m,i,i+1}(k)$ and $v_{m,i}(k)$, with $a_{\text{cross},m,i,i+1}(k)$ and $n_{\text{cross},m,i,i+1}(k)$ respectively given by (3.8) and (3.9).

Vehicles crossing a node

The emissions and fuel consumption of the vehicles crossing a node where merging and splitting links are connected is given by

$$\bar{J}_{\text{cross},\bar{y},m_i,\mu_j}(k) = n_{\text{cross},m_i,\mu_j}(k) \exp\left(\tilde{v}_{m_i,N_{m_i}}^{\top}(k) P_{\bar{y}} \tilde{a}_{\text{cross},m_i,\mu_j}(k)\right) \tag{3.23}$$

$$\bar{J}_{\text{cross},\text{CO}_2,m_i,\mu_j}(k) = n_{\text{cross},m_i,\mu_j}(k)\big(\delta_1 v_{m_i,N_{m_i}}(k) + \delta_2 \exp(\tilde{v}_{m_i,N_{m_i}}^{\top}(k) P_{\text{fuel}} \tilde{a}_{\text{cross},m_i,\mu_j}(k))\big) \tag{3.24}$$

where $\bar{J}_{\text{cross},\bar{y},m_i,\mu_j}(k)$ is the value of the variable $\bar{y} \in \bar{\mathcal{Y}}/\{\text{CO}_2\}$ of the vehicles moving from the link m_i to link μ_j at the simulation step k, $\bar{J}_{\text{cross},\text{CO}_2,m_i,\mu_j}(k)$ is the value of the CO_2 emission of the vehicles moving from link m_i to link μ_j at the simulation step k, the vectors $\tilde{a}_{\text{cross},m_i,\mu_j}(k)$ and $\tilde{v}_{m_i,N_{m_i}}(k)$ are respectively obtained using the vector operation $\tilde{\cdot}$ (cf., (3.3)) to $a_{\text{cross},m_i,\mu_j}(k)$ and $v_{m_i,N_{m_i}}(k)$ with $a_{\text{cross},m_i,\mu_j}(k)$ and $n_{\text{cross},m_i,\mu_j}(k)$ respectively given by (3.10) and (3.11), and $v_{m_i,N_{m_i}}(k)$ the average space-mean speed of the last segment of link m_i at simulation step k.

Overall emissions and fuel consumption model

The total emissions or fuel consumption of vehicles in a traffic network at simulation time step k is therefore

$$J_{\text{total},\bar{y}}(k) = \sum_{m\in\mathcal{M}} \sum_{i=1}^{N_m} \bar{J}_{\text{seg},\bar{y},m,i}(k) + \sum_{m\in\mathcal{M}} \sum_{i=1}^{N_m-1} \bar{J}_{\text{cross},\bar{y},m,i,i+1}(k) + \sum_{n\in\mathcal{N}} \sum_{m_i\in\mathcal{I}_n} \sum_{\mu_j\in\mathcal{O}_n} \bar{J}_{\text{cross},\bar{y},m_i,\mu_j}(k) \tag{3.25}$$

where $\bar{y} \in \bar{\mathcal{Y}} = \{\text{CO, CO}_2\text{, HC, NO}_x\text{, fuel}\}$, $\mathcal{M}$ is the set of links in the network, $\mathcal{N}$ is the set of nodes in the network, $\mathcal{I}_n$ is the set of links that enter node n, $\mathcal{O}_n$ is the set of links that leave node n, and $\bar{J}_{\text{seg},\bar{y},m,i}(k)$, $\bar{J}_{\text{cross},\bar{y},m,i,i+1}(k)$, and $\bar{J}_{\text{cross},\bar{y},m_i,\mu_j}(k)$ are respectively given by (3.19) (or (3.20)), (3.21) (or (3.22)), or (3.23) (or (3.24)).

Thus, the interface block and the VT-micro block in Fig. 3.2 forms a new macroscopic emissions and fuel consumption model. We call this new model the "VT-macro" emissions and fuel consumption model.

3.4.5 Analysis of VT-macro

In the previous section we have proposed the integration of the macroscopic traffic flow model METANET with the microscopic emissions and fuel consumption model VT-micro, which resulted in a macroscopic emissions and fuel consumption model VT-macro. Due to the approximation of the speed and acceleration of the individual vehicles by the average speed and the average acceleration over the number of vehicles, the model may introduce errors. Moreover, the motive for the development of the model is to gain computational speed while keeping the estimation error as small as possible. Therefore, analysis of the maximum error that can be introduced by this model is required. In the ensuing paragraphs, the analysis of this error is presented.

This section examines the effect of going from one individual vehicle (VT-micro) to a group of vehicles (VT-macro). In general, one could consider different macroscopic and microscopic simulation time steps, i.e., $T \neq T_{\mathrm{m}}$. However, this problem is mainly related to traffic flow models (e.g., METANET vs. IDM). Here the focus of the analysis is only on the VT-macro model. Since the METANET model is not directly based on microscopic modeling approaches, this thesis will not delve into the analysis of the approximation errors induced by the METANET traffic flow model. Hence, it is assumed here that $T = T_{\mathrm{m}}$.

Let the speed of an individual vehicle α and the average speed over a group of vehicles be respectively $v_\alpha(k_{\mathrm{m}})$ and $\bar{v}(k_{\mathrm{m}})$. If the relative deviation of the speed v of an individual vehicle α from the average speed is $\delta_{v,\alpha}(k_{\mathrm{m}})$, then the speed of an individual vehicle α can be expressed as

$$v_\alpha(k_{\mathrm{m}}) = \bar{v}(k_{\mathrm{m}})(1 + \delta_{v,\alpha}(k_{\mathrm{m}})). \tag{3.26}$$

Similarly, let the acceleration of vehicle α be $a_\alpha(k_{\mathrm{m}})$ and the average acceleration of its group be $\bar{a}(k_{\mathrm{m}})$, then the acceleration of vehicle α will be

$$a_\alpha(k_{\mathrm{m}}) = \bar{a}(k_{\mathrm{m}})(1 + \delta_{a,\alpha}(k_{\mathrm{m}})) \tag{3.27}$$

where $\delta_{a,\alpha}(k_{\mathrm{m}})$ is the relative deviation of the acceleration of vehicle α from the average acceleration $\bar{a}(k_{\mathrm{m}})$.

In Section 3.4, the speed and acceleration inputs are transformed into a vector through the operator $\tilde{\cdot}$ defined in (3.3). Using the approximation relation $(1+\delta)^n \approx (1+n\delta)$ for small δ, and the $\tilde{\cdot}$ operation, we get

$$\tilde{v}_\alpha(k_{\mathrm{m}}) = (I + E\delta_{v,\alpha}(k_{\mathrm{m}}))\tilde{\bar{v}}(k_{\mathrm{m}}), \quad \tilde{a}_\alpha(k_{\mathrm{m}}) = (I + E\delta_{a,\alpha}(k_{\mathrm{m}}))\tilde{\bar{a}}(k_{\mathrm{m}})$$

where I is an identity matrix of proper dimension, $E = \mathrm{diag}(0,1,2,3)$, $\tilde{\bar{v}}(k_{\mathrm{m}}) = [1\ \bar{v}(k_{\mathrm{m}})\ \bar{v}^2(k_{\mathrm{m}})\ \bar{v}^3(k_{\mathrm{m}})]^\top$, and $\tilde{\bar{a}}(k_{\mathrm{m}}) = [1\ \bar{a}(k_{\mathrm{m}})\ \bar{a}^2(k_{\mathrm{m}})\ \bar{a}^3(k_{\mathrm{m}})]^\top$.

Hence, the emissions or fuel consumption rate $J_{\alpha,\bar{y}}(k_{\mathrm{m}})$ of vehicle α with the speed $v_\alpha(k_{\mathrm{m}})$ and the acceleration $a_\alpha(k_{\mathrm{m}})$ can be expressed in terms of the average speed $\bar{v}(k_{\mathrm{m}})$, average acceleration $\bar{a}(k_{\mathrm{m}})$, speed deviation $\delta_{v,\alpha}(k_{\mathrm{m}})$, and acceleration deviation $\delta_{a,\alpha}(k_{\mathrm{m}})$ as

$$\begin{aligned} J_{\alpha,\bar{y}}(k_{\mathrm{m}}) = \exp\Big[& \tilde{\bar{v}}^\top(k_{\mathrm{m}}) P_{\bar{y}} \tilde{\bar{a}}(k_{\mathrm{m}}) + \delta_{v,\alpha}(k_{\mathrm{m}}) \tilde{\bar{v}}^\top(k_{\mathrm{m}}) E P_{\bar{y}} \tilde{\bar{a}}(k_{\mathrm{m}}) \\ & + \delta_{a,\alpha}(k_{\mathrm{m}}) \tilde{\bar{v}}^\top(k_{\mathrm{m}}) P_{\bar{y}} E \tilde{\bar{a}}(k_{\mathrm{m}}) \end{aligned}$$

$$+ \delta_{v,\alpha}(k_{\mathrm{m}})\delta_{a,\alpha}(k_{\mathrm{m}})\tilde{\bar{v}}^{\top}(k_{\mathrm{m}})EP_{\bar{y}}E\tilde{\bar{a}}(k_{\mathrm{m}})\Big] \quad (3.28)$$

for $\bar{y} \in \bar{\mathcal{Y}}/\{\mathrm{CO}_2\}$.

Using the Taylor series expansion and neglecting higher-order terms of the deviations $\delta_{v,\alpha}$ and $\delta_{a,\alpha}$, the emissions or fuel consumption $\bar{y}$ of vehicle α in (3.28) can be approximated by

$$J_{\alpha,\bar{y}}(k_{\mathrm{m}}) \approx \exp\left(\tilde{\bar{v}}^{\top}(k_{\mathrm{m}})P_{\bar{y}}\tilde{\bar{a}}(k_{\mathrm{m}})\right)\Big[1 + \delta_{v,\alpha}(k_{\mathrm{m}})\tilde{\bar{v}}^{\top}(k_{\mathrm{m}})EP_{\bar{y}}\tilde{\bar{a}}(k_{\mathrm{m}}) + \delta_{a,\alpha}(k_{\mathrm{m}})\tilde{\bar{v}}^{\top}(k_{\mathrm{m}})P_{\bar{y}}E\tilde{\bar{a}}(k_{\mathrm{m}})\Big]. \quad (3.29)$$

Therefore, the relative error of the estimation of emissions and fuel consumption $\bar{y}$ of individual vehicles due to the averaging of the speed and the acceleration is

$$\epsilon_{\mathrm{approx},\alpha,\bar{y}}(k_{\mathrm{m}}) \approx \delta_{v,\alpha}(k_{\mathrm{m}})\tilde{\bar{v}}^{\top}(k_{\mathrm{m}})EP_{\bar{y}}\tilde{\bar{a}}(k_{\mathrm{m}}) + \delta_{a,\alpha}(k_{\mathrm{m}})\tilde{\bar{v}}^{\top}(k_{\mathrm{m}})P_{\bar{y}}E\tilde{\bar{a}}(k_{\mathrm{m}}). \quad (3.30)$$

The VT-macro model is simulated in the operating region of the VT-micro model to determine an upper bound for the error in (3.30) for several possible combinations of the acceleration and speed ranges. Fig. 3.5 presents the maximum values of the approximate relative error (3.30) for all the possible speed and acceleration combinations within the operating region of the model when the deviations of the speed and acceleration are within $\pm 5\%$. The color-bars on the right side of the plots show the maximum values of the approximate relative errors introduced by the model for combinations of the deviations $\delta_{v,\alpha}$ and $\delta_{a,\alpha}$.

3.4.6 Empirical verification

In this section the macroscopic VT-macro emissions and fuel consumption model is evaluated by comparing it with the microscopic VT-micro emissions and fuel consumption model (3.2). To do so, the microscopic car-following "Intelligent Driver Model (IDM)" [186] is calibrated to a macroscopic traffic flow METANET model of a Dutch highway. In the sequel, the description of the freeway, its modeling, and the results of the simulation based on the calibrated models are discussed.

Freeway and scenario description

The freeway stretch that is considered for the analysis of the VT-macro model is a part of the Dutch A12 freeway going from the connection with the N11 at Bodegraven up to Harmelen, and is shown in Fig. 3.6. The freeway has three lanes in each direction. The part that is considered is approximately 14 km and it has two on-ramps and three off-ramps. The stretch is equipped with double-loop detectors at a typical distance of 500 to 600 m, measuring the average speed and flow every minute.

The data of the freeway has been used to calibrate the METANET model in [79]. The same parameters that have been obtained in the study [79] are now used to calibrate the microscopic car-following IDM model [186]. The IDM model is selected because, in Section 2.2.3 it has been motivated that this model improves some of the deficiencies of the well-known microscopic models GHR [67] and OVM [15]. The calibrated IDM car-

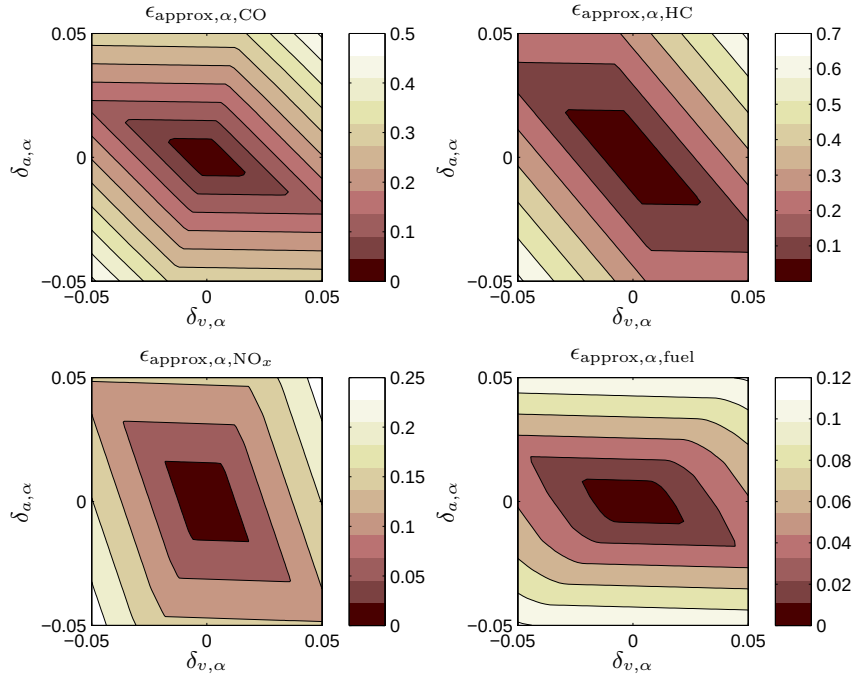

Figure 3.5: Upper bounds for the approximate error of (3.30) for different deviations of the speed $\delta_{v,\alpha}$ and acceleration $\delta_{a,\alpha}$ of an individual vehicle α for scenarios with average speeds (5–120 km/h) and average accelerations (-5–2.75 m/s^2) respectively.

Figure 3.6: A part of the Dutch A12 freeway going from the Bodegraven (left of the figure) up to Harmelen (right of the figure) considered for the empirical verification of the VT-macro emissions and fuel consumption model.

following model is subsequently coupled with the microscopic VT-micro emissions and fuel consumption model and the integrated models are considered as a benchmark.

In order to compare the performance of the integrated macroscopic traffic flow and emis-

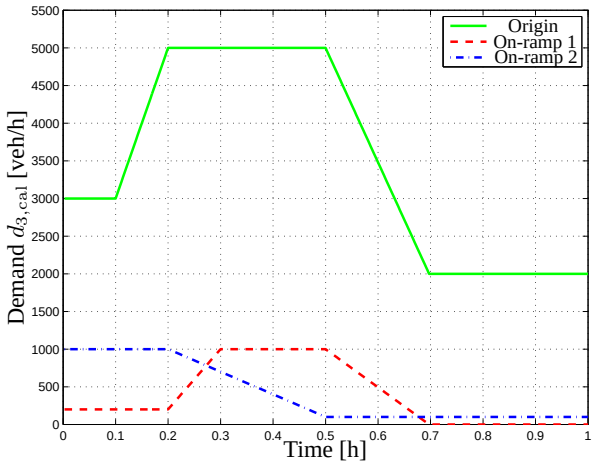

Figure 3.7: Traffic demands scenario used for the calibrating of the IDM model to the METANET model.

sions and fuel consumption models with the microscopic flow and emissions and fuel consumption models, four different traffic demand scenarios are used. In this way it is also possible to show to some extent the robustness of the modeling approach presented in this chapter. To provide a glimpse of the nature of the demand profiles, the calibrating demand $d_{3,\mathrm{cal}}$ is depicted in Fig. 3.7, where the other demand profiles are related to the calibrating demand profile as $d_1(k) = 0.8d_{3,\mathrm{cal}}(k)$, $d_2(k) = 0.9d_{3,\mathrm{cal}}(k)$, and $d_4(k) = 1.1d_{3,\mathrm{cal}}(k)$. The average of the space-mean speed and the average of the density of the traffic flow over the whole freeway network for the demand profile $d_1(k) = 0.8d_{3,\mathrm{cal}}(k)$ are depicted in Fig. 3.8. These quantities are obtained using the microscopic IDM model and the macroscopic METANET model of the freeway.

Now the two integrated models (microscopic and macroscopic approaches) are then simulated for the four scenarios and the corresponding emissions, fuel consumption, and CPU time are collected. The results of the simulation are presented and discussed afterwards.

Moreover, to compare the newly developed dynamic-macroscopic emissions and fuel consumption model, the VT-macro model[3], with the average-speed-based macroscopic emissions and fuel consumption model, the COPERT [139] model is considered. First the COPERT model is integrated to the METANET model and next the COPERT model is calibrated in such a way that the error between the emissions and fuel consumption estimates of the COPERT model and that of the VT-micro model is minimal. The demand profile $d_{3,\mathrm{cal}}$ is used for the calibration process. Since it is suggested that the accuracy of average-speed-based emissions and fuel consumption models can be improved if the speeds are averaged

[3]Recall that the VT-macro emissions and fuel consumption model consists of a transformation step that derives the accelerations and corresponding number of vehicles from the output of the METANET flow model and the VT-micro emissions and fuel consumption model that uses the speed and acceleration of the vehicles to compute the emissions and fuel consumption. Next, the resulting value of the emissions and fuel consumption corresponding to a single vehicle are multiplied by the number of vehicles subject to the speed-acceleration pairs used to determine the values. So the term “VT-macro” implicitly refers an integrated VT-micro and the interfacing block in Fig. 3.3.

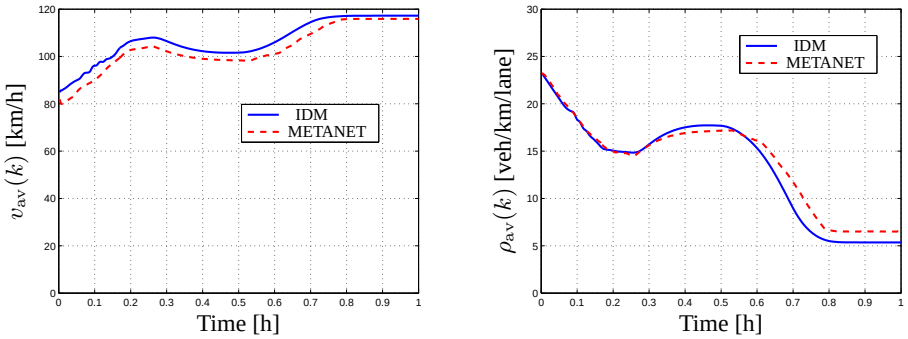

(a) Average speed (b) Average density

Figure 3.8: Average space-mean speed and average density of the freeway for the demand profile $d_1(k) = 0.8d_{3,\rm cal}(k)$ as generated using the IDM and METANET models.

at shorter time intervals [28], then the emissions and fuel consumption estimations are made at every simulation time. Finally, the COPERT model is simulated as integrated with the METANET model and the VT-micro model as integrated to the IDM model for the four aforementioned demand profiles.

For the macroscopic simulation case the simulation time step is set to be $T = 10$ s, while for the microscopic simulation the simulation time step is set to be $T_{\rm m} = 1$ s.

Validation and discussion

Recall that the VT-micro emissions and fuel consumption model estimates the emissions and fuel consumption of each vehicle at specific times (every 1 s) and specific places. Therefore, to compare the results of the VT-macro and COPERT models with the VT-micro model, we have aggregated the emissions and fuel consumption estimates of the VT-micro model (or individual vehicles) over 10 s time periods in order to determine the total emission and total fuel consumption in a specific segment of the freeway. These integrated emissions and fuel consumption values during each 10 s of the simulation of the VT-micro model are compared with the corresponding emissions and fuel consumption estimates of the VT-macro and the COPERT models.

Fig. 3.9 provides plots of the estimates of the CO, HC, and NO_x emissions, and fuel consumption of the freeway for the demand scenario $d_1(k) = 0.8d_{3,\rm cal}(k)$ that are estimated using the VT-micro, VT-macro, and COPERT models. The figure shows the evolution of the emissions and fuel consumption during the simulation period of 1 h. Fig. 3.9 clearly shows a very good fit of the estimates of the VT-macro model to the estimates of the VT-micro model, whereas the estimates of the COPERT show a bad fit. The corresponding relative error of the macroscopic approaches with respect to the VT-micro is presented in Fig. 3.10. The figure clearly indicates that the estimation error of the VT-macro model is small for the this particular scenario, while that of the COPERT model is large. Note, however, that the error in Fig. 3.10 is not only due to the error introduced by the VT-macro model as given in (3.30). The error is introduced both due to the mismatch between the METANET and

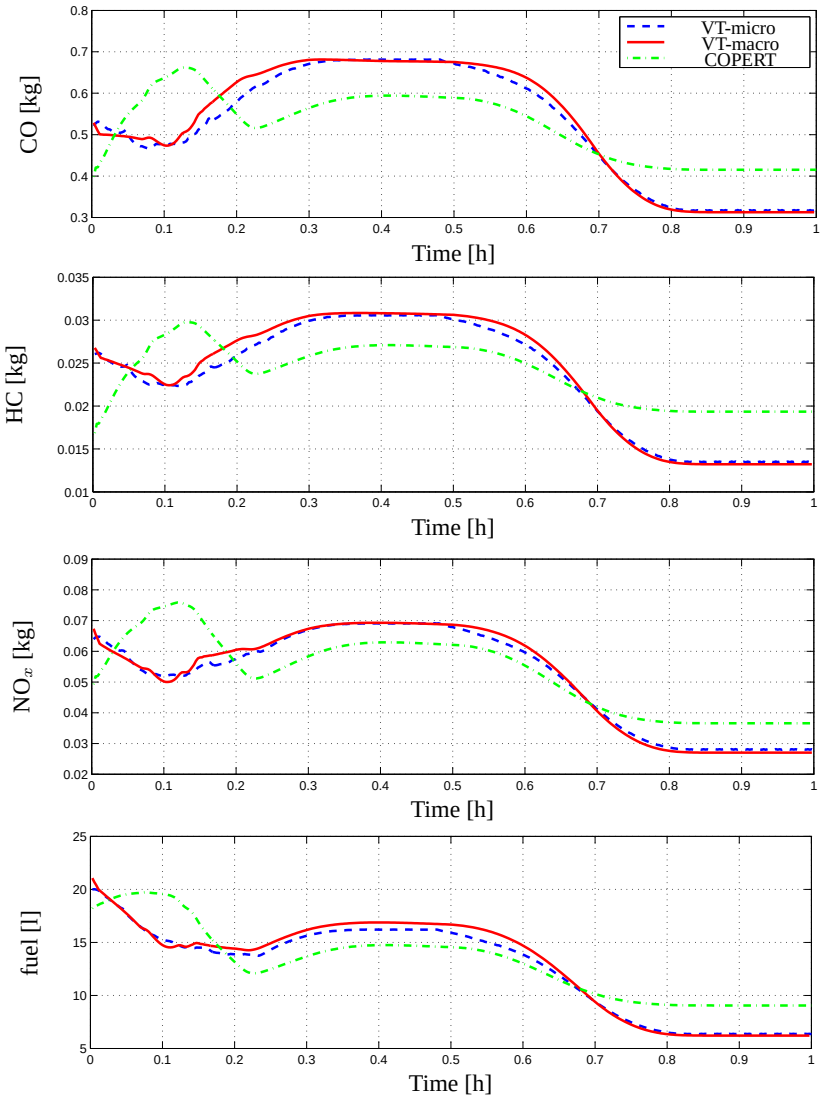

Figure 3.9: Comparison of the emissions and fuel consumption estimated using the macroscopic VT-macro and COPERT models and the microscopic VT-micro emissions and fuel consumption models for the demand profile $d_1(k) = 0.8 d_{3,\mathrm{cal}}(k)$.

the IDM traffic flow models and due to the mismatch between the VT-micro and the VT-macro emissions and fuel consumption models and between the VT-micro and the COPERT emissions and fuel consumption models. Therefore, it is not possible to relate the errors in Fig. 3.10 with the approximate errors in (3.30). It is neither possible to relate the error in Fig. 3.10 with the error due to the mismatch between the VT-micro model and the COPERT model.

The average of the absolute relative-estimation error of the emissions and fuel consump-

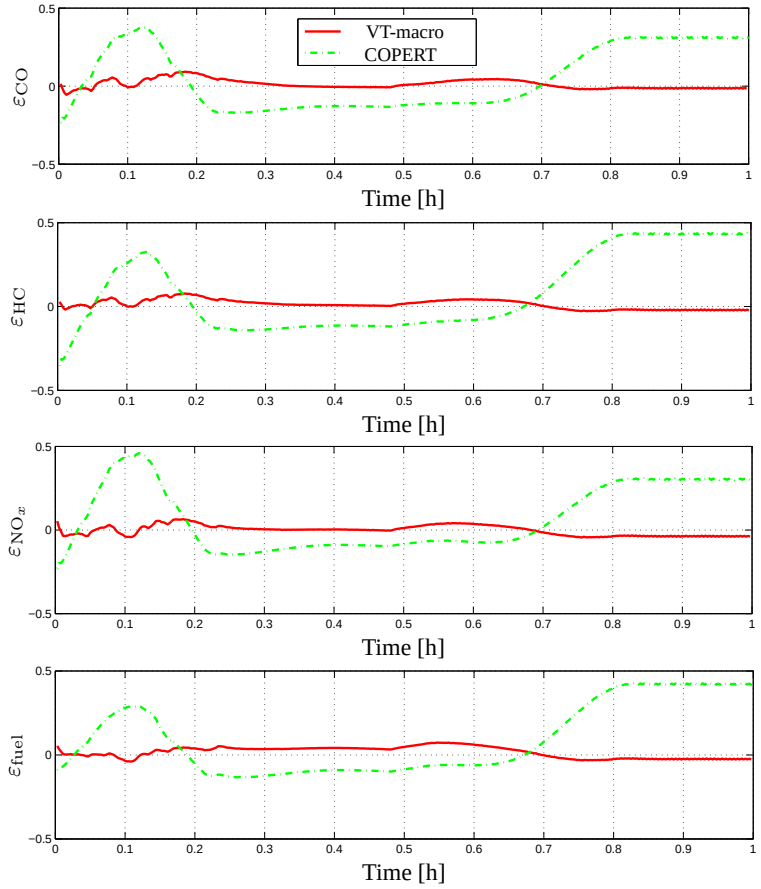

Figure 3.10: Relative-estimation error of the macroscopic VT-macro and COPERT models with respect to microscopic VT-micro model for the demand profile $d_1(k) = 0.8 d_{3,\mathrm{cal}}(k)$.

tion over the whole simulation time and the whole freeway is also computed. The average of the absolute relative-estimation error is determined using

$$e_{\mathrm{av},\bar{y}} = \frac{1}{N_{\mathrm{s}}} \sum_{k=1}^{N_{\mathrm{s}}} \frac{\|\bar{y}_{\mathrm{model}}(k) - \bar{y}_{\mathrm{VT-micro}}(k)\|}{\bar{y}_{\mathrm{VT-micro}}(k)} \times 100\% \tag{3.31}$$

where N_{s} is a positive integer that denotes the duration of the simulation and $\bar{y}_{(\cdot)}(k)$ denotes the value of the emissions or fuel consumption $\bar{y} \in \bar{\mathcal{Y}}/\{\mathrm{CO}_2\}$ of VT-micro, VT-macro, or COPERT at the simulation time step k.

The results are presented in Table 3.1 and Table 3.2. Table 3.1 indicates that the maximum average-absolute-relative error of the VT-macro model for these particular simulations is not more than 9.5%. So, although the model has been calibrated for a different demand profile, for the demand profiles d_1, d_2, and d_4 the estimates of the macroscopic approach

Table 3.1: The average of the absolute relative-estimation error of VT-macro with respect to VT-micro. The demand profiles are related as $d_1(k) = 0.8d_{3,\mathrm{cal}}(k)$, $d_2(k) = 0.9d_{3,\mathrm{cal}}(k)$, and $d_4(k) = 1.1d_{3,\mathrm{cal}}(k)$.

Scenarios	Average absolute relative-estimation error (%)				CPU time (s)	
	CO	HC	NO_x	fuel	VT-micro	VT-macro
d_1	2.4	2.5	2.5	3.2	112	1.70
d_2	2.3	1.9	2.7	2.6	124	1.52
$d_{3,\mathrm{cal}}$	3.4	2.9	4.5	3.7	142	1.65
d_4	9.4	7.0	9.2	6.6	162	1.61

Table 3.2: The average of absolute relative-estimation error of COPERT with respect to VT-micro. The demand profiles are related as $d_1(k) = 0.8d_{3,\mathrm{cal}}(k)$, $d_2(k) = 0.9d_{3,\mathrm{cal}}(k)$, and $d_4(k) = 1.1d_{3,\mathrm{cal}}(k)$.

Scenarios	Average absolute relative-estimation error (%)			
	CO	HC	NO_x	fuel
d_1	17.9	20.0	17.1	18.2
d_2	12.0	14.2	11.8	13.2
$d_{3,\mathrm{cal}}$	6.7	9.3	7.9	9.0
d_4	7.5	10.0	8.0	7.0

are not far from the estimates of the microscopic approach. From Table 3.2, one sees that the error that is introduced by the COPERT model is at least 100% more than the error introduced by the VT-macro for almost all the cases. Recall also that the COPERT model is calibrated to VT-micro, while the VT-macro model uses exactly the same parameters used by the VT-micro model.

In addition to the improvement of the emissions and fuel consumption estimation that can be obtained when microscopic emissions and fuel consumption models are integrated with macroscopic traffic flow models, the second motivation for the integration of the microscopic emissions and fuel consumption model with macroscopic traffic flow model is the need for reduced simulation time. In this regard the simulation times for the four different scenarios are compared. Table 3.1 provides the CPU time of the VT-micro (microscopic) and VT-macro (macroscopic) simulations for the different scenarios. It can be seen that the CPU time of the VT-macro simulation is independent of the demand (or number of vehicles) in the traffic network and is almost constant for all four scenarios. On the other hand, the CPU time required for the simulation of the VT-micro model increases as the demand increases. Moreover, the CPU time required for the simulation of the VT-micro model is very large relative to the CPU time required by the VT-macro model to simulate the same traffic scenario. Note that the CPU time required to simulate the VT-macro model and the COPERT model is the same, i.e., the difference is almost negligible.

3.5 Conclusions

This chapter has provided a general overview of emissions and fuel consumption models. After discussing the two modeling approaches viz. the technology-based engineering emissions and fuel consumption modeling approach and the traffic emissions and fuel consumption modeling approach, the attention of the chapter has shifted to the different traffic emissions and fuel consumption models. This chapter has elaborated on the different traffic emissions and fuel consumption models by categorizing them into three different groups, namely microscopic, macroscopic, and mesoscopic models. The chapter has also discussed two basic models, the VT-micro model from the microscopic group and the COPERT model from the macroscopic group.

This chapter has also presented a general framework for the integration of macroscopic traffic flow models with microscopic emissions and fuel consumption models. A distinction has been made between segmental and cross-segmental variables in order to capture the discrete temporal and spatial nature of macroscopic traffic flow models. The approach has been further demonstrated using the METANET traffic flow model and VT-micro emissions and fuel consumption model, which resulted in the VT-macro model.

Moreover, this chapter has presented an analysis of the maximum approximate error that can be introduced by the use of macroscopic variables to determine the emissions and fuel consumption of individual vehicles. Both the analytic and empirical results show that the errors introduced by using VT-macro are less than 10%. A comparison of the errors of the VT-macro model with the established average-speed-based macroscopic model COPERT also shows that the VT-macro model is more closer to the VT-micro model (which is claimed to be “better” than macroscopic emissions and fuel consumption models) than the COPERT model for the cases considered. Furthermore, the simulation results indicate that the simulation time (CPU time) can be tremendously decreased if one uses the macroscopically integrated emissions and fuel consumption model (VT-macro), while this only introduces errors less than 10% over the whole estimation for the particular scenarios.

Chapter 4

Traffic Emissions Dispersion Modeling

Reducing the amount of emitted gases of the traffic flow can improve the overall traffic network emissions. However, since dispersion of these emissions is dependent on the wind, temperature, rainfall, and topography of the freeway neighborhood, the dispersion of the emissions can be distributed unevenly. This means that certain areas can face higher emission levels than other areas. For example, protected target zones such as schools and hospitals could face high emission levels (pollution) despite the reduced total emission levels at the network level. Hence, it is unwise to affect the traffic flow (or compromise the travel time) of the whole freeway at all times. It is better to focus on the parts of the freeway that affect the target zones and on the time windows in which the corresponding emissions originate. This could be done by predicting the evolution of the emissions dispersion factors (such as the temperature, the wind speed, and wind direction) and by predicting freeway sections originating the emissions dispersed to a given target zone. In this way, only the traffic flow on the parts of the freeway that have negative impacts on the target zone have to be controlled dynamically so as to attain reduced traffic emissions and improved travel times.

Therefore, in order to predict the dispersion of the emissions, area-wide emission (dispersion) models are required. This chapter, therefore, presents computationally efficient emissions dispersion models. First, an overview and examination of existing dispersion models in the literature is presented in Section 4.1. Next, a point-source dispersion model, a basis for the development of enhanced models in the subsequent sections is discussed in Section 4.2. Section 4.3 presents computationally efficient grid-based dispersion models that are developed based on the point-source dispersion concept. Finally, the conclusions of the chapter are presented in Section 4.4.

Parts of this chapter are published in [213–217].

4.1 Overview of dispersion models

Despite the significant reduction of emissions in general and the factors that affect the emission rate of vehicles (such as engine efficiency, aerodynamic shape of vehicles), air pol-

lution, in particular, mainly associated with road traffic is still a significant environmental problem in most developed countries [127]. Consequently, the impact of traffic emissions has become an important research issue [26, 140], leading to numerous modeling studies related to the influence of meteorological, topological, and dispersion factors on pollutant accumulation/dissipation patterns [190]. In road traffic environments and especially in those areas where population and traffic density are relatively high, human exposure to hazardous substances is expected to be significantly increased [190]. This is often the case in and near busy urban and freeway traffic networks. Within these streets, pedestrians, cyclists, drivers, and residents are likely to be exposed to pollutant concentrations exceeding current air quality standards [190].

Dispersion of vehicular emissions is affected by several factors. Some of the main factors are the speed of the vehicles, the wind speed and wind direction, the temperature, rainfall, the topography of the area near to the freeway or urban roads, etc. However, it is difficult to consider all the factors that influence the dispersion of the vehicular emissions in the modeling process. Most models consider either the speed of the vehicles, the ambient temperature, the wind speed and wind direction, or the topography of the area around the freeway or urban traffic networks into account, whichever has significant effects [13, 25, 43, 112, 165].

Moreover, all the factors do not have a significant influence at all spatial and temporal scales of the dispersion process. For instance, the speeds of the vehicles influence the dispersion of the emissions in the close vicinity of the roads [13]. This means that the effect of traffic speed is important factor in the dispersion modeling process of urban traffic, while on the contrary its effect is not an important of consideration for models that consider the dispersion of freeway traffic emissions to sensitive target zones located at a relative distant location. This is because in the region far from the freeway, where most residence areas, schools, and other buildings are located, the dispersion of the emissions is primarily affected by the wind and the temperature [13], and thus the effect of the speed of the vehicles becomes negligible. On the other hand, the road side walls of the buildings in the urban canyon are important factors for the dispersion of vehicular emissions [51, 90, 135], because the walls block the dispersion of the emissions as wind blows perpendicular to the roadway, which creates circulation (or eddy like motion) of the emissions within the canyon.

4.1.1 Dispersion models

There is a multitude of dispersion models especially developed for street canyon applications (such as AEOLIUS [32], CALINE4 [25], CPRM [194], CAR [60]). There is, however, only a very limited number of models for the dispersion of emissions from freeway traffic. Although the basic governing modeling concepts for both the freeway and urban traffic networks are similar, they have certain important differences. Due to the generally complex geometrical structure of urban sites a variety of time and space scales is involved [174]. However, since the topology of freeways is relatively homogeneous uniform time and space scales are used. The dispersion of emissions from urban traffic is affected by the canyons of the urban streets and the dispersion distance of interest is short. However, the dispersion of emissions in freeways is less obstructed than the dispersion of the urban emissions. Moreover, the dispersion of the emissions in the near-wake (in the close vicinity of the freeway) is of less interest. Indeed, for freeways the dispersion of the emissions to relatively distant areas, where most public residences, schools, and parks are located is most often of interest.

According to the need and intended application of the models, the modeling approaches and modeling details of dispersion models can be different [127]. Although there are no clear-cut distinctions between different categories, dispersion models can be classified into groups according to their physical or mathematical principles (e.g., Gaussian, Computational Fluid Dynamic (CFD), and reduced-scale models) and their level of complexity (e.g., as parametric or numerical) [43, 190]. In this thesis the dispersion models are grouped into three categories: Gaussian models, CFD models, and reduced-scale models. In the following sections, a brief account on each of the modeling approaches is discussed.

Gaussian dispersion models

Gaussian dispersion models (such as STREET [90], CPBM [202], and OSPM [85]) are governed by a system of differential equations called the diffusion equations. These systems of equations describe the three-dimensional concentration field generated usually by a point source. With a set of assumptions that can reasonably be applied to atmospheric processes, the diffusion equation has a specific, closed-form algebraic solution that is Gaussian, i.e., the resulting solution of the diffusion equations describes the concentrations of emissions from a continuously emitting source to be proportional to the traffic emission rate and inversely proportional to the wind speed. Moreover, the horizontal and vertical time averaged pollutant concentrations are described by Gaussian distributions [127, 190].

In its simplest form, the Gaussian plume model assumes that there are no chemical or removal processes taking place and that pollutant material reaching the ground or the top of the mixing layer as the plume grows is reflected back towards the plume centerline [190]. Moreover, it assumes that the wind is constant during the time period of release and reception and has a constant direction. In other words, the model uses the time average of the wind speed and wind direction [121]. The classical Gaussian plume model also assumes that there is a continuous release of the emissions. The ensemble average (i.e., probabilistic) plume shape is approximated by the time average to sufficiently smooth the effects of plume meandering [121].

In Gaussian models, the atmospheric dispersion parameters are functions of either distance from the release point or time since release [43, 127]. They may also be functions of atmospheric stability and surface roughness. The equation for the Gaussian plume is a function only of the mean wind speed and the crosswind and vertical standard deviations $\big(\sigma_y(x)$ and $\sigma_z(x)\big)$. The contaminant concentration, $C(x, y, z)$, is given by

$$C(x,y,z) = \frac{Q}{2\pi\sigma_y\sigma_z v}\exp\left[-\frac{1}{2}\left(\frac{y}{\sigma_y}\right)^2\right]\left\{\exp\left[-\frac{1}{2}\left(\frac{z-h_\mathrm{s}}{\sigma_z}\right)^2\right] + \exp\left[-\frac{1}{2}\left(\frac{z+h_\mathrm{s}}{\sigma_z}\right)^2\right]\right\} \tag{4.1}$$

where Q is the source strength expressed as mass of released material per unit time, v is time averaged wind speed that is assumed to be uniform everywhere, σ_y is the standard deviation of $C(x, y, z)$ in the cross-wind direction (in this case in the $y-$axis) and σ_z is the standard deviation of $C(x, y, z)$ in the vertical direction. The z-dependent terms model the trapping effect of the ground by proposing a mirror source at a distance h_s beneath the ground [121]. Note that the dispersion parameters σ_y and σ_z are function of the downwind direction, x.

Gaussian models are not directly applicable to small-scale dispersion within the ur-

ban canopy, since they treat buildings and other obstacles only via a surface roughness parametrization [190]. The Gaussian dispersion models are applicable for pollutant emissions into uniform atmospheric flow [174]. The main problem of Gaussian models is their validation, as they include several empirical parameters often derived from experimental data [127]. Moreover, the validity of results is limited to street geometries and dispersion conditions similar to those for which the validation was carried out [127].

Although generally it is accepted that Gaussian dispersion models are not suitable for predicting flows and concentrations in complex-structure urban or industrial areas [174], many authors use them in urban streets by introducing surface roughness variables [43, 127] or error functions [112]. For short-range local problems (0-5 km) simple Gaussian type models have generally been used [174]. Despite their shortcomings, Gaussian dispersion models are used for industrial applications (i.e., point sources). Moreover, specially designed Gaussian plume models are used to calculate pollutant concentrations over urban agglomerations (i.e., area sources) and in the vicinity of highways (i.e., line sources) [190]. Gaussian tools are widely used in risk analysis procedures, providing fast dispersion estimations and usually reliable results when describing unobstructed gas flow over flat terrain [121]. For example the Gaussian models STREET [90], CPBM [202], and OSPM [85] have been developed as relatively simple tools that require less expertise and computational resources [127].

CFD dispersion models

The term Computational Fluid Dynamics (CFD) refers to a branch of fluid mechanics that uses numerical methods and algorithms to solve and analyze the dynamics of fluid (liquid and gas) flows. Computers are heavily used in order to perform the computations required for simulating the interaction of the fluids with the environment. Since the CFD modeling approaches are powerful modeling techniques, they are extensively used in the modeling of the dispersion of emissions from industries and traffic [70]. The CFD dispersion models are capable of dealing with irregularly shaped walls and other boundary conditions using flexible fine-scale grids [190]. Furthermore, since they usually include advanced turbulence treatment schemes, the CFD models are suitable for small-scale pollutant dispersion applications [174].

The governing fluid flow and dispersion equations of the CFD models are derived from the basic conservation and transport principles: mass conservation, momentum conservation, and pollutant transport [174, 190]. To directly solve these equations (especially in a turbulent flow) of dispersion of emissions, a very fine grid is required to capture all the relevant scales [174]. Furthermore, a time-dependent solution over a sufficiently long period is needed to yield stable time averages of the flow variables. This approach is called Direct Numerical Simulation (DNS). As the computational demand is too high, DNS is not applicable for real-time applications [121, 174].

The computational demand can be substantially reduced when the time-dependent equations are solved on a grid that is fine enough to resolve the larger atmospheric eddies [174]. This approach is called large eddy simulation [174]. However, since the large eddies are always unsteady, large eddy simulation models require input conditions that are time dependent as well [174]. Although less demanding than DNS, large eddy simulation dispersion models still require significant computation time, which renders them unsuitable for on-line applications [174, 190].

In order to tackle the computational issues, the Reynolds-Average Navier-Stokes approaches are most widely used in most CFD methods [161]. In these approaches the equations are averaged in time over all turbulent scales, to directly yield the statistically steady-state solution of the mean and turbulent flow [174]. Yet the computation time is still so high that such models cannot be used for real-time applications. However, despite the expensive computation time CFD models require, their popularity is increasing to describe the flow field in urban street canyons [126, 161, 201], because the CFD models provide accurate estimates of the dispersion of the emissions and they can also be applied to heterogeneous topologies which is the case in urban areas [34, 122, 127, 172, 190].

Reduced-scale dispersion models

Reduced-scale dispersion models are models that are developed based on the similarity principle [190]. By reducing the physical (geometrical) scale of a given flow domain, where the flow of the dispersion is required to be modeled, a similarity is established. The parameters in the reduced scale are adjusted to the original full-scale conditions such that the fundamental flow dynamics are reproduced. Then, based on the reduced scale of the dispersion environment, a model can be developed or all possible scenarios can be studied within the small-scale controlled environment.

The reduced-scale modeling is conducted in a wind tunnel or water tank facilities [190]. In either of these facilities, the dispersion of emissions is experimented and models are validated. In practice, wind tunnels are more often used for simulating pollutant dispersion than water tanks. However, the same principles and considerations can be also applied to methods based on water tank facilities [190]. Although it is a difficult task to scale the full-scale environment to a wind tunnel facility, the wind tunnel modeling can efficiently approximate real atmospheric conditions in urban streets. Moreover, it allows isolating and studying separately each one of the dispersion phenomena involved in micro-scale pollutant dispersion [190].

As [190] describes it, three monitoring techniques have been often used in wind tunnel experiments:

- Visualization of the flow: Visualization of the flow aids in exploring all possible flow and patterns of the dispersion of emissions that can be obtained for different arrangements of the buildings in the urban or freeway areas.
- Tracer dispersion: It is important to quantify the concentration of emissions (or tracer such as dye, ionic salt, or radioactive materials) at the receptor location near to freeway or urban streets. With the wind tunnel experiments it is possible to quantify the relationship between the quantity of the concentration and the position of the receptors in either urban or freeway streets.
- Laser Doppler Anemometry (LDA): This technique is used to study in more detail the patterns observed during flow visualization experiments.

Since the dispersion phenomena in the real environment (or full-scale reality) cannot be fully described by the reduced-scale wind tunnel models, most often reduced-scale modeling is used as a complementary tool to numerical modeling. Moreover, these models have been useful in model development and validation [14]. Nevertheless, differences between reduced-scale and full-scale systems should be carefully considered when validating numerical models [190].

4.1.2 Applications of dispersion models

Dispersion models have a wide range of applications. Although the main goal of all dispersion models is to provide an accurate estimate or prediction of the dispersion of emissions from an emission source, their application domains are diverse. Scientists use dispersion models to understand the physical and chemical phenomena that govern the diffusion and dispositions of pollutant both over time and space. The dispersion models can be used to underline the dominant factors of dispersion and to research methods or techniques that can be used to affect these factors.

Dispersion models can be used to assess the impact of new infrastructure on the dispersion of emissions to target zones. The models can be used in the design and development of new road infrastructures and new buildings near traffic networks with intense traffic flows. For example, the direction of windows, doors, and inclination of roofs can be designed in such a way that the pollution from road networks does not become a health threat. Dispersion models can also be used to study the resulting impact of pollution shields along the sides of traffic roads.

Moreover, traffic engineers and researchers can study the impact of traffic control solutions on the level of emissions dispersed to neighborhoods of the traffic networks. The models can be used to find a trade-off between the demand for reduced travel times and the need for reduced emission levels, in particular in specific target zones. Since reduction of the overall emissions of freeway does not necessarily mean reduced emission levels in a particular target zone (e.g., hospitals, schools, residences, and parks), consideration of dispersion of emissions to target zones during the design of traffic control strategies is of paramount importance. Therefore, dispersion models can be useful in such applications.

Dispersion models are now widely used for assessing road side air quality by providing predictions of present and future air pollution levels as well as temporal and spatial variations [176]. The models can also be used to prioritize locations for emergency medical responses in the immediate aftermath of a release of emissions due to any unexpected disasters [161].

In summary, the general overview of the existing emissions dispersion models highlights that the dispersion models described above cannot be used for on-line applications, which is the main core of the control approach proposed in Part II of this thesis. Although the Gaussian models are relatively faster than the CFD models, they still suffer from high computation times. Moreover, the Gaussian models assume constant wind speed and wind direction. Therefore, in the next sections of this chapter, new traffic emissions dispersion models that are computationally efficient and that take the variation of the wind speed and wind direction into account are presented. First, the basic concept on which the models are developed—the point-source model—is presented in Section 4.2. Next, new grid-based models are presented in Section 4.3.

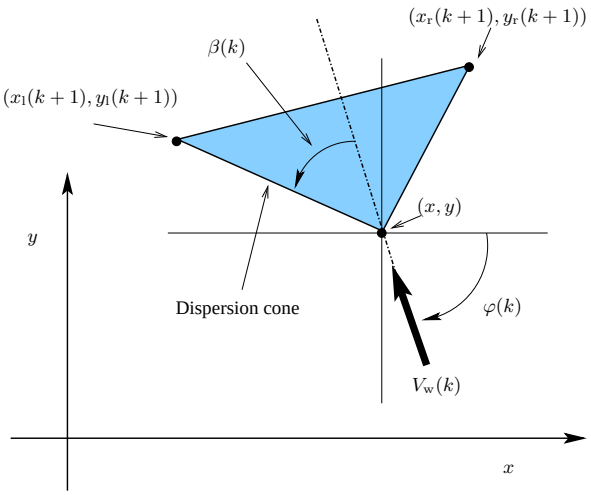

Figure 4.1: Dispersion of emissions from a point source in a 2D Cartesian coordinate system.

4.2 Point source dispersion modeling

4.2.1 Basic dispersion model

In this section, the dispersion of the emissions from vehicles in a section of a freeway is modeled using a point source approach. As an emission source, let us consider a point in a 2D Cartesian coordinate system denoted by (x, y) as shown in Fig. 4.1. The variables $V_w(k)$ and $\varphi(k)$ respectively denote the wind speed and wind direction at the point (x, y) and during the time interval $[kT, (k+1)T)$.

If the point emission source at the point (x, y) and at time step k has emitted a certain amount of emissions, the emissions will diverge and propagate due to the combined wind, temperature, and dispersion effects. For simplicity, at this point, the wavefronts of the emissions are assumed to be straight lines. Moreover, half of the divergence angle of the emissions from the point source at (x, y) at time step k is denoted by $\beta(k)$. This angle $\beta(k)$ describes the dispersion cone as depicted in Fig. 4.1. Since the emissions from vehicles are relatively more dense and have a higher temperature than the air particles, the emitted gases also expand sideways. The expansion of the emissions is inversely related to the wind speed [13]. Moreover, the sideways expansion of the emissions is dependent on other factors (such as the temperature and the inherent emissions characteristics). Since the emissions get dispersed in all directions when the wind speed is zero, the maximum value of $\beta(k)$ for a flat surrounding without any obstructions is $\beta_{\max} = \pi$. Moreover, the angle gets smaller as the wind speed increases. Hence, the relationship between the wind speed and dispersion parameter is considered to be

$$\beta(k) = \frac{\beta_{\max}}{1 + \beta_0 V_w(k)} \tag{4.2}$$

where $\beta_{\max} \in [0,\ \pi]$ denotes half of the maximum divergence angle at zero wind speed and

β_0 is model parameter that depends on the temperature and other dispersion factors.

As the emissions propagate (or disperse) in the direction of the wind, they form a dispersion cone as depicted in Fig. 4.1. The dispersion cone is represented by the left-most point $(x_{\mathrm{l}}(k+1), y_{\mathrm{l}}(k+1))$, the right-most point $(x_{\mathrm{r}}(k+1), y_{\mathrm{r}}(k+1))$, and the source point (x, y). The left-most point and the right-most point are computed as

$$x_{\mathrm{l}}(k+1) = x - TV_{\mathrm{w}}(k)\frac{\cos(\varphi(k) - \beta(k))}{\cos(\beta(k))} \tag{4.3}$$

$$y_{\mathrm{l}}(k+1) = y + TV_{\mathrm{w}}(k)\frac{\sin(\varphi(k) - \beta(k))}{\cos(\beta(k))} \tag{4.4}$$

$$x_{\mathrm{r}}(k+1) = x - TV_{\mathrm{w}}(k)\frac{\cos(\varphi(k) + \beta(k))}{\cos(\beta(k))} \tag{4.5}$$

$$y_{\mathrm{r}}(k+1) = y + TV_{\mathrm{w}}(k)\frac{\sin(\varphi(k) + \beta(k))}{\cos(\beta(k))} \tag{4.6}$$

if $\beta(k) \neq 0$.

These model equations are the basis for the derivation of the dispersion models in the subsequent sections. In the ensuing sections, the dispersion of the emissions for constant and variable wind cases is first presented. Next, these concepts will be used to develop an extended grid-based dispersion model in Section 4.3.1.

4.2.2 Variable-wind dispersion model

Throughout the modeling process in the following sections of this thesis, the areas near the freeways are assumed to be flat topographically. Moreover, as in [25, 43, 96, 123] it is assumed that the meteorological conditions are horizontally homogeneous. This means that the wind direction and wind speed responsible for transporting the plume from the emission source to the target zone and the turbulence and temperature responsible for diffusion are assumed not to change with location throughout the neighborhood of the freeway.

It has been pointed out that in the close vicinity of the road the speeds of the vehicles influence the dispersion of the emissions [13]. In the region far from the freeway, where most residences, schools, and other buildings are located, the dispersion of the emissions is primarily dependent on the speed and direction of the wind and the temperature of the atmosphere [13]. Since this thesis focuses on the dispersion of emissions (i.e., area-wide emissions) at specific locations at a large distance (e.g., 1 km or more) from a traffic freeway, the effect of the speed of the vehicles on the dispersion of the emissions is assumed to be negligible. Moreover, the wavefronts of the emissions are considered approximately planar at far distance from the freeway. Then, the emission particles will move due to wind and dispersion effects and the trajectory of the dispersion of the emissions will be captured by straight line wavefronts moving orthogonal to the wind direction and dispersion cones. The emissions are also assumed to emanate from the center point[1] of the segments of the links. This assumption is valid when the length of the freeway segment is much smaller than the distance from the segment to the target.

Fig. 4.2(a) shows the propagation of emissions of vehicles from segment i of a link m at

[1]This point modeling approach can also be extended to a line modeling approach, where the emissions are considered to emanate from a center line parallel and equal to the segments.

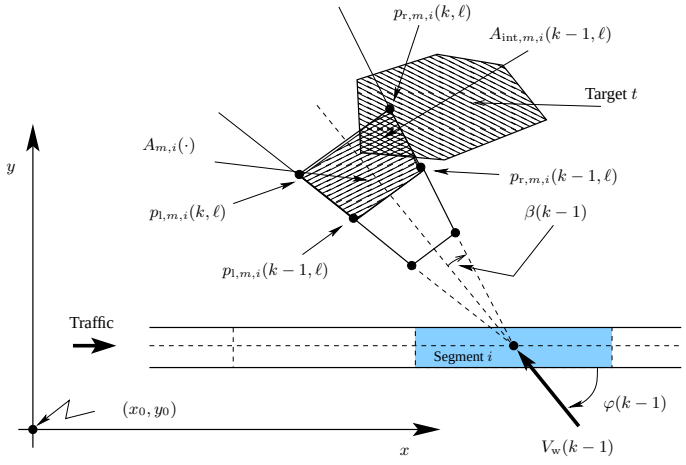

(a) At time instant $(k-1)T$

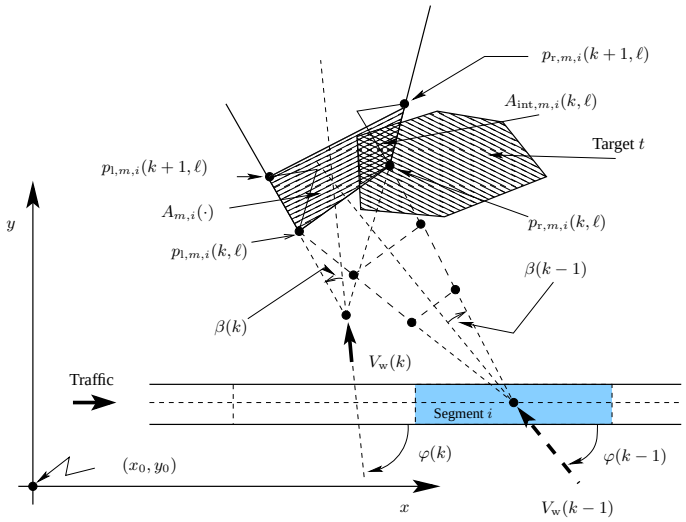

(b) At time instant kT

Figure 4.2: Schematic representation for a snapshot of horizontal dispersion of vehicle emissions with varying wind speed and angle.

time step $k-1$. The emissions propagate with a line wavefront in the direction of the wind. The sideways dispersion of the emissions from the source is modeled by the divergence angle $\beta(k)$ (4.2). At time step k the divergence angle corresponds to half of the angle of the dispersion cone (see Fig. 4.1).

Here we approximate wavefronts emanating from segment i of link m by lines with $p_{\mathrm{l},m,i}(k,\ell)$ as left-most[2] point of the emission front at time step k that was released from segment i of link m at time step ℓ, and $p_{\mathrm{r},m,i}(k,\ell)$ as right-most[2] point of the emission front at time step k that was released from segment i of link m at time step ℓ. Any emission

[2]With respect to the wind direction.

at a point of the wavefront formed by a line segment joining the points $p_{\mathrm{l},m,i}(k,\ell)$ and $p_{\mathrm{r},m,i}(k,\ell)$ diverge with an angle equal to $\beta(k)$ both to the left and to the right with respect to the wind direction (e.g., see the points $p_{\mathrm{l},m,i}(k,\ell)$ and $p_{\mathrm{r},m,i}(k,\ell)$ in Fig. 4.2(a) and 4.2(b)). Each of these points on the line between $p_{\mathrm{l},m,i}(k,\ell)$ and $p_{\mathrm{r},m,i}(k,\ell)$ results in a small cone due to wind and dispersion factors. Now, one can approximate the resulting wavefront by the line formed by joining the left-most point $p_{\mathrm{l},m,i}(k+1,\ell)$ of the emission cone for the left-most point and the right-most point $p_{\mathrm{r},m,i}(k+1,\ell)$ of the emission cone for the right-most point of the previous wavefront.

In general, the wind speed and the wind direction change in time and space. Let us suppose that the wind speed and direction have changed (see $V_{\mathrm{w}}(k)$ and $\varphi(k)$ in Fig. 4.2(b)) at time step k. This means that the dispersion speed and dispersion direction at every point of the wavefront formed by the line segment joining the points $p_{\mathrm{l},m,i}(k,\ell)$ and $p_{\mathrm{r},m,i}(k,\ell)$ will change (see the small cones at these points in Fig. 4.2(b)). During the time period $[kT,(k+1)T)$ the emissions at the wavefront formed by the line segment joining the points $p_{\mathrm{l},m,i}(k,\ell)$ and $p_{\mathrm{r},m,i}(k,\ell)$ will reach the wavefront formed by the line segment joining the points $p_{\mathrm{l},m,i}(k+1,\ell)$ and $p_{\mathrm{r},m,i}(k+1,\ell)$ due to the wind speed $V_{\mathrm{w}}(k)$ and wind direction $\varphi(k)$ as shown in Fig. 4.2(b). Then, the evolution of the end points of the wavefronts $p_{\mathrm{l},m,i}(k+1,\ell) = (x_{\mathrm{l},m,i}(k+1,\ell), y_{\mathrm{l},m,i}(k+1,\ell))$ and $p_{\mathrm{r},m,i}(k+1,\ell) = (x_{\mathrm{r},m,i}(k+1,\ell), y_{\mathrm{r},m,i}(k+1,\ell))$ is modeled by adapting (4.3)–(4.6) as

$$
\begin{aligned}
x_{\mathrm{l},m,i}(k+1,\ell) &= x_{\mathrm{l},m,i}(k,\ell) - TV_{\mathrm{w}}(k)\frac{\cos(\varphi(k)-\beta(k))}{\cos(\beta(k))},\\
y_{\mathrm{l},m,i}(k+1,\ell) &= y_{\mathrm{l},m,i}(k,\ell) + TV_{\mathrm{w}}(k)\frac{\sin(\varphi(k)-\beta(k))}{\cos(\beta(k))},\\
x_{\mathrm{r},m,i}(k+1,\ell) &= x_{\mathrm{r},m,i}(k,\ell) - TV_{\mathrm{w}}(k)\frac{\cos(\varphi(k)+\beta(k))}{\cos(\beta(k))},\\
y_{\mathrm{r},m,i}(k+1,\ell) &= y_{\mathrm{r},m,i}(k,\ell) + TV_{\mathrm{w}}(k)\frac{\sin(\varphi(k)+\beta(k))}{\cos(\beta(k))}.
\end{aligned}
$$

Now, let us consider the wavefront formed by the points $p_{\mathrm{l},m,i}(k,\ell)$ and $p_{\mathrm{r},m,i}(k,\ell)$ and let $J_{\bar{y},m,i}\big(p_{\mathrm{l},m,i}(k,\ell), p_{\mathrm{r},m,i}(k,\ell)\big)$ be the corresponding emission rate for emission $\bar{y} \in \bar{\mathcal{Y}}/\{\mathrm{fuel}\}$ at time step k (see Chapter 3). Then, the emission for the next wavefront is

$$
J_{\bar{y},m,i}(p_{\mathrm{l},m,i}(k+1,\ell), p_{\mathrm{r},m,i}(k+1,\ell)) = (1-\gamma)J_{\bar{y},m,i}(p_{\mathrm{l},m,i}(k,\ell), p_{\mathrm{r},m,i}(k,\ell)) \quad (4.7)
$$

where $0 \leq \gamma < 1$ is a factor that characterizes the vertical dispersion (evaporation).

Then the area that is subject to the emission $J_{\bar{y},m,i}\big(p_{\mathrm{l},m,i}(k+1,\ell), p_{\mathrm{r},m,i}(k+1,\ell)\big)$ during the time period $[kT,\ (k+1)T)$ is the tetragon formed by the points $p_{\mathrm{l},m,i}(k,\ell)$, $p_{\mathrm{l},m,i}(k+1,\ell)$, $p_{\mathrm{r},m,i}(k+1,\ell)$, and $p_{\mathrm{r},m,i}(k,\ell)$. The area of this tetragon is denoted by $A_{m,i}\big(p_{\mathrm{l},m,i}(k,\ell), p_{\mathrm{l},m,i}(k+1,\ell), p_{\mathrm{r},m,i}(k+1,\ell), p_{\mathrm{r},m,i}(k,\ell)\big)$. Let the area of the intersection of the target zone t and the tetragon formed by the emission wavefronts be denoted by $A_{\mathrm{int},m,i}(k,\ell)$. Then, the amount of emission $\bar{y}$ released at time step ℓ from segment i of link m and that is dispersed to the target zone t from segment i of link m during the time

period $[kT,\ (k+1)T)$ can be computed as

$$J_{\bar{y},t,m,i}(k+1,\ell) = \frac{TA_{\mathrm{int},m,i}(k,\ell)J_{\bar{y},m,i}\big(p_{\mathrm{l},m,i}(k+1,\ell), p_{\mathrm{r},m,i}(k+1,\ell)\big)}{A_{m,i}\big(p_{\mathrm{l},m,i}(k,\ell), p_{\mathrm{l},m,i}(k+1,\ell), p_{\mathrm{r},m,i}(k+1,\ell), p_{\mathrm{r},m,i}(k,\ell)\big)}. \tag{4.8}$$

Since the wavefronts are emanating from segment i of link m at each time step, we have to consider the sum of $J_{\bar{y},t,m,i}(k+1,\ell)$ over all wavefronts emitted in the past that intersect with the target zone t during the time period $[kT,(k+1)T)$. Let this total emission level be denoted by $J_{\mathrm{tot},\bar{y},t,m,i}(k+1)$. Thus the emission level of $\bar{y}$ at the target zone t over the time period $[kT,(k+1)T)$ due to all segments of the links in a freeway network will be

$$D_{\bar{y},t}(k) = \sum_{(m,i)\in\mathcal{M}_{\mathrm{all}}} J_{\mathrm{tot},\bar{y},t,m,i}(k) \tag{4.9}$$

where $\mathcal{M}_{\mathrm{all}}$ is the set of all pairs of segment and link indices.

Due to the continuous variation of the wind speed and wind direction, the geometrical shape and size of the intersection $A_{\mathrm{int},m,i}(k)$ between the target zone t and the dispersion tetragon $A_{m,i}(\cdot)$ changes frequently. Therefore, it is not possible to derive a general closed form analytical expression for $A_{\mathrm{int},m,i}(k)$ and its area. Moreover, as the number of target zones considered increases, the number of intersections that have to be determined increases. Consequently, the computation time is high and as a result this modeling approach cannot be applied for on-line based control applications. However, on the basis of the concepts presented above two computationally efficient grid-based dispersion models are presented in the following section.

4.3 Grid-based dispersion modeling

In this section two grid-based dispersion models are proposed. First, an extension of the variable-wind dispersion model is presented in Section 4.3.1. Next a more computationally efficient dispersion model is proposed in Section 4.3.2 by exploiting the basic concepts of the point-source dispersion model.

4.3.1 Extended grid-based dispersion model

Since the emissions from a segment of a freeway are better described in a narrow and long area emissions source, instead of approximating the emissions as a point source, the area around the neighborhood of the freeway is gridded as in Fig. 4.3(a), where the grid cells are of equal dimensions. Next, all the emissions from the part of the freeway within the cell are aggregated and assigned to the cell uniformly. Then, the evolution of the emission levels in each of the cell of the grid is modeled using the point-source approach. This means that the evolution of the emission sources within a cell, the effects of the emissions from the neighboring cells, and other external factors (e.g., polluting industries) are modeled. In the sequel a way these phenomena can be captured is presented.

The thick gray line represents a part of a freeway traffic network. Each cell is denoted by $C_{i_{\mathrm{c}},j_{\mathrm{c}}}$, where the subscript i_{c} indicates the position of the cell in the x direction and the subscript j_{c} indicates the position of the cell in the y direction. A cell $C_{i_{\mathrm{c}},j_{\mathrm{c}}}$ is described

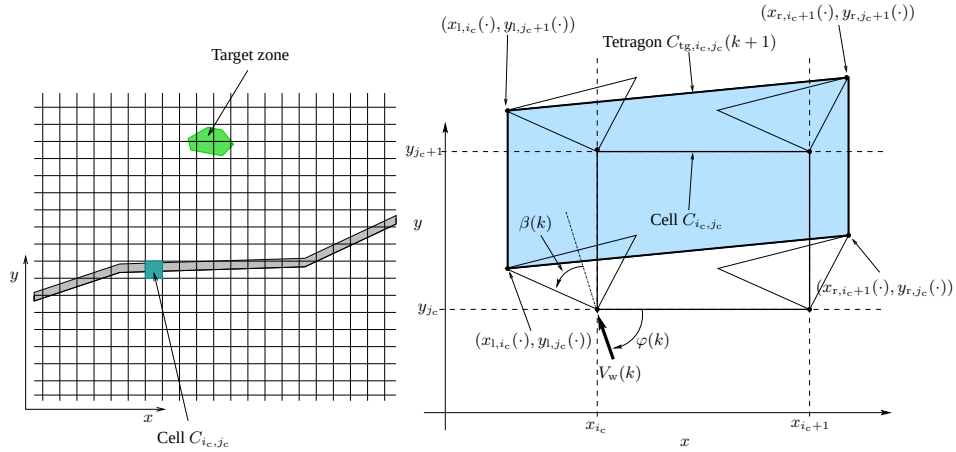

(a) Grid cells of the areas around a freeway. (b) Dispersion from cell C_{i_c,j_c}

Figure 4.3: Schematic representation of area-source dispersion of emissions in 2D space.

by the four corner points (x_{i_c}, y_{j_c}), (x_{i_c+1}, y_{j_c}), (x_{i_c+1}, y_{j_c+1}), and (x_{i_c}, y_{j_c+1}), where $x_{i_c} < x_{i_c+1}$ and $y_{j_c} < y_{j_c+1}$ (see also Fig. 4.3(b)).

Let the emission level in cell C_{i_c,j_c} for emission $\bar{y} \in \bar{\mathcal{Y}}/\{\mathrm{fuel}\}$ at a time step k be denoted by $J_{\bar{y},i_c,j_c}(k)$. The emission level $J_{\bar{y},i_c,j_c}(k)$ includes the rate at which the emission $\bar{y}$ is dispersed from the neighboring cells, the rate at which the emission $\bar{y}$ is generated by the part of the freeway in the cell, and the rate at which the emission $\bar{y}$ is dispersed from sources within the cell (e.g., polluting factories). Then, the emissions in cell C_{i_c,j_c} can be considered as emissions emanating from a continuum of uniformly distributed point sources. These emissions get dispersed according to the point source model discussed in Section 4.2. But, since it is assumed that the meteorological factors are horizontally homogeneous, it is not important to trace the dispersion of all the point sources. In fact, one only has to track the dispersion of the emissions at the corner points of the cells, where each corner point yields a dispersion cone as shown in Fig. 4.3(b).

During the time period $[kT,\ (k+1)T)$, the emission level $J_{\bar{y},i_c,j_c}(k)$ of emission $\bar{y}$ of cell C_{i_c,j_c} will propagate to the dispersion zone denoted by the tetragon $C_{\mathrm{tg},i_c,j_c}(k+1)$. This is schematically represented in Fig. 4.3(b) with the shaded area. The corner points of the tetragon $C_{\mathrm{tg},i_c,j_c}(k+1)$ are formed by the extremal points of the dispersion cones formed at the corner points of the cell C_{i_c,j_c} and these extremal points are denoted by $(x_{\mathrm{l},i_c}(k+1), y_{\mathrm{l},j_c}(k+1))$, $(x_{\mathrm{r},i_c+1}(k+1), y_{\mathrm{r},j_c}(k+1))$, $(x_{\mathrm{r},i_c+1}(k+1), y_{\mathrm{r},j_c+1}(k+1))$, and $(x_{\mathrm{l},i_c}(k+1), y_{\mathrm{l},j_c+1}(k+1))$.

Let us denote the area of the dispersion tetragon $C_{\mathrm{tg},i_c,j_c}(\cdot)$ by $A_{\mathrm{tg},i_c,j_c}(\cdot)$ and the area of the cell C_{i_c,j_c} by A_{i_c,j_c}. It is assumed that the cell C_{i_c,j_c} has at most eight neighboring cells that disperse emissions to the cell. This assumption is valid if the dimension of the cells is greater than the distance traveled by the emissions in one simulation time step, which is related to the CFL criterion encountered in [47]. Otherwise, the cells that disperse emissions to cell C_{i_c,j_c} can be different from just the immediate neighboring cells. The immediate neighboring cells are: C_{i_c-1,j_c+1}, C_{i_c,j_c+1}, C_{i_c+1,j_c+1} to the top, C_{i_c-1,j_c} and C_{i_c+1,j_c} to the left and right respectively, and C_{i_c-1,j_c-1}, C_{i_c,j_c-1}, C_{i_c+1,j_c-1} to the bottom

of the cell. Then, during the evolution of the emissions of cell C_{i_c,j_c}, the dispersion tetragon $C_{\mathrm{tg},i_c,j_c}(k+1)$ could be dispersed to each of the neighboring cells and part of it can remain in the original cell C_{i_c,j_c}. Moreover, emissions from the neighboring cells can be dispersed to cell C_{i_c,j_c}. Therefore, the emission level $J_{\bar{y},i_c,j_c}(k+1)$ at which the emission $\bar{y}$ will be dispersed in cell C_{i_c,j_c} during the time period $[kT,\ (k+1)T)$ is given by

$$\begin{aligned} J_{\bar{y},i_c,j_c}(k+1) &= J_{\mathrm{src},\bar{y},i_c,j_c}(k) + J_{\mathrm{ext},\bar{y},i_c,j_c}(k) \\ &\quad + (1-\gamma(k)) \sum_{(u_c,v_c)\in\mathcal{N}(i_c,j_c)} \frac{\mathcal{A}(C_{i_c,j_c} \bigcap C_{\mathrm{tg},u_c,v_c}(k+1))}{A_{\mathrm{tg},u_c,v_c}(k+1)} J_{\bar{y},u_c,v_c}(k) \end{aligned} \tag{4.10}$$

where $J_{\mathrm{src},\bar{y},i_c,j_c}(k)$ is the emission level at which emission $\bar{y} \in \bar{\mathcal{Y}}/\{\mathrm{fuel}\}$ generated by sources (e.g., vehicles in a part of a freeway in the cell) in cell C_{i_c,j_c} at time step k and $\bar{\mathcal{Y}} = \{\mathrm{CO}, \mathrm{CO_2}, \mathrm{HC}, \mathrm{NO}_x, \mathrm{fuel}\}$, $J_{\mathrm{ext},\bar{y},i_c,j_c}(k)$ is the emission level at which emission $\bar{y}$ is generated by external sources (e.g., factories) that contribute to the emission level of $\bar{y}$ in cell C_{i_c,j_c} at time step k, $\mathcal{N}(i_c,j_c)$ denotes the set of neighbors to cell C_{i_c,j_c} and the cell itself, $C_1 \bigcap C_2$ denotes the intersection of polytopes C_1 and C_2, $\mathcal{A}(C)$ denotes the area of the polytope C, and $0 \leq \gamma(k) < 1$ is a factor that characterizes the vertical dispersion of the emissions.

The emission level at the target zone t is therefore computed by summing up the fraction of the emissions contributed by each cell that intersects with the target zone t. Mathematically, the emission level of $\bar{y}$ at the target zone t at time step k is given by

$$D_{\bar{y},t}(k) = T \sum_{(i_c,j_c)\in\mathcal{T}_{\mathrm{int},t}} \frac{\mathcal{A}(C_{\mathrm{target},t} \bigcap C_{i_c,j_c})}{A_{i_c,j_c}} J_{\bar{y},i_c,j_c}(k) \tag{4.11}$$

where $C_{\mathrm{target},t}$ is the polytope describing the target zone t and $\mathcal{T}_{\mathrm{int},t}$ is the set of all cells in the grid that have a non-zero intersection with the target zone t.

To sum up, the main advantages of this extended grid-based dispersion model are that it can easily and without additional computational effort include multiple target zones; that it is computationally fast; that it takes the variation of wind speed and wind direction into account; that it provides the evolution of emissions over the region around the freeway rather than only focusing on the target zone; and that it also considers the effect of emissions from other emission sources like factories.

However, this model has one drawback that emanates from the point source approach. When the wind speed is zero, the dispersion of the emissions is not modeled. So, in the sequel we propose a grid-based approach that uses the point-source model as conceptual basis and that captures the dispersion of emissions in the no wind case. Moreover, this second grid-based model requires less computation time than the extended grid-based dispersion model. Since the coordinates of the dispersion tetragon in the extended grid-based dispersion model are dependent on the wind speed and direction, it is difficult to have a simple analytic solution to the intersection of the dispersion tetragon and the cells. This leads to a continuous computation of the intersections. In the model to be presented below, a general analytic solution for the intersections can be provided and thereby the computation time is reduced.

4.3.2 Expanding grid-based dispersion model

When the wind speed is zero and there are no other obstructions, emissions expand in all directions uniformly. However, this phenomenon is not reflected in the point source model or the extension of it presented above. This section presents how to model this phenomenon and how to reduce the computation time further. We call the resulting model the expanding grid-based dispersion model.

Dispersion modeling concept

When the wind speed is zero, the coordinate points that are computed using (4.3)–(4.6) are the same as the emission source point. Under such cases, the divergence angle in (4.2) becomes $\beta_{\max}$, which under no obstruction is equal to π. This indicates that the emission should be expanding (diverging) in all directions. The problem is that due to the zero wind speed the coordinate points do not move a distance away from the emission source point, which means that according to the model equations (4.3)–(4.6) there is no dispersion of the emissions over the horizontal 2D plane.

This problem could be solved by adding a term to the coordinate variables that is dependent on the temperature and the inherent dispersion factors of the emissions. But, since the point source dispersion model is based on the assumption that the emission wavefronts move as a straight line, which is valid for higher wind speeds, the added term will result in emissions moving into one direction along a line without dispersing sideways.

However, if one would consider the dispersion wavefront to be a curve, under no wind condition this curve would be a circle and the added term would be the expansion factor of the emissions. It is this analysis that led to the development of the expanding grid-based dispersion model. Hence, when there is no wind and no other external disturbances, emissions expand in all directions. In the ideal case, the shape of the expansion is a circle for a point emission source. When there is a non-zero wind speed, the expanding emissions (circles of emissions) will move in the direction of the wind while continuing to expand uniformly. This is the main concept for the development of the expanding grid-based dispersion model.

Expanding emission cells and emission levels

Just as in the case of the extended grid-based-dispersion model, we grid the region around the freeway into squares of equal dimensions. But, unlike in the extended grid-based dispersion model, where the corner points of a cell are considered, here the center of the cells is taken as a representative of the emissions in the cell.

We denote the expansion factor of the emissions of the grid at time step k cells by $\varpi(k)$ per unit time in each direction. For computational simplicity reasons it is assumed that the shape of the expanding emission cells remains intact. Hence, when the wind speed is zero, the emissions in the cell C_{i_c,j_c} expand due to dispersion factors as illustrated by the shaded region in Fig. 4.4(a) and the sides of the expanded cells at time step k are approximated by squares of length

$$L_e(k) = (1 + T\varpi(k))L \tag{4.12}$$

where L is the length of the sides of the grid cells.

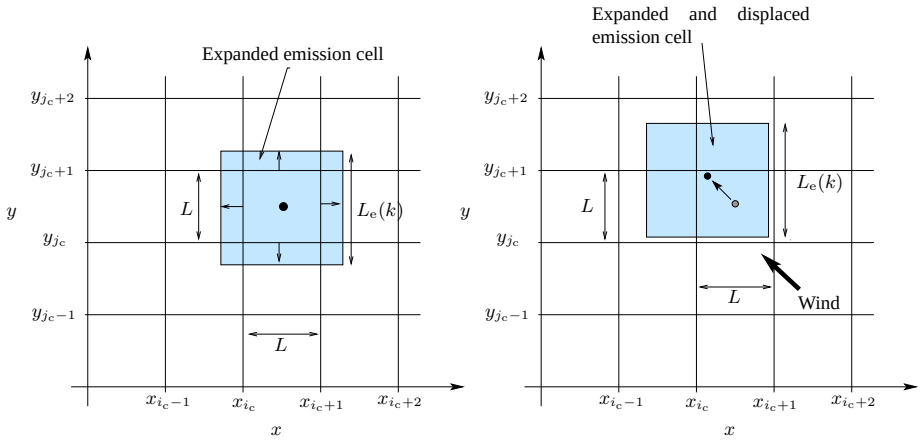

(a) Under no-wind condition (b) Under windy condition

Figure 4.4: Expansion of emissions from a cell under windy and no-wind conditions.

When the wind speed is non-zero, the expanded emission cell of cell C_{i_c,j_c} is displaced in the wind direction as depicted in Fig. 4.4(b). We use the center points of the (expanded) emission cells to represent the displacement of the (expanded) emission cells. The corner points of the expanded emission cells can be determined from the coordinates of the displaced center point and the expansion factor. Next, we can determine the emission level in cell C_{i_c,j_c}. Although the expression for the emission level in cell C_{i_c,j_c} can be expressed in a similar way as (4.10), in this particular approach it is possible to explicitly describe the equation of the intersections between the expanded emission cells (dispersion squares) and the original grid cells with simpler equations.

So, let us suppose the level of the emission $\bar{y} \in \bar{\mathcal{Y}}/\{\text{fuel}\}$ at time step k in cell C_{i_c,j_c} is $J_{\bar{y},i_c,j_c}(k)$, then at the end of the time period $[kT,\ (k+1)T)$ the emission level in the cell becomes

$$\begin{aligned} J_{\bar{y},i_c,j_c}(k+1) =& J_{\text{src},\bar{y},i_c,j_c}(k) + J_{\text{ext},\bar{y},i_c,j_c}(k) \\ &+ (1-\gamma(k)) \sum_{(u_c,v_c)\in\mathcal{N}(i_c,j_c)} \frac{\alpha^{(u_c,v_c)}_{(i_c,j_c)}(k)}{L_e^2(k)} J_{\bar{y},u_c,v_c}(k) \end{aligned} \tag{4.13}$$

where $\alpha^{(u_c,v_c)}_{(i_c,j_c)}(k)$ denotes the area of the part of the expanded emission cell (dispersion tetragon) of cell C_{u_c,v_c} that intersects with the cell C_{i_c,j_c} at time step k and by straightforward but somewhat elaborate calculations (see Appendix B), it is found that these quantities are given by

$$\alpha^{(u_c,v_c)}_{(i_c,j_c)}(k) = a_{2+i_c-u_c}(k) \cdot b_{2+j_c-v_c}(k)$$

with

$$a_1(k) = \max\left\{0, TV_w(k)\cos(\varphi(k)) + \frac{LT\varpi(k)}{2}\right\}$$

Table 4.1: The average CPU time per cell required to compute the intersections between the neighboring cells and the dispersion tetragon (or square) of a given cell for the extended grid-based and the expanding grid-based dispersion models.

Dispersion model	CPU time [s]
Extended grid-based	0.680
Expanding grid-based	0.010

$$
\begin{aligned}
a_2(k) &= L_{\mathrm{e}}(k) - a_1(k) - a_3(k) \\
a_3(k) &= \max\left\{0, -TV_{\mathrm{w}}(k)\cos(\varphi(k)) + \frac{LT\varpi(k)}{2}\right\}
\end{aligned}
$$

$$
\begin{aligned}
b_1(k) &= \max\left\{0, -TV_{\mathrm{w}}(k)\sin(\varphi(k)) + \frac{LT\varpi(k)}{2}\right\} \\
b_2(k) &= L_{\mathrm{e}}(k) - b_1(k) - b_3(k) \\
b_3(k) &= \max\left\{0, TV_{\mathrm{w}}(k)\sin(\varphi(k)) + \frac{LT\varpi(k)}{2}\right\}
\end{aligned}
$$

provided that $T < \frac{2}{\varpi(k)}$ and $L > \frac{2TV_{\mathrm{w}}(k)}{2-T\varpi(k)}$ for all time step k. If these CFL-like conditions on T and L are not satisfied, it is still possible to derive similar formulas, which also require redefinition of the neighborhood set $\mathcal{N}(i_{\mathrm{c}}, j_{\mathrm{c}})$ of cell $C_{i_{\mathrm{c}},j_{\mathrm{c}}}$.

Note also that the computation of the above intersections gives the same result for all the cells in the grid. This means that the computation has to be done only for one cell per every simulation time step k.

The emission level at the target zone is computed in a similar way as in the extended grid-based dispersion model of Section 4.3.1. Thus, the mathematical expression for the emission $\bar{y}$ level at the target zone t at time step k is given by (4.11).

4.3.3 Comparison of grid-based dispersion models

In Sections 4.3.1 and 4.3.2, two grid-based dispersion models have been presented. In order to quantify the required computation times and to determine their competitive speeds, the two models are simulated. Since the main difference of the extended grid-based dispersion model and the expanding grid-based dispersion model lies on the determination of the intersections of the dispersion regions and the gird cells, here the time required to compute the intersections of the dispersion tetragon (square) with the neighboring cells are compared. In order to compute the intersections and the area of the polytopes of the extended grid-based dispersion model the MATLAB® Multi-Parametric Toolbox (MPT) is used [106]. Recall that in the expanding grid-based dispersion model the intersections and the area of the polytopes (or squares) have analytical solutions and hence no computation tools are required there.

The average computation time per cell required to determine the intersections of each dispersion tetragon or square for the two models is presented in Table 4.1. The results indicate that the time consumed by the extended grid-based dispersion model is much higher

than the time consumed by the expanding grid-based dispersion model. This is because the expressions for the intersections in the extended grid-based dispersion model are more complicated than those for the expanding grid-based model.

Note that since the computations are done for a single cell, these intersection values are also the same for the remaining cells in the grid. Each cell in the grid only has to update its emission levels based on the dynamic equation given by (4.10) for the extended grid-based dispersion model and by (4.13) for the expanding grid-based dispersion model. Since the computation time required to update the emission levels is negligible for each cell (i.e., only (4.10) and (4.13) have to be evaluated for each cell in the grid) and since the computation time of both the models is less than a second, both models are suitable for on-line applications that have more than 1 s simulation time step size. But if the number of the cells in the grid is very large, the update time can be large, which in turn affects the applicability of the models for on-line based applications. It can be seen that the computation time of the expanding grid-based dispersion model is even very small and thus it can also be used for on-line based control applications that perform multiple runs with in a second.

4.4 Conclusions

As dispersion of emissions to the neighborhoods of traffic networks is an important aspect that requires due attention during the development and deployment of traffic solutions, the development of computationally efficient and accurate dispersion models is of paramount importance. In cases where the reduction of overall emissions has a severe impact on the travel time, traffic managers can instead consider the reduction of the dispersion of emissions to a target zone so that the effect on the travel time can be reduced.

Bearing this in mind, this chapter has first elaborated on the existing dispersion models from literature. It has discussed the general dispersion modeling strategies and their applications. Moreover, it has highlighted on the computation demand of the models. It has also been pointed out that the existing dispersion models, in particular the CFD and Gaussian models, are not suitable for on-line based traffic control approaches.

So this chapter has proposed new dispersion models that can be used for on-line applications. The chapter has first presented a point source dispersion model. Next, a direct extension of the point source dispersion model (extended grid-based dispersion model) has been discussed. However, it was found out that the extended grid-based dispersion model has one drawback. When there is no wind, the model does not model the dispersion of the emissions. So a more elegant, expanding grid-based dispersion model has been presented. In addition to its capability to model dispersion of emissions when there is no wind, the expanding grid-based dispersion model is also faster than the extended grid-based dispersion model.

A simulation has been performed to compare the computation time required to determine the intersections of the dispersion tetragon or square and the grid cells of the two grid-based dispersion models. The simulations have shown that the computation demand of the models is less than a second, which makes both of the models suitable for on-line applications, in particular for simulation that use macroscopic traffic emission models where the simulation time step size is more than a second. Moreover, the expanding grid-based dispersion model has required very small computation time, which makes it even suitable for on-line control applications where multiple runs are performed every control time step.

In the subsequent chapters, these models will be used in an on-line based traffic control approaches.

Part II

TRAFFIC CONTROL DESIGN

Chapter 5

Model Predictive Traffic Control

Dynamic traffic control methods continuously measure the state of the traffic network and respond accordingly. Dynamic traffic control methods can either be non-predictive [145, 221] or predictive [22, 75, 220]. Since traffic systems are highly non-linear and time-variant systems, model-based predictive traffic control approaches [19, 75, 77, 220] such as Model Predictive Control (MPC) are promising candidates.

MPC is a model-based control approach that is based on the optimization of control inputs that improve a given performance criterion (objective function) over some prediction horizon. The performance criterion of MPC is formulated as a cost function of the predicted system states, outputs, or inputs. The MPC approach can be used for non-linear and time-variant systems. In addition, it can incorporate constraints on the inputs, states, and outputs of the system.

Since the core control strategy used in this thesis is MPC, this chapter provides a brief account of the basic concepts of MPC and MPC for traffic systems in Sections 5.1 and 5.2 respectively. For detailed discussions on MPC, we refer the reader to [35, 116, 120, 167]. Continuing, the traffic performance criteria and multi-criteria optimization approaches considered in this thesis are presented in Sections 5.3 and 5.4 respectively. The MPC controller is demonstrated in two simulation-based case studies for a balanced reduction of travel time, emissions, fuel consumption, and dispersion of emissions in Section 5.5. The chapter concludes with Section 5.6.

Parts of this chapter are published in [57, 208, 211, 213, 215].

5.1 Philosophy of model predictive control

Model Predictive Control (MPC) [35, 116, 120, 167], also known as Moving Horizon Control or Receding Horizon Control is a popular technique for the control of slow dynamical systems, such as those encountered in chemical process control in the petrochemical, pulp and paper industries, and in gas pipeline control [66, 98]. As in [66], this thesis too refers to MPC as family of control strategies that explicitly use models. MPC, in general, computes optimal control solutions of an on-line optimization problem that is formulated to reflect the desired performance of a system. All MPC-based control approaches share five main concepts:

System and disturbance modeling: Since the control solutions of MPC are determined based on the future evolution of the system states and outputs, and on the evolution of either the known disturbances or the probabilistic properties (or bounds) of the unknown disturbances, whether it is for off-line or on-line design, MPC requires models of the system and the unknown disturbances in order to make predictions of these variables over a future prediction period.

Performance criterion: The MPC control strategy provides optimal control solutions that improve a predefined performance criterion. Usually, the performance criterion is defined as a cost function. The cost function is defined over a future prediction period (finite or infinite). MPC then seeks optimal control solutions that minimize the cost function. Hence, definition of an appropriate cost function is an important step in the design of an MPC controller.

Constraints: MPC can handle both equality and inequality constraints on the system states, outputs, and inputs. The constraints can be motivated by the operational limits of the system, economic requirements, environmental demands, safety requirements, and the like. The constraints can be linear or non-linear. In the design of an MPC controller, the description of the constraints involved is another important aspect that requires due attention.

Optimization: MPC uses optimization techniques and tools to optimize the control inputs in such a way that the value of the given cost function is minimal. Depending on the system model, the constraints, and the cost function, the solutions obtained can be optimal or sub-optimal. In principle MPC uses on-line optimization to design optimal control inputs. But to gain some computational speeds it is also possible (in some cases) to design MPC based on off-line optimization (such MPC is known as explicit MPC [23]).

Receding horizon principle: The principle of receding horizon (or moving horizon), which is the core of MPC, was first introduced by Propoi [160] in 1963 [66]. This means that after computation of the optimal future control sequence, only the first control sample is implemented, subsequently the horizon is shifted one sample and the optimization is restarted with new information of the system. This is illustrated in Fig. 5.1(b). At every control time step k_{c}, the MPC controller determines the optimal control input that minimizes a given performance criterion over the prediction period $[k_{\mathrm{c}}, k_{\mathrm{c}} + N_{\mathrm{p}} - 1]$. The dashed line in Fig. 5.1(b) shows the control input as designed based on the predicted states (which are indicated by the dots). At the next control time step $k_{\mathrm{c}} + 1$, the MPC controller again takes the new prevailing system state and uses it to make new predictions by shifting the prediction horizon one step forward. This process is repeated continuously in the receding horizon approach discussed here.

Fig. 5.1(a) presents the interrelationship of the five concepts presented above. Measurements of the system state are collected through sensors every sampling time step k_{s} with a sampling time step size T_{s}. However, the controller receives the measurements (such as speed, density, flow, and traffic demand) every control time step k_{c} (with step size T_{c}). For the sake of simplicity and ease of implementation the control time step T_{c} is defined to be an integer multiple of the sampling time step T_{s}: $T_{\mathrm{c}} = M_1 T_{\mathrm{s}}$, where $M_1 \in \mathbb{N}$. Thus, at every control time step the sampling time and the control time are related by $k_{\mathrm{s}}(k_{\mathrm{c}}) = M_1 k_{\mathrm{c}}$.

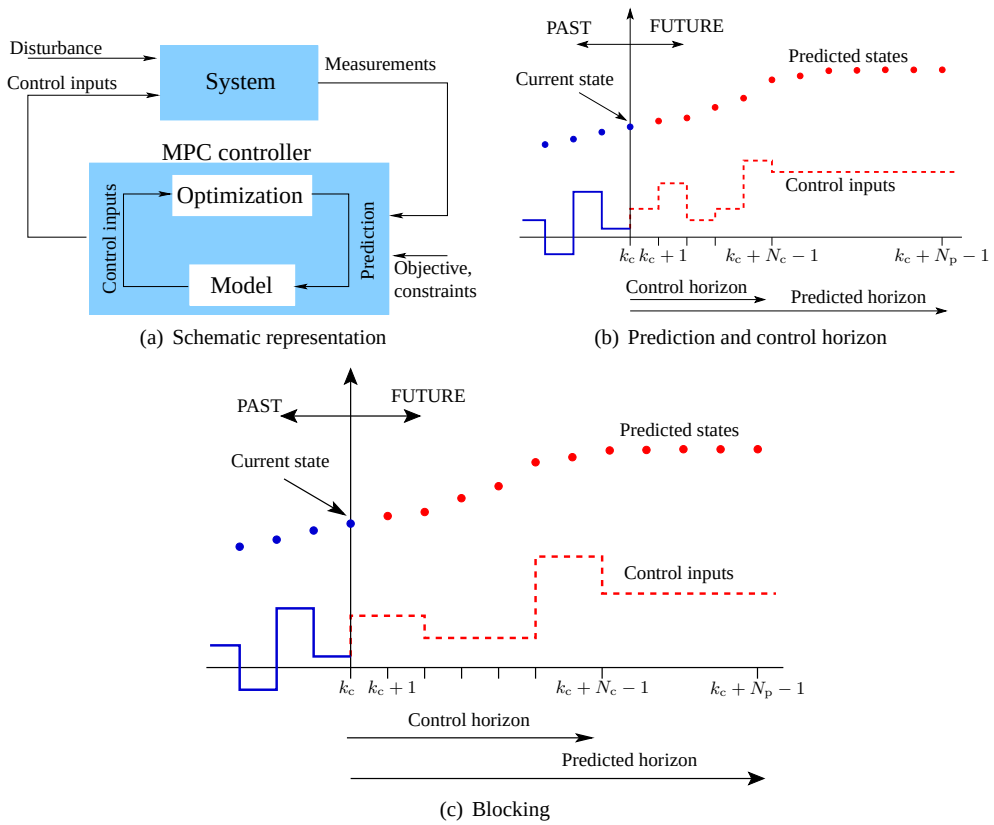

(a) Schematic representation

(b) Prediction and control horizon

(c) Blocking

Figure 5.1: Conceptual representation of model predictive control.

In addition, usually a distinction is made between the control time step k_c and the simulation time step k (or k_m for microscopically modeled systems). At every time instant of the form $t = k_\mathrm{c}T_\mathrm{c} = kT$, the control time step k_c is an integer divisor of the simulation time step k (with simulation time step size T). Thus, these are related by $k(k_\mathrm{c}) = M_2 k_\mathrm{c}$ for a positive integer M_2 (for microscopic models $k_\mathrm{m}(k_\mathrm{c}) = M_3 k_\mathrm{c}$, where M_3 is a positive integer).

The main advantages of MPC are that it takes the effect of the control inputs on the future system states, that it is able to take both equality and inequality non-linear constraints of the manipulated and controlled variables into account, and that it can be used for non-linear systems. Moreover, MPC can handle several process models as well as many performance criteria of significance to the system [98, 120].

MPC, and in particular, MPC for non-linear systems also has certain disadvantages. The main disadvantage of MPC for non-linear systems emanates from the non-linear and non-convex optimization problem involved. Such optimization problems do not only pose difficulty in computing optimal solutions, but also the computation time involved to get the (sub-)optimal solutions may become very high. Usually, the computation time exponentially increases as the number of control inputs (optimization variables) or the prediction horizon increase.

To alleviate the computational problems of MPC several methods can be used. The simplest ones are the introduction of a control horizon and blocking [116]. Instead of varying the control inputs over the full prediction horizon N_{p}, one can define a control horizon $N_{\mathrm{c}} \leq N_{\mathrm{p}}$ after which the control input is kept constant (see Fig. 5.1(b)). The optimization time can also be reduced by introducing blocking in such a way that the control inputs are varied at an integer multiple of the control time step. So, instead of varying the control inputs every control time step, they can be kept constant (uniformly or non-uniformly) for some integer multiple times of the control time step (see Fig. 5.1(c)). In these ways, the computation time can be reduced. However, the reduction in the computation time is in general gained at the expense of reduced performance. Moreover, due to model mismatch and the involved non-linear and non-convex optimization problem, the MPC controller, in general, does not guarantee the stability and optimality of the control solutions. Although in most cases stability can be imposed though ad hoc approaches, optimality is difficult to guarantee, because due to the non-linearity and non-convexity of the optimization problem it is possible to find multiple local minima.

In the next section, this control strategy is discussed in relation to traffic systems.

5.2 Conventional MPC for traffic systems

Fig. 5.1 shows a general block diagram representation of an MPC controller. When it is used with traffic systems, the system and the model blocks in Fig. 5.1(a) respectively denote the real traffic system and the model of the traffic system (such as the traffic flow, emissions, and fuel consumption models). In general the control measures can be speed limits, ramp metering rates, route guidance instructions, and so on. The measurements denote the traffic states (such as the speed, flow, and density) at every sampling time k_{s}.

Remark 5.1 In Part I of the thesis the simulation time step for microscopic and macroscopic models are designated as k_{m} and k respectively. For simplicity of the proceeding discussions only the case of macroscopic models is considered next, unless specified explicitly. However, all the results to follow also apply to microscopic models (in fact to any dynamic model). For the microscopic models the variables k and M_2 in the macroscopic models should be replaced by k_{m} and M_3 respectively. □

Now, in the context of MPC, the dynamic traffic models in Part I can be described or approximated by a system of ordinary difference equations of the form

$$x(k+1) = f(x(k), u(k)), \quad y(k) = h(x(k)), \tag{5.1}$$

where $x(k) \in \mathbb{R}^{n_x}$ denotes the traffic state vector (e.g., the position, flow, speed, density of vehicles in a traffic network, etc.), $u(k) \in \mathbb{R}^{n_u}$ denotes the traffic control inputs vector (containing values for the variable speed limits, ramp metering rates, etc.), and $y(k) \in \mathbb{R}^{n_y}$ denotes the output of the traffic system (e.g., the total time spent, total emissions, total fuel consumption, or total emission dispersion level on target zones), $f : \mathbb{R}^{n_x} \times \mathbb{R}^{n_u} \to \mathbb{R}^{n_x}$ is the state vector field, and $h : \mathbb{R}^{n_x} \to \mathbb{R}^{n_y}$ is the output vector field, with n_x, n_u, and n_y being positive integer numbers.

It is customary to use $\hat{x}$ to denote the prediction of variable x and the notation $\hat{x}(k_2|k_1)$ to denote the predicted value of x at simulation time step k_2 using the information available

at control time step k_1 with $k_2 \geq M_2 k_1$. At every control time step k_c, the MPC controller predicts the traffic states vector

$$\boldsymbol{x}(k_\mathrm{c}) = [\hat{x}^\top(M_2 k_\mathrm{c}|k_\mathrm{c}) \;\; \hat{x}^\top(M_2 k_\mathrm{c}+1|k_\mathrm{c}) \;\; \ldots \;\; \hat{x}^\top(M_2(k_\mathrm{c}+N_\mathrm{p})-1|k_\mathrm{c})]^\top,$$

the traffic outputs vector

$$\boldsymbol{y}(k_\mathrm{c}) = [\hat{y}^\top(M_2 k_\mathrm{c}|k_\mathrm{c}) \;\; \hat{y}^\top(M_2 k_\mathrm{c}+1|k_\mathrm{c}) \;\; \ldots \;\; \hat{y}^\top(M_2(k_\mathrm{c}+N_\mathrm{p})-1|k_\mathrm{c})]^\top,$$

and the initial control input vector

$$\boldsymbol{u}(k_\mathrm{c}) = [u_\mathrm{c}^\top(k_\mathrm{c}|k_\mathrm{c}) \;\; u_\mathrm{c}^\top(k_\mathrm{c}+1|k_\mathrm{c}) \;\; \ldots \;\; u_\mathrm{c}^\top(k_\mathrm{c}+N_\mathrm{p}-1|k_\mathrm{c})]^\top$$

using the models of the traffic system in the MPC controller and the measurements as initial states. The input $u(k)$ at every simulation time step k is related to the control input $u_\mathrm{c}(k_\mathrm{c})$ at every control time step k_c according to $u(k) = u_\mathrm{c}(k_\mathrm{c})$ for $k = M_2 k_\mathrm{c}, M_2 k_\mathrm{c} + 1, \ldots, M_2(k_\mathrm{c}+1)-1$.

At this time, the control objective of the MPC controller (more specifically the conventional MPC) is to optimize the vector of control inputs $\boldsymbol{u}$ that solves the following optimization problem at control time step k_c

$$\begin{aligned} \min_{\boldsymbol{u}(k_\mathrm{c})} J(k_\mathrm{c}, \boldsymbol{u}(k_\mathrm{c})) :&= V(\boldsymbol{x}(k_\mathrm{c}), \boldsymbol{u}(k_\mathrm{c}), \boldsymbol{y}(k_\mathrm{c})) \\ \text{subject to: } &\mathcal{G}(\boldsymbol{x}(k_\mathrm{c}), \boldsymbol{u}(k_\mathrm{c}), \boldsymbol{y}(k_\mathrm{c})) \leq 0, \\ &\mathcal{Q}(\boldsymbol{x}(k_\mathrm{c}), \boldsymbol{u}(k_\mathrm{c}), \boldsymbol{y}(k_\mathrm{c})) = 0, \\ &\text{and system model (5.1)} \end{aligned} \tag{5.2}$$

where $J(k_\mathrm{c}, \boldsymbol{u}(k_\mathrm{c}))$ denotes the objective function (such as travel time, emissions, dispersion of emissions, or a combination of these) defined by a real-valued user-defined function $V(\cdot)$, $\mathcal{G}(\cdot)$ is the inequality constraint mapping, and $\mathcal{Q}(\cdot)$ is the equality constraint mapping.

As has been introduced in the previous section only the first control input $u_\mathrm{c}^*(k_\mathrm{c}|k_\mathrm{c})$ of the optimal sequence $\boldsymbol{u}^*(k_\mathrm{c})$ is applied to the system till the next control time step $k_\mathrm{c}+1$, after which the MPC controller repeats the above process all over again using a receding horizon approach. Since the control inputs are generated based on the current and predicted future states of the traffic, the predicted future states can be different from the actual ones due to unexpected internal and external effects and modeling errors. However, since only the first control input is applied for the next $k_\mathrm{c}+1$ and then a new measurement of the traffic states is undertaken, the prediction errors can be reduced. This mechanism introduces a feedback of the output of the system to the controller.

However, due to its high computational demand, conventional MPC for traffic systems is not tractable in practice [22, 56, 77, 109, 188]. There are many advancements in the literature (e.g., [24, 71, 98, 111, 179, 189, 195]) to address the computational complexity problems of MPC in general. Kotsialos et al. [105] and Papamichail et al. [151] used a model-predictive hierarchical control approach to coordinate ramp meters for a freeway network and reported computation times in the order of $15\,\mathrm{s}$ without further explaining the details of the optimization algorithm. In this regard, the efforts to address the computational issues of conventional MPC and a new and efficient MPC approach for freeway traffic systems will be the subject of the next chapter.

5.3 Traffic performance criteria

Since MPC can accept any quantifiable form of performance criterion, a special structure is not required to formulate the performance criteria of the MPC controller. The main aim of any traffic controller is to improve the performance of the traffic network. However, the performance could vary depending on the desire of the stakeholders of the network, the time of operation of the network, and the location of the network. For example, environmentalists would like reduced dispersion of emissions and propagation of sound pollution to a protected target zone, while transport authorities could be interested to improve traffic throughput and safety. Moreover, the desired performance criterion of a given network can vary from time to time. For example, depending on the wind direction, wind speed, the temperature, and so on, the desired performance criteria can be different. When the wind direction is in the opposite direction of a given target zone (e.g., a hospital or school), the traffic control performance criteria can be set to improve the traffic flow, while when the wind is blowing towards a given target zone, the performance can be set to take dispersion of emissions into account.

In light of the conflicting demands, this thesis considers four performance criteria viz. total time spent, emissions, fuel consumption, and dispersion of emissions to target zones. Due to the similarity and close inter-relationship between the last three performance criteria, these four traffic performance criteria are grouped into two as traffic flow performance criteria and emissions and fuel consumption performance criteria. These are discussed in the subsequent sections in detail.

Since the performance criteria are going to be used in an MPC control approach, the values of all the performance criteria are determined at every control time step k_{c} over the prediction horizon N_{p}. However, the expressions can also be used in general for the determination of an overall traffic performance criterion of a traffic network for an entire simulation period (see Remark 5.2).

5.3.1 Flow performance criteria

Traffic network flow performance can be described or formulated using different criteria. As a result, the objective of the traffic controllers can be different. The flow performance criteria can be the throughput, travel times, homogeneity of the traffic flow, or the safety level of the traffic flow both over space and time. Since the total time spent (TTS for short) is often considered as performance criterion of traffic controllers, in this thesis too the total time spent is used as flow performance criterion.

For microscopic approaches

The formulation of the total time spent is different for microscopic and macroscopic models. The main difference is the way the number of vehicles is determined and the time and space scale considered. In the microscopic approaches, the number of vehicles is determined by counting each vehicle in the traffic network. The travel time of each vehicle at every location is collected. Then, the total time spent is determined by adding up the travel time of each

vehicle in the network. This reads as

$$\mathrm{TTS}(k_\mathrm{c}) = T_\mathrm{m} \sum_{k_\mathrm{m}=M_3 k_\mathrm{c}}^{M_3(k_\mathrm{c}+N_\mathrm{p})-1} \mathcal{N}(k_\mathrm{m}) \tag{5.3}$$

where $\mathcal{N}(k_\mathrm{m})$ denotes the number of vehicles in the network at time $t = k_\mathrm{m} T_\mathrm{m}$ and the positive integer M_3 relates k_c and k_m as $k_\mathrm{m}(k_\mathrm{c}) = M_3 k_\mathrm{c}$. The number of vehicles $\mathcal{N}(k_\mathrm{m})$ can be measured using microscopic measurement techniques or can be predicted using microscopic traffic models (e.g., models presented in Section 2.1.2 and Section 2.2).

Remark 5.2 The total time spent (TTS) in (5.3) is determined over the prediction period $[M_3 k_\mathrm{c}, M_3(k_\mathrm{c} + N_\mathrm{p}) - 1]$. But it is also possible to determine the value of the TTS over the simulation period $[0, N_\mathrm{s}]$ as

$$\mathrm{TTS}(k_\mathrm{c}) = T_\mathrm{m} \sum_{k_\mathrm{m}=0}^{N_\mathrm{s}-1} \mathcal{N}(k_\mathrm{m}) \tag{5.4}$$

where N_s is the total number of simulation steps. □

For macroscopic approaches

In macroscopic approaches, the number of vehicles and the travel time is obtained by computing or measuring the average number of vehicles in part of a traffic network over a given period of time. The travel times for the parts of the networks and time periods are added together to obtain the total time spent by the vehicles in the traffic network. Mathematically, this is given by

$$\mathrm{TTS}(k_\mathrm{c}) = T \sum_{k=M_2 k_\mathrm{c}}^{M_2(k_\mathrm{c}+N_\mathrm{p})-1} \left[\sum_{(m,i)\in M_\mathrm{all}} L_m \lambda_m \rho_{m,i}(k) + \sum_{o\in O_\mathrm{all}} w_o(k) \right] \tag{5.5}$$

where M_all is the set of all pairs of segment and link indices and O_all is the set of all origins, where the macroscopic variables, density $\rho_{m,i}(k)$ and the queue length $w_o(k)$ are either estimated or measured quantities at the time instant $t = kT$, and M_2 is a positive integer that relates the control time step k_c and k as $k(k_\mathrm{c}) = M_2 k$. Since this thesis uses the METANET macroscopic flow model, these quantities are obtained from the METANET model presented in Section 2.3.

The first term in (5.5), $L_m \lambda_m \rho_{m,i}(k)$, indicates the number of vehicles in segment i of link m and hence multiplied by the time step size T gives the time spent by the vehicles in the corresponding segment of the link. The second term in (5.5) corresponds to the time spent by the vehicles queuing at the mainstream or on-ramp origins.

5.3.2 Emissions and fuel consumption performance criteria

Other important traffic performance criteria are the emissions and energy consumption of the vehicles. Environmentalists are much concerned to reduce the total emission levels or local emission levels, while drivers and policy makers may be interested to have energy-efficient traffic systems.

Like the flow performance criteria, in this thesis the traffic emissions and fuel consumption performance criteria are formulated as the performance of the whole traffic network and not the performance of individual vehicles. This means that the emissions and energy efficiency performance criteria of a traffic network are respectively defined as the total emissions and the total fuel consumption of the network. In the sequel, the total emissions released and the total fuel consumed by the vehicles in a traffic network are defined. However, the formulation of the expressions is different if one uses microscopic or macroscopic modeling or measurement approaches.

For microscopic approaches

For microscopic approaches, the total emissions (TE for short) are determined as the summation of the emissions of each vehicle in the traffic network over time and space. Moreover, the total fuel consumption (TFC) is determined in the same way. These are expressed as

$$\mathrm{TE}(k_\mathrm{c}) = T_\mathrm{m} \sum_{k_\mathrm{m}=M_3 k_\mathrm{c}}^{M_3(k_\mathrm{c}+N_\mathrm{p})-1} \sum_{\alpha\in\mathcal{V}(k_\mathrm{m})} \sum_{\bar{y}\in\bar{\mathcal{Y}}/\{\mathrm{fuel}\}} \mu_{\bar{y}} J_{\bar{y},\alpha}(k_\mathrm{m}) \tag{5.6}$$

$$\mathrm{TFC}(k_\mathrm{c}) = T_\mathrm{m} \sum_{k_\mathrm{m}=M_3 k_\mathrm{c}}^{M_3(k_\mathrm{c}+N_\mathrm{p})-1} \sum_{\alpha\in\mathcal{V}(k_\mathrm{m})} J_{\mathrm{fuel},\alpha}(k_\mathrm{m}) \tag{5.7}$$

where $\mathcal{V}(k_\mathrm{m})$ denotes the set of vehicles present in the network at the time $t = k_\mathrm{m}T_\mathrm{m}$, $\bar{\mathcal{Y}} = \{\mathrm{CO}, \mathrm{NO}_x, \mathrm{HC}, \mathrm{CO}_2, \mathrm{fuel}\}$, and $J_{\bar{y},\alpha}(k_\mathrm{m})$ for $\bar{y} \in \bar{\mathcal{Y}}$ denotes the emissions or fuel consumption of vehicle α at time step k_m and is obtained using (3.2) and (3.4). The value of $\mu_{\bar{y}} \geq 0$ is the weighting factor of each emission $\bar{y} \in \bar{\mathcal{Y}}/\{\mathrm{fuel}\}$.

The dispersion of emissions to target zone can be computed microscopically by considering the emission of each vehicle and the evolution of the emissions over time and space. The dispersion of emissions from traffic networks are in general determined by integrating the individual emission sources over a segment of a freeway. So, conceptually, this is a macroscopic approach, because it does not consider the dispersion of emissions from individual vehicles but the dispersion of emissions from the whole segment of a freeway. Thus, the dispersion level performance criterion is given in the sequel in relation to macroscopic approaches.

For macroscopic approaches

In Chapter 3, the macroscopic emissions and fuel consumption models provide the emissions and fuel consumption of a number of vehicles in a given segment during a given period of time. The total emissions (TE) of a traffic network over a given period of time is then obtained by adding the emissions contribution of every segment of a freeway over the whole span of time considered. The total fuel consumption is also obtained in the same way. In this case, at every control time step k_c, the total emissions and total fuel consumption of

vehicles in a given freeway over a prediction horizon N_{p} is determined by

$$\mathrm{TE}(k_{\mathrm{c}}) = T \sum_{k=M_2 k_{\mathrm{c}}}^{M_2(k_{\mathrm{c}}+N_{\mathrm{p}})-1} \sum_{\bar{y}\in\bar{\mathcal{Y}}/\{\mathrm{fuel}\}} \mu_{\bar{y}} J_{\mathrm{total},\bar{y}}(k) \tag{5.8}$$

$$\mathrm{TFC}(k_{\mathrm{c}}) = T \sum_{k=M_2 k_{\mathrm{c}}}^{M_2(k_{\mathrm{c}}+N_{\mathrm{p}})-1} J_{\mathrm{total,fuel}}(k) \tag{5.9}$$

where $\bar{\mathcal{Y}} = \{\mathrm{CO}, \mathrm{CO_2}, \mathrm{HC}, \mathrm{NO}_x, \mathrm{fuel}\}$ and $J_{\mathrm{total},\bar{y}}(k)$ is the emission or fuel consumption $\bar{y}$ of segment i of link m over the time period $[kT, (k+1)T)$ as defined in (3.25).

In regard to emission dispersion levels, in this thesis two performance criteria are considered, viz. the maximum dispersion level in the target zone and the total dispersion level in the target zone within the prediction period $[M_2 k_{\mathrm{c}}, M_2(k_{\mathrm{c}}+N_{\mathrm{p}})-1]$. At the control time step k_{c}, the weighted total maximum emission dispersion level $\mathrm{MDL}(k_{\mathrm{c}})$ of each emission gas $\bar{y}$ at all the target zones over the prediction period $[M_2 k_{\mathrm{c}}, M_2(k_{\mathrm{c}}+N_{\mathrm{p}})-1]$ is

$$\mathrm{MDL}(k_{\mathrm{c}}) = T \sum_{t\in\mathcal{T}_{\mathrm{all}}} \sum_{\bar{y}\in\bar{\mathcal{Y}}/\{\mathrm{fuel}\}} \mu_{\mathrm{d},\bar{y}} \max_{k\in\{M_2 k_{\mathrm{c}}, M_2 k_{\mathrm{c}}+1, \ldots, M_2(k_{\mathrm{c}}+N_{\mathrm{p}})-1\}} D_{\bar{y},t}(k) \tag{5.10}$$

where $D_{\bar{y},t}(k)$ is the target dispersion level of emission $\bar{y}$ at target zone t obtained using (4.9) or (4.11) and $\mathcal{T}_{\mathrm{all}}$ is the set of all target zones.

The second performance criterion involves the cumulative effect of the dispersed emissions. At control time step k_{c}, the total dispersion level (TDL) of all emissions at all the target zones over the prediction period $[M_2 k_{\mathrm{c}}, M_2(k_{\mathrm{c}}+N_{\mathrm{p}})-1]$ is given by

$$\mathrm{TDL}(k_{\mathrm{c}}) = T \sum_{t\in\mathcal{T}_{\mathrm{all}}} \sum_{\bar{y}\in\bar{\mathcal{Y}}/\{\mathrm{fuel}\}} \sum_{k=M_2 k_{\mathrm{c}}}^{M_2(k_{\mathrm{c}}+N_{\mathrm{p}})-1} \mu_{\mathrm{d},\bar{y}} D_{\bar{y},t}(k). \tag{5.11}$$

5.3.3 Variation in traffic control measures

Dynamic traffic control approaches, such as MPC, dynamically vary the settings of the traffic control measures such as variable speed limits and ramp metering rates both in time and in space. In general, frequent fluctuations and big changes in the values of the control measures are not desired from safety and driver comfort point of view. Since it is also possible to have different optimal traffic control settings that can result in the same traffic performance, priority is usually given to attain the same performance level with a minimal fluctuation in the traffic control measures.

In general, at control time step k_{c} the total fluctuation of the traffic control measures over time and space is expressed by

$$\begin{aligned} U_{\Delta}(k_{\mathrm{c}}) = \mu_{\mathrm{u},1} & \sum_{\ell=k_{\mathrm{c}}}^{k_{\mathrm{c}}+N_{\mathrm{p}}-1} \sum_{s\in\mathcal{U}_{\mathrm{all}}} \left(\bar{u}_s(\ell) - \bar{u}_s(\ell-1)\right)^2 \\ + \mu_{\mathrm{u},2} & \sum_{\ell=k_{\mathrm{c}}}^{k_{\mathrm{c}}+N_{\mathrm{p}}-1} \sum_{(s_1,s_2)\in\mathcal{C}_{\mathrm{all}}} \left(\bar{u}_{s_1}(\ell) - \bar{u}_{s_2}(\ell)\right)^2 \end{aligned} \tag{5.12}$$

where $\mu_{\mathrm{u},1} \geq 0$ and $\mu_{\mathrm{u},2} \geq 0$ are the weighting factors between the fluctuation in time and in space respectively, $\bar{u}_s(k_\mathrm{c})$ is the traffic control measure at control time step k_c and at location s, $\mathcal{U}_\mathrm{all}$ is the set of all traffic control measures, and $\mathcal{C}_\mathrm{all}$ is the set of all pairs of consecutive traffic control measures.

Although the formulation above is general, throughout this thesis the variable speed limits and ramp metering traffic control measures are used. In that case the expression for $U_\Delta(k_\mathrm{c})$ becomes

$$\begin{aligned} U_\Delta(k_\mathrm{c}) = \sum_{\ell=k_\mathrm{c}}^{k_\mathrm{c}+N_\mathrm{p}-1} \Bigg[& \sum_{s\in\mathcal{S}_\mathrm{all}} \mu_\mathrm{s}\big(u_s(\ell)-u_s(\ell-1)\big)^2 \\ & + \sum_{(s_1,s_2)\in\mathcal{P}_\mathrm{all}} \mu_\mathrm{cs}\big(u_{s_1}(\ell)-u_{s_2}(\ell)\big)^2 \\ & + \sum_{r\in\mathcal{R}_\mathrm{all}} \mu_\mathrm{r}\big(u_r(\ell)-u_r(\ell-1)\big)^2 \Bigg] \end{aligned} \tag{5.13}$$

with $u_s(k_\mathrm{c})$ denoting the speed limits at control time step k_c, $u_r(k_\mathrm{c})$ denoting the ramp metering rate at control time step k_c, $\mathcal{S}_\mathrm{all}$ denoting the set of all speed limits, $\mathcal{P}_\mathrm{all}$ denoting the set of all pairs of consecutive speed limits, $\mathcal{R}_\mathrm{all}$ denoting the set of all controlled on ramps, and $\mu_\mathrm{s} = (\#(\mathcal{S}_\mathrm{all})v_\mathrm{step}^2)^{-1}$, $\mu_\mathrm{cs} = (\#(\mathcal{P}_\mathrm{all})v_\mathrm{step}^2)^{-1}$, and $\mu_\mathrm{r} = (\#(\mathcal{R}_\mathrm{all}))^{-1}$ respectively are the weighting of the variation of the speed limits over time, the variation of the speed limits in space, and the variation of the ramp metering rate over time, where $\#(\cdot)$ denotes the set cardinality and v_step is the maximum speed limit step change allowed.

5.4 Multi-criteria optimization

In the above sections, different traffic performance criteria were discussed. In an MPC control approach, the formulation of an appropriate optimization problem is required. For a multi-criteria traffic control approach a systematic combination of the different performance criteria is required. Generally, an optimization problem of MPC is formulated as in (5.2). The objective function of the optimization problem can be a vector of control objectives. For convenience let us consider a multi-criteria optimization problem given by

$$\begin{aligned} & \min_x J_\mathrm{vector}(x) \\ & \text{s.t.} \quad g(x) \leq 0 \ \text{ and } \ h(x) = 0 \end{aligned} \tag{5.14}$$

where $J_\mathrm{vector}(k) \in \mathbb{R}^m$ denotes a vector of m objective functions and $g(x)$ and $h(x)$ are the inequality and equality constraint functions.

Most often, the objective functions are competing, which require trade-offs as there may be no solution that minimizes all the criteria at the same time. As the number of the objectives increases, the trade-offs are likely to become more complex and less easily quantified [68]. So for such competing multi-objective criteria, the multi-objective optimization must generate and select the Pareto-optimal[1] solutions [62]. Multi-objective techniques such as

[1] A solution is a Pareto-optimal if and only if there does not exist any other solution that results in a lower value of all the cost functions [39, 125].

the weighted sum strategy, the ϵ-constraint method, and the goal attainment method can be used in case of competing objective functions [62, 68]. For its simplicity in the context of MPC, in this thesis, the weighted-sum multi-objective optimization strategy is used. In the sequel, the formulation of the multi-criteria objective function, the normalization of the weights, and the optimization method employed are discussed.

5.4.1 Weighted sum

The weighted sum strategy converts the multi-objective problem of minimizing the vector $J_{\text{vector}}(x)$ into a problem with a scalar objective function by constructing a weighted sum of all the objectives. This results in the following optimization problem

$$\begin{aligned} \min_x J(x) &= \sum_{i=1}^{m} \zeta_i J_{\text{vector},i}(x) \\ \text{s.t.} \quad & g(x) \leq 0 \ \text{ and } \ h(x) = 0 \end{aligned} \tag{5.15}$$

where $\zeta_i \geq 0$ for $i = 1, 2, \ldots, m$.

Using this strategy, at every control time step k_{c}, a single objective function of a traffic control system with the objectives of reducing the total time spent by vehicles in a traffic network, the total emissions and total fuel consumption of vehicles in the traffic network, and the dispersion of the emissions of the vehicles to a target zone t can be formulated as

$$\begin{aligned} J(k_{\text{c}}) = \zeta_1 \frac{\text{TTS}(k_{\text{c}})}{\text{TTS}_{\text{n}}} + \zeta_2 \frac{\text{TE}(k_{\text{c}})}{\text{TE}_{\text{n}}} + \zeta_3 \frac{\text{TFC}(k_{\text{c}})}{\text{TFC}_{\text{n}}} \\ + \zeta_{4,\text{MDL}} \frac{\text{MDL}(k_{\text{c}})}{\text{MDL}_{\text{n}}} + \zeta_{4,\text{TDL}} \frac{\text{TDL}(k_{\text{c}})}{\text{TDL}_{\text{n}}} + \zeta_5 \frac{U_\Delta(k_{\text{c}})}{U_{\Delta,\text{n}}} \end{aligned} \tag{5.16}$$

where $\text{TTS}(k_{\text{c}})$, $\text{TE}(k_{\text{c}})$, $\text{TFC}(k_{\text{c}})$, MDL, $\text{TDL}(k_{\text{c}})$, and $U_\Delta(k_{\text{c}})$ are respectively given by (5.5) (or (5.3)), (5.8) (or (5.6)), (5.9) (or (5.7)), (5.10), (5.11), and (5.12) and where the subscript 'n' denotes the normalization of TTS, TE, TFC, MDL, TDL, and U_Δ. The normalizations are discussed in the next section.

5.4.2 Normalization

One of the challenges with the weighted-sum approach is the determination of the weights for the different performance criteria. This is because the different performance criteria mostly have different dimensions and values. Some can have very large values while others can have very small values and thus the determination of the weights can be difficult. In order to have the same order of magnitude and dimension and in order to make the weight assignment between the different performance criteria easy and physically interpretable, the unbalanced values and dimensions of the performance criteria can be equalized by normalizing them to unity and dimensionless quantities.

So, these normalization values have to be determined beforehand. Usually, these values have to be the maximum possible values of the performance criteria. However, in some cases, like in the traffic system, it is difficult to determine the maximum possible value of the performance criteria. So, throughout this thesis the nominal values are taken as the normalization values of the performance criteria. These nominal values are determined

under the uncontrolled natural traffic flow conditions. This means that the variable speed limits are set to the free-flow speed, and the ramp metering installations are uncontrolled (set green always).

Since the different variation terms in control input $U_{\Delta,\mathrm{n}}$ is already normalized at every control time step k_{c} in (5.13), here the normalization is the prediction horizon N_{p}.

5.4.3 Optimization method

Optimization is one of the main elements in an MPC control strategy. It is also one of the main bottlenecks potentially resulting in extensive computational requirements. Since the traffic flow models are highly non-linear, the objective functions are also non-linear with respect to the traffic control measures. Moreover, the objective functions are non-convex with respect to the traffic control measures. This leads to a non-linear and non-convex optimization problem.

There is no optimization method that can guarantee to reach an optimal solution of a non-convex optimization problem in finite time. Therefore, since the MPC traffic control problem considered in this thesis is non-linear and non-convex and since it has to be solved within a limited time frame (at least within T_{c} time units), it is difficult to obtain global optimal solutions. It is therefore important to make a proper choice of an optimization technique. Due to the non-convex nature of the objective functions, global or multi-start local optimization methods are required. In this case multi-start Sequential Quadratic Programming (SQP) [27, 152], pattern search [10], genetic algorithms [55], or simulated annealing [61] can be used.

Throughout this thesis, the SQP local optimization method in combination with a multi-start approach is used. SQP is a powerful method for solving non-convex and constrained continuous optimization problems. This approach has been extensively applied in MPC based traffic control approaches in [21, 75, 77, 99, 102, 103]. Since SQP is a local optimization problem, in order to increase the possibility of attaining the global optimal solution, the optimization process is repeated several times with different initial points. This is called a multi-start approach. For more details of SQP we refer the reader to [27, 136, 152, 166].

5.5 Case studies

In this section different cases studies that illustrate the conventional MPC presented in this chapter as applied to traffic systems are presented. Since models are required to make predictions of the traffic states, the MPC controller uses the models presented in Part I of the thesis. Section 5.5.1 presents case studies where reduction of travel time, emissions, and fuel consumption are defined as the performance criteria of the MPC controller. In Section 5.5.2 the reduction of dispersion of emissions to target zones is also considered.

5.5.1 Balanced reduction of travel times, emissions, and fuel consumption

In this section two case studies are presented: Case study A presents the use of variable speed limits to provide a balanced trade-off between travel times and emissions; Case study B illustrates the integrated use of variable speed limits and ramp metering for sustainable

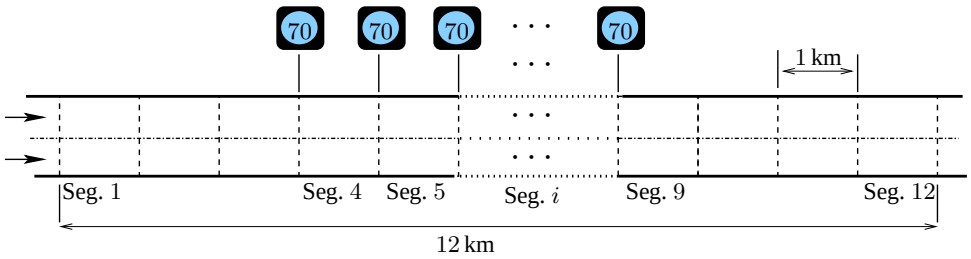

Figure 5.2: A two-lane single-link freeway considered for Case study A.

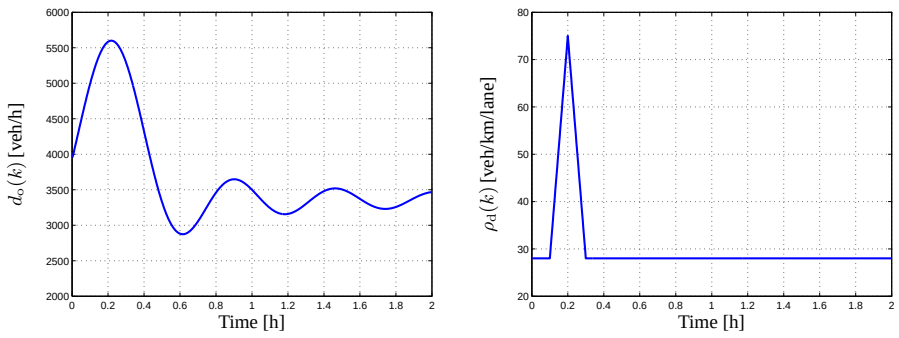

(a) Demand (b) Demand

Figure 5.3: Demand $d_o(k)$ at the origin and density $\rho_d(k)$ at the end of the freeway segments considered for Case study A.

mobility, in particular for the reduction of total time spent, emission of NO_x, and fuel consumption of vehicles in a given traffic network.

Case study A

The use of variable speed limits for improved traffic flow and emissions is presented in this section. A case study with a 12 km two-lane freeway is considered. The freeway is divided into 12 segments, where only the middle 6 segments are controlled with dynamic speed limits (see Fig. 5.2; this is similar to the network considered in [78]). The freeway is modeled using the METANET traffic flow model presented in Section 2.3. As emissions model the VT-macro model of Section 3.4 is used. The demand of the traffic flow at the origin of the freeway is given in Fig. 5.3(a). Moreover, a density profile at the end of the freeway is presented in Fig. 5.3(b). These profiles provide one particular example of a traffic scenario where there is a dynamic demand with a peak during the rush hour and a shock wave (see Fig. 5.4) that can cause traffic jams.

In this case study the network parameters $T = 10\,\text{s}$, $\tau = 18\,\text{s}$, $b_m = 1.867$, $\kappa = 40\,\text{veh/km/lane}$, $\eta_\text{h} = 65\,\text{km}^2\text{/h}$, $\eta_\text{l} = 30\,\text{km}^2\text{/h}$, $\rho_{\text{jam},m} = 180\,\text{veh/km/lane}$, $\rho_{\text{cr},m} = 33.5\,\text{veh/km/lane}$, and $v_\text{min} = 10\,\text{km/h}$ are used [78]. Furthermore, the noncompliance factor is assumed to be $\varrho = 0$ (i.e., all drivers comply to traffic control measures), the

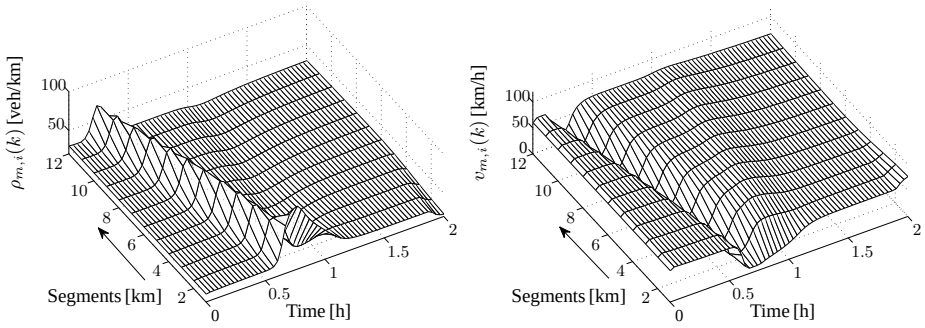

(a) Density profile

(b) Speed profile

Figure 5.4: Density and speed profiles of the traffic flow under uncontrolled Scenario S_1 of Case study A. The arrows indicate the driving direction.

free-flow speed $v_{\mathrm{free},m} = 102$ km/h, and the capacity of the link is $C_o = 2000$ veh/h/lane.

The simulation period for this case is 2 hours. The traffic system is simulated for both controlled and uncontrolled scenarios. An MPC controller is designed for the controlled scenarios with a control time step size $T_{\mathrm{c}} = 1$ min, a prediction horizon of $N_{\mathrm{p}} = 30$ (corresponding to 30 min), control horizon $N_{\mathrm{c}} = 10$ (corresponding to 10 min), and with eight initial points for the multi-start SQP optimization. The eight initial points of the multi-start optimization include: the control inputs of the previous control step, the upper bound and the lower bound of the control inputs, the average of the upper and lower bounds, and four random points. Three different control objectives are defined for the MPC controller. Thus, in total four scenarios are simulated, and these are:

$\mathbf{S}_1$: Uncontrolled

$\mathbf{S}_2$: Controlled, total time spent (TTS) only

$\mathbf{S}_3$: Controlled, total emissions (TE) only, and

$\mathbf{S}_4$: Controlled, weighted sum of total time spent (TTS) and total emissions (TE).

For the first Scenario S_1, no controller is implemented. The density and speed profile of the traffic under this scenario are presented in Fig. 5.4. As can be seen, the shock wave that started at the end of the freeway propagates in the upstream direction. The total time spent in this case is 2142.3 veh·h. The total emissions (of CO, HC, and NO_x) for the same case is 15.9 kg. As has been discussed in the previous sections, these values (determined under the uncontrolled scenario) are used as the nominal values for the normalization of the control objectives.

For the TTS controlled Scenario S_2, the weights[2] in (5.16) are set to $\zeta_1 = 1$ and $\zeta_2 = \zeta_3 = \zeta_{4,\mathrm{MDL}} = \zeta_{4,\mathrm{TDL}} = \zeta_5 = 0$. In the third Scenario S_3, only the total emission (TE) is taken as MPC control objective. In this case (Scenario S_3), the weights are $\zeta_1 = \zeta_3 =$

[2] In this simulation we did not take the variation of the control input into account. Thus, the weight ζ_5 corresponding to the variation in control input is set to be $\zeta_5 = 0$. In hindsight, it is better to consider non-zero weight. In the subsequent sections non-zero weight for the variation of the control inputs are considered.

Table 5.1: Simulation results for Case study A. The values inside the brackets indicate the relative change of the performance criteria as compared to the uncontrolled Scenario S_1. Negative values indicate a decrease (i.e., improvement) in the value of the performance criteria, while positive values indicate an increase in the value of the performance criteria as compared to the uncontrolled scenario.

Scenarios	Performance Criteria	
	TTS [veh·h]	TE [kg]
S_1: Uncontrolled	2142.3	15.907
S_2: TTS	1687.7 (-21.2%)	16.131 ($+1.3\%$)
S_3: TE	2167.2 ($+1.2\%$)	14.657 (-7.6%)
S_4: TTS + TE	2037.9 (-4.9%)	14.747 (-7.6%)

$\zeta_{4,\mathrm{MDL}} = \zeta_{4,\mathrm{TDL}} = \zeta_5 = 0$, $\zeta_2 = 1$, $\mu_{\mathrm{CO}} = \mu_{\mathrm{HC}} = \mu_{\mathrm{NO_x}} = 1$, and $\mu_{\mathrm{CO_2}} = 0$. For the last Scenario S_4, where a weighted combination of the TTS and TE is considered, the weights are set to $\zeta_1 = \zeta_2 = 1$, $\zeta_3 = \zeta_{4,\mathrm{MDL}} = \zeta_{4,\mathrm{TDL}} = \zeta_5 = 0$, $\mu_{\mathrm{CO}} = \mu_{\mathrm{HC}} = \mu_{\mathrm{NO_x}} = 1$, and $\mu_{\mathrm{CO_2}} = 0$.

The simulation results are listed in Table 5.1. Moreover, Table 5.1 provides the relative change of the performance indicators of the different controlled scenarios as compared to the uncontrolled Scenario S_1. These values are computed as

$$I_p = \frac{p_{\mathrm{controlled}} - p_{\mathrm{uncontrolled}}}{p_{\mathrm{uncontrolled}}} \tag{5.17}$$

where $p_{\mathrm{uncontrolled}}$ denotes the value of the performance criteria $p \in \{\mathrm{TTS}, \mathrm{TE}\}$ for the uncontrolled scenario and $p_{\mathrm{controlled}}$ is the value of the performance criteria p for the controlled scenarios.

Under the considered traffic conditions, the results in Table 5.1 indicate that when the objective of the controller is to reduce the travel time (Scenario S_2), the MPC controller reduces the total time spent by 21.2% (as compared to the uncontrolled Scenario S_1) at the expense of increased emissions by 1.3%. However, when the objective of the MPC controller is to reduce total emissions (Scenario S_3), the total emissions are reduced by 7.6% relative to the uncontrolled scenario. But the total time spent is increased by 1.2%. These results indicate that a control strategy that focuses either only on the total time spent or only on the total emissions may impact the emissions or the travel time negatively. On the other hand, in particular in this case study, when the objective of the controller is set to be the weighted sum of total emissions and total time spent (Scenario S_4), the controller results in an improvement of the total time spent and total emissions by 4.9% and 7.6% respectively as compared to the uncontrolled scenario.

The variation of the traffic densities and speeds for the Scenarios S_2, S_3 and S_4 over the whole link are depicted in Fig. 5.5, Fig. 5.6, and Fig. 5.7 respectively. Recall that under the uncontrolled Scenario S_1, the shock wave created around the time $t = 0.25\,\mathrm{h}$ propagates through the entire link upstream from segment 12 to segment 1 (see Fig. 5.4). However, when the MPC controller is implemented to reduce the travel time (Scenario S_2) the shock wave is reduced and dissolves in time as it propagates upstream (see Fig. 5.5), i.e., the controller creates a relatively smooth traffic flow. Moreover, the peak of the shock wave at segment 12 of Scenario S_2 is less than that of Scenario S_1. This shows that the proposed

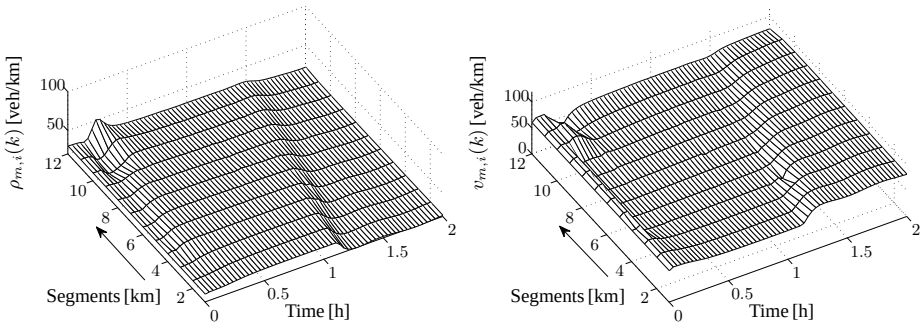

(a) Density profile (b) Speed profile

Figure 5.5: Density and speed profiles of the traffic flow under TTS*-controlled Scenario S_2 of Case study A. The arrows indicate the driving direction.*

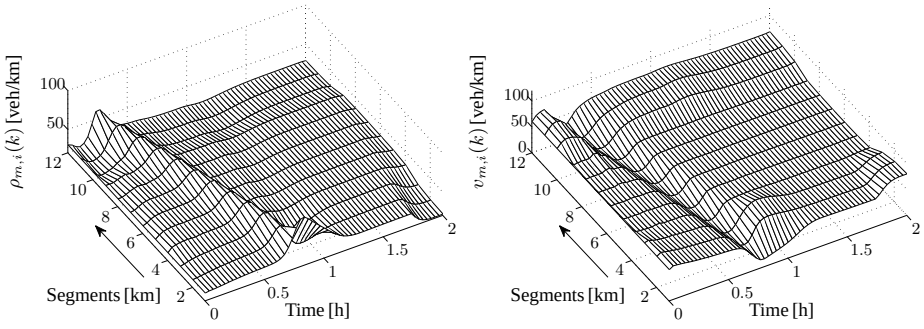

(a) Density profile (b) Speed profile

Figure 5.6: Density and speed profiles of the traffic flow under TE*-controlled Scenario S_3 of Case study A. The arrows indicate the driving direction.*

MPC controller is able to avoid the appearance of the shock waves in the uncontrolled scenario. However, this is at the expense of increased emissions (see Table 5.1). In Scenario S_1, the MPC controller has reduced and smoothened the space-mean speed and it has increased the density. But, since the emission reduction resulting from the homogenized space-mean speed is over-compromised by the increase in emission resulting from the increased density (number of vehicles), the net effect has resulted in increased total emissions.

Fig. 5.6 shows the density and speed profiles for the scenario where the objective of the MPC controller is to reduce only the total emissions. Although the differences of these profiles from the uncontrolled case are not significant, one can see that the speed under the Scenario S_3 (i.e., the controller focusing on the reduction of total emissions only) is lower than under the uncontrolled case (Scenario S_1). As a result the travel time has been increased while the emissions have been reduced (see Table 5.1). In this case (Scenario S_3) the MPC controller has slightly improved the shock wave (reduces emission levels), has

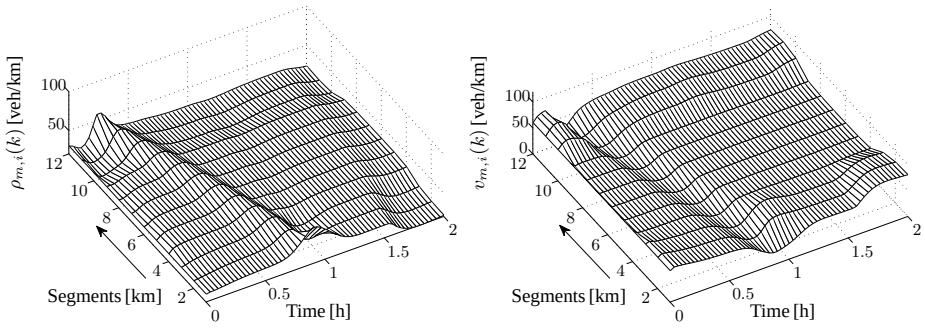

(a) Density profile (b) Speed profile

Figure 5.7: Density and speed profiles of the traffic flow under $\mathrm{TTS} + \mathrm{TE}$*-controlled Scenario* S_4 *of Case study A. The arrows indicate the driving direction.*

reduced and homogenized the higher speeds (reduces emission levels), and has increased the density slightly (increases emission levels) as compared to the uncontrolled case. Thus, as a net effect, the controller results in reduced total emissions.

Fig. 5.7 presents the density and speed profiles for the scenario in which the objective of the MPC controller is to reduce both the total emissions and total time spent (Scenario S_4). The figure and the values in Table 5.1 of the scenario show that the MPC has offered a balanced trade-off between reducing the total emissions and the total time spent. Fig. 5.7 shows that the shock waves get reduced as compared to the uncontrolled scenario. The trade-off between the total time spent and the total emissions can be adjusted by changing the weight of the performance criterion in (5.16). One can see that the total emissions (TE) for Scenario S_3 and S_4 are almost the same, while the total time spent (TTS) are different (see Table 5.1). Since the optimization process is a non-convex problem, it is possible to have multiple local minima. As a result, if the MPC controller focuses only on the TE, it may not compromise small loss in TE that could result in better TTS. However, with the addition of TTS on the cost function of the controller, the controller can seek solutions (local minima) that can reduce TTS while still reducing TE. Scenario S_4 shows such situation.

Case study B

In this case study, two traffic control measures are considered, viz. variable speed limits and ramp metering. A simple freeway network similar[3] to the network considered in [75, 76] is used for this case study (see Fig. 5.8). The network consists of one mainstream freeway link with two speed limits and one metered on-ramp. The on-ramp is located at a distance of 4 km from the mainstream origin of the freeway link, and it has a capacity of 2000 veh/h. The mainstream freeway link has two lanes with a capacity of 2100 veh/h each. Segments 3 and 4 of the freeway are equipped with variable message signs where speed limits can be displayed. The outflow at the end of the freeway is considered to be unrestricted. It

[3] In [75, 76], the considered freeway network has been used to reduce the travel time using MPC. In this case study the same network is considered to reduce travel time, emissions, and fuel consumptions using MPC.

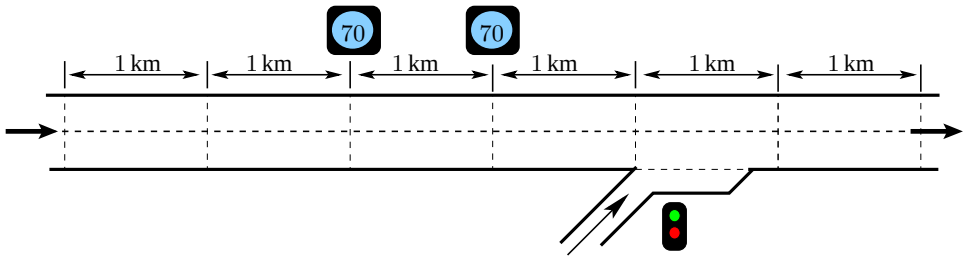

Figure 5.8: A 6 km freeway with metered on-ramp and two dynamic speed limits considered for Case study B.

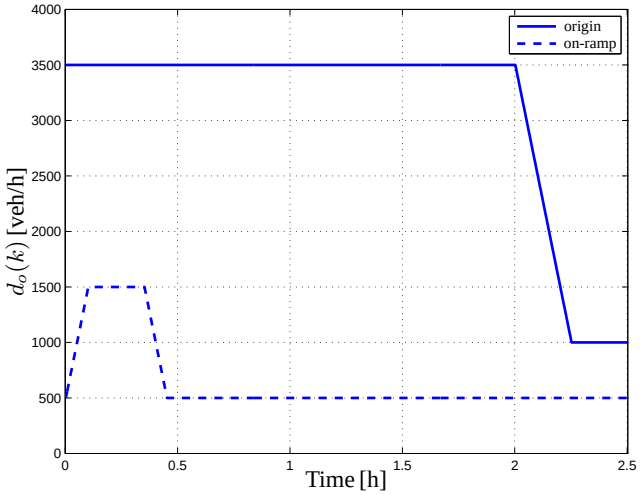

Figure 5.9: On-ramp demand (dashed line) and mainstream demand (solid line) profiles considered for Case study B.

is assumed that the queue length at the on-ramp may not exceed 100 vehicles, in order to prevent spill-back to a surface street intersection.

The network parameters used for this case are the same as used in Case study A of this section, except that the on-ramp model parameter is $\delta = 0.0122$ and the desired speed is 10% higher than the displayed speed limit, i.e., the drivers' noncompliance factor is $\varrho = 0.1$. These values are based on [75, 76]. The controller sampling time T_c is again chosen to be 1 min. The prediction horizon and the control horizon of the MPC are selected to be respectively $N_\mathrm{p} = 15$ (corresponding to 15 min) and $N_\mathrm{c} = 7$ (corresponding to 7 min) as used in [75].

To examine the effect of the combination of variable speed limits and ramp metering typical demand profiles are considered for the mainstream origin and the on-ramp (see Figure 5.9). The mainstream demand has a constant, relatively high level and a drop after 2 h to a low value in a time span of 15 min. The demand on the on-ramp increases to near capacity,

Table 5.2: Simulation results for Case study B. The values in the bracket indicate the relative change of the performance criteria as compared to the uncontrolled Scenario S_1. Negative values indicate a decrease (i.e., an improvement) in the value of the performance criteria, while positive values indicate an increase in the value of the performance criteria as compared to the uncontrolled scenario.

Scenarios	Performance Criteria		
	TTS [veh·h]	Total NO_x [kg]	TFC [l]
S_1: Uncontrolled	1459	8.719	6108
S_2: TTS	1247 (−14.6%)	8.288 (−4.9%)	5274 (−13.7%)
S_3: TTS + TFC	1257 (−13.9%)	8.147 (−6.6%)	4934 (−19.2%)
S_4: TTS+NO_x	1412 (−3.2%)	7.654 (−12.2%)	5290 (−13.4%)
S_5: TTS + TFC+NO_x	1336 (−8.5%)	7.786 (−10.7%)	5088 (−16.7%)

remains constant for 15 min, and decreases finally to a constant low value.

For the given demand profiles one uncontrolled (Scenario S_1) and four controlled (Scenarios S_2 to S_5) situations are compared. Scenario S_1 is considered as a benchmark to compare the results of the simulations when an MPC controller is implemented. For all the controlled scenarios, in order to give less emphasis to the variation of the control input, the weight corresponding to the variation of the control inputs in (5.16) is taken to be $\zeta_5 = 0.4$ (as in [75, 76]). The following performance criteria are considered for the MPC controller in the controlled scenarios:

S_2: Total time spent (i.e., $\zeta_1 = 1$, $\zeta_2 = \zeta_3 = \zeta_{4,\mathrm{MDL}} = \zeta_{4,\mathrm{TDL}} = 0$),

S_3: Total fuel consumption and total time spent (i.e., $\zeta_1 = \zeta_3 = 1$, $\zeta_2 = \zeta_{4,\mathrm{MDL}} = \zeta_{4,\mathrm{TDL}} = 0$),

S_4: Total NO_x emissions and total time spent (i.e., $\zeta_1 = \zeta_2 = 1$, $\zeta_3 = \zeta_{4,\mathrm{MDL}} = \zeta_{4,\mathrm{TDL}} = 0$, and $\mu_{\mathrm{CO}} = \mu_{\mathrm{HC}} = \mu_{\mathrm{CO_2}} = 0$, $\mu_{\mathrm{NO_x}} = 1$), and

S_5: Total fuel consumption, total NO_x emissions, and total time spent (i.e., $\zeta_1 = \zeta_2 = \zeta_3 = 1$, $\zeta_{4,\mathrm{MDL}} = \zeta_{4,\mathrm{TDL}} = 0$, $\mu_{\mathrm{CO}} = \mu_{\mathrm{HC}} = \mu_{\mathrm{CO_2}} = 0$, and $\mu_{\mathrm{NO_x}} = 1$).

Table 5.2 gives the simulation results of the uncontrolled simulation (Scenario S_1) and the controlled simulations (Scenarios S_2 to S_5). Moreover, the table gives the relative change as defined in (5.17) with $p \in \{\mathrm{TTS}, \mathrm{TFC}, \mathrm{NO}_x\}$. When the MPC controller is implemented (Scenarios S_2 to S_5) the values of all the performance indicators are reduced by a certain amount compared to the uncontrolled situation. But the reduction of the respective performance indicators is dependent on the objective of the controller. As can be seen in the table, when the objective of the controller is to reduce the TTS (Scenario S_2), the TTS is reduced by 14.6%. Moreover, the total NO_x emissions and the total fuel consumption are reduced by 4.9% and 13.7% respectively. This indicates that under the given traffic demand and traffic scenario, reducing the TTS can also help in reducing the total NO_x emissions and the total fuel consumption.

When the objective of the controller also includes the total fuel consumption as well as the TTS (Scenario S_3), the results for TTS differ slightly compared to Scenario S_2, while the total fuel consumption shows a significant reduction. So for Scenario S_3 more fuel is

saved by making a small sacrifice in the TTS that can be saved when only TTS is the control objective (Scenario S_2).

In Scenario S_4 the objective of the controller is to reduce the total NO_x emissions and the TTS where both criteria are weighted equally. In this scenario, the TTS does not show a significant improvement compared to the uncontrolled scenario. On the other hand, the total NO_x emissions decrease significantly. Moreover, we can see that the total fuel consumption is reduced by 13.4%, which is less than the improvement in Scenario S_3. Thus, although the combination of a larger TTS and more fuel consumption indicates inefficient driving behavior in terms of the economic performance indicators (travel time and energy consumption), there is a positive impact on the NO_x emission.

Scenario S_5 encompasses the concerns regarding the travel time, energy consumption, and the environment, as it addresses all three performance indicators by weighting them equally. The simulation results in Table 5.2 show that in this case the MPC controller achieves a balanced trade-off between total time spent, the total fuel consumption, and the total NO_x emission. As can be seen from the table, the three performance indicators are respectively improved by 8.5%, 10.7%, and 16.7%. Fig. 5.11 also provides more information on the states of the system when the objective of the controller is to address the total fuel consumption, total NO_x emission, and total time spent.

The action of the MPC controller in Scenario S_5 can be more clear when we compare Fig. 5.10 and Fig. 5.11. Fig. 5.10 and Fig. 5.11 depict the traffic states (density and space-mean speed), the queue length (at the on-ramp and mainstream origins), the flows at the on-ramp and mainstream origins, and the control inputs (the variable speed limits and ramp metering rate) of the traffic system under Scenarios S_2 and S_5 respectively[4]. The dynamics of the queue length in the Fig. 5.11 is different than in Fig. 5.10. This can be explained as follows. Since the initial speed and the number of the vehicles in the freeway origin is larger than the initial speed and the number of the vehicles at the on-ramp, the emissions and fuel consumption of the vehicles at the freeway origin will have more effect on the value of the control objective function than their waiting time or than the emissions and fuel consumption of the vehicles at the on-ramp. Thus, the controller tries to avoid a queue on the freeway origin without violating the on-ramp queue length (see Fig. 5.11). This has resulted in frequent fluctuation of the control inputs. This can be seen in Fig. 5.11, where the control input fluctuates during the simulation periods where the queue lengths fluctuate (i.e., between 0.5 h and 2 h of the simulation periods). In Scenario S_2 a queue can develop in the mainstream origin under two conditions. One possible condition is when the queue length at the on-ramp has reached its maximum limit (the same as in Fig. 5.11). The second possibility is when the contribution of the queue on the TTS is the same whether it is formed at the on-ramp or at the mainstream origin. But if in the long run the TTS can be reduced by forming a queue at the mainstream origin, the controller can let a queue develop on the mainstream origin. This can be one of the reasons for the formation of the queue in Scenario S_2 while the queue in the on-ramp is below its limit.

[4]Since detailed results of the MPC controller under different control performance indicators are given in Table 5.2, the evolution of the traffic states of all the scenarios is not presented. As an illustration and as good representatives, Scenarios S_2 and S_5 are chosen and the evolution of the traffic states of these scenarios are respectively depicted in Fig. 5.10 and Fig. 5.11, because Scenario S_2 shows a traffic problem where most traffic control approaches focus on and Scenario S_5 shows the potential of MPC to provide a balanced trade-off between possibly conflicting traffic performance criteria.

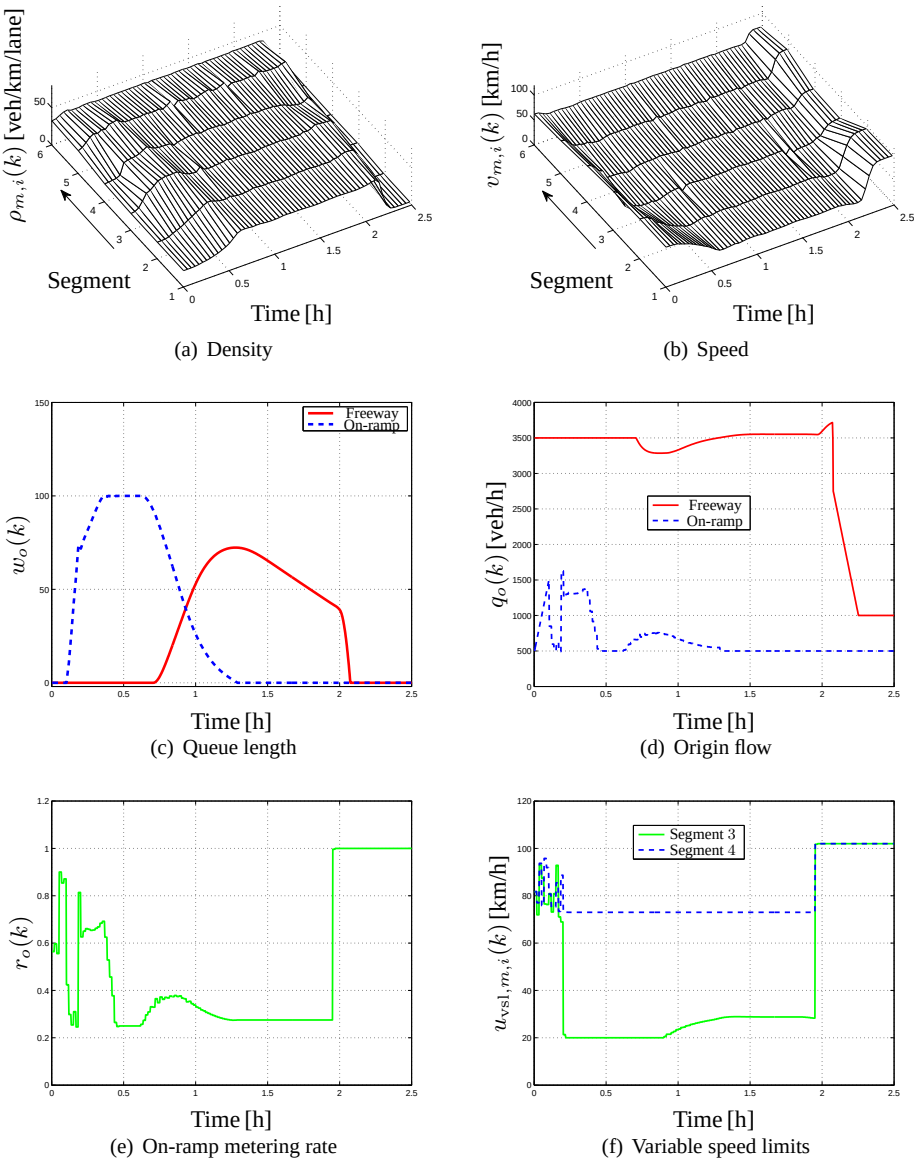

Figure 5.10: The trajectory of the traffic states and the control signals of Case study B when the objective of the controller is reducing the total time spent only (Scenario S_2). The arrows indicate the driving direction.

In the two case studies presented above, macroscopic traffic models are used. However, similar conclusions are reached using microscopic models in our papers [207, 209, 210]. To avoid presentation of similar concepts and to focus on the main relevant points, those

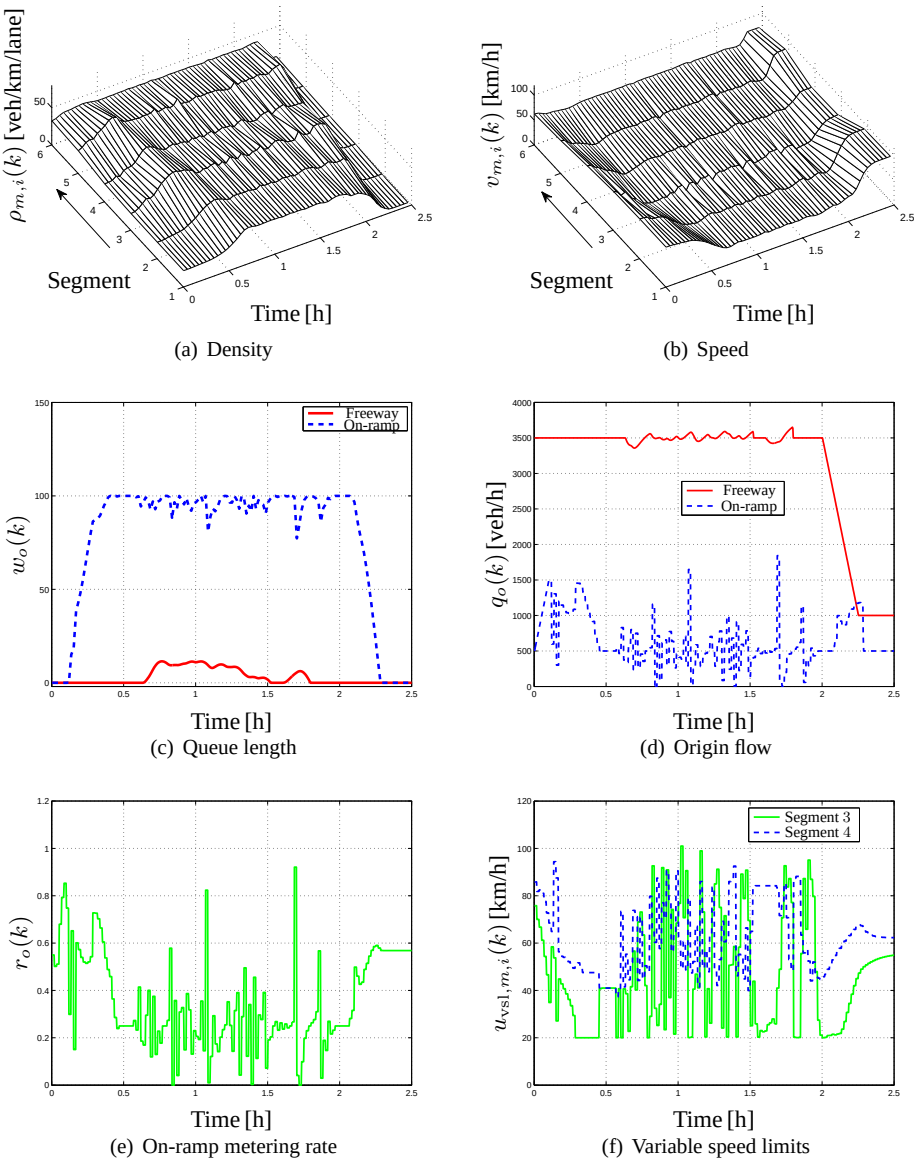

Figure 5.11: The trajectory of the traffic states and the control signals of Case study B when the objective of the controller is to minimize the total fuel consumption, total NO_x emissions, and total time spent (Scenario S_5). The arrows indicate the driving direction.

results are not discussed in this thesis. Moreover, the MPC approach is so generic that it can be applied with other complex and extensive models. Hence, throughout this thesis, the simulations are based on the macroscopic models, because this eases the computational

demands of the approach.

5.5.2 Reduction of area-wide emissions

In the previous section, the use of MPC for the reduction of traffic travel time, emissions, and fuel consumption was presented. Two control measures, variable speed limits and ramp metering, were considered. In this section the dispersion of the emissions to a given target zone is considered as an additional performance criterion of the MPC controller. Two case studies are presented. In the first case (Case study C), only variable speed limit is used as a traffic control measure. Moreover, the dispersion of emissions under constant wind speed and wind direction is considered. In the second case (Case study D), an additional traffic control measure, ramp metering, and variable wind speed and wind direction are considered.

Case study C

In this case study, a $12\,\mathrm{km}$ three-lane freeway stretch, which is sectioned into twelve equal segments of size $1\,\mathrm{km}$ is considered. Each section of the freeway is equipped with a variable speed limit control (see Fig. 5.12). Since the intention is to illustrate the use of MPC with multi-objective traffic control performance criteria, for computational reasons, the speed limits are coupled in groups of four, where each group displays the same speed limit at the same time. In general, it is possible that the performance of MPC can decrease due to this grouping. For this case study, since the main goal is to demonstrate the potential of MPC, we allow a small loss in performance for increased computation speed.

In this case study, a protected zone (e.g., school) with an area of $200\,\mathrm{m}\times 200\,\mathrm{m}$ is located at $2\,\mathrm{km}$ north and $6\,\mathrm{km}$ east of the origin of the freeway (see Fig. 5.12). The freeway and its neighborhood are subject to a wind blowing with speed $V_\mathrm{w} = 8\,\mathrm{m/s}$ and with an angle $\varphi = \pi/3$ radians with respect to the freeway as shown in Fig. 5.12. Fig. 5.13 depicts the traffic demand at the origin of the freeway.

The traffic flow, emissions, and dispersion of the emissions of the freeway considered are modeled using the METANET, VT-macro, and point-source dispersion models presented in respectively Sections 2.3, 3.4, and 4.2. The freeway parameters have the same values as in Case study B of Section 5.5.1.

An uncontrolled Scenario S_1 of the traffic setup is used as the benchmark to compare the performance of the MPC controller for different traffic performance criteria. For the controlled Scenarios S_2 to S_5, a multi-objective performance criterion defined in (5.16), with $\zeta_3 = \zeta_{4,\mathrm{TDL}} = 0$, $\zeta_5 = 0.01$, $\mu_\mathrm{CO} = \mu_\mathrm{HC} = \mu_{\mathrm{NO_x}} = 1$, and $\mu_{\mathrm{CO_2}} = \mu_\mathrm{fuel} = 0$ is considered throughout this case study. By varying the weights ζ_1, ζ_2, and $\zeta_{4,\mathrm{MDL}}$ in (5.16), the following control objectives are considered:

S_2: Total time spent (i.e., $\zeta_1 = 1$ and $\zeta_2 = \zeta_3 = \zeta_{4,\mathrm{MDL}} = \zeta_{4,\mathrm{TDL}} = 0$),

S_3: Total emissions (i.e., $\zeta_2 = 1$ and $\zeta_1 = \zeta_3 = \zeta_{4,\mathrm{MDL}} = \zeta_{4,\mathrm{TDL}} = 0$),

S_4: Dispersion level (i.e., $\zeta_{4,\mathrm{MDL}} = 1$ and $\zeta_1 = \zeta_2 = \zeta_3 = \zeta_{4,\mathrm{TDL}} = 0$), and

S_5: Total time spent, total emissions, and dispersion level with $\zeta_1 = 10$, $\zeta_2 = 1$, $\zeta_3 = \zeta_{4,\mathrm{TDL}} = 0$, and $\zeta_{4,\mathrm{MDL}} = 5$.

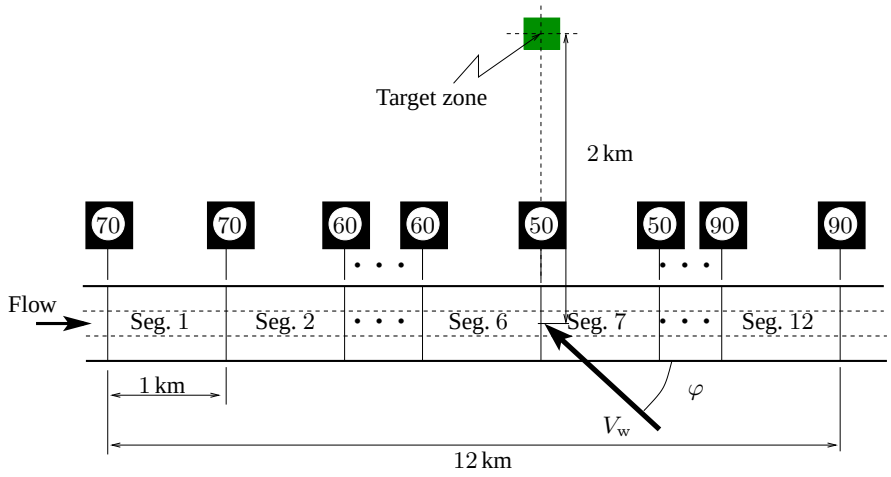

Figure 5.12: A 12 km 3-lane traffic freeway considered for Case study C. The freeway is equipped with 12 variable speed limits and there is a neighboring school of area 0.04 km^2 at a distance of 2 km from the center. It is subjected to wind with wind speed $V_w = 8$ m/s and wind direction $\varphi = \pi/3$ radians.

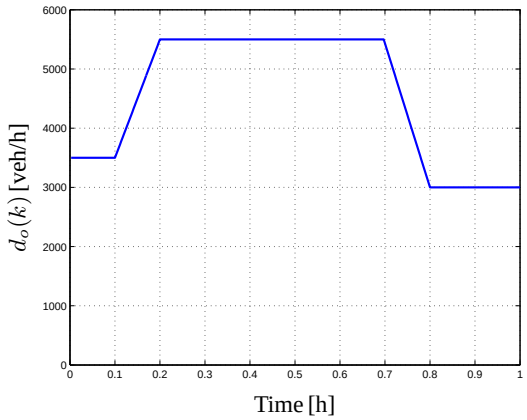

Figure 5.13: Traffic demand profile for Case study C.

The control time step $T_c = 2$ min, the prediction horizon $N_p = 7$ (corresponding to 14 min), and the control horizon $N_c = 5$ (corresponding to 10 min) are used. The duration of the simulation is 1 h with a simulation time step size $T = 10$ s.

The simulation results for the different scenarios are tabulated in Table 5.3. The first row of the table shows the results of the simulation for a case where no controller is implemented. Under this scenario, the evolution of the dispersion of the emissions of the freeway to the school area is depicted in Fig. 5.14 (solid line). The second to the fifth rows of the table provide the simulation results under the controlled scenarios and the relative percentage change as compared to the uncontrolled scenario using the expression given in (5.17) with

Table 5.3: Simulations results under uncontrolled and different traffic control objectives of Case study C. The values in brackets indicate the relative change of the performance criteria of the controlled scenarios compared to the uncontrolled scenario. Negative values indicate a decrement (i.e., an improvement) of the performance criteria as compared to the uncontrolled scenario, while positive values indicate an increment in the performance criteria.

Scenarios	Performance Criteria		
	TTS [veh·h]	TE [kg]	MDL [μg/m^2]
S_1: Uncontrolled	1488.8	133.3	56.3
S_2: TTS	1100.7 (-26%)	162.5 ($+22\%$)	62.1 ($+10\%$)
S_3: TE	1783.9 ($+20\%$)	64.8 (-51%)	19.3 (-66%)
S_4: MDL	1783.9 ($+20\%$)	64.8 (-51%)	19.3 (-66%)
S_5: 10TTS + TE + 5MDL	1382.6 (-7%)	85.6 (-36%)	34.1 (-39%)

$p \in \{\mathrm{TTS}, \mathrm{TE}, \mathrm{MDL}\}$.

The levels in Fig. 5.14 have the same initial value for all the scenarios. This is because the initial emission levels of the freeway cannot be affected by the controller. Hence, only the impact of the emissions emitted after the start of the simulation can be affected.

When the objective of the controller is to reduce the TTS (Scenario S_2), the dispersion level is smaller than in the uncontrolled case only for about 15 min (see Fig. 5.14). However, after about 30 min of the simulation time, the dispersion level of the TTS controlled case in the target area becomes higher for the rest of the simulation time. As a result, in Table 5.3 we see that the maximum dispersion level MDL and the total emissions TE for the TTS controlled case increase by 10% and 22% respectively compared to the uncontrolled case. However, the TTS is improved by 26% relative to the uncontrolled case. This indicates that reducing the travel time can have a negative impact on the area-wide emissions. Obviously, the negative impact of the improved travel time on the emissions can be accounted to the increase in speed of the vehicles as can be seen in Fig. 5.15.

When the objective of the controller is to reduce either the TE (Scenario S_3) or the MDL (Scenario S_3), the results are almost the same (see Table 5.3 and Fig. 5.14). In these two scenarios the travel time is increased by 20% compared to the uncontrolled case. But, the TE and the MDL are respectively reduced by about 51% and 66%. Moreover, the evolution of the dispersion levels on the target zone is smaller throughout the simulation (see Fig. 5.14). This shows that the emissions and dispersion levels are lower when the speed of the vehicles is lower (see Fig. 5.15), which is consistent with the emission rate models. On the contrary, the travel time increases as the speed of the vehicles decreases. So the results are consistent with the traffic flow and emission rate theory. For the TTS controlled case (Scenario S_2) and around 0.45 h, the emission levels at the target zone have abruptly increased (see TTS controlled scenario of Fig. 5.14). The abrupt increase in emission levels is caused due to the abrupt increase in the speed of vehicles at around 0.3 h (see TTS controlled scenario of Fig. 5.15). Due to the distance of the target zone from the freeway (2 km from the center) and due to the low wind speed (8 m/s), the high emission levels released from the freeway are experienced after about 0.15 h at the target zone. Since the significant increase in the average speed at about 0.5 h is accompanied by a significant reduction in the number of vehicles (see Fig. 5.15), the emissions have not shown significant

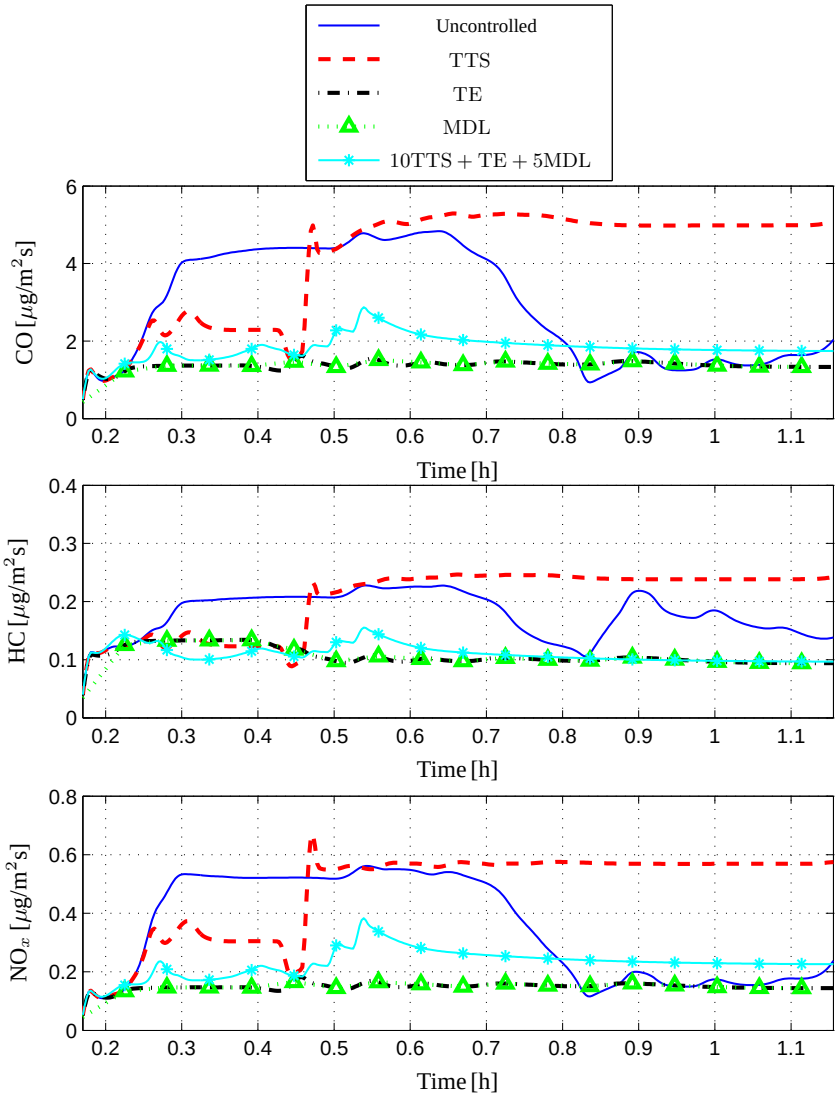

Figure 5.14: Evolution of dispersion levels for the uncontrolled and the controlled scenarios of Case study C.

change.

Finally, all the performance criteria (TTS, TE, and MDL) are combined in the objective function of the controller as in the last row of Table 5.3. In this case the TTS is reduced by 7% compared to the uncontrolled scenario. Furthermore, the TE and MDL are respectively reduced by 36% and 39% relative to the uncontrolled scenario. However, the reduction in percentage of the performance criteria is less than the scenarios where the objective of the controller is focused only on either of these measures.

In general, the simulation results demonstrate that variable speed limits can be used in

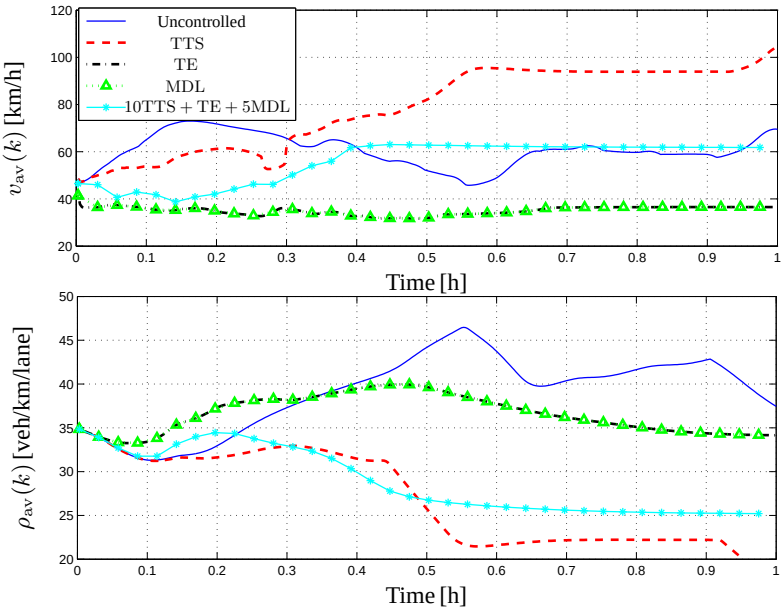

Figure 5.15: Evolution of average speed $v_{\mathrm{av}}(k)$ and average density $\rho_{\mathrm{av}}(k)$ over all the segments of the freeway for the uncontrolled and the controlled scenarios of Case study C.

some cases to alleviate, in a balanced way, the problem of emissions and of lost time due to traffic jams. Note, however, that there are also cases where the variable speed limit is not effective, e.g., if all segments of a traffic freeway are congested [75].

Case study D

In Case study C, variable speed limits are applied to reduce travel time, emissions, and the dispersion of emissions into a given target zone. The point-source dispersion model with constant wind speed and wind direction has been used. In the current case study, ramp metering traffic control is also taken into account. Moreover, the wind speed and wind direction are assumed to vary in time. A 12 km three-lane freeway stretch with one on-ramp is considered. The freeway is divided into 12 segments with the on-ramp at the sixth segment from the left as depicted in Fig. 5.16. Each segment of the freeway is equipped with a variable speed limit. In this case study, the variable speed limits are grouped in groups of two such that each segment in a group will have the same speed limit signs. This implies the MPC controller optimizes only 6 speed limits and 1 on-ramp metering rate. So, in total there are 7 control variables at each control time step.

The traffic flow demand at the mainstream origin and the on-ramp origin is shown in Fig. 5.17. In addition, the freeway is subject to a wind with speed and direction (see Fig. 5.16) given by

$$V_{\mathrm{w}}(k) = 7 + 2\sin(0.005\pi k + \pi/6)\sin(0.01\pi k) \tag{5.18}$$

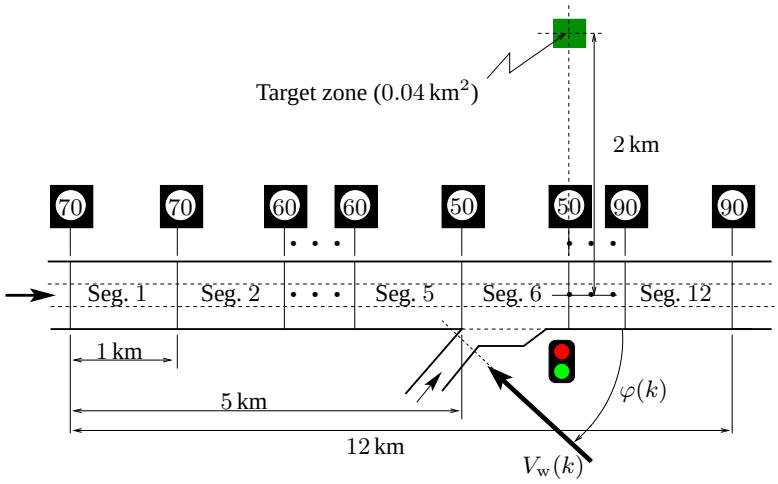

Figure 5.16: A 12 km freeway with 12 variable speed limits and 1 on-ramp for Case study D.

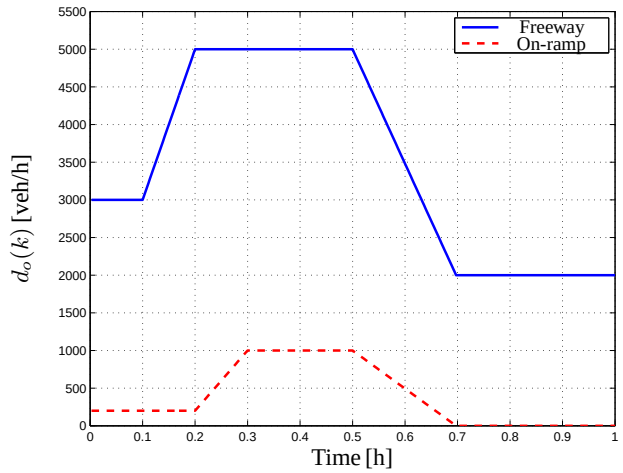

Figure 5.17: Traffic demand flow at the mainstream and on-ramp origins for Case study D.

$$\varphi(k) = \frac{2\pi}{5} + \frac{\pi}{4}\cos(0.004\pi k) \tag{5.19}$$

where the wind speed $V_w(k)$ is expressed in m/s and the wind direction (angle) $\varphi(k)$ in radians.

Similar to Case study C, a multi-objective performance criterion that accommodates the emissions, dispersion of emissions, and travel time is considered in addition to the uncontrolled scenario. The performance criteria for this case study are the same as in Case study

Table 5.4: Simulations results under uncontrolled and different traffic control objectives of Case study D. The values in the brackets indicate the relative change of the performance criteria of the controlled scenarios compared to the uncontrolled scenario. Negative values indicate a decrement (i.e., an improvement) of the performance criteria as compared to the uncontrolled scenario, while the positive values indicate an increment of the performance criteria.

Scenarios	Performance Criteria		
	TTS [veh·h]	TE [kg]	MDL [μg/m^2]
S_1: Uncontrolled	1362	127.5	163.2
S_2: TTS	692 (-49%)	148.2 ($+16\%$)	160.6 (-1%)
S_3: TE	1621 ($+20\%$)	65.6 (-49%)	87.7 (-46%)
S_4: MDL	1606 ($+15\%$)	71.8 (-44%)	104.7 (-36%)
S_5: 10TTS + TE + 5MDL	749 (-45%)	109.4 (-15%)	142.6 (-13%)

C. Moreover, the parameters of the MPC controller are set the same as that of the MPC controller in Case study C. For all the five scenarios (one uncontrolled and four controlled), the case study is simulated for an hour. The simulation results for these scenarios are tabulated in Table 5.4.

Table 5.4 compares the performance of the MPC controller with respect to the uncontrolled scenario using (5.17) with $p \in \{\mathrm{TTS}, \mathrm{TE}, \mathrm{MDL}\}$. The performance measures considered are the total time spent (TTS), the total emissions (TE), and the maximum dispersion level (MDL) at the target zone. As can be seen, when the objective of the controller is the TTS, the TE is worsened and the MDL in the target zone is almost unchanged as compared to the uncontrolled scenario. Similarly, if the objective of the controller is to reduce the TE or the MDL, the TTS gets worse than for the uncontrolled scenario. But there is an important difference between the two scenarios. The TTS gets much worse when the objective of the controller is TE than when it is MDL. Moreover, the MDL in Scenario S_4 is larger than the MDL in Scenario S_3, which in fact should not be the case (see Remark 5.3 for possible reasons).

Remark 5.3 In general, the MDL is expected to be lower when the objective of the controller is reducing MDL than when the objective of the controller is reducing TE. However, the results in Table 5.4 show the opposite. This can happen for two possible reasons, viz.

1. When the prediction horizon of the MPC controller is not large enough to capture the important dispersion dynamics. Under such cases, the traffic solutions that give better performance for the prevailing traffic situation may have negative impact on the future traffic conditions. This is because that since the traffic state changes at every control time step and since the controller uses this state as an initial condition to predict the future traffic states, any change to the state (which can be good for the current traffic situation) may lead to a situation that may turn out to be bad for the future traffic performance.

2. The second reason is due to the optimization process. Since the optimization is nonlinear and non-convex problem and since the control objectives for the two cases have different non-linearity and non-convexity, it is possible that the MDL can be minimal under Scenario S_3 than Scenario S_4.

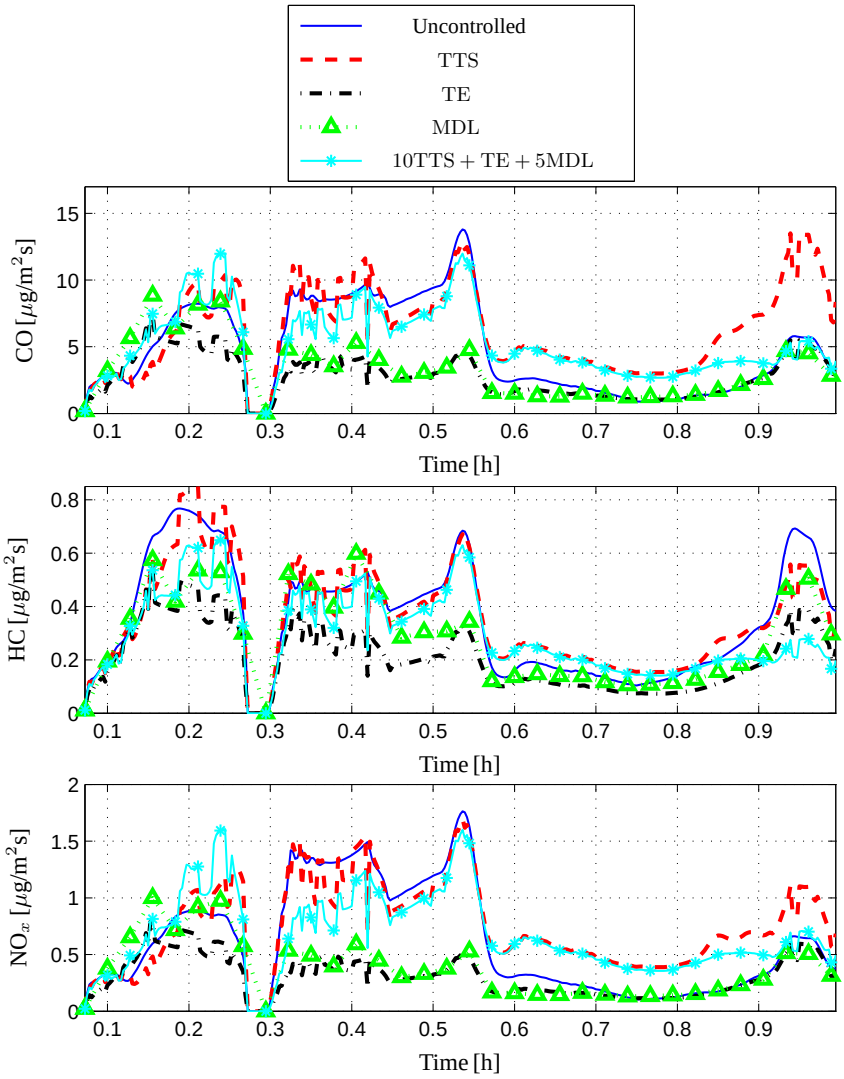

Figure 5.18: Evolution of dispersion levels for the controlled and uncontrolled scenarios of Case study D.

□

More can be observed by also looking into the evolution of the dispersion levels. The evolution of the dispersion level in the target area is plotted in Fig. 5.18. The figure depicts the dispersion level for the different controlled scenarios and for the uncontrolled scenario. To have more insight in what is happening the space-mean speed of the complete freeway in shown in Fig. 5.19.

From Fig. 5.19 one can see that the two shock waves of the traffic flow observed in the uncontrolled case are dissolved when the objective of the controller is to reduce only the

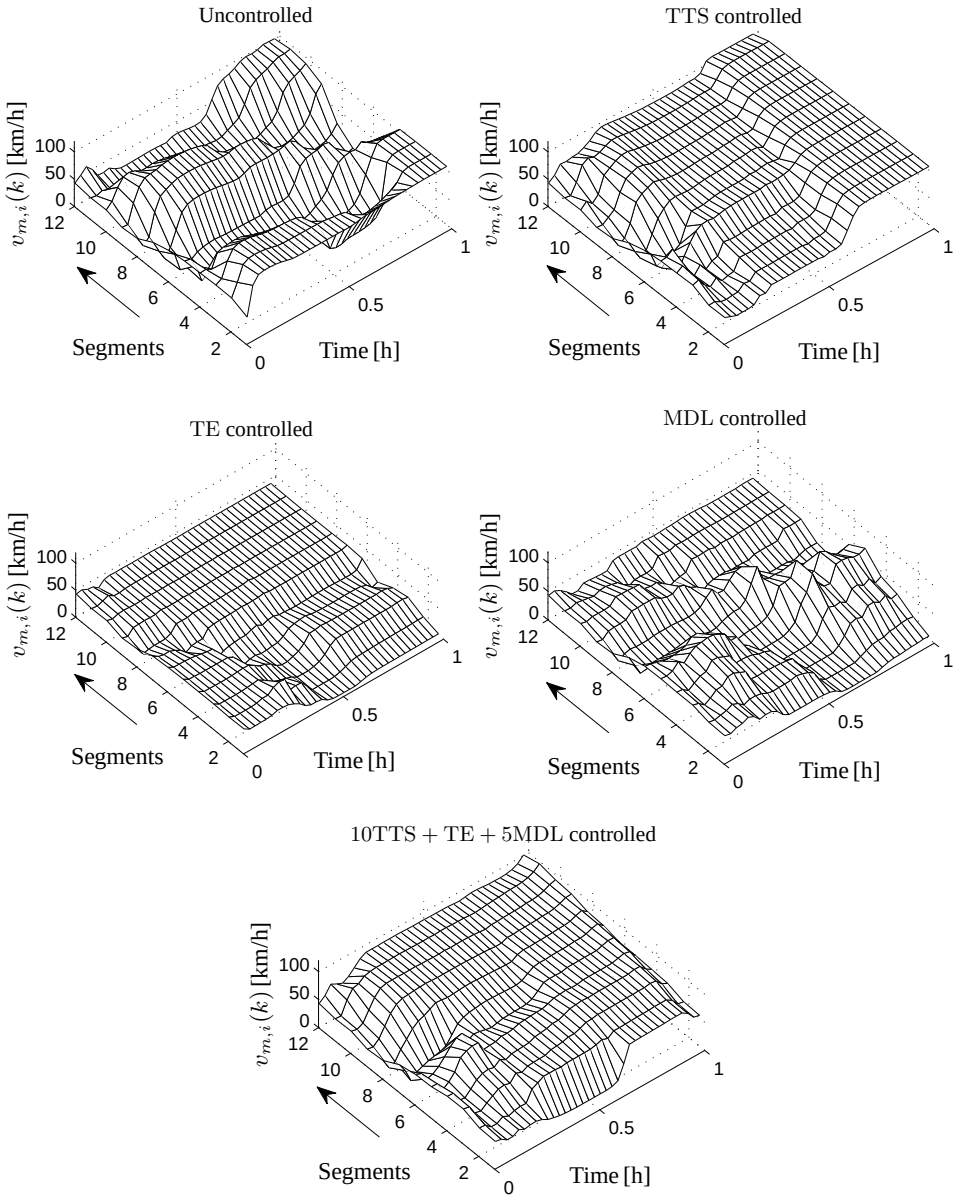

Figure 5.19: Space-mean speed over segments and time for controlled and uncontrolled scenarios of Case study D. The arrows indicate the driving direction.

total time spent (Scenario S_1). Under this situation the dispersion level becomes even more worse than for the uncontrolled case (see Fig. 5.18), i.e., despite the fact that the maximum dispersion level (MDL) at about $t = 0.53$ h is less than the uncontrolled scenario, it can be seen that the dispersion levels during most of the time under the TTS controlled case are

higher than for the uncontrolled scenario. However, if the objective of the controller is set to reduce the maximum dispersion level, one sees that the TTS of the traffic flow gets worse by 15% (see Fig. 5.19 and Table 5.4), but the dispersion level is reduced by 36%.

When the objective of the controller is the weighted sum of the TTS, TE, and MDL, the TTS is improved relatively to both the uncontrolled scenario and to the scenario where only TE or MDL are the objective of the controller. Moreover, the TE and MDL are also reduced compared to the uncontrolled scenario. However, their decrement relative to Scenario S_3 (TE controlled) or Scenario S_4 (MDL controlled) is small. In general, it can be observed that as the weights of the performance indicators vary, the controller can shift its focus towards the improvement of the indicators with higher weighting factor. In this way the model predictive controller can be used to specifically improve the traffic performance.

5.6 Conclusions

Model predictive traffic control is a potentially very promising control approach since it is able to use non-linear and complex system models, it takes both system and operational constraints into account, and it makes decisions based on the evolution of the current and the future possible traffic states. In many papers in the literature it has been shown that the model predictive control, in particular model predictive traffic control, is able to optimally coordinate different control measures and to provide (sub-)optimal solutions to improve the traffic flow. In this chapter, a short account on the concept of MPC and how it can be used for traffic control has been discussed.

In addition to the travel time as the performance criterion of traffic controllers, the fuel consumption and the emissions of vehicles in a traffic network, and the dispersion of the emissions to neighborhoods of traffic networks are important traffic performance criteria. In this context, this chapter has presented how these quantities can be formulated. Moreover, the formulation of a multi-objective criterion for the MPC traffic controller has been discussed.

Finally, four cases studies, two that focus on the reduction of combined travel time, emissions, fuel consumption, and two that focus on the reduction of combined travel time, emissions, and dispersion of emissions have been presented. In the case studies, the use of variable speed limits alone and variable speed limits integrated with ramp metering have been illustrated. The case studies demonstrated that MPC is able to provide a balanced trade-off between the travel times, emissions, fuel consumption, and dispersion of the emissions to a target zone.

However, the simulations in all the cases consumed long computation times, which makes the control approach intractable for real-time applications. So an improvement in the computation time is required. The following chapter will present a version of the MPC controller that has lower computation times which makes it tractable in practice.

Chapter 6

Receding-Horizon Parametrized Control

As has been indicated in the previous chapter, Model Predictive Control (MPC), and in particular, non-linear MPC has certain disadvantages. The main disadvantage emanates from the non-linear and non-convex optimization involved. Usually, in practice the computation time exponentially increases as the number of control inputs or the prediction horizon increases. To alleviate the computational problems the introduction of a control horizon or blocking has been discussed in Chapter 5. However, these approaches do not bring down the computation time to the level at which MPC can be applied for freeway traffic in practice, unless the performance is compromised significantly.

Another interesting approach that can reduce the computation time considerably is the parametrization of the control inputs (by a smaller number of parameters than the number of control inputs), so that the controller optimizes a set of parameters instead of optimizing a sequence of control inputs as in the case of conventional MPC. In this approach the parameters are optimized in such a way that a given performance criterion is improved in a receding horizon fashion. To do so, the control inputs are described using certain control laws that are dictated by the values of the parameters.

This chapter then presents parametrized MPC, more specifically called Receding Horizon Parametrized Control (RHPC). This chapter begins by providing some introductory notes on parametrized MPC in Section 6.1. Next, the philosophy of the RHPC controller and its general formulation is elaborated in Section 6.2. Following the design of RHPC for variable speed limits and ramp metering in Section 6.3, case studies are presented in Section 6.4. At the end, the conclusions of the chapter are put forward in Section 6.5.

Parts of this chapter are published in [216, 217].

6.1 Parametrized MPC

It has been indicated that the freeway traffic system is complex, non-linear, and time-variant. Controlling the traffic network to get a system (or user) optimum traffic flow, while at the same time reducing the externalities of traffic flow (such as emissions and fuel consumption)

is a day-to-day challenge. In this regard, many studies that focus on the design of traffic controllers to improve the traffic flow under certain traffic conditions [42, 79, 149, 150] have been conducted for decades. The freeway traffic controllers in [78, 79] are designed to avoid or at least to reduce shock waves on freeways. The freeway controllers designed in [42, 149, 150] are state feedback control policies where the parameters of the control policies are determined using off-line optimization approaches based on simulation or historical data of the given freeway. This means the control policies perform well for the specific scenarios they are optimized to. In [104] an optimal open-loop freeway controller called AMOC (Advanced Motorway Optimal Control) is proposed. However, the traffic conditions change so frequently that the performance of the controllers is then most often reduced.

An excellent traffic control solution for freeway traffic problems is a controller that takes the current and future traffic situation into account and that predicts the consequences of its control actions. One such control strategy, Model Predictive Control (MPC), has been proposed more than three decades ago [50, 168] and has been discussed in Chapter 5. Recall that an MPC approach can handle model uncertainties, include constraints, support multi-objective performance criteria, and can be used with non-linear models [35, 116]. Moreover, in several case studies, MPC has proved to yield significant gains in the performance of the traffic network [22, 77, 220]. However, it has been pointed out that this comes with one main limitation; the computation time is very large [22, 77] (see also Section 5.6).

Indeed, there are many advancements and efforts described in the literature (e.g., [24, 37, 71, 98, 111, 179, 183, 189, 195]) to address the computation problems of MPC in general. Most available papers in literature deal either with linear time-invariant systems or specific classes of non-linear systems (such as linear time-varying, linear parameter-varying, and piecewise affine systems). However, traffic systems are too complex and non-linear such that they do not fall within the specific classes of non-linear systems for which the methods to reduce the computation time have been developed.

In an effort to formulate the model structure of the METANET traffic flow model [103, 124, 145, 146] to suit for advanced control approaches, the authors in [113, 115] have approximated the METANET traffic flow model by a Linear Parameter-Varying (LPV) model. That model has been extended in [213] to include emission models in an LPV form. But the models do not have the provision to use variable speed limits, which is an important freeway control measure [79, 180]. These models use only ramp metering as a traffic control measure. Moreover, the number of scheduling variables of the LPV models increases as the size of the traffic network increases, which increases the computation time exponentially. Although the LPV approach may have potential to reduce the computation time with some errors introduced, the approach requires further research. The authors of [69] have proposed to use a game-theoretic approach with *distributed* controllers to address the computational complexity of MPC for traffic systems. Moreover, in [105, 151] it is proposed to use a model-predictive hierarchical control approach, which is also reported to be computationally tractable in practice. In [64] it is also proposed to apply an artificial neural network as an offline control approach for optimal freeway traffic control instead of using on-line optimization.

In this chapter, however, a centralized traffic control approach that yields fast computation speeds is presented. A Receding-Horizon Parametrized Controller (RHPC for short) is proposed as a traffic control approach that combines the advantages of conventional MPC (i.e., prediction, adaptation, and handling constraints, multi-objective criteria, and non-linear models) and the advantages of state feedback controllers (i.e., faster computa-

tion speed and easier implementation). The control approach does not impose any specific structure on the traffic models. This idea is related to the parametrization concept introduced by [71, 98, 111, 179]. In general, depending on the parametrization the proposed RHPC approach can introduce loss in performance relative to its counterpart, conventional MPC.

In the conventional MPC approach the control inputs of a system are optimized directly. In parametrized MPC approach the control signals are parametrized according to some control policies (laws) and the parameters of the control policies are optimized over a given time horizon to reduce a pre-defined objective (cost) function [71, 98, 111, 179]. Therefore, the control inputs in parametrized MPC are optimized indirectly as opposed to the conventional MPC approach. The parameters of the control policies can be optimized in such a way that they are constant over the prediction horizon [98, 111, 179] or they can be considered to be time-varying over the prediction horizon [71]. In addition to the fact that the approaches of [71, 98, 111, 179] are not well developed to handle the general class of non-linear systems (such as traffic systems), all the parametrization concepts in [71, 98, 111, 179] revolve around the transformation of the non-convex optimization problem of conventional MPC into a convex optimization problem through the parametrization of the control inputs. This means that the number of parameters can be (and usually also is) larger than the number of control inputs of conventional MPC. So if the parametrization cannot transform the optimization into a convex problem, the computation time of the MPC will not be reduced.

But if the parametrization is defined appropriately and if the number of parameters that describe the laws of the control signals is smaller than the number of control signals, it is possible to reduce the computation time of the MPC controller without necessarily transforming the MPC optimization problem into a convex problem, which is the approach proposed in this chapter. This means that for the same problem set-up, in general the parametrized MPC results in lower computation times than conventional MPC. However, note that since the space of the control signals is in principle reduced due to the parametrization process, in general the performance of parametrized MPC may be less optimal than that of conventional MPC.

6.2 Basic concepts of RHPC

In this section the proposed Receding-Horizon Parametrized Control (RHPC) is discussed in detail. First, the general philosophy of the RHPC traffic controller is discussed. The different possible variants of the controller and their relative computation speeds under the same conditions are examined. Next, the general description on how the method can be employed to design dynamic traffic control laws is put forward.

6.2.1 Philosophy of RHPC traffic controller

The concept of RHPC can be illustrated with the schematic diagram depicted in Fig. 6.1. The system block represents the real traffic system where the measurement of the traffic state (such as the speed, density, and flow) is fed to the RHPC controller. The RHPC controller contains two layers: the feedback layer and the optimization layer. The feedback layer has a control law block that receives the traffic state and determines the value of traffic control measures at every control time step $k_{\mathrm{c,i}}$ (with control time step size $T_{\mathrm{c,i}}$). The control laws

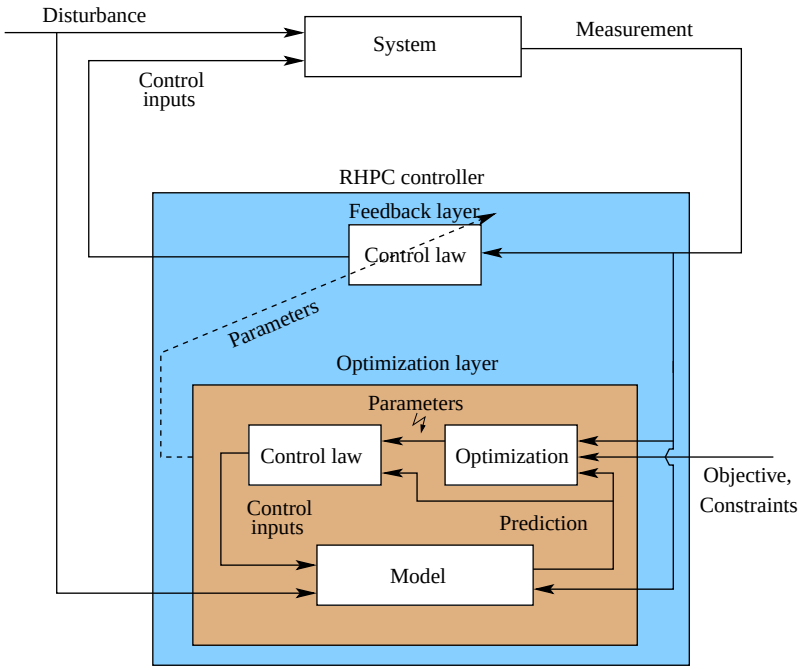

Figure 6.1: Schematic representation of model-based receding-horizon parametrized control (RHPC).

of the feedback layer are described by a set of parameters which are updated every control (parameter-update) time step k_c where $k_{\mathrm{c,i}}(k_\mathrm{c}) = M_4 k_\mathrm{c}$ with M_4 being a positive integer.

The optimization layer contains the model of the traffic system, the optimization tool, and the control law (which is the same as that of the feedback layer) blocks (see Fig. 6.1). Similar to the conventional MPC controller, with the measurements of the traffic states at control (parameter-update) time step k_c as the initial states of the model, the RHPC controller predicts the evolution of the system states using the system model (such as traffic flow, emissions, and dispersion models). The optimization block optimizes a set of parameters that describe the control policy in such a way that the defined control objective (cost) function is reduced over the prediction period while the constraints are met. The optimal set of parameters is fed to the control law block. The control law block uses the parameters along with the measured and predicted traffic states from the model to generate the traffic control measures (such as speed limits, ramp metering rate, and route guidance signals). The parameters are optimized and generated as if they are intended to be used for the whole prediction horizon. However, the optimization layer of the RHPC controller applies only the parameter values of the first control time step to the feedback layer. At the next control time step, the prediction horizon shifts one control time step, and the RHPC controller repeats the optimization process all over again, which is called the receding horizon concept (see also Section 5.1).

Although RHPC and conventional MPC are based on the same concept, they have four major differences. First, the number of optimization variables is different. Due to the parametrization RHPC is designed in such a way that the number of parameters required

to describe the control laws is smaller than the number of control inputs. Note that in RHPC the parameters of the control laws are the optimization variables while in conventional MPC the control inputs are the optimization variables. Second, unlike the conventional MPC controller, the RHPC controller does not necessarily optimize the parameters every control time step $k_{\mathrm{c,i}}$ as does conventional MPC (i.e., the control (parameter-update) time step size T_{c} of the optimization layer is in general greater than the control time step size $T_{\mathrm{c,i}}$). The optimization of the RHPC controller is undertaken at every control time step k_{c}, which is related to the control time step $k_{\mathrm{c,i}}$ as $k_{\mathrm{c,i}}(k_{\mathrm{c}}) = M_4 k_{\mathrm{c}}$ where M_4 is a positive integer. Third, due to the parametrization with few number of parameters, the range of the control signals of RHPC is reduced as compared to conventional MPC. In this context RHPC is more conservative than conventional MPC, since in general the full space of optimal control inputs cannot be reached from the parameter space (see Section 7.1). This may result in a loss of performance compared to conventional MPC. Fourth, since the number of the optimization variables of RHPC is smaller than that of conventional MPC, the computation time of RHPC is smaller than the computation time of conventional MPC. In the ensuing sections the difference between conventional MPC and RHPC will be more clear.

Remark 6.1 From now on, for the sake of simplicity of the exposition, we just take the control (parameter-update) time step size T_{c} of the optimization layer to be equal to the control time step size $T_{\mathrm{c,i}}$ of the feedback layer. However, expansion of the subsequent theories to the case where $T_{\mathrm{c}} \neq T_{\mathrm{c,i}}$ is straightforward. □

The computation time of RHPC depends on the way the parameters are allowed to vary over the control horizon. This can be realized in three different ways:

1. *Control policies with constant parameters.* This option is used in most of the literature [71, 98, 111, 179]. In this approach a state feedback controller (control law) with constant parameter is designed. So in this option (control policies with constant parameters), the parameters of the control law do not change over the prediction horizon as shown in Fig. 6.2(a). Although the parameters are kept constant throughout the prediction horizon, the control inputs in general vary due to the variation in the states of the system (see Fig. 6.2(a)). Thus, the number of parameters over the entire prediction horizon is small, which leads to reduced computation time, while in the conventional MPC approach—if the control inputs have to vary over the prediction horizon as in this case—the number of control inputs that have to be optimized increases proportionally to the control horizon. However, in general, since this option of control input parametrization limits the space of the parameters, it is conservative and could have a lower performance than the two approaches presented next.

2. *Control policies with variable parameters.* In contrast to the first option, where the parameters are kept constant throughout the control horizon, in this approach the parameters of the control policies vary over the whole control horizon (see Fig. 6.2(b)). So, both the control input and the parameters vary at the same time (see Fig. 6.2(b)). Since the parameters can vary over the entire control horizon, the space of the control inputs is larger than the first option elaborated above. In this approach the computation time of the RHPC controller is smaller than that of the conventional MPC controller provided that the number of parameters describing the control laws is less than the number of control inputs of the system. This control approach requires higher computation time

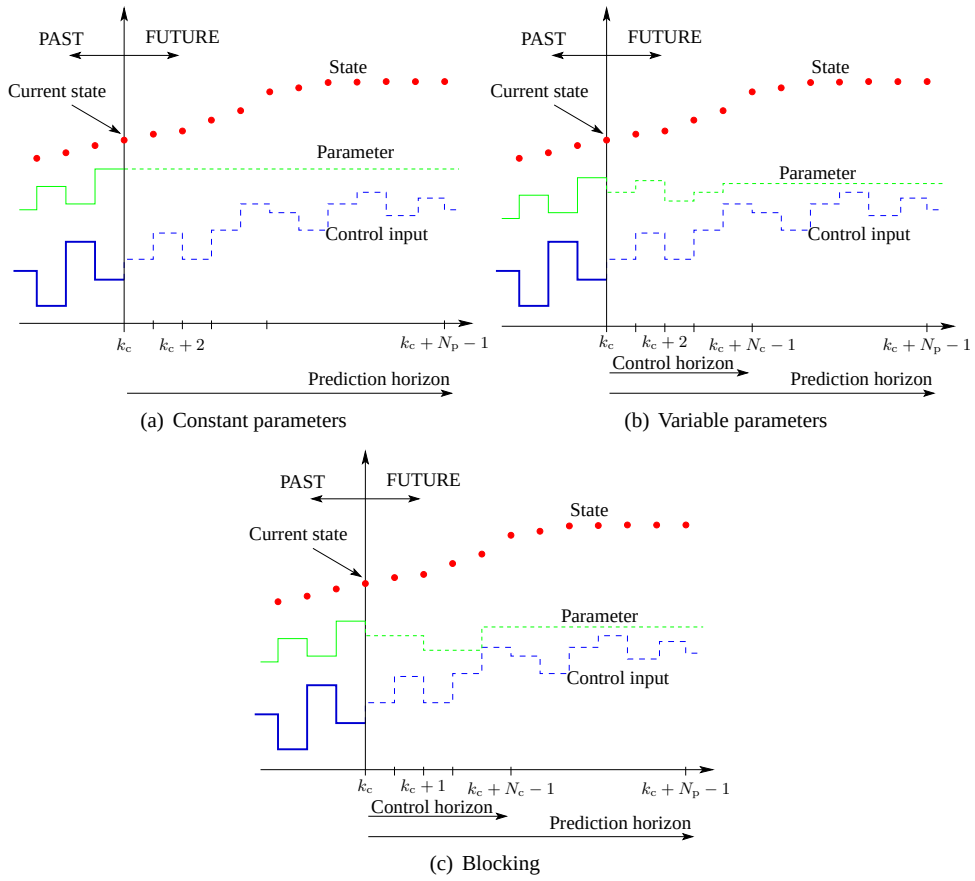

(a) Constant parameters (b) Variable parameters

(c) Blocking

Figure 6.2: Control policy parametrization options over a control horizon in an RHPC scheme.

than the first option. However, since it is rich, this option yields better performance than the first option.

3. *Control policies with limited parameters variations.* To reduce the computation time of the second option and to relax the conservativeness of the first option, one can combine the two options, which results in a hybrid option called blocking. There, the parameters are forced to remain constant during some pre-defined uniform or non-uniform intervals over the prediction horizon. In this way, it is possible to find a balanced trade-off between the performance and the computation time of the RHPC control approach.

6.2.2 General formulation of RHPC for traffic systems

Recall that, in general, the traffic system can be described by the systems of non-linear difference equations given in (5.1). Depending on the model type, the state vector $x(\cdot)$ represents the dynamic states of the traffic system. For example, for macroscopic traffic

models, it contains the average speeds, flows, densities, and queue lengths. The variable $u(\cdot)$ represents the control signals (such as the dynamic speed limits and the ramp metering rates), and the variable $y(\cdot)$ contains the outputs of the traffic system. This could be the travel time, throughput, and emissions.

In Chapter 5 it has been explained that the sampling (measurement) time size $T_{\rm s}$ and the simulation time step size T are in general different. Moreover, the control time step size $T_{\rm c}$ is not necessarily equal to the sampling time step size $T_{\rm s}$. In this thesis, for computational convenience the sampling time step size and the control time step size has been assumed to be related by $T_{\rm c} = M_1 T_{\rm s}$ for a positive integer M_1. In this thesis the system states and outputs at every control time step $k_{\rm c}$ are used in the formulation of the control policies. Therefore, we introduce new variable $x_{\rm c}(k_{\rm c})$, $y_{\rm c}(k_{\rm c})$, $u_{\rm c}(k_{\rm c})$, and $r_{\rm c}(k_{\rm c})$ that denote the traffic system state, output, control input, and reference signal at control time step $k_{\rm c}$. These variables are equal to the corresponding system variables at a every measurement time step $k_{\rm s} = M_1 k_{\rm c}$, where $k_{\rm s}$ is the sampling (measurement) time step counter.

Therefore, in the RHPC control formulation, at every control time step $k_{\rm c}$ the discrete-time control input $u_{\rm c}(k_{\rm c})$ can be defined as a parametrized function of the measured or estimated traffic state vector $x_{\rm c}(k_{\rm c}-1)$, the output vector $y_{\rm c}(k_{\rm c}-1)$, and the parameter vector $\theta(k_{\rm c}-1)$. So, the RHPC control law is in general given by

$$u_{\rm c}(k_{\rm c}+1+j'|k_{\rm c}) = f\big(\hat{x}_{\rm c}(k_{\rm c}+j'|k_{\rm c}), \hat{y}_{\rm c}(k_{\rm c}+j'|k_{\rm c}), \theta(k_{\rm c}+j'|k_{\rm c})\big) \tag{6.1}$$

for $j' = 0, 1, \ldots, N_{\rm p}-1$, where $f(\cdot)$ is a user-defined mapping and the $\hat{x}_{\rm c}(k_{\rm c}+j'|k_{\rm c})$ and $\hat{y}_{\rm c}(k_{\rm c}+j'|k_{\rm c})$ denote the predicted values of respectively $x_{\rm c}$ and $y_{\rm c}$ at time step $k_{\rm c}+j'$ using the information available at time step $k_{\rm c}$.

At every control time step $k_{\rm c}$, the RHPC controller collects all the parameters of the control law (6.1) into a vector $\boldsymbol{\theta}(k_{\rm c}) = [\theta^\top(k_{\rm c}|k_{\rm c}), \ldots, \theta^\top(k_{\rm c}+N_{\rm p}-1|k_{\rm c})]^\top$ and solves the following optimization problem

$$\begin{aligned} &\min_{\boldsymbol{\theta}(k_{\rm c})} J(k_{\rm c}, \boldsymbol{\theta}(k_{\rm c})) := V\big(\boldsymbol{x}(k_{\rm c}), \boldsymbol{y}(k_{\rm c}), \boldsymbol{\theta}(k_{\rm c})\big) \\ &\text{subject to: } \mathcal{G}\big(\boldsymbol{x}(k_{\rm c}), \boldsymbol{y}(k_{\rm c}), \boldsymbol{\theta}(k_{\rm c})\big) \le 0, \\ &\qquad\qquad \mathcal{Q}\big(\boldsymbol{x}(k_{\rm c}), \boldsymbol{y}(k_{\rm c}), \boldsymbol{\theta}(k_{\rm c})\big) = 0, \\ &\qquad\qquad \text{system model (5.1) and control law (6.1)}, \end{aligned} \tag{6.2}$$

where $\boldsymbol{x}(k_{\rm c})$, $\boldsymbol{y}(k_{\rm c})$, $V(\cdot)$, $\mathcal{G}(\cdot)$, and $\mathcal{Q}(\cdot)$ are defined in a similar way as in (5.2).

Next, only the first value of the parameter vector $\boldsymbol{\theta}(k_{\rm c})$, i.e., $\theta(k_{\rm c}|k_{\rm c})$ is implemented for the traffic system, until the next control time step $k_{\rm c}+1$, at which the RHPC controller repeats the above process all over again using a receding horizon approach as described in the previous sections.

Since the RHPC optimization problem is non-linear and non-convex, global or multi-start local optimization methods are required (see Section 5.4.3). Moreover, the formulation of the traffic performance criteria (cf. Section 5.3) and definition of multi-criteria objective functions and normalizations (cf. Section 5.4) of each performance criterion used for this RHPC approach are exactly the same as for conventional MPC. In the sequel the way parametrized control laws for variable speed limits and ramp metering can be formulated is presented.

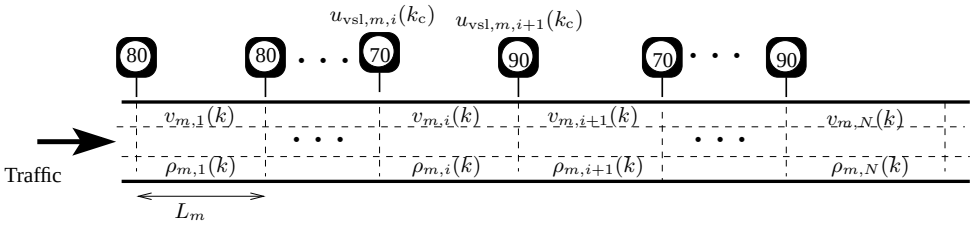

Figure 6.3: A freeway link with N segments and variable speed limits.

6.3 RHPC for variable speed limits and ramp metering

Variable speed limits and ramp metering rates are two of the traffic control measures that are often used for freeway traffic control. In general, traffic control measures and in particular variable speed limits and ramp metering are extensively discussed in [75]. The potential of these control measures to control and to improve the traffic flow have been illustrated in many papers [21, 76–78, 99, 103, 148, 149]. In Chapter 5, it has also been demonstrated that the variable speed limits and ramp metering sometimes can be coordinated in such a way that the emissions and fuel consumption can be reduced while at the same time the traffic flow is improved.

In this section the control policies for variable speed limits and ramp metering to be used in an RHPC approach are formulated in general. From the general expression of the control policies, specific examples are formulated and used in subsequent case studies. It is important to note that the formulation of the control policies does not necessarily have to follow the structures to be presented. The concept discussed in Section 6.2 is so general that it can be applied to different formulations and traffic control measures.

6.3.1 RHPC for variable speed limits

Although one can design an RHPC controller for any dynamic traffic models, in this thesis the RHPC controller is designed based on macroscopic models. Actually, since speed limits are used to limit the speed of all vehicles within the same segment of a link, it is logical to use the macroscopic variables such as the average speed, density, or flow of the vehicles to design the RHPC controller for speed limit control. So, in this particular case a link with a number of segments as depicted in Fig. 6.3 is considered. There are two ways to control the variable speed limits on a link of the freeway. One option is to control the variable speed limits of each segment independently, and the second option is to group a number of neighboring variable speed limits together and to assign them the same value. The general strategy to be presented below holds for both options. Here the former option will be presented and the second option easily follows.

One of the main causes of traffic jams or shock waves is the heterogeneous traffic density and speed in the traffic network. Differences in vehicles speeds and densities between segments of a freeway occur so often. This results in frequent acceleration and deceleration of vehicles in the freeway. Then, due to the difference in acceleration and deceleration of vehicles the operational capacity of a freeway is reduced. Therefore, the intention of traffic control solutions using speed limits is to obtain homogenized traffic flows (such as homogenized speed and density of vehicles on the freeway [7, 180]) so that the desired per-

formance measure can be met (could be increased flow, reduced emissions, and improved safety). Hence, the control laws of the variable speed limits designed below make use of this discussion.

From traffic theory, it has become apparent that the density of every segment is affected by the density of the downstream segment (cf. (2.18)). It means if upstream traffic density is low and if the vehicles upstream flow at certain speed to a dense downstream segment, due to the perspective of the drivers (despite the speed downstream), the speed of the upstream vehicles is affected negatively. On the contrary, if the downstream density is low, drivers tend to increase their speed. Hence, it is important to consider the density of the downstream segment in determining the speed limit of a segment. Assigning high speed limits while the downstream segment is congested will not change the speed of the vehicles in the current segment nor will it improve the flow.

However, density alone cannot describe the flow relation of the two consecutive segments. It is also required to use the speed to determine the control signal that can produce the desired flow. In fact, it is logical to take the downstream speed, because drivers can only adapt their speeds to the speeds of the vehicles in front of them. This means that in addition to the downstream density, the downstream speed is also important in the parametrization of the control signals. Note however that, the use of the speeds and densities of the downstream is not limited only to those of the neighboring segments. One can also use the speeds and densities of multiple downstream segments as long as the number of parameters in the parametrization of the control inputs does not exceed the number of control signals. This is because that the computational advantage of the RHPC approach lies in the reduced number of parameters that has to be optimized. Moreover, it is also possible to use a larger number of parameters than the number of the control inputs, if the first or third options in Section 6.2 are used.

Now, using the downstream speed and density of the traffic flow, a general approach in designing the dynamic speed limit controller for a link of a freeway depicted in Fig. 6.3 can be formulated as follows. The dynamic speed limit $u_{\mathrm{vsl},m,i}(k_{\mathrm{c}}+1)$ of segment i of link m at control time step $k_{\mathrm{c}}+1$ can in general be expressed as

$$\begin{aligned} u_{\mathrm{vsl},m,i}(k_{\mathrm{c}}+1) = f_m\big(&v_{\mathrm{c},m,i}(k_{\mathrm{c}}), v_{\mathrm{c},m,i+1}(k_{\mathrm{c}}), \\ &\rho_{\mathrm{c},m,i}(k_{\mathrm{c}}), \rho_{\mathrm{c},m,i+1}(k_{\mathrm{c}}), \theta_m(k_{\mathrm{c}})\big) \end{aligned} \tag{6.3}$$

where $f_m(\cdot)$ is a general user-defined mapping function that determines the control law of the speed limit of segment i of link m, $\theta_m(k_{\mathrm{c}})$ is the parameter vector, $v_{\mathrm{c},m,i}(k_{\mathrm{c}})$ is the measured or estimated average speed of segment i of link m at time $t = k_{\mathrm{c}}T_{\mathrm{c}}$, and $\rho_{\mathrm{c},m,i}(k_{\mathrm{c}})$ is the measured or estimated average density of segment i of link m at time $t = k_{\mathrm{c}}T_{\mathrm{c}}$.

The function $f_m(\cdot)$ can be a reflection of the error (difference) between the traffic variables (in this particular case the speed and density) of different segments that has an influence on the speed and density of a segment under consideration. The function can be linear or non-linear. Depending on the way $f_m(\cdot)$ is defined the number of parameters required could be small or large. However, it is only important to be aware of the fact that the number of the parameters needed to describe $f_m(\cdot)$ has to be less than the number of the variable speed limits for improved computation times.

In general one can use different relations for $f_m(\cdot)$. In this thesis a linear expression is

proposed, viz.

$$\begin{aligned} u_{\mathrm{vsl},m,i}(k_\mathrm{c}+1) = \theta_{m,0}(k_\mathrm{c})u_{\mathrm{vsl,ref},m}(k_\mathrm{c}) \\ + \theta_{m,1}(k_\mathrm{c})f_{m,1}\big(v_{\mathrm{c},m,i}(k_\mathrm{c}), v_{\mathrm{c},m,i+1}(k_\mathrm{c})\big) \\ + \theta_{m,2}(k_\mathrm{c})f_{m,2}\big(\rho_{\mathrm{c},m,i}(k_\mathrm{c}), \rho_{\mathrm{c},m,i+1}(k_\mathrm{c})\big) \end{aligned} \tag{6.4}$$

where $u_{\mathrm{vsl,ref},m}(k_\mathrm{c})$ is the reference speed that can be either the maximum allowed speed limit of the link or the speed limit that is currently being displayed on the speed limit board, $f_{m,1}(\cdot)$ and $f_{m,2}(\cdot)$ are state feedback functions that relate respectively the speeds and densities to the variable speed limit control, and $\theta_{m,0}(k_\mathrm{c})$, $\theta_{m,1}(k_\mathrm{c})$, and $\theta_{m,2}(k_\mathrm{c})$ are time-dependent parameters that parametrize the speed limit control signals. In the sequel we provide a specific example of the speed limit controller given in (6.4).

Speed limit controller

The speed limit controller presented in (6.4) is general. The functions $f_{m,1}(\cdot)$ and $f_{m,2}(\cdot)$ could be defined in different ways. In the sequel, the two functions are defined by considering the relative difference of the corresponding variables of the functions. This is motivated by the reason that if for a certain performance level the reference speed of a link of a freeway is determined, the controller has to seek a way to minimize the speed difference between the segments and the reference speed. However, since the traffic states in the preceding segments also affect the traffic states of an actual segment, then the traffic states of the preceding states also have to be considered in the speed limit control laws. In this context, the function $f_{m,1}(\cdot)$ is defined as the relative-speed difference of a segment with respect to the speed of downstream segment, and the function $f_{m,2}(\cdot)$ is defined as the relative-density difference of a segment with respect to the density of downstream segment. Thus,

$$f_{m,1}(v_{\mathrm{c},m,i}(k_\mathrm{c}), v_{\mathrm{c},m,i+1}(k_\mathrm{c})) = \frac{v_{\mathrm{c},m,i+1}(k_\mathrm{c}) - v_{\mathrm{c},m,i}(k_\mathrm{c})}{v_{\mathrm{c},m,i+1}(k_\mathrm{c}) + \kappa_v}, \tag{6.5}$$

$$f_{m,2}(\rho_{\mathrm{c},m,i}(k_\mathrm{c}), \rho_{\mathrm{c},m,i+1}(k_\mathrm{c})) = \frac{\rho_{\mathrm{c},m,i+1}(k_\mathrm{c}) - \rho_{\mathrm{c},m,i}(k_\mathrm{c})}{\rho_{\mathrm{c},m,i+1}(k_\mathrm{c}) + \kappa_\rho}, \tag{6.6}$$

where κ_v and κ_ρ respectively denote the minimum non-zero speed and density model parameters. Moreover, the variables $v_{\mathrm{c},m,i}(k_\mathrm{c})$, $v_{\mathrm{c},m,i+1}(k_\mathrm{c})$, $\rho_{\mathrm{c},m,i}(k_\mathrm{c})$, and $\rho_{\mathrm{c},m,i+1}(k_\mathrm{c})$ represent the traffic variables of segment i and $i+1$ of link m at the control time step k_c. However, if the speed limits are going to be applied for a group of segments, these variables should be the average of the traffic state variables of the segments grouped together, because since the speed limits determined by the control laws are going to be applied for the entire group, then the values of the speed limits have to be determined based on the average traffic states of the segments in the group.

In this thesis, the reference speed $u_{\mathrm{vsl,ref},m}(k_\mathrm{c})$ in (6.4) is chosen to be constant independent of time and it is taken to be equal to the maximum speed limit $v_{\mathrm{free},m}$ of the given link. So, depending on the performance criterion of the RHPC controller, the parameter $\theta_{m,0}(k_\mathrm{c})$ corresponding to the reference speed can be optimized such that the reference speed that results in better performance can be set. Therefore, the control policies have to systematically harmonize the traffic flow (by minimizing the difference in speed and density of neighboring segments of a link) while at the same time pushing the speed limits towards

the reference speed ($\theta_{m,0}(k_\mathrm{c})v_{\mathrm{free},m}$). Now, the RHPC speed limit control law becomes

$$u_{\mathrm{vsl},m,i}(k_\mathrm{c}+1) = \theta_{m,0}(k_\mathrm{c})v_{\mathrm{free},m} + \theta_{m,1}(k_\mathrm{c})\frac{v_{\mathrm{c},m,i+1}(k_\mathrm{c}) - v_{\mathrm{c},m,i}(k_\mathrm{c})}{v_{\mathrm{c},m,i+1}(k_\mathrm{c}) + \kappa_v} + \theta_{m,2}(k_\mathrm{c})\frac{\rho_{\mathrm{c},m,i+1}(k_\mathrm{c}) - \rho_{\mathrm{c},m,i}(k_\mathrm{c})}{\rho_{\mathrm{c},m,i+1}(k_\mathrm{c}) + \kappa_\rho}. \tag{6.7}$$

The proposed controller has only

- 3 parameters (if the first option of Section 6.2 is used),
- $3 \times N_\mathrm{p}$ parameters[1] (if the second option of Section 6.2 is used), and
- between 3 and $3 \times N_\mathrm{p}$ parameters (if the third option of Section 6.2 is used)

to be optimized at every control time step k_c in the RHPC control strategy. This means that this speed limit controller can reduce the computation time if it is used with a freeway link with at least N independent variable speed limits such that the $N \times N_\mathrm{p}$ is larger than the number of parameters in either of the three possible options listed above.

Usually, the speed limits are constrained. Maximum allowable speed limits are set for safety reasons, while the lower speed limits are set such that displaying speed limits below the lower limit does not have any physical advantage. For example, a freeway speed limit of 20 km/h is not useful as a speed limit lower than 40 km/h is considered congested traffic. These upper and lower bounds of the speed limits can also be described as constraints for the parameters of the control policies. This can be recast as

$$\begin{bmatrix} v_{\mathrm{free},m} & f_{m,1}(\cdot) & f_{m,2}(\cdot) \\ -v_{\mathrm{free},m} & -f_{m,1}(\cdot) & -f_{m,2}(\cdot) \end{bmatrix} \begin{bmatrix} \theta_{m,0}(k_\mathrm{c}) \\ \theta_{m,1}(k_\mathrm{c}) \\ \theta_{m,2}(k_\mathrm{c}) \end{bmatrix} \leq \begin{bmatrix} V_{\mathrm{u},m} \\ -V_{\mathrm{l},m} \end{bmatrix} \tag{6.8}$$

where $V_{\mathrm{l},m}$ and $V_{\mathrm{u},m}$ are respectively the lower and upper speed limits.

6.3.2 RHPC for ramp metering control

The design of an RHPC controller for ramp metering is similar to the way the RHPC variable speed limit controller is designed. In the case of ramp metering control, the main goal of the controller is to increase the traffic performance level (e.g., throughput, emissions, etc.) of the on-ramp without affecting the traffic flow in the freeway. The on-ramp flow is basically dependent on the current density $\rho_{m,1}(k)$ of the freeway segment and the critical density $\rho_{\mathrm{cr},m}$ of the freeway link (see Fig. 6.4). When the density of the freeway link is below the critical density, the traffic flow can move freely if the downstream traffic is unrestricted. However, as the density of the first segment of link m (of Fig. 6.4) approaches the critical density (which is the meta-stable state of the traffic system) any small disturbance can create a traffic jam (see also Fig. 2.2). Hence, the ramp metering control signal has to take this effect into account. In view of this, a ramp metering control that is affine with respect to the time dependent parameter $\theta_{3,m}(k_\mathrm{c})$ is proposed and it reads as

$$u_{\mathrm{r},m}(k_\mathrm{c}+1) = u_{\mathrm{r,ref},m}(k_\mathrm{c}) + \theta_{m,3}(k_\mathrm{c})f_{m,3}\big(\rho_{\mathrm{c},m,1}(k_\mathrm{c}), \rho_{\mathrm{cr},m}\big) \tag{6.9}$$

[1] Recall that N_p is the prediction horizon.

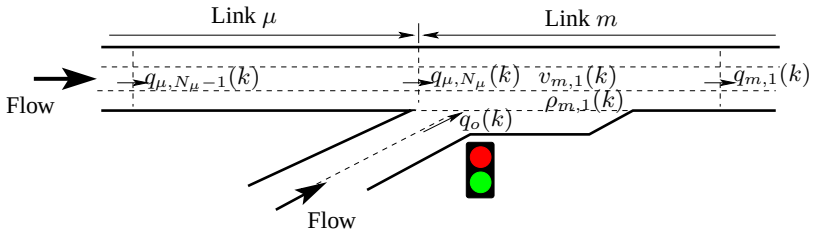

Figure 6.4: Freeway on-ramp.

for $k = M_2 k_\mathrm{c}$, where $u_{\mathrm{r,ref},m}(k_\mathrm{c})$ is the reference ramp metering rate and $f_{m,3}(\cdot)$ is a user-defined mapping.

The reference ramp metering rate $u_{\mathrm{r,ref},m}(k_\mathrm{c})$ can be either the maximum rate that results in desired flow or the currently applied metering rate. One possible specific on-ramp controller is presented in the sequel.

On-ramp controller

With similar reasoning as in (6.5) and (6.6), for the on-ramp control, this thesis considers the RHPC ramp metering control law

$$u_{\mathrm{r},m}(k_\mathrm{c}+1) = u_{\mathrm{r},m}(k_\mathrm{c}) + \theta_{m,3}(k_\mathrm{c}) \frac{\rho_{\mathrm{cr},m} - \rho_{\mathrm{c},m,1}(k_\mathrm{c})}{\rho_{\mathrm{cr},m}}. \tag{6.10}$$

In this RHPC ramp metering controller, the reference $u_{\mathrm{r,ref},m}(k_\mathrm{c})$ is taken to be the currently applied ramp metering rate. The idea behind the structure of the controller is the same as that of ALINEA [149]. In the RHPC approach, the parameter $\theta_{m,3}(k_\mathrm{c})$ is updated every control time step and it is optimized on-line, while in ALINEA the parameter is optimized off-line and is constant irrespective of the prevailing traffic conditions.

Note, however, that ALINEA is a special case of the on-ramp controller presented in Section 6.3.2. One can obtain the ALINEA on-ramp controller from (6.10) by setting $\theta_{m,3}(k_\mathrm{c}) = K$ (a constant gain parameter).

Similar to the speed limit control, the constraint on the on-ramp metering rate can be translated to a constraint on the parameter $\theta_{m,3}(k_\mathrm{c})$: the constraint $0 \leq u_{\mathrm{r},m}(k_\mathrm{c}+1) \leq 1$ can be recast as

$$\begin{bmatrix} f_{m,3}(\cdot) \\ -f_{m,3}(\cdot) \end{bmatrix} \theta_{m,3}(k_\mathrm{c}) \leq \begin{bmatrix} 1 - u_{\mathrm{r,ref},m}(k_\mathrm{c}) \\ u_{\mathrm{r,ref},m}(k_\mathrm{c}) \end{bmatrix}. \tag{6.11}$$

6.4 Reduction of area-wide emissions

Now the RHPC traffic controller discussed above is illustrated with two case studies. In these case studies, the reduction of travel time, emissions, and dispersion of emissions using variable speed limits and ramp metering as traffic control measures are presented. The two traffic control measures are generated using the control laws given in (6.7) and (6.10).

Both case studies presented below use the macroscopic traffic flow model METANET described in Section 2.3 and the macroscopic emission and fuel consumption model VT-

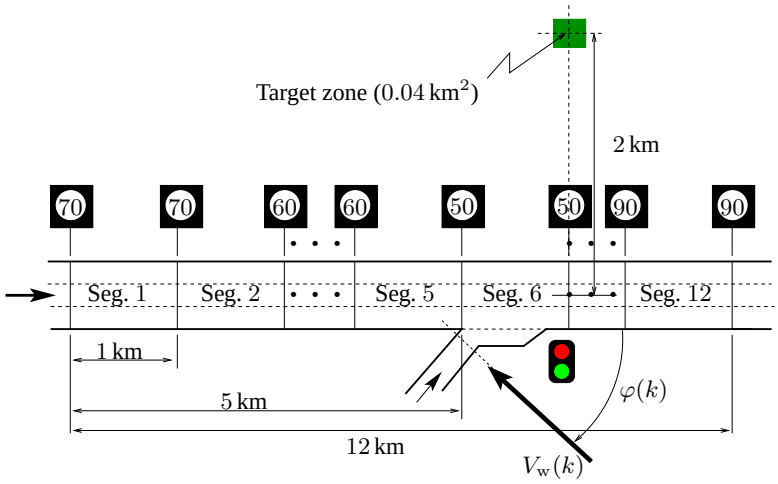

Figure 6.5: A 12 km freeway with 12 variable speed limits and 1 on-ramp for Case study E.

macro proposed in Section 3.4. The first case study in Section 6.4.1 uses the point-source emission dispersion model, while the second case study in Section 6.4.2 uses the extended grid-based dispersion model discussed respectively in Section 4.2 and Section 4.3.1.

6.4.1 Case study E: Using a point source model

In this case study, the RHPC controller uses the point-source emission dispersion model with variable wind speed and wind direction. The case study illustrates the proposed control approach by considering the same 12 km three-lane freeway stretch as in Case study D of Section 5.5.2. The layout of the case study is repeated in Fig. 6.5 for convenience. The freeway is divided into 12 equal segments with an on-ramp at the sixth segment from the left (see Fig. 6.5) and each segment is provided with a variable speed limit. Moreover, a target is located at a distance 2 km from the freeway as shown in the figure.

Like in Case study D of Section 5.5.2, the freeway in this case study is also subject to a wind with speed and direction given by

$$V_{\mathrm{w}}(k) = 7 + 2\sin(0.005\pi k + \pi/6)\sin(0.01\pi k) \tag{6.12}$$

$$\varphi(k) = \frac{2\pi}{5} + \frac{\pi}{4}\cos(0.004\pi k) \tag{6.13}$$

where the wind speed $V_{\mathrm{w}}(k)$ is expressed in m/s and the wind direction (angle) $\varphi(k)$ in radians.

The evolution of the wind speed and wind direction is shown in Fig. 6.6. The demand profile of the traffic at the mainstream and on-ramp origins is also the same as in Case study D, and is shown in Fig. 6.7. Moreover, the downstream traffic is assumed to be unrestricted.

In this case study, different scenarios with different control objectives are simulated. First, the uncontrolled Scenario S_1 is simulated. This scenario is considered as the bench-

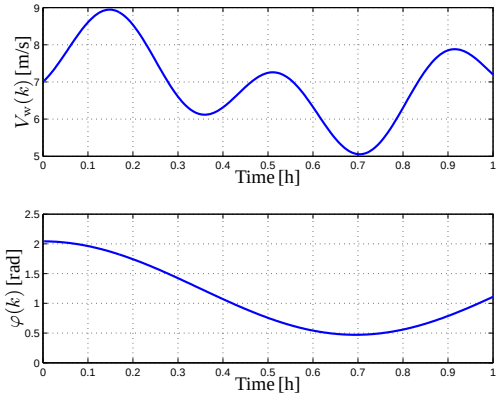

Figure 6.6: The wind speed $V_{\mathrm{w}}(k)$ and wind direction $\varphi(k)$ given by (6.12) and (6.13) respectively.

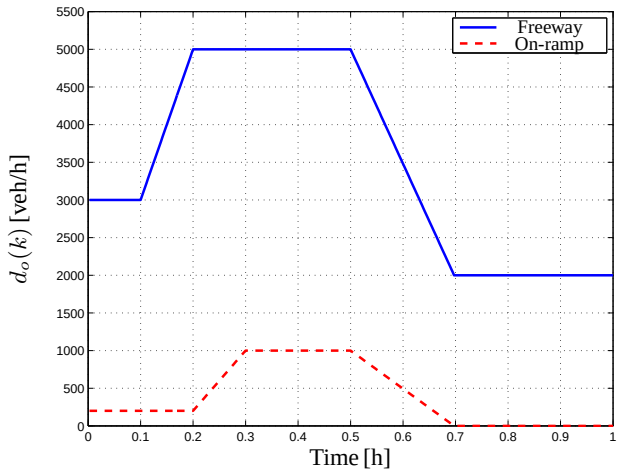

Figure 6.7: Traffic demand flow at the mainstream and on-ramp origins for Case study E.

mark to compare the performance of the RHPC controller under four different control objectives. The control objectives of the RHPC controller are defined by varying the weights of the cost function presented in (5.16). Accordingly, four combinations (corresponding to four controlled scenarios) as listed next are examined. In all the cases, the weight corresponding to the variation of the control inputs is set as $\zeta_5 = 0.01$, because the emphasis on the variation of the control inputs is required to be less as compared to the travel time, emissions, or dispersion of emissions.

$\mathbf{S}_2$: Focuses on the reduction of the total time spent (TTS). This is obtained by setting $\zeta_1 = 1$, $\zeta_2 = \zeta_3 = \zeta_{4,\mathrm{MDL}} = \zeta_{4,\mathrm{TDL}} = 0$, and all the weights $\mu_{(\cdot)}$ for the emissions

Table 6.1: Simulation results for uncontrolled and controlled scenarios for the Case study E. The values in the brackets indicate the relative change of the performance criteria as compared to the uncontrolled Scenario S_1. Negative values indicate a decrease (i.e., an improvement) in the value of the performance criteria, while positive values indicate an increase in the value of performance criteria as compared to the uncontrolled scenario.

Scenarios	Performance Criteria		
	TTS [veh·h]	TE [kg]	MDL [μg/m^2]
S_1: Uncontrolled	1362.1	127.5	163.2
S_2: TTS	875.3 (-36%)	145.4 ($+14\%$)	196.9 ($+25\%$)
S_3: TE	1590.3 ($+17\%$)	66.4 (-48%)	100.0 (-37%)
S_4: MDL	1509.0 ($+11\%$)	70.8 (-44%)	101.2 (-36%)
S_5: 10TTS + TE + 5MDL	874.1 (-36%)	120.3 (-6%)	194.4 ($+23\%$)

and fuel consumption are zero.

S_3: Minimizes the total emissions TE (CO, HC, and NO_x). In this case $\zeta_1 = \zeta_3 = \zeta_{4,\mathrm{MDL}} = \zeta_{4,\mathrm{TDL}} = 0$, $\zeta_2 = 1$, $\mu_{\mathrm{CO}} = \mu_{\mathrm{HC}} = \mu_{\mathrm{NO_x}} = 1$, and $\mu_{\mathrm{CO_2}} = 0$.

S_4: The controller focuses on the reduction of the maximum dispersion level (MDL) in the target zone as defined in (5.10). This is obtained by setting $\zeta_1 = \zeta_2 = \zeta_3 = \zeta_{4,\mathrm{TDL}} = 0$, $\zeta_{4,\mathrm{MDL}} = 1$, $\mu_{\mathrm{CO}} = \mu_{\mathrm{HC}} = \mu_{\mathrm{NO_x}} = 1$, $\mu_{\mathrm{CO_2}} = 0$, $\mu_{\mathrm{d,CO}} = \mu_{\mathrm{d,HC}} = \mu_{\mathrm{d,NO_x}} = 1$, and $\mu_{\mathrm{d,CO_2}} = 0$.

S_5: The combination of travel time, emissions, and dispersion of emissions to the target zone is considered. In this scenario the weights are set as $\zeta_1 = 10$, $\zeta_2 = 1$, $\zeta_3 = \zeta_{4,\mathrm{TDL}} = 0$, $\zeta_{4,\mathrm{MDL}} = 5$, $\mu_{\mathrm{CO}} = \mu_{\mathrm{HC}} = \mu_{\mathrm{NO_x}} = 1$, $\mu_{\mathrm{CO_2}} = 0$, $\mu_{\mathrm{d,CO}} = \mu_{\mathrm{d,HC}} = \mu_{\mathrm{d,NO_x}} = 1$, and $\mu_{\mathrm{d,CO_2}} = 0$.

The simulation was conducted for 1 h and the tuning parameters of the RHPC controller are set exactly the same as that of the conventional MPC controller used in Section 5.5.2, i.e., $T_{\mathrm{c}} = 2$ min, $N_{\mathrm{p}} = 7$ (corresponding to 14 min), and $N_{\mathrm{c}} = 5$ (corresponding to 10 min) with simulation time step size $T = 10$ s. The simulation results of the uncontrolled and controlled scenarios are given in Table 6.1. Table 6.1 also provides the relative changes of the performance criteria in the controlled scenarios as compared to the uncontrolled scenario. These relative changes are computed using

$$I_p = \frac{p_{\mathrm{controlled}} - p_{\mathrm{uncontrolled}}}{p_{\mathrm{uncontrolled}}} \times 100\% \tag{6.14}$$

where $p_{\mathrm{uncontrolled}}$ denotes the value the performance criteria $p \in \{\mathrm{TTS}, \mathrm{TE}, \mathrm{MDL}\}$ for the uncontrolled scenario and $p_{\mathrm{controlled}}$ is the value of the performance criteria p for the controlled scenarios.

As can be seen from the table, when the objective of the RHPC controller is set to reducing either the total emissions (Scenario S_3) or the dispersion level (Scenario S_4), the travel time increases by more than 11% relative to the uncontrolled Scenario S_1. Both the dispersion level and the total emission are reduced by more than 44% and 36% respectively

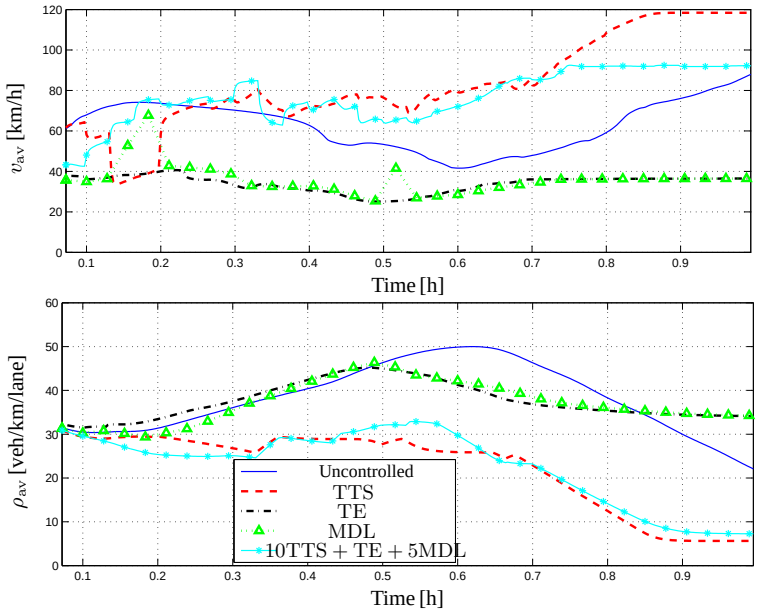

Figure 6.8: Evolution of average speed $v_{\rm av}(k)$ and average density $\rho_{\rm av}(k)$ over all the segments of the freeway for uncontrolled and controlled scenarios of Case study E.

as compared to the uncontrolled scenario. This is so because when the RHPC controller is focusing on the reduction of total emissions TE of the freeway or the dispersion level MDL over the target area, the speed of the traffic is reduced (see Fig. 6.8). This means that the travel time is increased. An important point to notice here is the difference in TTS when the objective of the controller is to reduce either TE only or MDL only. When the focus of the RHPC controller is on the TE, the TTS becomes worse than when the objective of the controller is to reduce MDL (see Scenarios S_3 and S_4 in Table 6.1). This is because of the fact that when the controller is focusing on the reduction of TE, it will reduce the total emissions caused by all vehicles over the whole traffic network. However, when the intention of the controller is to reduce the dispersion MDL at the target area, it only focuses on the reduction of the emissions caused by vehicles in those parts of the traffic network that affect this particular target. Thus, the parts of the traffic network that do not cause emissions that affect the target area are allowed to have better traffic flow when the focus of the controller is on reducing the MDL. As it has been pointed out in Section 5.5.2, in general, the MDL is expected to be lower when the objective of the controller is reducing MDL than when the objective of the controller is reducing TE. However, the results in Table 6.1 show the opposite. This can happen for two possible reasons discussed in Remark 5.3 for Case Study D.

The evolution of the dispersion level at the target zone is presented in Fig. 6.9. The figure depicts the total dispersion for different control objectives. It shows that the dispersion level becomes higher than in the uncontrolled case if the control objective is to reduce TTS or the combination of TTS, TE, and MDL (see also Table 6.1). This is probably due to the higher

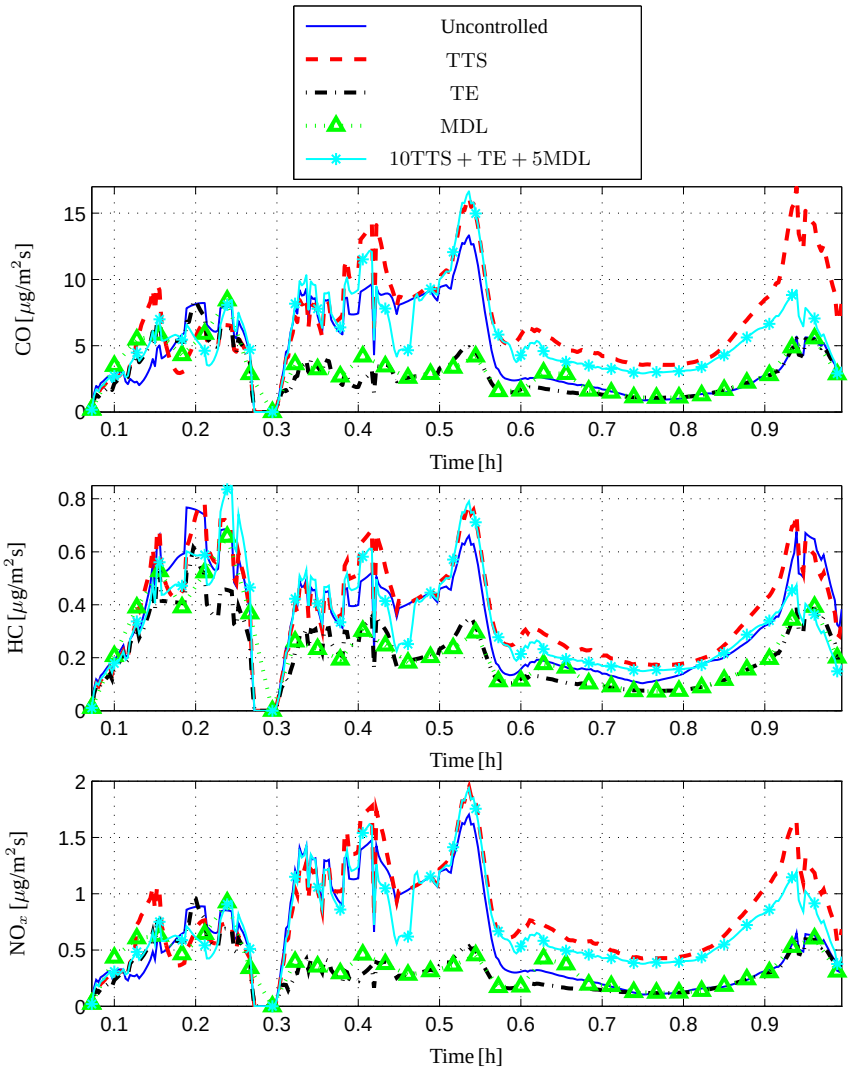

Figure 6.9: Evolution of dispersion levels in target zone for the uncontrolled and the controlled scenarios of Case study E.

average traffic speed shown in Fig. 6.8, because higher traffic speeds favor traffic flow while they have a negative impact on emissions. Thus, the dispersion level becomes higher as the travel time gets lower as a result of increased traffic speed. It is also important to note that in this case study the TE has decreased while MDL has increased under Scenario S_5, which indicates that reduction of emissions may not necessarily mean reduction of the dispersion level to a target zone.

Finally, Fig. 6.10 depicts the evolution of the emissions of the freeway over time. The variation of the emissions in Fig. 6.10 and the dispersion level in Fig. 6.9 show different characteristics due to two reasons. One, due to the location of the freeway segments relative

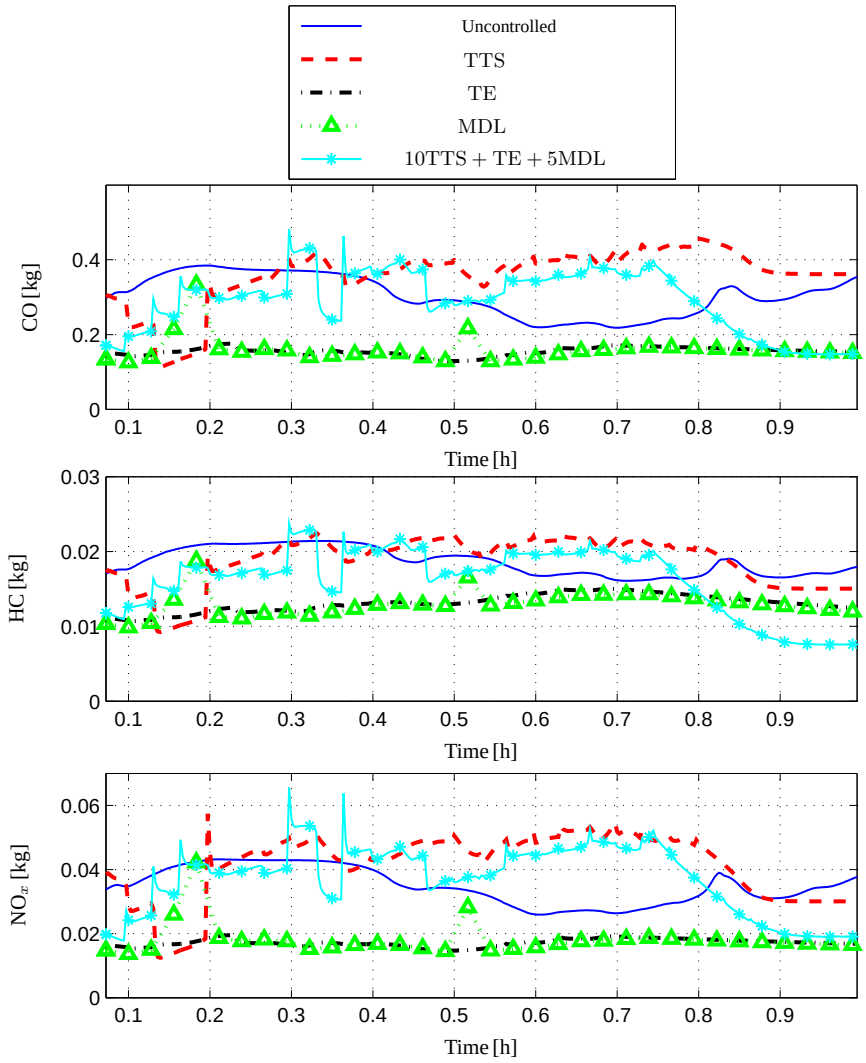

Figure 6.10: Evolution of emission levels of the freeway for the uncontrolled and the controlled scenarios of Case study E.

to the target, the emissions do not necessarily reach the target location from *all* segments. Second, due to the variation of the wind speed and wind direction, the dispersion of the emissions of the segments that affect the target varies. This phenomenon is observed in Fig. 6.9. At around $0.3\,\mathrm{h}$ the dispersion level is zero. This is the time range where none of the segments disperse emissions to the target location. This zero dispersion-level window in Fig. 6.9 is also due to an intrinsic shortcoming of the point-source dispersion model. Since the centers of the segments of the freeway are considered as the emission sources with the point-source dispersion model, at high wind speeds the dispersion cones will be narrow so that the regions between the dispersion cones of the segments may not encounter emissions

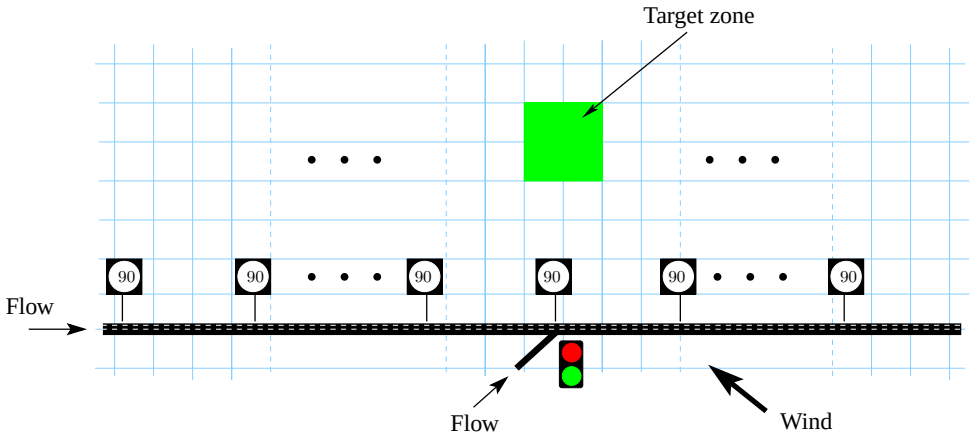

Figure 6.11: A 12 km three-lane freeway stretch considered for the Case study F. Each cell in the grid is 200 m by 200 m.

in the model (whereas in reality they do). Under such cases the dispersion level experienced by the target zone can become zero.

6.4.2 Case study F: Using extended grid-based dispersion model

In this case study, the extended grid-based dispersion model presented in Section 4.3.1 is used to predict the dispersion of the emissions to a target zone. The traffic flow and emission models are the same models as that of the first case study reported in Section 6.4.1. Fig. 6.11 shows a 12 km three-lane freeway stretch, which is the same as freeway considered in Case study E of Section 6.4.1. As in Case study E, the freeway shown in Fig. 6.11 is divided into 12 segments with each of length 1 km and equipped with a variable speed limit. Only the sixth segment of the freeway has a metered on-ramp.

A time-varying traffic demand is assumed at the on-ramp and mainstream origins as shown in Fig. 6.7. The traffic flow at the end of the mainstream is considered to be unrestricted. Moreover, the neighborhood of the freeway is considered to be flat with no obstructions and is subject to varying wind speed and wind direction. For this case study, the wind speed and wind direction are the same as given in (6.12) and (6.13), which are depicted in Fig. 6.6.

Since this case study also takes into account the dispersion of emissions to a target zone, a target zone that is 1 km away from the middle of the segment with the on-ramp (see Fig. 6.11) is considered. The target zone has an area of $400\,\mathrm{m}\times 400\,\mathrm{m}$. Moreover, since the extended grid-based dispersion model is employed, the neighborhood of the freeway is meshed into a grid of square cells of dimension 200 m as shown in Fig. 6.11. This means that there are $12\,000\,\mathrm{m}/200\,\mathrm{m}= 60$ cells along the freeway stretch and 5 cells from the center of the freeway to the center of the target zone. This means that $5 \times 60 = 300$ emission dispersion states have to be updated every simulation time step.

As a performance measure of the RHPC controller, the multi-objective function defined in (5.16) is used. To quantify the performance of the controller under different controlled scenarios, the results of the controlled scenarios are compared to the uncontrolled situation.

Table 6.2: Simulation results for the uncontrolled and the controlled scenarios of Case study F. The values in the brackets indicate the relative change of the performance criteria as compared to the uncontrolled Scenario S_1. Negative values indicate a decrease (i.e., an improvement) in the value of the performance criteria, while positive values indicate an increase in the value of the performance criteria as compared to the uncontrolled scenario.

Scenarios	Performance Criteria		
	TTS [veh·h]	TE [kg]	MDL [μg/m^2]
S_1: Uncontrolled	1362.1	127.5	137.6
S_2: TTS	860.5 (-37%)	140.9 ($+11\%$)	145.2 ($+6\%$)
S_3: TE	1618.1 ($+19\%$)	66.1 (-48%)	96.4 (-30%)
S_4: MDL	1613.2 ($+18\%$)	70.7 (-45%)	93.5 (-32%)
S_5: 10TTS + TE + 5MDL	1528.7 ($+12\%$)	77.5 (-39%)	119.2 (-13%)

In all the controlled scenarios considered, the weight corresponding to the variation of the control inputs is set as $\zeta_5 = 0.01$, so that less emphasis is given to the minimization of the variation of the control inputs than the other traffic performance measures. Moreover the weights of the emissions are set $\mu_{\mathrm{CO}} = \mu_{\mathrm{HC}} = \mu_{\mathrm{NO_x}} = 1$ and $\mu_{\mathrm{CO_2}} = 0$ so that equal weight is given to CO, HC, and NO_x; and CO_2 is not taken into account. Note that since there is an affine relationship between fuel consumption and CO_2 as described in Section 3.2 reduction of CO_2 or fuel consumption would mean almost the same. In addition, the same emission gases are also considered for the dispersion cost function, i.e., $\mu_{\mathrm{d,CO}} = \mu_{\mathrm{d,HC}} = \mu_{\mathrm{d,NO_x}} = 1$ and $\mu_{\mathrm{d,CO_2}} = 0$.

For the RHPC-controlled scenarios, the control objectives are set to reduce:

S_2: The total time spent TTS, which is obtained by setting $\zeta_1 = 1$ and $\zeta_2 = \zeta_3 = \zeta_{4,\mathrm{MDL}} = \zeta_{4,\mathrm{TDL}} = 0$ of the general control objective given in (5.16),

S_3: The total emissions TE obtained by setting $\zeta_2 = 1$ and $\zeta_1 = \zeta_3 = \zeta_{4,\mathrm{MDL}} = \zeta_{4,\mathrm{TDL}} = 0$ of (5.16),

S_4: The maximum dispersion level MDL obtained with $\zeta_{4,\mathrm{MDL}} = 1$ and $\zeta_1 = \zeta_2 = \zeta_3 = \zeta_{4,\mathrm{TDL}} = 0$ of (5.16), and

S_5: The weighted combination of the TTS, TE, and MDL with $\zeta_1 = 10$ and $\zeta_2 = 1$, $\zeta_3 = \zeta_{4,\mathrm{TDL}} = 0$, $\zeta_{4,\mathrm{MDL}} = 5$ of the general control objective given in (5.16).

The simulation period is 1 h with a simulation time step of $T = 10$ s. The prediction horizon and the control horizon are set to $N_{\mathrm{p}} = 14$ min and $N_{\mathrm{c}} = 10$ min with the control time step $T_{\mathrm{c}} = 2$ min. Under the uncontrolled scenario, the free-flow speed $v_{\mathrm{free},m} = 120$ km/h is used. The simulation results are shown in Table 6.2, Fig. 6.12, and Fig. 6.13. Table 6.2 provides the value of the performance criteria and relative changes of the performance criteria of the controlled scenarios as compared to the uncontrolled scenario. These values are computed using the expression in (6.14).

As can be seen from the Table 6.2 and Fig. 6.12 both the total emissions and the dispersion levels are worse if the objective of the controller is to reduce the TTS. Indeed the TTS is reduced by 37%. However, when the objective function of the RHPC controller is

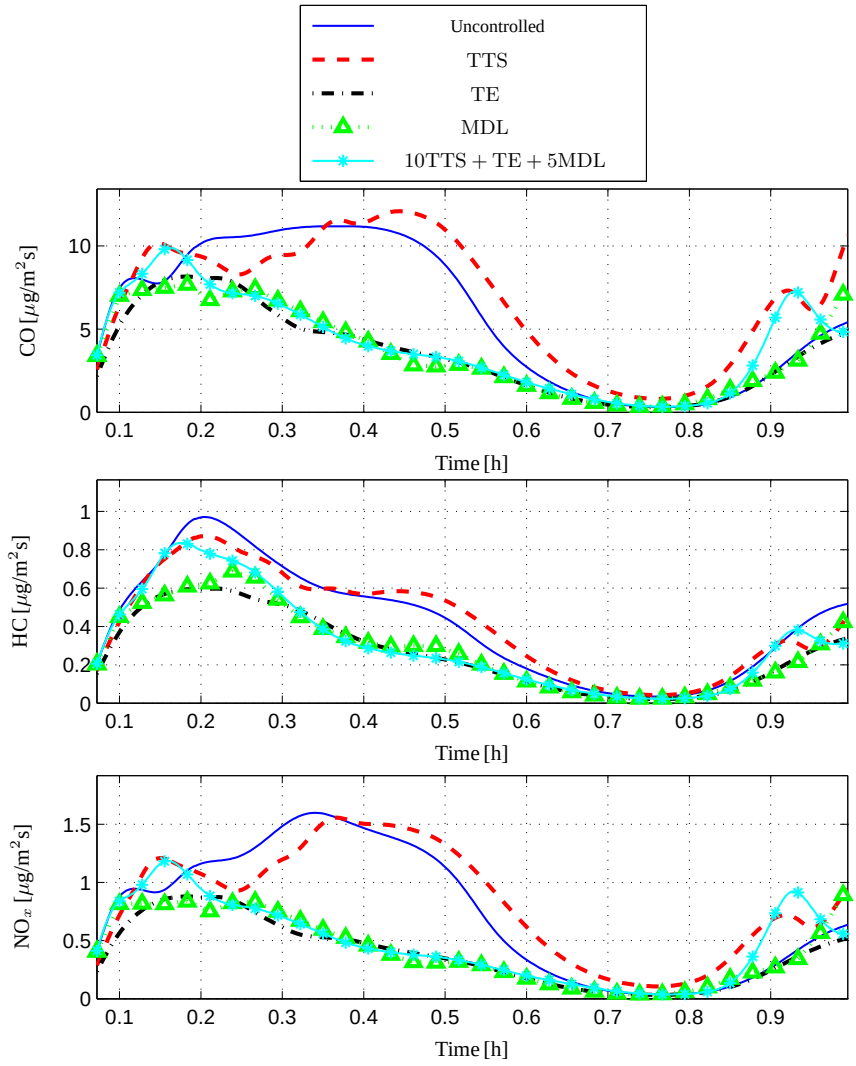

Figure 6.12: Evolution of dispersion levels at the target zone for uncontrolled and RHPC-controlled scenarios of Case study F.

set either TE or MDL, the TTS increases by at least 18% while the TE and the MDL are reduced by more than 30%. For those cases (Scenarios S_1 to S_5) Fig. 6.12 also shows the evolution of the dispersion levels at the target zone. When the objective of the controller is either TE or DL, the dispersion levels are lower than the uncontrolled and the TTS-controlled scenarios for almost all of the simulation time. The dispersion levels of all the cases are the same only at the beginning (about 4 min after the simulation—the time the emissions take to reach the target zone) where the initial traffic conditions are the same for all the scenarios. Differences are created after the controller starts influencing the traffic flow.

The last scenario, where a weighted combination of the performance criteria is defined as the objective of the RHPC controller, shows that the controller provides a balanced trade-off between total time spent, total emissions, as well as maximum dispersion levels of the emissions. In fact, the travel time is worsened compared to the uncontrolled scenario and to the TTS-controlled scenario. But it is better as compared to the scenarios where the control objectives are TE and MDL.

The space-time evolution of the space-mean speeds under the uncontrolled and controlled scenarios are also plotted in Fig. 6.13. These plots show the effect of the different traffic control performance measures on the space-mean speed of the traffic flow. Under the uncontrolled scenario, two shock waves are observed. These shock waves are resolved when the objective of the RHPC controller is minimizing TTS, which results in reduced travel time. However, then the emission and dispersion levels are high, which is consistent with the fact that higher speeds favor flow while negatively impact the emissions. On the contrary, the space-mean speed is lower than in the uncontrolled and the TTS-controlled scenarios when the objective of the RHPC controller is either TE or MDL. The space-mean speed is slightly improved when the objective of the RHPC controller is the weighted sum of TTS, TE, and MDL as in Scenario S_5, resulting in improved traffic flow at the cost of increased emissions and dispersion levels as compared to Scenarios S_3 and S_4 (see also Table 6.2).

6.5 Conclusions

Since the computational demand of conventional MPC makes it intractable in practice, a new parametrized MPC approach called Receding-Horizon Predictive Control (RHPC) has been presented in this chapter. The general concept and general formulation of RHPC have been discussed. Unlike conventional MPC, RHPC optimizes a set of parameters that describe control laws in such a way that a given objective function is minimized. Since the number of parameters used for the description of the control laws is smaller than the control inputs, the computation time of RHPC is smaller as compared to conventional MPC which directly optimizes the control inputs. However, it has been discussed that the performance of the RHPC controller can be reduced as the number of control inputs described by the same parameters increases.

As an example the speed limits and ramp metering traffic control measures have been formulated in this control approach. Under different options, the theoretical background why the RHPC controller can be faster than the conventional MPC is elaborated. Simulation-based comparisons of these controllers will be presented in the next chapter.

This chapter has also demonstrated the use of RHPC for the reduction of travel time, emissions, and dispersion of emissions to a target zone using two case studies. The first case study (Case study E) has used the point-source dispersion model and the second case study (Case study F) has used the extended grid-based dispersion model. For both case studies time-varying traffic demand and wind have been considered. These case studies illustrate that the RHPC controller can provide a balanced trade-off between travel times, emissions, and dispersion of emissions to a given target zone.

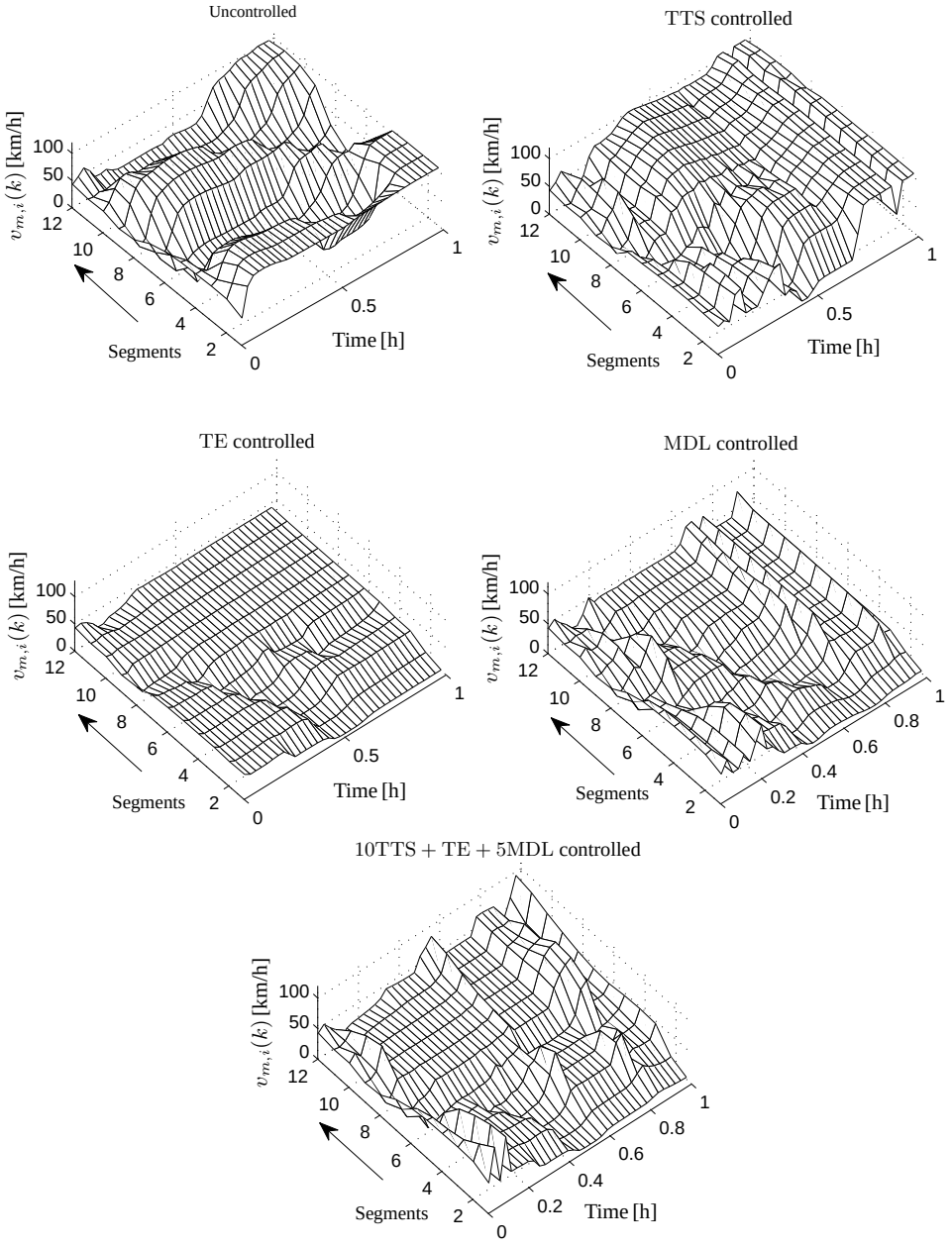

Figure 6.13: The evolution of the space-mean speed over space and time for uncontrolled and controlled scenarios for the Case study F. The arrows indicate the driving direction.

Chapter 7

Conventional MPC versus RHPC

In the last two chapters, Chapter 5 and Chapter 6, the conventional Model Predictive Control (MPC) and the Receding-Horizon Parametrized Control (RHPC) approaches have been discussed. These two control approaches have been illustrated with a number of case studies to reduce travel times, emissions, fuel consumption, and dispersion of emissions to target zones. Moreover, the ability of the control approaches to provide a balanced trade-off between these conflicting control performance criteria has been demonstrated.

However, in neither of the two chapters, the computation time of the controllers for the different cases were presented. Furthermore, the performance indicators of the controllers were not compared. Therefore, the two control approaches are compared in detail in this chapter. The computation time required by the two control approaches under the same traffic conditions is presented. The performance of the controllers for different control objectives are compared.

In this chapter, first a general qualitative comparison of the controllers is discussed in Section 7.1. This section highlights the challenges for theoretical comparison of conventional MPC (designated as cMPC hereafter) and RHPC and it sheds light on future research directions in this area. Next, two case studies are considered to compare the cMPC and the RHPC controllers. The first case study, Section 7.2, presents the comparison of the cMPC and RHPC controllers using a part of the A12 Dutch freeway. The traffic performance criteria and the computation time of the two controllers are discussed. In Section 7.3, further comparison of the cMPC and RHPC controllers is conducted using the traffic scenario described in Section 6.4.2. In this second case study, in addition to the travel time and the emissions, the dispersion of emissions to a target zone is also considered as the control performance criterion. Finally, the conclusions of the chapter are given in Section 7.4.

7.1 Qualitative comparison of controllers

Both the cMPC controller and the RHPC controller require the five basic elements of MPC discussed in Section 5.1, i.e., system and disturbance modeling, performance criterion, description of constraints, optimization, and the receding horizon principle. In general, the utilization of these concepts makes the RHPC controller and the cMPC controller similar.

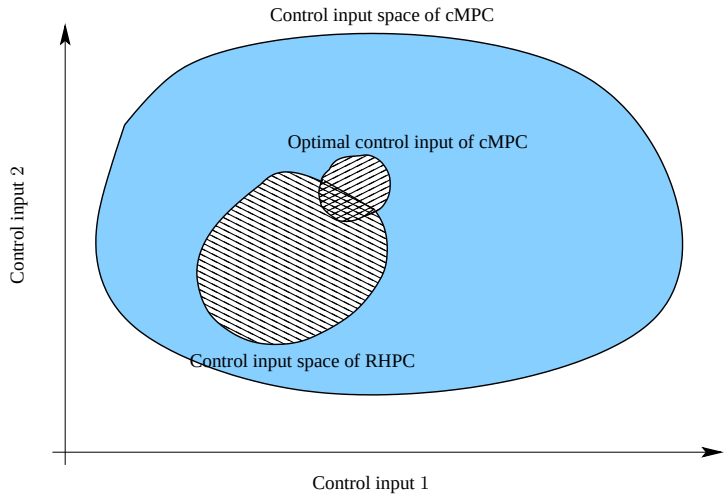

Figure 7.1: Control space of the cMPC controller and the RHPC controller provided that the number of the control inputs is larger than the number of parameters of the control laws of the RHPC controller and if $T_{\mathrm{c}} = T_{\mathrm{c,i}}$ and $N_{\mathrm{c}} = N_{\mathrm{p}}$.

In the RHPC approach, whether the control horizon is large or small, the actual control inputs (the variable speed limits and the ramp metering rates for example) can in general always vary for every control time step over the entire prediction horizon. This is because of the fact that the control laws in the RHPC controller are dependent on the state of the system. Thus, as far as there is variation in the state of the system, the control inputs vary according to the control laws provided that the parameters of the control laws are non-zero. However, this is not the case when the cMPC controller is used. Based on the size of the control horizon and the blocking introduced, the variation of the control inputs can differ. For example, if the control horizon is set to $N_{\mathrm{c}} = 1$, the control inputs cannot vary over the prediction horizon if one uses the cMPC controller, while they can if one uses the RHPC controller.

However, there is one catch. Since at every control time step k_{c} the RHPC controller describes the control inputs based on control laws with a number of parameters that is less than the number of the control inputs, the dimension of the control input space of RHPC is less than the dimension of the control input space of conventional MPC.Therefore, if $T_{\mathrm{c}} = T_{\mathrm{c,i}}$ and $N_{\mathrm{c}} = N_{\mathrm{p}}$, the possible input space of the RHPC approach over the prediction period might be limited as compared to the cMPC approach. This is illustrated in Fig. 7.1. Thus, if the number of the parameters of the RHPC control laws is smaller than the number of the control inputs and if $T_{\mathrm{c}} = T_{\mathrm{c,i}}$ and $N_{\mathrm{c}} = N_{\mathrm{p}}$, the control space of the RHPC controller over the prediction period will be a subset of the control input space of the cMPC controller (see also Fig. 7.1). However, if $T_{\mathrm{c}} \neq T_{\mathrm{c,i}}$ or $N_{\mathrm{c}} \neq N_{\mathrm{p}}$, the optimal control input spaces of the two controller may or may not have common point. Hence, depending on the control laws of the RHPC controller, the intersection of the control input space of the RHPC controller and the optimal control input space of the cMPC controller can be anything. Due to this fact, a general comparison of the two controllers becomes difficult.

Under the condition that $T_{\mathrm{c}} = T_{\mathrm{c,i}}$ and $N_{\mathrm{c}} = N_{\mathrm{p}}$, the RHPC control law of the speed

limit defined in (6.7) can be compactly recast as

$$u_{\mathrm{vsl,RHPC},m,i}(k_\mathrm{c}+j) = z_{m,i}^\top(k_\mathrm{c}+j)\theta_m(k_\mathrm{c}+j) \tag{7.1}$$

for $j = 0, 1, 2, \ldots, N_\mathrm{p}-1$, where $u_{\mathrm{vsl,RHPC},m,i}(k_\mathrm{c})$ is the variable speed limit of segment i of link m obtained using the RHPC controller, $z_{m,i}(k_\mathrm{c}) = [v_{\mathrm{free},m}\ f_{m,1}(\cdot)\ f_{m,2}(\cdot)]^\top$, and $\theta_m(k_\mathrm{c}) = [\theta_{m,0}(k_\mathrm{c})\ \theta_{m,1}(k_\mathrm{c})\ \theta_{m,2}(k_\mathrm{c})]^\top$.

Now, at every control time step k_c and over the prediction period $[T_\mathrm{c}k_\mathrm{c}, T_\mathrm{c}(k_\mathrm{c}+N_\mathrm{p}-1)]$, all speed limits $u_{\mathrm{vsl,RHPC},m,i}(k_\mathrm{c}+j)$ described by the same parameter vector $\theta_m(k_\mathrm{c}+j)$ can be concatenated as

$$\underbrace{\begin{bmatrix} U_{\mathrm{vsl,RHPC},m}(k_\mathrm{c}) \\ U_{\mathrm{vsl,RHPC},m}(k_\mathrm{c}+1) \\ \vdots \\ U_{\mathrm{vsl,RHPC},m}(k_\mathrm{c}+N_\mathrm{p}-1) \end{bmatrix}}_{\boldsymbol{U}_{\mathrm{vsl,RHPC},m}(k_\mathrm{c})} = \underbrace{\begin{bmatrix} Z_m(k_\mathrm{c}) & 0 & \ldots & 0 \\ 0 & Z_m(k_\mathrm{c}+1) & \ldots & 0 \\ \vdots & \vdots & \ddots & \vdots \\ 0 & 0 & \ldots & Z_m(k_\mathrm{c}+N_\mathrm{p}-1) \end{bmatrix}}_{\boldsymbol{Z}_m^\top(k_\mathrm{c})} \boldsymbol{\Theta}_m(k_\mathrm{c}) \tag{7.2}$$

where $U_{\mathrm{vsl,RHPC},m}(k_\mathrm{c}) = [u_{\mathrm{vsl,RHPC},m,1}(k_\mathrm{c})\ u_{\mathrm{vsl,RHPC},m,2}(k_\mathrm{c}) \ldots\ u_{\mathrm{vsl,RHPC},m,N_\mathrm{vsl}}(k_\mathrm{c})]^\top$ $\boldsymbol{\Theta}_m(k_\mathrm{c}) = [\theta_m^\top(k_\mathrm{c})\ \theta_m^\top(k_\mathrm{c}+1)\ \ldots\ \theta_m^\top(k_\mathrm{c}+N_\mathrm{p}-1)]^\top$, $Z_m(k_\mathrm{c}) = [z_{m,1}(k_\mathrm{c})\ z_{m,2}(k_\mathrm{c})\ \ldots\ z_{m,N_\mathrm{vsl}}(k_\mathrm{c})]^\top$, and N_vsl is the number of speed limits that are described by the same parameter vector $\theta_m(k_\mathrm{c}+j)$.

The control input space of RHPC is equal to that of conventional MPC, if for any vector $\boldsymbol{U}_{\mathrm{vsl,cMPC},m}(k_\mathrm{c})$ in the control input space of conventional MPC, one can find a vector $\boldsymbol{\Theta}_m(k_\mathrm{c})$ that solves the following equation

$$\boldsymbol{U}_{\mathrm{vsl,cMPC},m}(k_\mathrm{c}) = \boldsymbol{U}_{\mathrm{vsl,RHPC},m}(k_\mathrm{c}) = \boldsymbol{Z}_m^\top(k_\mathrm{c})\boldsymbol{\Theta}_m(k_\mathrm{c}). \tag{7.3}$$

Note that $\boldsymbol{Z}_m(k_\mathrm{c})$ in fact depends on the control inputs that are applied over the prediction horizon. Hence, for every $\boldsymbol{U}_{\mathrm{vsl,cMPC},m}(k_\mathrm{c})$, the value of $\boldsymbol{Z}_m(k_\mathrm{c})$ can be determined. Therefore, if for the $\boldsymbol{Z}_m(k_\mathrm{c})$ corresponding to $\boldsymbol{U}_{\mathrm{vsl,cMPC},m}(k_\mathrm{c})$ we have

$$\mathrm{Rank}\Big(\boldsymbol{Z}_m(k_\mathrm{c})\Big) = \mathrm{Rank}\Big(\Big[\boldsymbol{Z}_m^\top(k_\mathrm{c})\Big|\boldsymbol{U}_{\mathrm{vsl,cMPC},m}(k_\mathrm{c})\Big]\Big), \tag{7.4}$$

then (7.3) has a solution $\boldsymbol{\Theta}_m^*(k_\mathrm{c})$. In such cases, the performance of the conventional MPC $J_\mathrm{cMPC}(\boldsymbol{U}_{\mathrm{vsl,cMPC},m}^*(k_\mathrm{c}))$ and the performance of the RHPC controllers $J_\mathrm{RHPC}(\boldsymbol{\Theta}_m^*(k_\mathrm{c}))$ are equal.

However, if the rank condition in (7.4) is not satisfied, the control inputs generated by the RHPC controller will not be able to reach the full control input space of the cMPC controller. This will in general negatively impact the performance of the RHPC controller.

In general, the performance of the cMPC controller and the performance of the RHPC controller have to be compared using the value of the control objective given in (5.16)

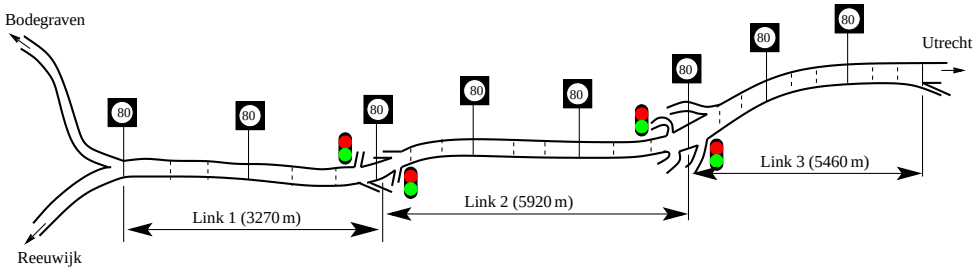

Figure 7.2: Schematic representation of the part of the Dutch A12 freeway considered for Case study G. The map of the freeway is also depicted in Fig. 3.6.

under the two control schemes. However, even if the control objectives are equal (i.e., $J_{\mathrm{cMPC}}(\boldsymbol{U}^*_{\mathrm{vsl,cMPC},m}(k_{\mathrm{c}})) = J_{\mathrm{RHPC}}(\boldsymbol{U}^*_{\mathrm{vsl,RHPC},m}(k_{\mathrm{c}}))$), it does not necessarily imply that the control inputs generated using the conventional MPC and the RHPC controllers are equal (i.e., it does not mean that $\boldsymbol{U}^*_{\mathrm{vsl,cMPC},m}(k_{\mathrm{c}}) = \boldsymbol{U}^*_{\mathrm{vsl,RHPC},m}(k_{\mathrm{c}})$) unless the rank condition in (7.4) is satisfied and $\boldsymbol{Z}_m(k_{\mathrm{c}})$ is a full column rank matrix. This is due to two reasons: first, since the objective function of the controllers are non-linear and non-convex with respect to the control inputs, then the optimization problem can have multiple possible global minima, second even if the minimum of the control objective function is unique and the rank condition in (7.4) is satisfied, multiple values of $\boldsymbol{\Theta}_m(k_{\mathrm{c}})$ are possible in case $\boldsymbol{Z}_m(k_{\mathrm{c}})$ is not of full column rank. Hence, in general qualitative comparison of the RHPC controller and the cMPC controller is not possible, and therefore, in this thesis, case studies are used to compare the performance of the cMPC and the RHPC controllers. Although the case studies cannot generalize on the comparison of the two control approaches, the results can provide an understanding on the performance of the control approaches.

7.2 Case study G: Reduction of travel times and emissions

In this case study, the cMPC and the RHPC control approaches are applied to reduce the travel time and emissions with different weights for both criteria. The two control approaches, cMPC and RHPC, are compared to each other and to the uncontrolled scenario.

7.2.1 Set-up of the case study

The freeway stretch considered for this case study is a part of the Dutch A12 freeway going from the connection with the N11 at Bodegraven up to Harmelen, and is shown in Fig. 3.6. The schematic representation of the freeway is depicted in Fig. 7.2. The freeway has three lanes in each direction. In this case study, the traffic flow in the direction from left to right of Fig. 7.2 is simulated. The part of the A12 freeway that is considered is approximately $14650\,\mathrm{m}$ long and it has two on-ramps (near Waarder and Woerden) and three off-ramps (near Waarder, Woerden, and Harmelen). The stretch is equipped with double-loop detectors at a typical distance of $500\,\mathrm{m}$ to $600\,\mathrm{m}$, measuring the average speed and flow every minute. It has 24 segments, each of which is equipped with a dynamic speed limit.

In [79] real-life data of the part of A12 freeway described above has been used to calibrate a METANET model. In this case study, the parameters that have been obtained in [79]

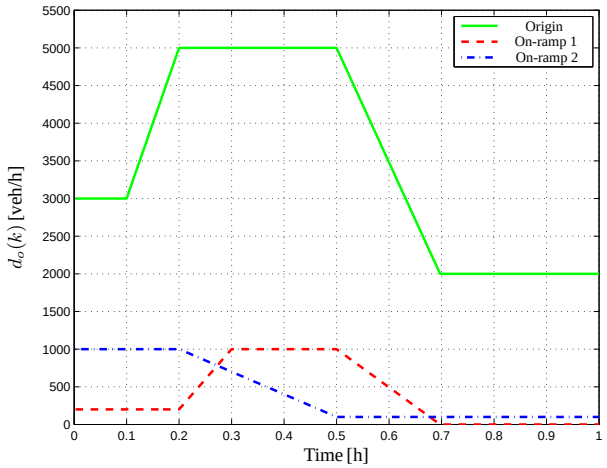

Figure 7.3: Time-varying demand profile for the main-stream and on-ramp origins of the A12 freeway considered in Case study G.

are used. The parameters of the freeway as obtained in [79] are listed in Appendix A.2.

A time-varying demand at the mainstream origin and at on-ramp origin is considered. The demand profile for a duration of one hour is shown in Fig. 7.3. With the given traffic demand, the traffic flow on the freeway in the uncontrolled case evolves as shown in Fig. 7.4. The spatial-temporal profile of the space-mean speed and the density of the traffic show a shock wave created at the beginning of the simulation at the 20^{th} segment counted from the origin of the freeway. The shock wave propagates till the 2^{nd} segment before it gets dissolved at $0.8\,\text{h}$.

Under this (uncontrolled) scenario, the total time spent by the vehicles is $1045.8\,\text{veh·h}$ and the total emissions of the traffic flow is $219.5\,\text{kg}$. In the subsequent simulations these values will be used as a benchmark and as nominal values of the performance measures.

7.2.2 Control objective

A general weighted-sum control objective has been given in (5.16). In this case study, since the travel time and emissions are considered as the performance criteria to compare the cMPC controller and the RHPC controller, the weights of the control objective are set as $\zeta_3 = \zeta_{4,\text{MDL}} = \zeta_{4,\text{TDL}} = 0$, $\zeta_5 = 0.01$, and $\mu_{\text{CO}} = \mu_{\text{HC}} = \mu_{\text{NO}_\text{x}} = 1$, and $\mu_{\text{CO}_2} = 0$. By varying the weights ζ_1 and ζ_2 different controlled scenarios with different emphasis on TTS and TE are considered. For the fixed values of ζ_3, ζ_4, and ζ_5 listed above the control objective of the cMPC and the RHPC controllers reads as

$$J(k_\text{c}) = \zeta_1 \frac{\text{TTS}(k_\text{c})}{\text{TTS}_\text{n}} + \zeta_2 \frac{\text{TE}(k_\text{c})}{\text{TE}_\text{n}} + 0.01 \frac{U_\Delta(k_\text{c})}{U_{\Delta,\text{n}}} \tag{7.5}$$

where the nominal (normalization) values TTS_n, TE_n, and $U_{\Delta,\text{n}}$ are the values when no controller is implemented (see Section 7.2.1).

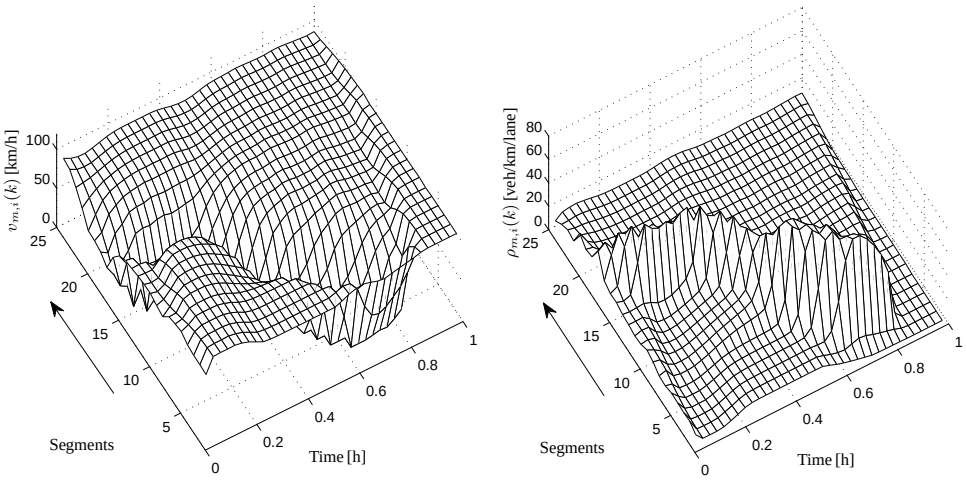

Figure 7.4: Traffic states of the A12 freeway of Case study G for the traffic demand in Fig. 7.3 and when no controller is implemented. The arrows indicate the driving direction.

The total time spent $\mathrm{TTS}(k_\mathrm{c})$ is determined using (5.5), the total emissions $\mathrm{TE}(k_\mathrm{c})$ is obtained using the macroscopic emission model given in (5.8), and the variation of the control input $U_\Delta(k_\mathrm{c})$ for both control approaches is determined using (5.13) with $\mu_\mathrm{s} = (8N_\mathrm{p}v_\mathrm{step}^2)^{-1}$, $\mu_\mathrm{cs} = (7N_\mathrm{p}v_\mathrm{step}^2)^{-1}$, and $\mu_\mathrm{r} = (2N_\mathrm{p})^{-1}$ for $v_\mathrm{step} = 10\,\mathrm{km/h}$.

For the controlled scenarios discussed below, the 24 speed limits of the freeway stretch are coupled in groups of 3, where each speed limit control in the group is assigned the same value (see Fig. 7.2). Thus, there are 8 variable speed limit values. Moreover, 2 ramp meters are controlled independently. This means that there are 10 control variables (8 speed limit values and 2 ramp metering rates) for both the cMPC controller and the RHPC controller. The grouping of the speed limits is done so that the computation time of the cMPC controller can be sped up to a level where the simulation can be finished within a maximum of $24\,\mathrm{h}$ while it does not have any effect on the speed of the RHPC controller. Note that when using the RHPC controller for the grouped speed limits, the states required for the control laws are the average values of the states of the segments in a group. In this way, the RHPC controller can also result in speed limits that are the same for the segments of a group. Moreover, the same parameter values are used for the whole freeway stretch.

Moreover, the speed limits are constrained by the upper speed limit $V_{\mathrm{u},m} = v_{\mathrm{ref},m} = 120\,\mathrm{km/h}$ and the lower speed limit $V_{\mathrm{l},m} = 40\,\mathrm{km/h}$. At every control time step k_c, the optimization problem that minimizes the cost function (7.5) is solved using multi-start Sequential Quadratic Programming (SQP) introduced in Section 5.4.3. More specifically, 5 initial starting points are used, of which 1 is random, while the rest consists of the lower bounds of the optimization variables, the upper bounds, the average of the lower and upper bounds, and the one time-step forward-shifted version of the solutions of the previous optimization step.

For both the cMPC and the RHPC controlled cases, the control time step $T_\mathrm{c} = 1\,\mathrm{min}$, the prediction horizon $N_\mathrm{p} = 15$ (corresponding to $15\,\mathrm{min}$), and the simulation time step

$T = 10\,\mathrm{s}$ are used. The control horizon $N_\mathrm{c} = 10$ (corresponding to $10\,\mathrm{min}$) for the cMPC controller. For the RHPC controller, since the control laws given in (6.7) and (6.10) under the first option of the RHPC strategy in Section 6.2.1 is employed, the control horizon is set $N_\mathrm{c} = 1$ (corresponding to $1\,\mathrm{min}$). This means that the number of optimization variables of the RHPC controller is equal to the number of the controller parameters, i.e., 4 (3 for the variable speed limits and 1 for the ramp metering rates). The number of the optimization variables of the cMPC controller is $10 \times N_\mathrm{c} = 100$.

In this case study, the weights ζ_1 and ζ_2 are related by $\zeta_2 = 10 - \zeta_1$, where $\zeta_1 \in \{0, 1, 2, \ldots, 10\}$. Therefore, 11 possible combinations of the TTS and TE are considered. The evolution of system states is simulated for $1\,\mathrm{h}$. The simulation results are discussed in the sequel.

7.2.3 Results and discussion

Let us first look at the simulation results of the cMPC and the RHPC controllers when the control objectives are either only TTS, TE, or $9\mathrm{TTS} + \mathrm{TE}$, i.e., when the weights are set as:

1. $\zeta_1 = 10$ and $\zeta_2 = 0$, i.e., the focus of the controllers is on reducing only the total time spent TTS.

2. $\zeta_1 = 0$ and $\zeta_2 = 10$: in this scenario the focus of the controllers is on reducing the total emissions (TE).

3. $\zeta_1 = 9$ and $\zeta_2 = 1$, i.e., the controllers focus on the reduction of the TTS and the TE with a different degree of emphasis. This combination should result in a trade-off between travel time and emissions.

The results of the simulations of these three cases are presented in Table 7.1. The results give the values of each performance criterion for each control scenario. For comparison reasons, Table 7.1 also tabulates the results of the cMPC and the RHPC controllers. It can be seen that the difference between the performance criteria (TTS and TE) of the two control approaches is not significant for the three different combinations of weights. However, the difference in the average computation time (CPU Time) per control time step is significant. The average computation time step per control time step is computed as the average of all computation time steps required at every control time step by the controllers to minimize the given objective function by optimizing the control inputs over the prediction horizon.

Table 7.2 provides the relative performance of the proposed RHPC traffic controller as compared to the cMPC traffic controller for the three cases presented in Table 7.1. The relative comparison of the RHPC controller is obtained using the equation

$$R_c = \frac{c_\mathrm{RHPC} - c_\mathrm{cMPC}}{c_\mathrm{cMPC}} \times 100\% \tag{7.6}$$

where c_cMPC denotes the value of the performance criterion $c \in \{\mathrm{TTS}, \mathrm{TE}, \text{CPU Time}\}$ for the cMPC controller and c_RHPC is the value of the performance criterion c for the RHPC controller. So a negative value of the relative comparison indicates the RHPC controller performs better than the cMPC controller and a positive value indicates a worse performance of the RHPC controller as compared to the cMPC controller.

Table 7.1: Simulation results of the cMPC traffic controller and the RHPC traffic controller for Case study G. The CPU time is the average computer computation time required to compute the control variables in one control time step, where one control time step is $T_c = 60$ s.

Scenarios	Controller	Performance Criteria		
		TE [veh·h]	TE [kg]	CPU Time [s]
Uncontrolled	—	1045.8	219.5	0.0
TTS	RHPC	841.1	216.9	10.9
	cMPC	811.5	230.5	375.2
TE	RHPC	2377.5	82.7	25.7
	cMPC	2283.1	92.0	1862.7
9TTS + TE	RHPC	842.7	213.9	40.4
	cMPC	807.4	214.0	1809.3

Table 7.2: Relative comparison of the RHPC traffic controller with respect to the cMPC traffic controller for Case study G. Negative values indicate the RHPC controller performs better than the cMPC controller and positive values indicate a worse performance of the RHPC controller as compared to the cMPC controller.

Scenarios	Relative Comparison	
	Control Performance Criterion	CPU Time
TTS	+4%	−97%
TE	−10%	−99%
9TTS + TE	−2%	−98%

As can be seen from Table 7.2, the loss in the performance of the RHPC controller is at most 4% for each case. But, the improvement in the computation times in all cases is more than 97%.

In Fig. 7.5 the spatial-temporal profile of the space-mean speed and the density of the traffic flow are presented to compare the performance of the controllers with respect to each other and the uncontrolled scenario. The shock wave created at the 20^{th} segment from the origin of the freeway in Fig. 7.4 propagates till the 2^{nd} segment before it gets dissolved at about 0.8 h. However, when the system is controlled to reduce the TTS (see Fig. 7.5(a) and Fig. 7.5(b)) using either the cMPC or the RHPC controllers the shock wave is suppressed at the very early stage. The profiles of the space-mean speed and the density generated through the two controllers (cMPC and RHPC) are almost the same. However, the evolution of the space-mean speed in the cMPC-controlled case is smoother than in the RHPC-controlled case. Moreover, the space-mean speed under the cMPC-controlled case is on average higher than the RHPC-controlled case.

The above comparison of the controllers gives a detailed comparison for three combinations of the weights ζ_1 and ζ_2 in (7.5). Now, the RHPC and the cMPC controllers are simulated for several possible weight combinations. In particular, that the relation $\zeta_2 = 10 - \zeta_1$,

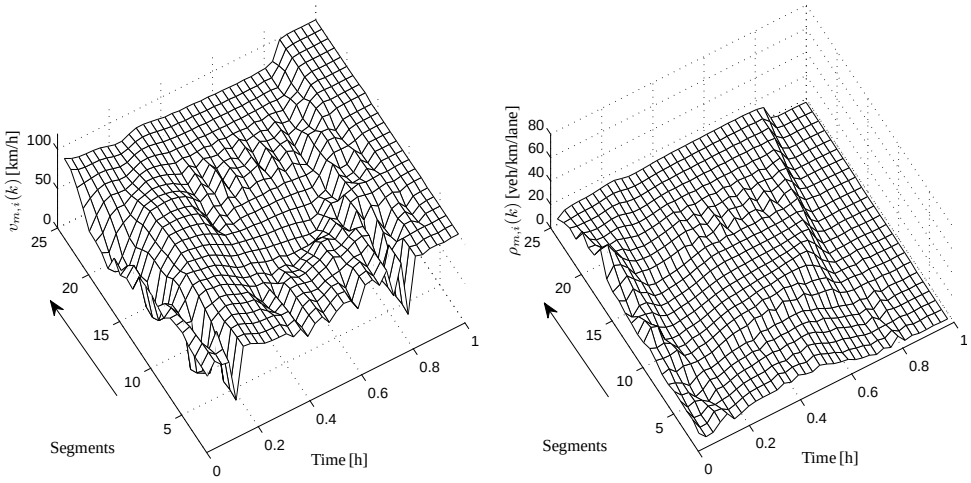

(a) TTS controlled using RHPC

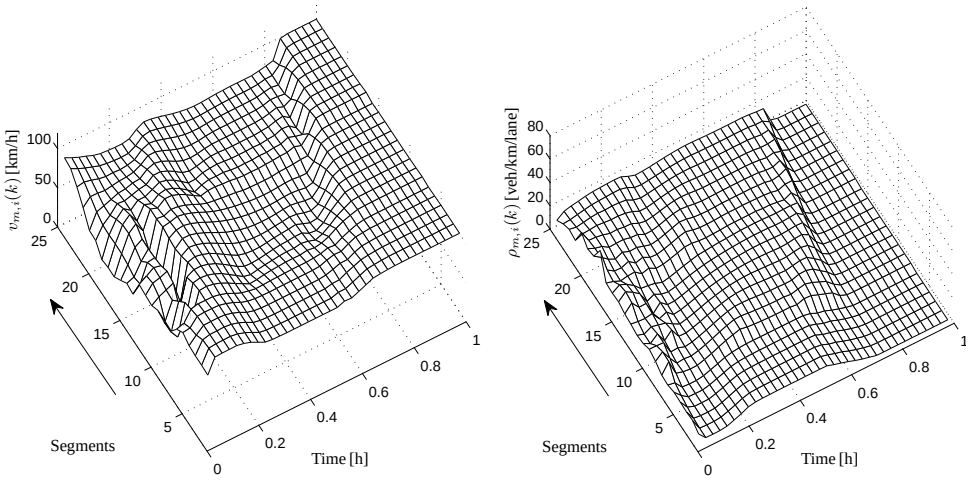

(b) TTS controlled using cMPC

Figure 7.5: Space-mean speed and density profiles of Case study G as a function of time and space using different controllers. The arrows indicate the driving direction.

for $\zeta_1 \in \{0, 1, 2, \ldots, 10\}$ is considered. The results of the simulation for the different weight combinations are depicted in Fig. 7.6. The figure provides the relative change of the performance criteria, in particular TTS and TE, as compared to the uncontrolled scenario, which is computed using

$$I_p = \frac{p_{\text{controlled}} - p_{\text{uncontrolled}}}{p_{\text{uncontrolled}}} \times 100\% \tag{7.7}$$

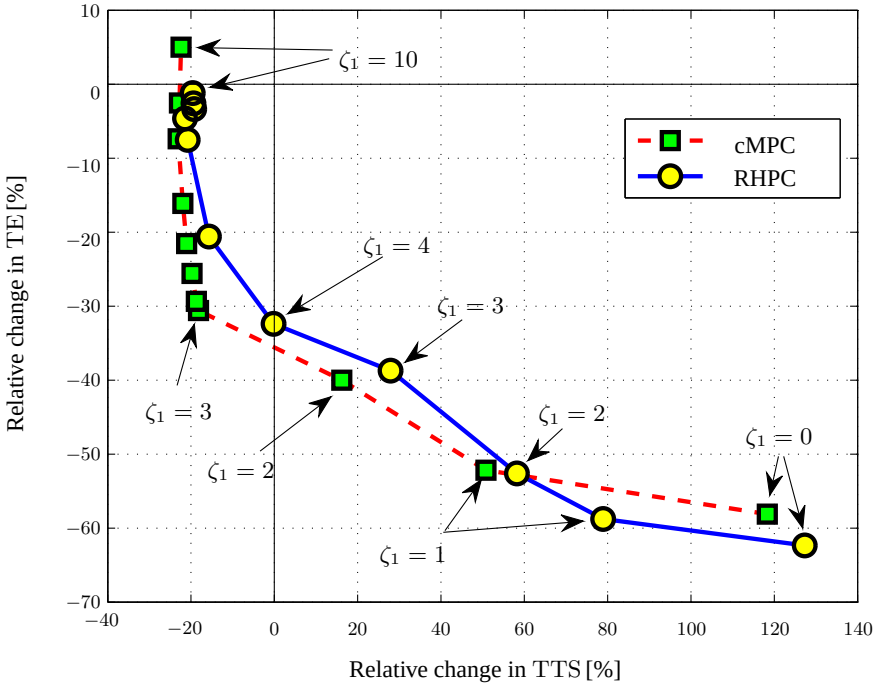

Figure 7.6: Trade-off curve for Case study G, where the objective function $J = \zeta_1 \mathrm{TTS} + (10 - \zeta_1)\mathrm{TE} + 0.01 U_\Delta$ *for* $\zeta_1 = 0, 1, \ldots, 10$*. Each point on the graph indicates the relative change of the* TTS *and* TE *of the controlled scenarios as compared respectively to the* TTS *and* TE *of the uncontrolled scenario. Negative values indicate a decrease (i.e., an improvement) of the value of the performance criteria as compared to the uncontrolled scenario and a positive value indicate an increase of the value of the performance criteria compared to the uncontrolled scenario.*

where $p_{\text{controlled}} \in \{\mathrm{TTS}, \mathrm{TE}\}$ is the performance criteria of either the RHPC controller or the cMPC controller of the different controlled scenarios and $p_{\text{uncontrolled}} \in \{\mathrm{TTS}, \mathrm{TE}\}$ is the performance criteria of the uncontrolled scenario.

The figure shows that the TTS can be reduced by a factor of more than 19% and the TE by less than 2% when the focus of the RHPC controller is on TTS ($\zeta_1 = 10, \zeta_2 = 0$) only. With the cMPC controller and the same control objective, the travel time TTS is reduced by more than 20% while the emissions TE increase by more than 5%. Moreover, the figure shows that the TE can be reduced by more than 58% if the focus of the two controllers is on TE ($\zeta_1 = 0$, $\zeta_2 = 10$) only, but then the TTS increases by more than 110%. The figure also indicates that a reduction of more than 30% in emissions can be attained without significantly affecting the travel time if the relative weight of the TTS is about $\zeta_1 = 4$ while the TE has a weight of $\zeta_2 = 6$ when the controller is RHPC and if the relative weight of the TTS is about $\zeta_1 = 2.5$ while the TE has a weight of $\zeta_2 = 7.5$ when the controller is cMPC.

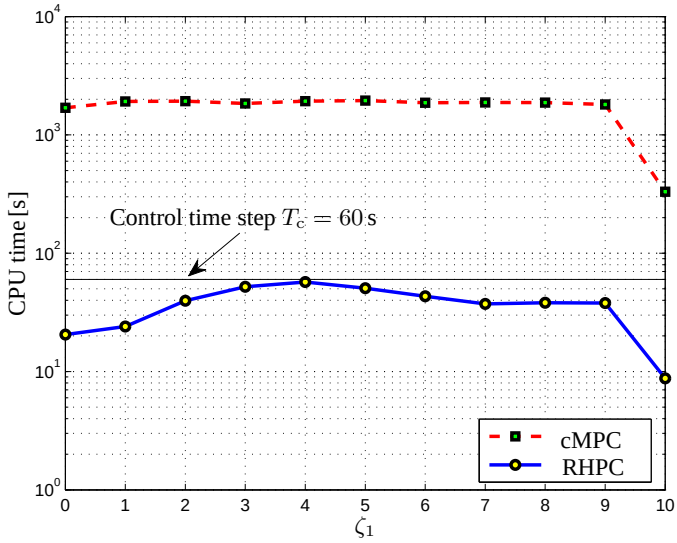

Figure 7.7: Computer CPU computation time per every control time step of the cMPC controller and the RHPC controller of Case study G.

This indicates that the optimal control inputs generated by the two controllers are different and that the same weights of the performance measures of the control objectives may not have the same impact on the performance of the controllers.

Although the trade-off curves generated using the RHPC controller and the cMPC controller are more or less similar, there are important differences when the combinations of the weights are one of $\zeta_1 \in \{1, 2, \ldots, 7\}$ and $\zeta_2 = 10 - \zeta_1$. For these values the RHPC controller gives better improvement to the TE than the cMPC controller does. But the cMPC controller results in lower TTS than the RHPC controller does. In general, however, one can see that the RHPC controller has somehow comparable performance to the cMPC controller.

Since the main motivation for the design of the RHPC controller is to reduce the computation time of the cMPC controller so that the control approach can be tractable in practice, the average computation time required at every control time step is also depicted in Fig. 7.7. As can be seen, for all the weight combinations considered in this case study, the computation time of the RHPC controller is below the control time step $T_c = 60$ s line. This means that the RHPC controller is feasible in practice for this particular case study. On the contrary, the computation times of the cMPC controller for all the cases are way above the control time step, which makes it intractable in practice. Clearly, the computation time of the RHPC controller and the cMPC controller are very different. However, the gain in the computation time of the RHPC controller is obtained at the cost of small loss in performance.

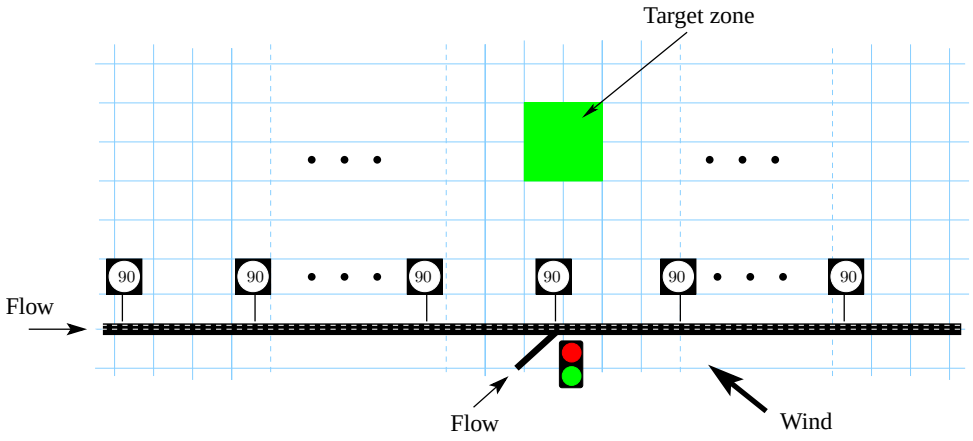

Figure 7.8: A 12 km three-lane freeway stretch considered for the Case study H. Each cell in the grid is 200 m by 200 m.

7.3 Case study H: Reduction of dispersion of emissions

In the previous section, a case study that focuses on the reduction of travel times and emissions has been simulated to compare the cMPC and the RHPC controllers. In this section, another dimension of the performance measure, the dispersion of emissions to a target zone, is also taken into account.

7.3.1 Set-up of the case study

In this case study, a 12 km freeway stretch described in Section 6.4.2 is considered. The schematic representation of the freeway is again depicted in Fig. 7.8 for convenience. As in Section 6.4.2, the neighborhood of the freeway is assumed to be flat with no obstructions and is subject to varying wind speed and wind direction described by

$$V_{\mathrm{w}}(k) = 7 + 2\sin(0.005\pi k + \pi/6)\sin(0.01\pi k) \tag{7.8}$$

$$\varphi(k) = \frac{2\pi}{5} + \frac{\pi}{4}\cos(0.004\pi k) \tag{7.9}$$

where the wind speed $V_{\mathrm{w}}(k)$ is expressed in m/s and the wind direction (angle) $\varphi(k)$ in radians.

Moreover, in order to study the dispersion of the emissions, a target zone of interest that is 1 km away from the middle of the segment with the on-ramp (see Fig. 7.8) is assumed. Just as in the case study of Section 6.4.2, the target zone has an area of $400\,\mathrm{m}\times 400\,\mathrm{m}$ and the neighborhood of the freeway is meshed into a grid of square cells of dimension $200\,\mathrm{m}$ as shown in Fig. 7.8.

The freeway traffic of this case study is modeled using the METANET traffic flow model of Section 2.3 with the model parameters presented in Section 6.4.2. The VT-macro emission and fuel consumption model of Section 3.4 is used to model the emissions of the traffic flow of the freeway. In this section, the dispersion of the emissions to the given target zone

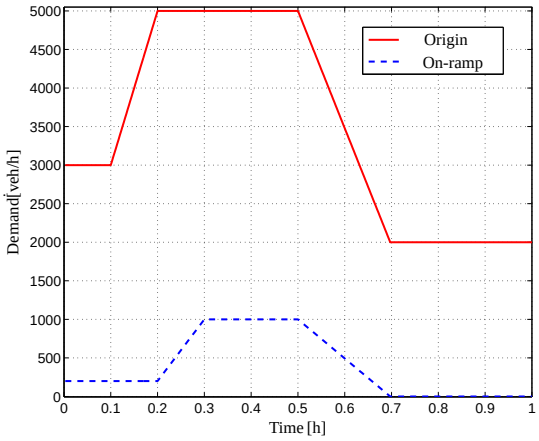

Figure 7.9: Traffic demand profile at the mainstream origin and the on-ramp origin of Case study H.

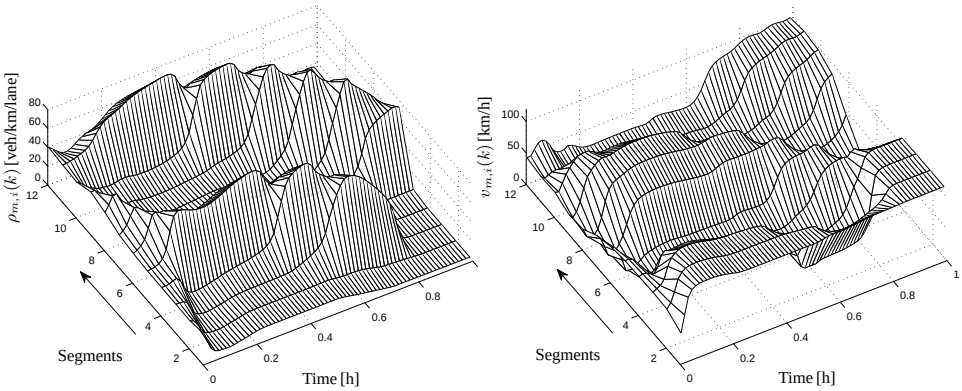

(a) Density (b) Space-mean speed

Figure 7.10: Traffic flow characteristics when no traffic control is applied for the demand profile depicted in Fig. 7.9 of Case study H. The arrows indicate the driving direction.

is modeled using the expanding grid-based dispersion model[1] of Section 4.3.2, with the expansion factor $\varpi = 0.05\ (5\%)$ and the vertical dispersion factor $\gamma = 0.1\ (10\%)$.

The traffic at the downstream of the traffic flow is considered to be unrestricted. A time-varying traffic demand both at the mainstream origin and the on-ramp origin is considered. The demand profile is also the same as the demand used in the case study presented in Section 6.4.2. For convenience the demand profile is depicted again in Fig. 7.9. The simulation period is 1 h with a simulation time step of $T = 10\,\text{s}$.

[1] Note that in Section 6.4.2, the extended grid-based dispersion model discussed in Section 4.3.1 is used.

7.3.2 Control objective

In all the controlled scenarios of this case study, the performance measure of the cMPC and the RHPC controllers are defined using the multi-criteria objective function defined in (5.16). In all the controlled scenarios, the weight for the variation of the control input is set $\zeta_5 = 0.01$. Moreover, $\zeta_3 = \zeta_{4,\mathrm{TDL}} = 0$ so that the controllers do not consider the reduction of fuel consumption and total dispersion level TDL. The weights of the emissions are $\mu_{\mathrm{CO}} = \mu_{\mathrm{HC}} = \mu_{\mathrm{NO}_x} = 1$ to give equal weight to CO, HC, and NO_x; moreover, $\mu_{\mathrm{CO}_2} = 0$. The values of ζ_1, ζ_2, and $\zeta_{4,\mathrm{MDL}}$ are varied depending on the effect the controllers are required to induce. In particular, the following four different combinations are considered:

- S_2: $[\zeta_1\, \zeta_2\, \zeta_{4,\mathrm{MDL}}] = [1\ 0\ 0]$, where the controllers focus on the reduction of TTS only,
- S_3: $[\zeta_1\, \zeta_2\, \zeta_{4,\mathrm{MDL}}] = [0\ 1\ 0]$, where the controllers focus on the reduction of TE only,
- S_4: $[\zeta_1\, \zeta_2\, \zeta_{4,\mathrm{MDL}}] = [0\ 0\ 1]$, where the controllers focus on the reduction of MDL only, and
- S_5: $[\zeta_1\, \zeta_2\, \zeta_{4,\mathrm{MDL}}] = [10\ 1\ 1]$, where the controllers focus on the reduction of $10\mathrm{TTS} + \mathrm{TE} + \mathrm{MDL}$.

In all the above scenarios of this particular case study, the maximum dispersion level MDL is determined using (5.10) with $\mu_{\mathrm{d,CO}} = \mu_{\mathrm{d,HC}} = \mu_{\mathrm{d,NO_x}} = 1$ and $\mu_{\mathrm{d,CO_2}} = 0$.

The control time step $T_{\mathrm{c}} = 2\,\mathrm{min}$, the prediction horizon $N_{\mathrm{p}} = 7$ (corresponding to $14\,\mathrm{min}$), and the control horizon $N_{\mathrm{c}} = 5$ (corresponding to $10\,\mathrm{min}$) are used for both the cMPC and the RHPC controllers. The RHPC controller used in this case study employs the third option of the RHPC control concept discussed in Section 6.2.1, i.e., the parameters of the control laws are allowed to vary only until the control horizon N_{c} after which they are kept constant. Since the optimization problem is non-linear and non-convex, multi-start Sequential Quadratic Programming (SQP) with 8 initial points is used. Four of the initial points are random, while the rest consists of the lower bounds of the optimization variables, the upper bounds, the average of the lower and the upper bounds, and one time-step forward-shifted values of the optimization variables (either the parameters in the case of the RHPC controller and the control inputs in the case of the cMPC controller).

The values of the performance measures under the uncontrolled condition (Scenario S_1) are taken to be the nominal values used for normalization in the objective function. In the uncontrolled situation, the traffic demand creates the traffic flow that is characterized by the density and space-mean speed profiles depicted in Fig. 7.10. Due to high initial traffic densities at the end of the freeway and high traffic demands at the on-ramp origin of the freeway, two shock waves are created that propagate upstream. Under these traffic conditions, the total time spent TTS is $1362.1\,\mathrm{veh{\cdot}h}$, the values of the total emissions TE is $127.5\,\mathrm{kg}$, and the maximum dispersed emission level MDL at the target zone is $61.6\,\mu\mathrm{g/m^2}$. In the following section these values will also be used as benchmark to evaluate the performance of the traffic controllers.

7.3.3 Results and discussion

The simulation results for each of the controlled Scenarios S_2 to S_5 of the two control approaches (cMPC and RHPC) are compared to each other and to the uncontrolled Scenario

Table 7.3: Performance criteria for the uncontrolled and RHPC-controlled and cMPC-controlled scenario of Case study H. The controlled scenarios have the following control objectives: S_2 : TTS, S_3 : TE, S_4 : MDL, and S_5 : 10TTS+TE+MDL. The CPU Time is the average computer computation time required by the controllers to compute the control variables in one control time step, where one control time step is $T_c = 120$ s.

Scenarios	Controller	Performance Criteria			
		TTS [veh·h]	TE [kg]	MDL [μg/m^2]	CPU Time [s]
S_1 :	Uncontrolled	1362.1	127.5	61.6	0
S_2 :	RHPC	875.8	141.6	78.7	110
	cMPC	704.0	147.7	78.3	345
S_3 :	RHPC	1611.5	66.2	29.9	214
	cMPC	1624.5	65.9	30.6	731
S_4 :	RHPC	1604.5	66.5	30.0	1690
	cMPC	1624.8	69.6	34.4	11933
S_5 :	RHPC	1526.0	70.6	34.5	2075
	cMPC	1030.4	92.7	45.3	10400

S_1. First, let us analyze the comparison of the controlled simulation scenarios with the uncontrolled scenario. The comparison results are listed in Table 7.3. From the table it can be observed that both controllers perform well according to the intention of the control objective. The controllers reduce the traffic control performance criteria and provide a balanced trade-off when the combined objective function (Scenario S_5) is considered.

The controllers clearly show differences in performance. From Table 7.3, it is observed that in some cases the cMPC controller performs better than the RHPC controller. This is quantified and explicitly presented in Table 7.4. Table 7.4 lists the relative comparison of the RHPC controller with respect to the cMPC controller. It is determined using the equation given in (7.6). In this particular case study, the performance measure c in (7.6) is $c \in \{\mathrm{TTS}, \mathrm{TE}, \mathrm{MDL}, \text{CPU Time}\}$. Then, as can be seen from Table 7.4, the cMPC controller mostly performs better than the RHPC controller as expected (cf. Section 7.1). However, the computation time (see Table 7.3 and Table 7.4) of the RHPC controller is significantly lower than that of the cMPC controller. The RHPC controller improves the computation time (expressed in CPU Time) by more than 68% with respect to the cMPC controller for the considered scenarios. The CPU time in Table 7.3 increases as one progresses from Scenario S_2 to Scenario S_5 of the controlled cases. This is because in each scenario only the models that are required to generate the corresponding performance criteria are simulated. This means that in Scenario S_2 only the METANET traffic flow model is simulated, while for example in Scenario S_3 the METANET model and the VT-macro model are simulated. Therefore, the computation time of the scenarios with multiple performance criteria becomes high (e.g., in this particular case Scenario S_5 has higher CPU Time, because it uses traffic flow, emissions, and dispersion of emissions models).

The space-mean speed profiles under the different control objectives are also presented through Fig. 7.11 to Fig. 7.13. These figures compare the space-time speeds of the traffic network when the control approaches are cMPC and RHPC. As can be seen from all the figures, the shock waves observed in Fig. 7.10 are dissolved both by the cMPC and RHPC controllers. However, cMPC results in a smoother speed evolution than RHPC.

Table 7.4: Relative comparison of the values of the performance criteria of the RHPC controller and the cMPC controller of Case study H for the different controlled scenarios. Negative values of the performance criteria indicate the RHPC controller performs better than the cMPC controller while positive values of the performance criteria indicate the RHPC controller performs worse than the cMPC controller.

	Relative Comparison	
Scenarios	Control Performance Criterion	CPU Time
S_2 : TTS	$+24\%$	-68%
S_3 : TE	$+0\%$	-71%
S_4 : MDL	-12%	-86%
S_5 : 10TTS + TE + MDL	$+36\%$	-80%

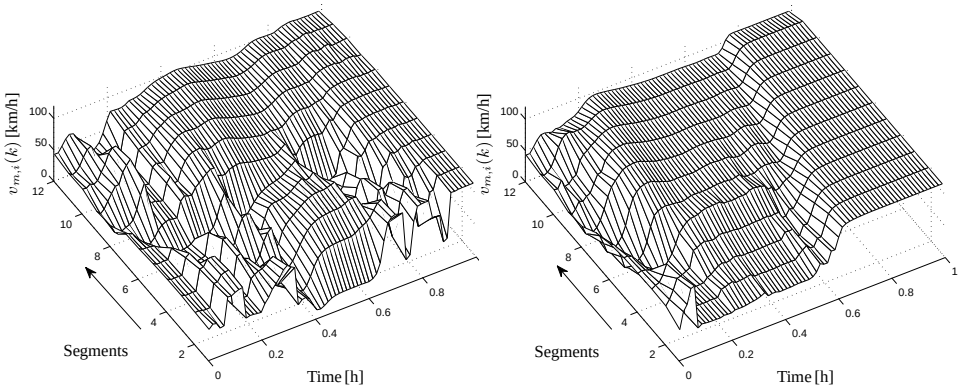

(a) RHPC controlled (b) cMPC controlled

Figure 7.11: Time-space evolution of space-mean speed of Case study H when the control objective of the cMPC and the RHPC controllers is TTS*. The arrows indicate the driving direction.*

In Fig. 7.13, it can be seen that the speed is higher when the control approach is cMPC than when the control approach is RHPC. This is reflected in the higher travel times and lower emissions and dispersion levels in the RHPC-controlled case than the cMPC-controlled case (see also the last row of Table 7.3).

Furthermore, the evolution of the dispersion level in the target zone is depicted in Fig. 7.14. Under the TTS-controlled Scenario S_2, both the cMPC and the RHPC control approaches worsen the dispersion level. However, the dynamics of the evolutions of the dispersion of the emissions under the two control strategies are completely different. The RHPC controller causes a higher fluctuation in the dispersion level than the cMPC controller, regardless of the difference in the values of the dispersion levels. This can be explained by the speed variation observed in Fig. 7.11. A similar situation is also observed in Fig. 7.14(b), where the dispersion level fluctuates more in the cMPC-controlled case than in the RHPC-controlled case. This is because that the space-mean speed fluctuates less in the RHPC-controlled case than in the cMPC-controlled case (see Fig. 7.12).

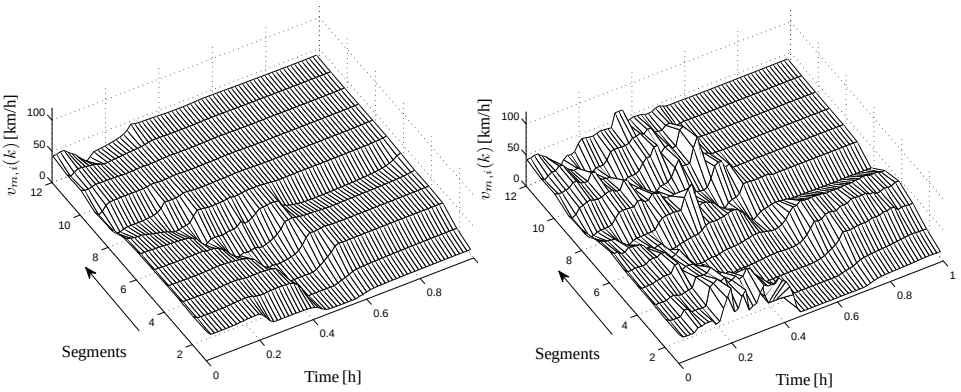

(a) RHPC controlled (b) cMPC controlled

Figure 7.12: Time-space evolution of space-mean speed of Case study H when the control objective of the cMPC and the RHPC controllers is MDL*. The arrows indicate the driving direction.*

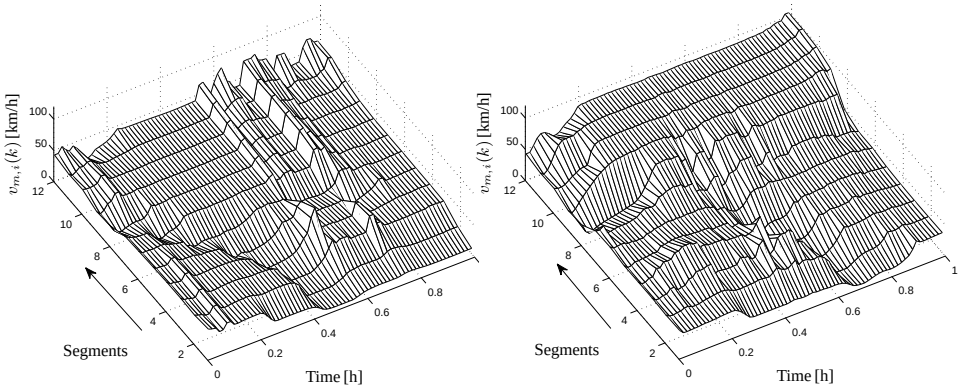

(a) RHPC controlled (b) cMPC controlled

Figure 7.13: Time-space evolution of space-mean speed of Case study H when the control objective of the cMPC and the RHPC controllers is $10\mathrm{TTS} + \mathrm{TE} + \mathrm{MDL}$*. The arrows indicate the driving direction.*

A similar phenomenon is observed from Fig. 7.13 and Fig. 7.14(c). However, in general, despite the difference in the value of the performance improvement (TTS, TE, MDL, and CPU Time), the two control approaches (cMPC and RHPC) produce similar trends in the evolution of the emissions and the speed of the traffic for the various scenarios.

7.4 Conclusions

This chapter has presented the general similarities and differences between conventional Model Predictive Control (cMPC) and Receding-Horizon Predictive Control (RHPC). It

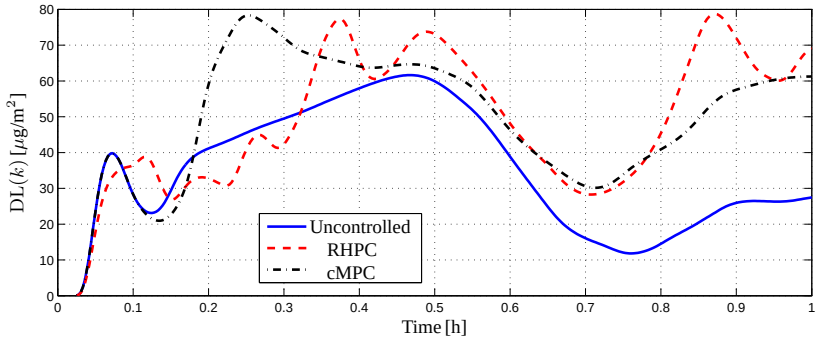

(a) TTS controlled

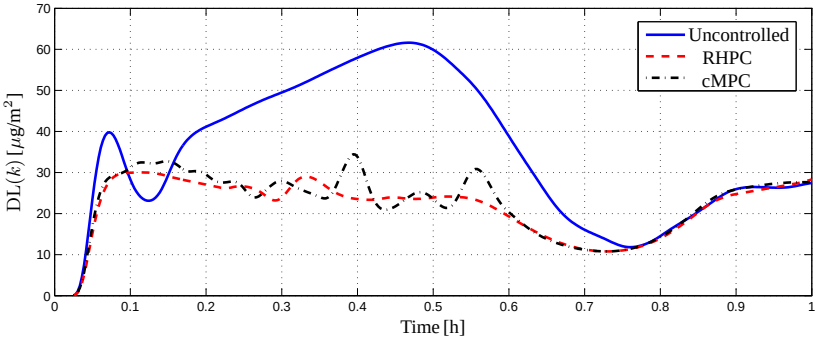

(b) MDL controlled

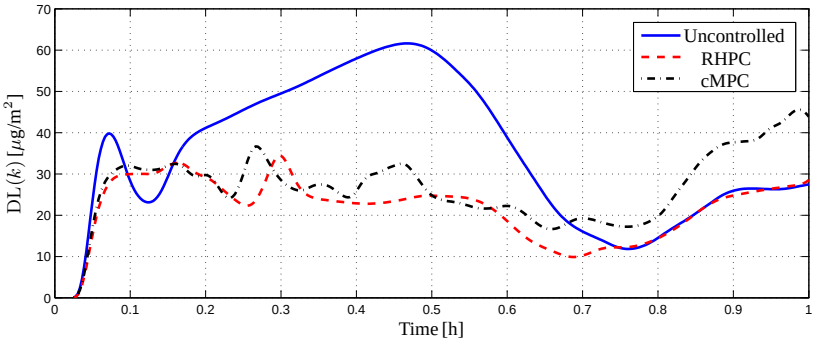

(c) $10\mathrm{TTS} + \mathrm{TE} + 5\mathrm{MDL}$ controlled

Figure 7.14: The influence of cMPC and RHPC control approaches on the evolution of the dispersion level $\mathrm{DL}(k)$ *in the target zone under different control scenarios of Case study H. The dispersion level* $\mathrm{DL}(k)$ *is the total sum of emission levels CO, HC, and* NO_x *in the target zone at every simulation time step* k *as expressed in* $\mu g/m^2$.

further has compared the two control approaches using simulation-based case studies.

The first case study illustrated that RHPC may have relatively good performance while

featuring a very low computation time, which makes it feasible for practical applications. With all the scenarios considered (different combinations of the total time spent and the total emissions) the computation time demand of the RHPC controller has been less than one control time step while still improving the control performance measures as compared to the uncontrolled scenario. Moreover, for this case study the performance of the RHPC controller was comparable to that of the cMPC controller.

In the second case study, where dispersion of emissions was taken into account, both the RHPC and the cMPC controllers were too slow (i.e., the computation time required at every control time step is larger than one control time step size), which makes them unsuitable for practical applications. In fact this is due to the added computation time required by the dispersion model and due to the larger number of initial points used for the optimization process (i.e., the number of the initial points of the optimization was 5 in the first case study, while it is increased to 8 in the second case study.). Nonetheless, even in this second case, the RHPC controller has proved to be very much faster than the cMPC controller, albeit at the cost of a lower performance. The reduction in the computation time as compared to the loss in performance measure of the RHPC controller relative to the cMPC controller is small.

Chapter 8

Conclusions and Open Issues

This thesis has presented and discussed freeway traffic flow models, freeway traffic emissions and fuel consumption models, freeway traffic emissions dispersion models, and model-based freeway traffic control approaches. In this chapter the main conclusions of the thesis are summarized. Moreover, as has been pointed out in some of the chapters, this thesis also leaves some open issues that require further research work. This chapter highlights the main issues that can be researched in the future and in some cases the chapter provides some pointers (recommendations) for the pursuit of the solutions to the open issues.

8.1 Conclusions

Traffic systems are non-linear and complex systems. Due to the unpredictable behavior of drivers and unknown disturbances, development of traffic flow models that provide accurate estimates and predictions of traffic states and that are applicable to all situations is very challenging. Thus, models are developed with a minor acceptable mismatch from the reality. Using such models to make predictions of traffic states and making decisions based on the uncertain predictions can have a negative impact, especially if decisions are based on longer prediction horizons, where the introduction of prediction errors is highly plausible.

In cases where models have some uncertainty or are complex, the receding-horizon-based model predictive control approaches are good candidates due to two main reasons. On the one hand, the control approaches make use of predicted traffic states to design control measures so that a given traffic control objective is attained, and thus future travel times and traffic demands can be considered when allocating the limited infrastructure. On the other hand, since such control approaches rely on the predictability of the traffic states, when there are errors in the prediction of the traffic states, the errors can be corrected during the next prediction step as it uses the receding-horizon-feedback concept. This means that the model-based traffic controllers presented in this thesis adapt themselves to the prevailing traffic situations and update the traffic control measures that can improve the traffic performance.

This thesis has considered multi-objective traffic control performance measures. In particular, the reduction of travel time, emissions, fuel consumption, and dispersion of emissions to neighborhoods have been taken into account. This means that the controllers have to predict these performance indicator on-line for every possible combination of traffic con-

trol measures, in particular the variable speed limits and ramp metering discussed in this thesis. Therefore, it is imperative to select models that can be used for on-line applications and to design model-based controllers that are tractable in practice. To this end, models have been selected and compared and traffic controllers have been designed and compared. The main conclusions of the process and the results are summarized as follows:

Traffic flow modeling: Initially, a brief overview of the traffic flow models has been given in Chapter 2. From the literature it can be concluded that, despite the fact that microscopic traffic flow models such as the GHR (Gazis-Herman-Rothery) model [67] and IDM (Intelligent Driver Model) [186] provide a relatively accurate description of individual vehicles in a traffic flow, due to the limited contemporary computational capability of computers and the current state of microscopic models, macroscopic models are much better suited for on-line applications, because macroscopic models demand low computation time and memory size. In particular, model-based traffic control (where models are required to make on-line predictions and estimations) require macroscopic traffic flow models. Moreover, as long as traffic control measures are not tailored for individual vehicles, macroscopic traffic flow models are suitable for on-line based traffic control applications, where control measures (such as speed limits and ramp metering) are assigned arbitrarily to collection of vehicles.

In this thesis, the METANET [103, 124, 145, 146] traffic flow model, which is macroscopic and discrete in time and space is selected to describe the traffic flow of freeway systems. Moreover, in many occasions this model has been proved to result in a good description of the traffic phenomenon of the freeway traffic systems [103, 145, 146]. As has been demonstrated in several articles, the computation time of the METANET traffic flow model and its extensions [77] does not depend on the number of the vehicles in the traffic network. Therefore, the METANET model and its extensions can be used for the simulation of large-scale networks. Moreover, in addition to the ramp metering control, it is relatively easy to include variable speed limits explicitly in the METANET model.

Traffic emissions modeling: Literature suggests that microscopic emissions and fuel consumptions models are more accurate than macroscopic emissions and fuel consumption models. Since the macroscopic traffic flow model METANET is chosen for the simulation and prediction of the traffic flow, the use of macroscopic emissions and fuel consumption models would have decreased the accuracy of the estimation of the traffic emissions and fuel consumption. Therefore, it has been imperative to find a way to integrate the microscopic emissions and fuel consumption models with macroscopic traffic flow models in order to increase the estimation or prediction accuracy of the emissions and the fuel consumption. To this end, Chapter 3 of this thesis has presented a general framework for the integration of macroscopic traffic flow models with microscopic emissions and fuel consumption models. The approach has been further demonstrated using the METANET traffic flow model and the VT-micro [2] emissions and fuel consumption model, which resulted in the VT-macro emissions and fuel consumption model.

The analytical and empirical examination of the errors that can enter due to the integration of the VT-micro microscopic emissions and fuel consumption model with the METANET macroscopic traffic flow model have been shown to be small for small deviations in the speed and in the acceleration of the vehicles from their average values.

Comparison of the newly developed macroscopic VT-macro model to the established average-speed-based macroscopic model, COPERT [139], has shown the excellent performance of the VT-macro model. Moreover, the VT-macro emissions and fuel consumption model shows a significant reduction of the computation time relative to its parent microscopic emissions and fuel consumption model, VT-micro.

Freeway traffic emissions dispersion modeling: As not only the emissions from vehicles on a freeway but also the dispersion of the emissions to protected areas is important, traffic management and control practices should also take the dispersion of released emissions into account. The prediction or analysis of the impact of different traffic control and management actions on the dispersion of emissions can be done with emissions dispersion models. Emissions dispersion models require the emissions of vehicles in the traffic networks (either measured on-line or predicted) as an input. In prediction-based control approaches (such as the model predictive control discussed in this thesis), prediction of the traffic states and thereby determination of the emissions is required before one can predict the dispersion of the emissions to a given target zone. In general, this entails a higher demand for computation time. Therefore, dispersion models with a low computation time while still offering considerably accurate estimation or prediction are required for the on-line model based control approaches as is the case in this thesis.

So, this thesis has presented new dispersion models that can be used for an on-line applications. First a point-source dispersion model was presented. This is used as a basis for the development of the subsequent efficient grid-based models, the extended grid-based and expanding grid-based dispersion models. These models take the effect of varying wind speed and wind direction on the dispersion of emissions into account. The variation of the dispersion of emissions with the variation of temperature can be considered. Moreover, the computation of the grid-based dispersion models is small and it is also independent of the number of target zones considered.

Conventional Model Predictive Control (cMPC): Due the non-linear and time-varying nature of freeway traffic systems and due to the potentially conflicting interests of different stakeholders of the traffic systems, this thesis has proposed Model Predictive Control (MPC) to dynamically steer the freeway traffic flow such that a balanced trade-off between the conflicting interests can be obtained. Chapter 5 has highlighted the basic concepts of the cMPC controller as applied to traffic systems; it has illustrated ways to describe the multi-objective traffic control performance criteria; and it has formulated model predictive traffic control optimization problem.

In this thesis, case studies have been used to demonstrate cMPC for freeway traffic applications with multifaceted and sometimes conflicting objectives (e.g., reduction of travel times and emissions are conflicting requirements in case of low to medium traffic, while under congested traffic conditions both requirements are in essence the same). In this regard, the case studies have illustrated that—depending on the weights assigned to the individual control performance criteria—it is possible to reduce not only the travel times of vehicles in a traffic network, but also the emissions and the dispersion of the emissions to a given target zone. This means that assigning different weights in the control approach offers the capability for different stakeholders to affect the traffic flow in order to favor the traffic performance criteria they would like to focus on. Moreover, the case studies have also illustrated the ability and potential of cMPC to efficiently coordinate variable speed limits and ramp metering.

The simulation results of the case studies have also illustrated the potential of coordinated and integrated variable speed limits and ramp metering to improve the performance of the traffic network. In this regard, the cMPC controller has been able to integrate and coordinate the traffic measures. Depending on the wind speed and wind direction, the cMPC controller has been able to steer the traffic flow in such a way that the dispersion of emissions to a given target zone is reduced. The simulation results suggest that—instead of focusing on the total emissions—reduction of the dispersion of emissions to a specific target zone is best strategy in areas where there is frequent traffic jams and where there is the need to reduce the emission levels on a given target zone. In this way, only the parts of the traffic network that have effects on the emission levels of a protected target zone can be regulated to produce low emission levels. Hence, the constraint on the traffic flow of the parts of the traffic network that have no effect on the protected target zone is relaxed, as such the traffic flow in these parts of the traffic network can be improved.

However, as other papers from literature already suggested before, the simulation studies have shown that the computation time demand of the cMPC controller is very high, which makes it not suitable for practical on-line applications.

Receding-Horizon Predictive Control (RHPC): Since the large computational demands of the cMPC controller makes it intractable in practice, in Chapter 6 of this thesis a parametrized MPC strategy called Receding-Horizon Predictive Controller (RHPC) has been proposed. Under the same conditions, if the control measures of the traffic system can be described by control laws with a number of parameters that is less than the number of the control measures, the computation time of the RHPC controller can be decreased. To this end, Chapter 6 has discussed the general concept behind the RHPC controller and the parametrization of the control laws. Specifically, the concepts have been applied to design the RHPC controller for variable speed limits and ramp metering.

Similar to the cMPC controller, the RHPC controller has been used in simulation-based case studies to reduce the travel times, the emissions, and the dispersion of the emissions to a target zone. Moreover, the RHPC controller has been used to integrate and coordinate variable speed limits and ramp metering in such a way that a given traffic performance criterion is improved. The case studies have illustrated that the RHPC controller, as its parent cMPC controller, can improve the traffic flow, the emission levels, and the dispersion of the emissions to a target zone. The RHPC controller has also shown the trade-off involved between the travel times, emissions, and dispersion of emissions to a target zone. Based on the weights assigned to the traffic performance criteria, the RHPC controller has been able to provide a balanced trade-off between the conflicting and sometimes concurring traffic performance criteria.

Comparison of cMPC and RHPC: Since the control objectives of the controllers are nonlinear and non-convex, the performance of the cMPC and the RHPC controllers could not be compared (or quantified) analytically. Hence, the performance loss induced by the parametrization of the control measures cannot be generalized.

Due to lack of analytical description of the performance of the RHPC controller as compared to the cMPC controller, this thesis has compared the control approaches using simulation-based case studies in Chapter 7. The case studies have indicated that the

RHPC controller, in particular when the control objective is reduction of travel times, has very low computation time which makes it suitable for practical applications. However, the computational gain of the RHPC controller has been obtained at the expense of a performance loss relative to the cMPC controller. The loss in performance in general increases as the number of control inputs that are determined by the same control laws increases. Hence, a trade-off has to be made between computational efficiency and loss in performance relative to the cMPC controller.

8.2 Open issues

Although this thesis answers several important questions related to the application of model-based predictive control to solve the potentially conflicting traffic control performance criteria, there are many open issues that still require further investigation and research work. In this section some of the open issues that are worth of attention in relation to this thesis work are discussed.

This thesis has developed macroscopic emissions and fuel consumption models and dispersion of freeway traffic emissions models. These models have not yet been validated nor calibrated to real-life data. The VT-macro emissions and fuel consumption model presented uses the parameters of the VT-micro emissions and fuel consumption model [2] that is calibrated based on microscopic real-life data. The dispersion models are neither compared to established models nor calibrated to real-life data. Therefore, these models cannot be used in practice before assessing them with respect to real-life data. In order to improve the quality and assert the use of the models for practical applications, it is recommended to make further extensive research on the validation and comparison of the models with real data and available models. In this regard, some open issues that require further examination and research are:

Extensive validation of the VT-macro emissions and fuel consumption model: The newly developed VT-macro emissions and fuel consumption model has been compared only to the parent VT-micro model [2] and the COPERT model [139]. Moreover, the VT-macro model has not yet been calibrated with the original data of the VT-micro model. Calibration of the VT-macro model with the original data of the VT-micro model or some other data could improve the quality and reliability of the model. Additionally, comparison of the VT-macro model with other macroscopic and microscopic emissions and fuel consumption models both in terms of the computation time and estimation or prediction accuracy is an important step before exploitation of the model.

Moreover, the error introduced during the empirical comparison of the VT-macro model with the VT-micro model could have been caused due to the mismatch between the microscopic and macroscopic traffic flow models. This issue has not been investigated and could not be quantified in this thesis. Therefore, further research is suggested to find relations or explanation to the emissions or fuel consumption estimation errors that can be caused due to the mismatch between the different traffic flow models.

A general framework to integrate the macroscopic traffic flow models with microscopic emissions and fuel consumption models has been presented in Chapter 3. This framework has been demonstrated only with the METANET flow model and the VT-micro emissions and fuel consumption model. The applicability (or the shortcomings) of the

framework can also be investigated for other models (e.g., the cell transmission flow model [52, 53] with the VT-micro model).

Calibration, validation, and extension of dispersion models: Similarly to the emissions and fuel consumption models, the proposed dispersion models are neither calibrated nor compared with any real-life data or existing dispersion models. The accuracy of the models when calibrated with real data or models is not known. Therefore, it is recommended that the freeway emissions dispersion models are calibrated and validated with real-life data and are also compared with other existing models both in terms of their computation time and their estimation or prediction accuracy.

Furthermore, the dispersion models developed in this thesis do not describe the evolution of the dispersion of the emissions in the vertical direction. The dispersion models describe the evolution of the emissions horizontally while considering a vertical dispersion factor that to some extent reflects the effect of the vertical dispersion on the horizontal dispersion level. However, it is therefore recommended to also extend the developed models to fully describe the vertical dispersion of the emissions (i.e., to extend them to 3D models).

The wind speed and wind direction in the dispersion models are assumed to be homogeneous spatially (i.e., every point in the horizontal space—all at the same time—experience the same wind speed and wind direction). However, the wind speed and wind direction vary in space. So, we recommend to extend the dispersion models by including a wind model for each cell in the grid that depends on the wind speed and wind direction of the neighboring cells.

Consideration of traffic composition: In reality, the traffic composition is not homogeneous. It comprises light and heavy duty vehicles and old and new vehicles driven by drivers of different age and experience level. But throughout this thesis homogeneous traffic composition has been assumed. This means that all vehicles are assumed to be characterized by the same behavior. Therefore, it is recommended that the models be assessed for the cases with heterogeneous traffic compositions. Moreover, the impact of the controllers designed under such traffic compositions should be examined.

Other important issue is related to the traffic control design. As has been indicated in this thesis, the main shortcoming of the cMPC controller is that the required computation time is very high. To alleviate this issue the RHPC controller has been introduced at the cost of some performance loss. However, even the RHPC control approach still has some unresolved issues, in particular the relative loss or improvement of the RHPC controller with respect to the cMPC controller is not determined in general. Moreover, other dynamic control strategies (or even control laws of the RHPC controller) that may result in better outcomes have not been investigated. Thus, it is recommended that future research is conducted to study:

Quantifying possible or maximum performance loss: The performance loss of the RHPC controller with respect to the cMPC controller due to the parametrization of the control laws requires both extensive analytic approximations and empirical investigations. In other words, the research question “What is the (approximate) relation between the control objectives of the RHPC and the cMPC controllers for the respective control input spaces of the controllers?” requires detailed examination. This is because the

relation between the control objective functions of the controllers in terms of the parameter space for the RHPC controller and in terms of the control inputs for the cMPC controller can give a clear understanding in the amount of performance loss of the RHPC controller with respect to the cMPC controller.

Systematic approach for the formulation of control laws: In general, in this thesis, the control laws of the RHPC controller have been developed heuristically with the help of a priori knowledge of traffic systems. But could there be a general approach that can be used to formulate control laws in a systematic way? The development of a strategy to define a control law such that the control input space of the RHPC approximates the optimal control input space of the cMPC as closely as possible can improve the performance of the RHPC and the time to attain the optimal values.

Alternative control approaches: In this thesis, the RHPC controller has been introduced to reduce the computation time of the cMPC controller. In general, this is at the expense of loss in performance relative to the cMPC controller. However, there are also new control strategies for special system model structures. One of these approaches is Linear Parameter Varying (LPV)-MPC, which requires LPV models of the systems. For many non-linear systems the LPV-based control approaches have proved to increase the performance of traditional control approaches. In this regard, there have been efforts to model the traffic flow, emissions, and fuel consumption models in an LPV form [113, 115, 213]. However, since these models are not able to use variable speed limits as a control measure, these models have not been used in LPV-MPC or other LPV-based traffic control approaches. So, such approaches can also be investigated and can be compared to the RHPC control approach presented in this thesis.

Including and assessing other traffic control measures: In this thesis, only the speed limits and ramp metering have been used as traffic control measures. Utilization and impact assessment of other traffic control measures, such as route guidance, lane closure, and road pricing, within the scope of the proposed control approaches is also an important subject to be considered in future research.

Simulation versus prediction models: All the case studies presented in this thesis use the same model as a simulator of the real traffic system and as a predictor of the traffic states required by the model-based controllers. However, if the cMPC and the RHPC controllers would be implemented in practice, the reality will be definitely different from the prediction models used by the controllers. This mismatch can have consequences on the performance of the controllers. Hence, the performance of the controllers also has to be investigated by using different models for the simulation and prediction of the controllers. Such an approach would give some idea of how the controllers would cope with such a model mismatch when applied in reality.

In this thesis, centrally governed traffic controllers have been designed for system optimal operations of traffic systems. However, system optimal operations of traffic systems does not necessarily mean that all stakeholders are at equilibrium. Moreover, in this thesis, intelligent (or fully autonomous) vehicles have not been considered. In view of these, it is also interesting to investigate the following research questions in the future.

System optimum versus user equilibrium traffic operation: In this thesis the traffic control performance criteria were defined to be total time spent, total emissions, total fuel con-

sumption, and the dispersion level on a target zone of the total traffic network considered. But, minimum total time spent, total fuel consumed, or total emissions released does not mean that every driver has the same travel cost per unit time. The systems' optimal solutions that were sought using the control approaches presented in this thesis do not show a user equilibrium. Therefore, the traffic solutions that resulted in system optimal operations are not efficient in allocating resources equally. On the other hand, user equilibrium traffic operations are in general viewed as a reasonable approximation of the non-cooperative decisions made by commuters and are not efficient for the allocation of the scarce traffic network capacities [198]. Therefore, a traffic control approach is efficient if it can provide both system optimal and user equilibrium traffic solutions.

However, at least for some cases, it can be possible that the same system optimum can be obtained with different combination of traffic control measures or the same user equilibrium operations can be attained with different combination of traffic control measures. Then, a traffic control strategy can select the combinations of traffic control measures that results in the minimum difference between the user equilibrium and system optimal traffic operations. In this sense, it is interesting to research the user equilibrium approach of the model-based traffic control approaches presented in this thesis. Moreover, a combination of both user equilibrium and system optimal approaches can be considered as a future research direction.

Platooning: As has been briefly presented in Chapter 1, platooning of vehicles can decrease the fuel consumption and emissions of vehicles [6, 17]. Moreover, the number of vehicles occupying a traffic network can increase, because the inter-vehicle distance is reduced. The question is then, how can the model-based traffic control strategies influence intelligent vehicles to formulate platoons in such a way that a given traffic performance criterion is improved? Since travel time, fuel consumption, and emissions of the vehicles depend on the platooning, modifications are required in the available traffic flow, fuel consumption, and emission models. Therefore, further research is recommended to investigate platooning as a traffic control measure to improve travel time, fuel consumption, emissions, and dispersion of emissions to a given target zone.

Appendix A

Model Parameters

This appendix lists the values of the parameters of the macroscopic VT-macro emissions and fuel consumption model and the values of the parameters of the METANET traffic flow model for the part of the A12 Dutch freeway. These parameter values are used in the simulation studies presented throughout this thesis.

A.1 VT-macro (VT-micro) parameters

The values of the parameters of the VT-macro model are the same as that of the VT-micro model [2]. But since the values of VT-micro are given for speed inputs in ft/s and acceleration in ft/s^2 and the outputs are in mg/s for the emissions and gal/h for the fuel consumption, the values of the parameters are transformed in order to use SI-units for the inputs and for the outputs. Thus, the values of the model parameter $P_{\bar{y}}$ for the emissions and fuel consumption variable $\bar{y} \in \bar{\mathcal{Y}}/\{\mathrm{CO}_2\} = \{\text{CO, HC, NO}_x\text{, fuel}\}$ are given by:

$$P_{\mathrm{CO}} = 0.01 \begin{bmatrix} -1292.81 & 48.8324 & 32.8837 & -4.7675 \\ 23.2920 & 4.1656 & -3.2843 & 0 \\ -0.8503 & 0.3291 & 0.5700 & -0.0532 \\ 0.0163 & -0.0082 & -0.0118 & 0 \end{bmatrix},$$

$$P_{\mathrm{HC}} = 0.01 \begin{bmatrix} -1454.4 & 0 & 25.1563 & -0.3284 \\ 8.1857 & 10.9200 & -1.9423 & -1.2745 \\ -0.2260 & -0.3531 & 0.4356 & 0.1258 \\ 0.0069 & 0.0072 & -0.0080 & -0.0021 \end{bmatrix},$$

$$P_{\mathrm{NO_x}} = 0.01 \begin{bmatrix} -1488.32 & 83.4524 & 9.5433 & -3.3549 \\ 15.2306 & 16.6647 & 10.1565 & -3.7076 \\ -0.1830 & -0.4591 & -0.6836 & 0.0737 \\ 0.0020 & 0.0038 & 0.0091 & -0.0016 \end{bmatrix},$$

and

$$P_{\mathrm{fuel}} = 0.01 \begin{bmatrix} -753.7 & 44.3809 & 17.1641 & -4.2024 \\ 9.7326 & 5.1753 & 0.2942 & -0.7068 \\ -0.3014 & -0.0742 & 0.0109 & 0.0116 \\ 0.0053 & 0.0006 & -0.0010 & -0.0006 \end{bmatrix},$$

when the inputs of the emissions and fuel consumption model are in SI-units and the outputs are in kg/s for emissions and l/s for fuel consumption.

A.2 Parameters of part of the A12 Dutch freeway

The METANET traffic flow model has been calibrated to the data collected from part of the A12 Dutch freeway by [79] (these values are also used in Chapters 3 and 7 of this thesis). The values of the parameters as obtained by [79] are listed below.

Parameters	**Values**	**Units**
b_m	2.8260	–
λ	3	–
δ	0.8942	–
ϱ	1	–
τ	14.76	s
T	10	s
κ	32.9010	veh/km/lane
$\rho_{\mathrm{cr},m}$	24.1801	veh/km/lane
$\rho_{\mathrm{jam},m}$	187.6495	veh/km/lane
$v_{\mathrm{ref},m}$	117.6946	km/h
$v_{\min}$	13.0010	km/h
η_{h}	26.2669	km^2/h
η_{l}	64.2005	km^2/h
$C_{o,1}$	None	veh/h
$C_{o,2}$	1 751.2	veh/h
$C_{o,3}$	1 976.2	veh/h
L_{m_1}	[530 530 535 600 595 480]	m
L_{m_2}	[800 640 785 700 725 656 600 600 414]	m
L_{m_3}	[653 527 494 616 665 635 600 688 582]	m
$\beta_{m_1,\mathrm{off}}$	0.0234	–
$\beta_{m_2,\mathrm{off}}$	0.1618	–
$\beta_{m_3,\mathrm{off}}$	0.1228	–

Appendix B

Derivation of The Intersection Formulas

In the derivations of the intersection equations given in Section 4.3.2, two conditions are stated: $T < \frac{2}{\varpi(k)}$ and $L > \frac{2TV_{\mathrm{w}}(k)}{2-T\varpi(k)}$. If the simulation time step size T and the grid square length L are selected in such a way that these conditions are satisfied, then any dispersion square of a cell will only be able to cover at most nine neighboring cells as depicted in Fig. B.1.

Now let us first consider the displacement of the center point $(0, 0)$ to $(x_{\mathrm{e}}, y_{\mathrm{e}})$ due to the wind $V_{\mathrm{w}}(k)$ with a direction $\varphi(k)$. The displaced center point of the expanded square is then

$$(x_{\mathrm{e}}(k), y_{\mathrm{e}}(k)) = \big(-TV_{\mathrm{w}}(k)\cos(\varphi(k)), TV_{\mathrm{w}}(k)\sin(\varphi(k))\big) \tag{B.1}$$

Since, the expanded dispersion square is expanded by a factor $\varpi(k)$ per unit time from L to $L_{\mathrm{e}}(k) = (1 + T\varpi(k))L$, then the corner points $c_1(k)$, $c_2(k)$, $c_3(k)$, and $c_4(k)$ can be described as

$$c_1(k) = \left(x_{\mathrm{e}}(k) - \frac{L_{\mathrm{e}}(k)}{2}, y_{\mathrm{e}}(k) + \frac{L_{\mathrm{e}}(k)}{2}\right) \tag{B.2}$$

$$c_2(k) = \left(x_{\mathrm{e}}(k) + \frac{L_{\mathrm{e}}(k)}{2}, y_{\mathrm{e}}(k) + \frac{L_{\mathrm{e}}(k)}{2}\right) \tag{B.3}$$

$$c_3(k) = \left(x_{\mathrm{e}}(k) + \frac{L_{\mathrm{e}}(k)}{2}, y_{\mathrm{e}}(k) - \frac{L_{\mathrm{e}}(k)}{2}\right) \tag{B.4}$$

$$c_4(k) = \left(x_{\mathrm{e}}(k) - \frac{L_{\mathrm{e}}(k)}{2}, y_{\mathrm{e}}(k) - \frac{L_{\mathrm{e}}(k)}{2}\right) \tag{B.5}$$

In order to determine the values of $\alpha_{(i_{\mathrm{c}},j_{\mathrm{c}})}^{(u_{\mathrm{c}},v_{\mathrm{c}})}(k)$, we need to determine the magnitude of $a_1(k)$, $a_2(k)$, $a_3(k)$, $b_1(k)$, $b_2(k)$, and $b_3(k)$. With straightforward calculations the value of $a_1(k)$ is

$$a_1(k) = TV_{\mathrm{w}}(k)\cos(\varphi(k)) + \frac{TL\varpi(k)}{2}. \tag{B.6}$$

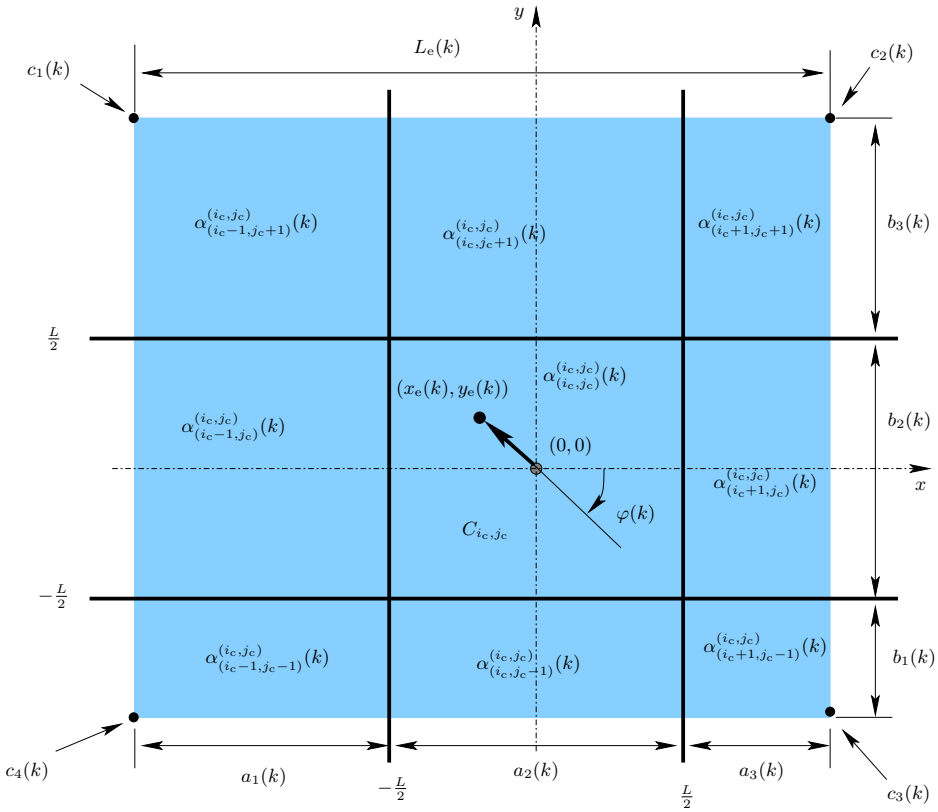

Figure B.1: Expanded and displaced dispersion square of the cell C_{i_c,j_c}. The point $(x_e(k), y_e(k))$ denotes the new center of the expanded and dispersed dispersion square. The areas of the parts of the dispersion square of cell C_{i_c,j_c} that intersect the grid cells C_{u_c,v_c} are denoted by $\alpha^{(u_c,v_c)}_{(i_c,j_c)}$. The variable $\varphi(k)$ denotes the direction of the wind $V_w(k)$ in which the emissions are dispersed.

However, due to the variation of the wind speed $V_w(k)$, wind direction $\varphi(k)$, and the expansion factor $\varpi(k)$, the value of $a_1(k)$ can be negative. This indicates that the dispersion square does not intersect to the neighboring cell in the left side of a cell. Moreover, using this negative value to determine the area of the intersection could result in invalid values. Therefore, to avoid such cases, the value for $a_1(k)$ is modified as

$$a_1(k) = \max\left\{0,\ TV_w(k)\cos(\varphi(k)) + \frac{TL\varpi(k)}{2}\right\}. \tag{B.7}$$

Using similar reasoning, $a_3(k)$, $b_1(k)$, and $b_3(k)$ are given by

$$a_3(k) = \max\left\{0,\ -TV_w(k)\cos(\varphi(k)) + \frac{TL\varpi(k)}{2}\right\} \tag{B.8}$$

$$b_1(k) = \max\left\{0,\ -TV_{\mathrm{w}}(k)\sin(\varphi(k)) + \frac{TL\varpi(k)}{2}\right\} \tag{B.9}$$

$$b_3(k) = \max\left\{0,\ TV_{\mathrm{w}}(k)\sin(\varphi(k)) + \frac{TL\varpi(k)}{2}\right\}. \tag{B.10}$$

The values for $a_2(k)$ and $b_2(k)$ are then

$$a_2(k) = L_{\mathrm{e}}(k) - a_1(k) - a_2(k) \tag{B.11}$$

$$b_2(k) = L_{\mathrm{e}}(k) - b_1(k) - b_2(k). \tag{B.12}$$

So, the areas of the $\alpha^{(u_{\mathrm{c}},v_{\mathrm{c}})}_{(i_{\mathrm{c}},j_{\mathrm{c}})}(k)$ can be obtained as

$$\alpha^{(u_{\mathrm{c}},v_{\mathrm{c}})}_{(i_{\mathrm{c}},j_{\mathrm{c}})}(k) = a_{2+i_{\mathrm{c}}-u_{\mathrm{c}}}(k)\cdot b_{2+j_{\mathrm{c}}-v_{\mathrm{c}}}(k). \tag{B.13}$$

Bibliography

[1] K. Ahn and H. Rakha. The effects of route choice decisions on vehicle energy consumption and emissions. *Transportation Research Part D*, 13(3):151–167, May 2008.

[2] K. Ahn, A. A. Trani, H. Rakha, and M. Van Aerde. Microscopic fuel consumption and emission models. In *Proceedings of the 78$^{\text{th}}$ Annual Meeting of the Transportation Research Board*, Washington, DC, USA, January 1999. CD-ROM.

[3] K. Ahn, H. Rakha, A. Trani, and M. Van Aerde. Estimating vehicle fuel consumption and emissions based on instantaneous speed and acceleration levels. *Journal of Transportation Engineering*, 128(2):182–190, March/April 2002.

[4] T. Akamatsu. An efficient algorithm for dynamic traffic equilibrium assignment with queues. *Transportation Science*, 35(4):389–404, November 2001.

[5] R. Akçelik. An interpretation of the parameters in the simple average travel speed model of fuel consumption. *Australian Road Research*, 15(1):46–49, 1985.

[6] A. A. Alam, A. Gattami, and K. H. Johansson. An experimental study on the fuel reduction potential of heavy duty vehicle platooning. In *The 13$^{\text{th}}$ International IEEE Conference on Intelligent Transportation Systems*, pages 306–311, Södertälje, Sweden, September 2010.

[7] A. Alessandri, A. Di Febbraro, A. Ferrara, and E. Punta. Optimal control of freeways via speed signaling and ramp metering. *Control Engineering Practice*, 6(6):771–780, June 1998.

[8] A. Alvarez, J. J. Brey, and J. M. Casado. A simulation model for traffic flow with passing. *Transportation Research Part B*, 24(3):193–202, June 1990.

[9] F. An, M. Barth, J. Nobeck, and M. Ross. Development of comprehensive modal emissions model operating under hot-stabilized conditions. In *Proceedings of the 76$^{\text{th}}$ Annual Meeting of the Transportation Research Board*, pages 52–62, Washington, DC, USA, 1997.

[10] C. Audet and J. E. Dennis Jr. Analysis of generalized pattern searches. *SIAM Journal on Optimization*, 13(3):889–903, 2007.

[11] W. Bachman, W. Sarasua, and R. Guensler. Geographic information system framework for modeling mobile-source emissions. *Transportation Research Record*, (1551):123–132, 1996.

[12] W. Bachman, W. Sarasua, S. Hallmark, and R. Guensler. Modeling regional mobile source emissions in a geographic information system framework. *Transportation Research Part C*, 8(1-6):205–229, February-December 2000.

[13] C. J. Baker. Outline of a novel method for the prediction of atmospheric pollution dispersal from road vehicles. *Journal of Wind Engineering and Industrial Aerodynamics*, 65(1-3):395–404, 1996.

[14] C. J. Baker and D. M. Hargreaves. Wind tunnel evaluation of a vehicle pollution dispersion model. *Journal of Wind Engineering and Industrial Aerodynamics*, 89(2): 187–200, February 2001.

[15] M. Bando, K. Hasebe, A. Nakayama, A. Shibata, and Y. Sugiyama. Dynamical model of traffic congestion and numerical simulation. *Physical Review E*, 51(2):1035–1042, February 1995.

[16] R. Barlovic, L. Santen, A. Schadschneider, and M. Schreckenberg. Metastable states in cellular automata for traffic flow. *The European Physical Journal B*, 5(3):793–800, April 1998.

[17] M. Barth. An emissions and energy comparison between a simulated automated highway system and current traffic conditions. In *Proceedings of IEEE Conference on Intelligent Transportation Systems*, pages 358–363, Dearborn, Michigan, USA, October 2000.

[18] M. Barth, F. An, T. Younglove, G. Scora, C. Levine, M. Ross, and T. Wenzel. Development of a comprehensive modal emissions model-CMEM. Technical Report Project 25-11, NCHRP, Transportation Research Board National Research Council, USA, 2000.

[19] L. D. Baskar, B. De Schutter, and H. Hellendoorn. Dynamic speed limits and on-ramp metering for IVHS using model predictive control. In *Proceedings of the 11$^{\text{th}}$ International IEEE Conference on Intelligent Transportation Systems*, pages 174–179, Beijing, China, October 2008.

[20] T. Bellemans. *Traffic Control on Motorways*. PhD thesis, Katholieke Universiteit Leuven, Leuven, Belgium, May 2003.

[21] T. Bellemans, B. De Schutter, and B. De Moor. Model predictive control with repeated model fitting for ramp metering. In *Proceedings of the IEEE 5$^{\text{th}}$ International Conference on Intelligent Transportation Systems*, pages 236–241, Singapore, September 2002.

[22] T. Bellemans, B. De Schutter, and B. De Moor. Model predictive control for ramp metering of motorway traffic: A case study. *Control Engineering Practice*, 14(7): 757–767, July 2006.

[23] A. Bemporad, F. Borrelli, and M. Morari. Model predictive control based on linear programming—the explicit solution. *IEEE Transactions on Automatic Control*, 47 (12):1974–1985, December 2002.

[24] A. Bemporad, M. Morari, V. Dua, and E. N. Pistikopoulos. The explicit linear quadratic regulator for constrained systems. *Automatica*, 38(1):3–20, January 2002.

[25] P. E. Benson. A review of the development and application of the CALINE3 and 4 models. *Atmospheric Environment*, 26(3):379–390, September 1992.

[26] A. Bitan. The high climatic quality city of the future. *Atmospheric Environment. Part B. Urban Atmosphere*, 26B(3):313–329, September 1992.

[27] P. T. Boggs and J. W. Tolle. Sequential quadratic programming. *Acta Numerica*, 4: 1–51, 1995.

[28] P. G. Boulter, T. Barlow, I. S. McCrae, S. Latham, D. Elst, and E. van der Burgwal. Road traffic characteristics, driving patterns and emission factors for congested situations. Technical report, TNO Automotive, Department Powertrains-Environmental Studies & Testing, Delft, The Netherlands, 2002. OSCAR Deliverable 5.2.

[29] M. Brackstone and M. McDonald. Car-following: a historical review. *Transportation Research Part F*, 2(4):181–196, December 2000.

[30] E. Brannvall and V. Špakauskas. Experimental and theoretical study of pollutant dispersion along a highway. *Geologija*, 60:27–32, 2007.

[31] D. Branston. Models of single lane time headway distributions. *Transportation Science*, 10(2):125–148, May 1976.

[32] A. T. Buckland and D. R. Middleton. Nomograms for calculating pollution within street canyons. *Atmospheric Environment*, 33(7):1017 – 1036, March 1999.

[33] D. J. Buckley. A Semi-Poisson model of traffic flow. *Transportation Science*, 2(2): 107–133, May 1968.

[34] J. Burman. An evaluation of topographical effects on neutral and heavy-gas dispersion with a CFD model. *Journal of Wind Engineering and Industrial Aerodynamics*, 74-76:315–325, April 1998.

[35] E. F. Camacho and C. Bordons. *Model Predictive Control in the Process Industry*. Springer-Verlag, Berlin, Germany, 1995.

[36] A. Cappiello, I. Chabini, E. K. Nam, A. Lue, and M. A. Zeid. A statistical model of vehicle emissions and fuel consumption. In *Proceedings of the IEEE 5$^{\text{th}}$ International Conference on Intelligent Transportation Systems*, pages 801–809, Singapore, September 2002.

[37] A. Casavola, D. Famularo, and G. Franze. A predictive control strategy for norm-bounded LPV discrete-time systems with bounded rates of parameter change. *International Journal of Robust and Nonlinear Control*, 18(7):714–740, August 2007.

[38] M. J. Cassidy and R. L. Bertini. Some traffic features at freeway bottlenecks. *Transportation Research Part B*, 33(1):25–42, February 1999.

[39] Y. Censor. Pareto optimality in multiobjective problems. *Applied Mathematics and Optimization*, 4:41–59, 1977.

[40] M. F. Chang and R. Herman. Trip time versus stop time and fuel consumption characteristics in cities. *Transportation Science*, 15(3):183–209, August 1981.

[41] D. Chen, J. Zhang, S. Tang, and J. Wang. Freeway traffic stream modeling based on principal curves and its analysis. *IEEE Transactions on Intelligent Transportation Systems*, 5(4):246–258, December 2004.

[42] C. C. Chien, Y. Zhang, A. Stotsky, and P. Ioannou. Roadway traffic controller design for automated highway systems. In *Proceedings of the 33*$^{\mathrm{rd}}$ *IEEE Conference on Decision and Control*, pages 2425–2430, Lake Buena Vista, Florida, USA, December 1994.

[43] D. P. Chock. A simple line-source model for dispersion near roadways. *Atmospheric Environment*, 12(4):823–829, 1978.

[44] M. C. Coelho, T. L. Farias, and N. M. Rouphail. Impact of speed control traffic signals on pollutant emissions. *Transportation Research Part D*, 10(4):323–340, July 2005.

[45] M. C. Coelho, T. L. Farias, and N. M. Rouphail. Effect of roundabout operations on pollutant emissions. *Transportation Research Part D*, 11(5):333–343, September 2006.

[46] A. Colorni, E. Laniado, and S. Muratori. Decision support systems for environmental impact assessment of transport infrastructures. *Transportation Research Part D*, 4(1): 1–11, January 1999.

[47] R. Courant, K. Friedrichs, and H. Lewy. On the partial difference equations of mathematical physics. *IBM Journal of Research and Development*, 11(2):215–234, March 1967.

[48] M. Cremer and J. Ludwig. A fast simulation model for traffic flow on the basis of boolean operations. *Mathematics and Computers in Simulation*, 24(4):297–303, August 1986.

[49] M. Cremer and M. Papageorgiou. Parameter identification for a traffic flow model. *Automatica*, 17(6):837–843, 1981.

[50] C. R. Cutler and B. L. Ramaker. Dynamic matrix control – A computer control algorithm. In *Proceedings of the 86*$^{\mathrm{th}}$ *AIChE National Meeting*, Houston, Texas, USA, April 1979.

[51] W. F. Dabberdt, F. L. Ludwig, and W. B. Johnson. Validation and applications of an urban diffusion model for vehicular pollutants. *Atmospheric Environment*, 7(6): 603–618, June 1973.

[52] C. F. Daganzo. The cell transmission model: A dynamic representation of highway traffic consistent with the hydrodynamic. *Transportation Research Part B*, 28(4): 269–287, August 1994.

[53] C. F. Daganzo. The cell transmission model, Part II: Network traffic. *Transportation Research Part B*, 29(2):79–93, April 1995.

[54] J. Dargay and D. Gately. The response of world energy and oil demand to income growth and changes in oil prices. *Annual Review of Energy and the Environment*, 20: 145–178, November 1995.

[55] L. Davis, editor. *Handbook of Genetic Algorithms*. Van Nostrand Reinhold, New York, New York, USA, 1991.

[56] L. B. de Oliveira and E. Camponogara. Multi-agent model predictive control of signaling split in urban traffic networks. *Transportation Research Part C*, 18(1):120–139, February 2010.

[57] B. De Schutter, H. Hellendoorn, A. Hegyi, M. van den Berg, and S. K. Zegeye. Model-based control of intelligent traffic networks. In R. R. Negenborn, Z. Lukszo, and H. Hellendoorn, editors, *Intelligent Infrastructures*, volume 42 of *Intelligent Systems, Control and Automation: Science and Engineering*, chapter 11, pages 277–310. Springer, Dordrecht, The Netherlands, 2010.

[58] T. Dijker, P. H. L. Bovy, and R. G. M. M. Vermijs. Car-following under congested conditions: Empirical findings. *Transportation Research Record*, (1644):20–28, 1998.

[59] D. W. Dockery and C. A. Pope III. Acute respiratory effects of particulate air pollution. *Annual Reviews of Public Health*, 15(-):107–132, 1994.

[60] H. C. Eerens, C. J. Sliggers, and K. D. van den Hout. The CAR model: The Dutch method to determine city street air quality. *Atmospheric Environment*, 27(4):389–399, December 1993.

[61] R. W. Eglese. Simulated annealing: a tool for operations research. *European Journal of Operational Research*, 46(3):271–281, 1990.

[62] G. Eichfelder. Scalarizations for adaptively solving multi-objective optimization problems. *Computational Optimization and Applications*, 44:249–273, 2009.

[63] L. Evans and R. Herman. Automobile fuel economy on fixed urban driving schedules. *Transportation Science Information*, 12(2):137–152, 1978.

[64] A. Di Febbraro, T. Parisini, S. Sacone, and R. Zoppoli. Neural approximations for feedback optimal control of freeway systems. *IEEE Transactions on Vehicular Technology*, 50(1):302–313, January 2001.

[65] T. L. Friesz. A variational inequality formulation of the dynamic network user equilibrium problem. *Operations Research*, 41(1):179–191, January-February 1993.

[66] C. E. García, D. M. Prett, and M. Morari. Model predictive control: Theory and practice–A survey. *Automatica*, 25(3):335–348, May 1989.

[67] D. Gazis, R. Herman, and R. Rothery. Nonlinear follow the leader models of traffic flow. *Operations Research*, 9(4):545–567, June 1961.

[68] F. Gembicki and Y. Haimes. Approach to performance and sensitivity multiobjective optimization: The goal attainment method. *IEEE Transactions on Automatic Control*, 20(6):769–771, dec 1975.

[69] A. H. Ghods, L. Fu, and A. Rahimi-Kian. An efficient optimization approach to real-time coordinated and integrated freeway traffic control. *IEEE Transactions on Intelligent Transportation Systems*, 11(4):873–884, December 2010.

[70] A. D. Gosman. Developments in CFD for industrial and environmental applications in wind engineering. *Journal of Wind Engineering and Industrial Aerodynamics*, 81 (1-3):21–39, May 1999.

[71] P. J. Goulart, E. C. Kerrigan, and M. Maciejowski. Optimization over state feedback policies for robust control with constraints. *Automatica*, 42(4):523–533, April 2006.

[72] F. L. Hall and K. Agyemang-Duah. Freeway capacity drop and the definition of capacity. *Transportation Research Record*, (1320):99–109, 1991.

[73] R. Y. Harrison and J. Yin. Particulate matter in the atmosphere: which particle properties are important for its effects on health? *The Science of The Total Environment*, 249(1-3):85–101, April 2000.

[74] S. Hausberger, M. Rexeis, M. Zallinger, and R. Luz. Emission factors from the model PHEM for the HBEFA version 3. Technical Report I-20/2009, Graz University of Technology, Graz, Austria, December 2009.

[75] A. Hegyi. *Model Predictive Control for Integrating Traffic Control Measures*. PhD thesis, Delft University of Technology, Delft, The Netherlands, February 2004.

[76] A. Hegyi, B. De Schutter, H. Hellendoorn, and T. van den Boom. Optimal coordination of ramp metering and variable speed control – An MPC approach. In *Proceedings of the 2002 American Control Conference*, pages 3600–3605, Anchorage, Alaska, USA, May 2002.

[77] A. Hegyi, B. De Schutter, and H. Hellendoorn. Model predictive control for optimal coordination of ramp metering and variable speed limits. *Transportation Research Part C*, 13(3):185–209, June 2005.

[78] A. Hegyi, B. De Schutter, and H. Hellendoorn. Optimal coordination of variable speed limits to suppress shock waves. *IEEE Transactions on Intelligent Transportation Systems*, 6(1):3600–3605, March 2005.

[79] A. Hegyi, S. P. Hoogendoorn, M. Schreuder, H. Stoelhorst, and F. Viti. SPECIALIST: A dynamic speed limit control algorithm based on shock wave theory. In *Proceedings of the 11$^{\text{th}}$ International IEEE Conference on Intelligent Transportation Systems*, pages 827–832, Beijing, China, October 2008.

[80] D. Helbing. Improved fluid-dynamic model for vehicular traffic. *Physical Review E*, 51(4):3164–3169, April 1995.

[81] D. Helbing. Gas-kinetic derivation of Navier-Stokes-like traffic equations. *Physical Review E*, 53(3):2366–2381, March 1996.

[82] D. Helbing, A. Hennecke, V. Shvetsov, and M. Treiber. Micro- and macro-simulation of freeway traffic. *Mathematical and Computer Modelling*, 35(5–6):517–547, March 2002.

[83] B. Hellinga and M. van Aerde. INTEGRATION: A model for simulating ITS in integrated traffic networks. *User's Guide for Model Version 1.5x3*, February 1995.

[84] D. A. Hennessy and D. L. Wiesenthal. The relationship between traffic congestion, driver stress and direct versus indirect coping behaviours. *Ergonomics*, 40(3):348–361, March 1997.

[85] O. Hertel and R. Berkowicz. Modelling pollution from traffic in a street canyon. evaluation of data and model development. Technical Report DMU Luft-A129, National Environment Research Institute, Roskilde, Denmark, 1989.

[86] G. Hoek, B. Brunekreef, A. Verhoeff, J. van Wijnen, and P. Fischer. Daily mortality and air pollution in The Netherlands. *Journal of Air and Waste Management Association*, 50(8):1380–1389, August 2000.

[87] S. P. Hoogendoorn and P. H. L. Bovy. State-of-the-art of vehicular traffic flow modelling. *Proceedings of the Institution of Mechanical Engineers, Part I: Journal of Systems and Control Engineering*, 215(4):283–303, August 2001.

[88] Z. Huang and X. Ma. Integration of emission and fuel consumption computing with traffic simulation using a distributed framework. In *Proceedings of the 12$^{\text{th}}$ International IEEE Conference on Intelligent Transportation Systems*, pages 154–159, St. Louis, Missouri, USA, October 2009.

[89] J. H. Johnson. Automotive emissions. In A. Y. Waton, R. R. Bates, and D. Kennedy, editors, *Air Pollution, the Automobile, and Public Health*, pages 39–75. National Academy Press, Washington, DC, USA, 1988.

[90] W. B. Johnson, F. L. Ludwig, W. F. Dabberdt, and R. J. Allen. An urban diffusion simulation model for carbon monoxide. *Air Pollution Control Association*, 23(6): 490–498, June 1973.

[91] R. Joumard, P. Jost, J. Hickman, and D. Hassel. Hot passenger car emissions modelling as a function of instantaneous speed and acceleration. *The Science of The Total Environment*, 169(1-3):167–174, July 1995.

[92] R. Joumard, J. M. André, M. Rapone, M. Zallinger, N. Kljun, M. André, Z. Samaras, S. Roujol, J. Laurikko, M. Weilenmann, K. Markewitz, S. Geivanidis, D. Ajtay, and L. Paturel. Emission factor modeling and database for light vehicles. Technical Report LTE 0523, Institut National de Recherche sur les Transport et Leur Securite, Bron, France, June 2007.

[93] S. Jun, Y. Fubing, L. Gesheng, and G. Xiaohong. A new approach of spark ignition engine fueled with ethanol. In *Proceedings of the Asia-Pacific Power and Energy Engineering Conference*, pages 1–4, Chengdu, China, March 2010.

[94] B. S. Kerner and P. Konhäuser. Cluster effect in initially homogeneous traffic flow. *Physical Review E*, 48(4):2335–2338, October 1993.

[95] B. S. Kerner and P. Konhäuser. Structure and parameters of clusters in traffic flow. *Physical Review E*, 50(1):54–83, July 1994.

[96] M. Khare and P. Sharma. Performance evaluation of general finite line source model for Delhi traffic conditions. *Transportation Research Part D*, 4(1):65–70, January 1999.

[97] Y. Kishi, S. Katsuki, Y. Yoshikawa, and I. Morita. A method for estimating traffic flow fuel consumption-using traffic simulations. *The Society of Automotive Engineers of Japan Review*, 17(3):307–311, July 1996.

[98] M. V. Kothare, V. Balakrishnan, and M. Morari. Robust constrained model predictive control using linear matrix inequalities. *Automatica*, 32(10):1361–1379, 1996.

[99] A. Kotsialos and M. Papageorgiou. Optimal coordinated ramp metering with advanced motorway optimal control. *Transportation Research Record*, (1748):55–65, 2001.

[100] A. Kotsialos and M. Papageorgiou. Nonlinear optimal control applied to coordinated ramp metering. *IEEE Transactions on Control Systems Technology*, 12(6):920–933, November 2004.

[101] A. Kotsialos, M. Papageorgiou, and A. Messner. Integrated optimal control of motorway traffic networks. In *Proceedings of the 1999 American Control Conference*, pages 2183–2187, San Diego, California, USA, June 1999.

[102] A. Kotsialos, M. Papageorgiou, and F. Middelham. Optimal coordinated ramp metering with advanced motorway optimal control. In *Proceedings of the 14$^{\text{th}}$ International Symposium on Transportation and Traffic Theory (ISTTT)*, pages 621–644, Jerusalem, Israel, July 1999.

[103] A. Kotsialos, M. Papageorgiou, C. Diakaki, Y. Pavlis, and F. Middelham. Traffic flow modeling of large-scale motorway networks using the macroscopic modeling tool METANET. *IEEE Transactions on Intelligent Transportation Systems*, 3(4): 282–292, December 2002.

[104] A. Kotsialos, M. Papageorgiou, M. Mangeas, and H. Haj-Salem. Coordinated and integrated control of motorway networks via nonlinear optimal control. *Transportation Research Part C*, 10(1):65–84, February 2002.

[105] A. Kotsialos, M. Papageorgiou, and F. Middelhan. Local and optimal coordinated ramp metering for freeway networks. *Journal of Intelligent Transportation Systems*, 9(4):187–203, 2005.

[106] M. Kvasnica, P. Grieder, and M. Baotić. Multi-Parametric Toolbox (MPT), 2004. URL http://control.ee.ethz.ch/~mpt/.

[107] Y. Li, B. Waterson, and M. McDonald. Collection and use of environmental data for transport management: a view from local authorities. *IET Intelligent Transport Systems*, 3(1):95–101, January 2009.

[108] M. Lighthill and G. Whitman. On kinematic waves II: a traffic flow theory on long crowded roads. *Proceedings of the Royal Society of London Series A*, 229(1178): 317–345, March 1995.

[109] S. Lin, B. De Schutter, Y. Xi, and H. Hellendoorn. Study on fast model predictive controllers for large urban traffic networks. In *Proceedings of the 12$^{\text{th}}$ International IEEE Conference on Intelligent Transportation Systems*, pages 691–696, St. Louis, Missouri, USA, October 2009.

[110] S. Lin, B. De Schutter, S. K. Zegeye, H. Hellendoorn, and Y. Xi. Integrated urban traffic control for the reduction of travel delays and emissions. In *Proceedings of the 13$^{\text{th}}$ International IEEE Conference on Intelligent Transportation Systems (ITSC 2010)*, pages 677–682, Madeira Island, Portugal, September 2010.

[111] J. Löfberg. Approximations of closed loop minimax MPC. In *Proceedings of the 42$^{\text{nd}}$ IEEE Conference on Decision and Control*, pages 1438–1442, Maui, Hawaii, USA, December 2003.

[112] A. K. Luhar and R. S. Patil. A general finite line-source model for vehicular pollution prediction. *Atmospheric Environment*, 23(3):555–562, 1989.

[113] T. Luspay, B. Kulcsár, I. Varga, and J. Bokor. Parameter-dependent modeling of freeway traffic flow. *Transportation Research Part C*, 18(4):471–488, August 2010.

[114] T. Luspay, B. Kulcsár, I. Varga, S. K. Zegeye, B. De Schutter, and M. Verhaegen. On acceleration of traffic flow. In *Proceedings of the 13th International IEEE Conference on Intelligent Transportation Systems (ITSC 2010)*, pages 741–746, Madeira Island, Portugal, September 2010.

[115] T. Luspay, B. Kulcsár, J. van Wingerden, M. Verhaegen, and J. Bokor. Linear parameter varying identification of freeway traffic models. *IEEE Transactions on Control Systems Technology*, 19(10):31–45, January 2011.

[116] J. M. Maciejowski. *Predictive Control with Constraints*. Prentice Hall, Harlow, England, 2002.

[117] Hani S. Mahmassani, R. Jayakrishnan, and Robert Herman. Network traffic flow theory: Microscopic simulation experiments on supercomputers. *Transportation Research Part A*, 24(2):149–162, March 1990.

[118] A. Matzoros and D. van Vliet. A model of air pollution from road traffic, based on the characteristics of interrupted flow and junction control: Part II – model results. *Transportation Research Part A*, 26(4):331–355, July 1992.

[119] A. D. May. *Traffic Flow Fundamentals*. Prentice-Hall, Englewood Cliffs, New Jersey, USA, 1990.

[120] D. Q. Mayne, J. B. Rawlings, C. V. Rao, and P. O. M. Scokaert. Constrained model predictive control: stability and optimality. *Automatica*, 36(6):789–814, 2000.

[121] A. Mazzoldi, T. Hill, and J. J. Colls. CFD and Gaussian atmospheric dispersion models: A comparison for leak from carbon dioxide transportation and storage facilities. *Atmospheric Environment*, 42(34):8046–8054, November 2008.

[122] M. A. Mcbride, A. B. Reeves, M. D. Vanderheyden, C. J. Lea, and X. X. Zhou. Use of advanced techniques to model the dispersion of chlorine in complex terrain. *Process Safety and Environmental Protection*, 79(2):89–102, March 2001.

[123] S. A. McGuire, J. V. Ramsdell, and G. F. Athey. RASCAL 3.0.5: Description of models and methods. Technical Report NUREG-1887, U.S. Nuclear Regulatory Commission, Washington, DC, USA, August 2007.

[124] A. Messmer and M. Papageorgiou. METANET: a macroscopic simulation program for motorway networks. *Traffic Engineering and Control*, 31(9):466–470, 1990.

[125] K. Miettinen. Some methods for nonlinear multi-objective optimization. In Eckart Zitzler, Lothar Thiele, Kalyanmoy Deb, Carlos Coello Coello, and David Corne, editors, *Evolutionary Multi-Criterion Optimization*, Lecture Notes in Computer Science, pages 1–20. Springer, Berlin, Germany, 2001.

[126] M. Milliez and B. Carissimo. Numerical simulations of pollutant dispersion in an idealized urban area, for different meteorological conditions. *Boundary-Layer Meteorology*, 122(2):321–342, 2006.

[127] F. Murena, G. Favale, S. Vardoulakis, and E. Solazzo. Modelling dispersion of traffic pollution in a deep street canyon: Application of CFD and operational models. *Atmospheric Environment*, 43(14):2303–2311, May 2009.

[128] K. Nagel. Particle hopping models and traffic flow theory. *Physical Review E*, 53(5): 4655–4672, May 1996.

[129] K. Nagel. From particle hopping models to traffic flow theory. *Transportation Research Record*, (1644):1–9, 1998.

[130] K. Nagel and A. Scheicher. Microscopic traffic modeling on parallel high performance computers. *Parallel Computing*, 20(1):125–146, January 1994.

[131] A. Nagurney. Congested urban transportation networks and emission paradoxes. *Transportation Research Part D*, 5(2):145–151, March 2000.

[132] E. Negrenti. The 'corrected average speed' approach in ENEA's TEE model: an innovative solution for the evaluation of the energetic and environmental impacts of urban transport policies. *The Science of The Total Environment*, 235(1-3):411–413, September 1999.

[133] G. F. Newell. Nonlinear effects in the dynamics of car following. *Operations Research*, 9(1):209–229, April 1961.

[134] G. F. Newell. A simplified theory of kinematic waves in highway traffic, part II: Queuing at freeway bottlenecks. *Transportation Research Part B*, 27(4):289–303, August 1993.

[135] S. E. Nicholson. A pollution model for street-level air. *Atmospheric Environment*, 9 (1):19–31, January 1975.

[136] J. Nocedal and S. J. Wright. *Numerical Optimization*. Springer-Verlag, New York, New York, USA, 1999. Springer Series in Operations Research.

[137] R. B. Noland. Relationships between highway capacity and induced vehicle travel. *Transportation Research Part A*, 35(1):47–72, January 2001.

[138] NRC. Expanding metropolitan highways: Implications for air quality and energy use. Technical Report 245, National Academy Press, Washington, DC, USA, 1995.

[139] L. Ntziachristos and Z. Samaras. COPERT III. Computer program to calculate emissions from road transport. Methodology and emission factors. Technical Report 49, European Environment Agency, Copenhagen, Denmark, 2000.

[140] T. R. Oke. Street design and urban canopy layer climate. *Energy and Buildings*, 11 (1-3):103–113, March 1988.

[141] M. T. Oliver-Hoyo and G. Pinto. Using the relationship between vehicle fuel consumption and CO_2 emissions to illustrate chemical principles. *Journal of Chemical Education*, 85(2):218–220, February 2008.

[142] D. M. Levinson P. Parthasarathi and R. Karamalaputi. Induced demand: a microscopic perspective. *Urban Studies*, 40(7):1335–1351, June 2003.

[143] L. I. Panis, S. Broekx, and R. Liu. Modelling instantaneous traffic emission and the influence of traffic speed limits. *The Science of The Total Environment*, 371(1-3): 270–285, December 2006.

[144] M. Papageorgiou. *Application of Automatic Control Concepts to Traffic Flow Modelling and Control*. Springer, Berlin, Germany, 1983.

[145] M. Papageorgiou. Dynamic modelling, assignment, and route guidance in traffic networks. *Transportation Research Part B*, 24B(6):471–495, December 1990.

[146] M. Papageorgiou. Modeling and real-time control of traffic flow on the southern part of Boulevard Peripherique in Paris: part I: modeling. *Transportation Research Part A*, 24A(5):345–359, September 1990.

[147] M. Papageorgiou. Some remarks on macroscopic traffic flow modelling. *Transportation Research Part A*, 32(5):323–329, 1998.

[148] M. Papageorgiou and A. Kotsialos. Freeway ramp metering: An overview. *IEEE Transactions on Intelligent Transportation Systems*, 3(4):271–281, December 2002.

[149] M. Papageorgiou, H. Hadj-Salem, and J. M. Blosseville. ALINEA: A local feedback control law for on-ramp metering. *Transportation Research Record*, (1320):58–64, 1991.

[150] I. Papamichail and M. Papageorgiou. Traffic-responsive linked ramp-metering control. *IEEE Transactions on Intelligent Transportation Systems*, 9(1):111–121, March 2008.

[151] I. Papamichail, A. Kotsialos, I. Margonis, and M. Papageorgiou. Coordinated ramp metering for freeway networks - a model-predictive hierarchical control approach. *Transportation Research Part C*, 18(3):311– 331, June 2010.

[152] P. M. Pardalos and M. G. C. Resende. *Handbook of Applied Optimization*. Oxford University Press, Oxford, UK, 2002.

[153] S. L. Paveri-Fontana. On Boltzmann-like treatments for traffic flow: A critical review of the basic model and an alternative proposal for dilute traffic analysis. *Transportation Research*, 9(4):225–235, August 1975.

[154] H. J. Payne. Models of freeway traffic and control. *Simulation Council Proceedings*, 1:51–61, 1971.

[155] S. Peeta and H. Mahmassani. System optimal and user equilibrium time-dependent traffic assignment in congested networks. *Annals of Operations Research*, 60(1): 81–113, 1995.

[156] R. Pfiffner, F. Weber, A. Amstutz, and L. Guzzella. Modeling and model-based control of supercharged SI-engines for cars with minimal fuel consumption. In *Proceedings of the 1997 American Control Conference*, pages 304–308, Albuquerque, New Mexico, USA, June 1997.

[157] W. F. Phillips. A kinetic model for traffic flow with continuum implications. *Transportation Planning and Technology*, 5(3):131–138, 1979.

[158] L. A. Pipes. An operational analysis of traffic dynamics. *Journal of Applied Physics*, 24(3):274–281, March 1953.

[159] I. Prigogine and R. Herman. *Kinetic Theory of Vehicular Traffic*. American Elsevier, New York, New York, USA, 1971.

[160] A. Propoi. Use of linear programming methods for synthesizing sampled-data automatic systems. *Automation and Remote Control*, 24(7):837–844, 1963.

[161] J. Pullen, J. P. Boris, T. Young, G. Patnaik, and J. Iselin. A comparison of contaminant plume statistics from a Gaussian puff and urban CFD model for two large cities. *Atmospheric Environment*, 39(6):1049–1068, 2005.

[162] Y. G. Qi, H. H. Teng, and L. Yu. Microscale emission models incorporating acceleration and deceleration. *Journal of Transport Engineering*, 130(3):348–359, June 2004.

[163] H. Rakha and K. Ahn. Integration modeling framework for estimating mobile source emissions. *Journal of Transport Engineering*, 130(2):183–193, March 2004.

[164] T. A. Ranney. Psychological factors that influence car-following and car-following model development. *Transportation Research Part F*, 2(4):213–219, December 1999.

[165] K. S. Rao, R. L. Guner, J. R. White, and R. P. Hosker. Turbulence and dispersion modeling near highways. *Atmospheric Environment*, 36(27):4337–4346, September 2002.

[166] S. S. Rao. *Engineering Optimization: Theory and Practice*. New Age International Limited, New Delhi, India, 3^{rd} edition, 2004.

[167] J. B. Rawlings and D. Q. Mayne. *Model Predictive Control: Theory and Design*. Nob Hill Publishing, Madison, Wisconsin, USA, 2009. ISBN 978-0-9759377-0-9.

[168] J. Richalet, A. Rault, J.L. Testud, and J. Papon. Model predictive heuristic control: Applications to industrial processes. *Automatica*, 14(5):413–428, September 1978.

[169] P. I. Richard. Shock waves on the highway. *Operations Research*, 4(1):42–51, February 1956.

[170] A. J. Richardson and R. Akcelik. Fuel consumption models and data needs for the design and evaluation of urban traffic systems. In *Proceedings of the Transportation Conference 1981*, pages 21–28, Brisbane, Australia, 1981.

[171] K. Sanwal, K. Petty, J. Walrand, and Y. Fawaz. An extended macroscopic model for traffic flow. *Transportation Research Part B*, 30(1):1–9, February 1996.

[172] F. Scargiali, E. Di Rienzo, M. Ciofalo, F. Grisafi, and A. Brucato. Heavy gas dispersion modelling over a topographically complex mesoscale: A CFD based approach. *Process Safety and Environmental Protection*, 83(3):242–256, May 2005.

[173] W.J̃. Schakel, B. van Arem, and B.D̃. Netten. Effects of cooperative adaptive cruise control on traffic-flow stability. In *Proceedings of the* 13^{th} *International IEEE Conference on Intelligent Transportation Systems*, pages 759–764, Madeira Island, Portugal, September 2010.

[174] M. Schatzmann and B. Leitl. Issues with validation of urban flow and dispersion CFD models. *Journal of Wind Engineering and Industrial Aerodynamics*, 99(4):169–186, April 2011.

[175] S. Schmidt and R. P. Schäfer. An integrated simulation systems for traffic induced air pollution. *Environmental Modeling & Software*, 13(3-4):295–303, 1998.

[176] P. Sharma and M. Khare. Modelling of vehicular exhausts - a review. *Transportation Research Part D*, 6(3):179–198, May 2001.

[177] R. Smit, R. Smokers, and E. Rabe. A new modeling approach for road traffic emissions: VERSIT+. *Transportation Research Part D*, 12(6):414–422, August 2007.

[178] R. Smit, M. Poelman, and J. Schrijver. Improved road traffic emission inventories by adding mean speed distributions. *Atmospheric Environment*, 42(5):916–926, February 2008.

[179] R. S. Smith. Robust model predictive control of constrained linear systems. In *Proceedings of the 2004 American Control Conference*, pages 245–250, Boston, Massachusetts, USA, June 2004.

[180] S. Smulders. Control of freeway traffic flow by variable speed signs. *Transportation Research Part B*, 24B(2):111–132, 1990.

[181] D. Stokols, R. W. Novaco, J. Stokols, and J. Campbell. Traffic congestion, Type A behavior, and stress. *Journal of Applied Psychology*, 63(4):467–480, August 1978.

[182] P. J. Sturm, P. Boulter, P. de Haan, R. Joumard, S. Hausberger, J. Hickman, M. Keller, W. Niederle, L. Ntziachristos, C. Reiter, Z. Samaras, G. Schinagl, T. Schweizer, and R. Pischinger. Instantaneous emission data and their use in estimating passenger car emissions. Technical Report MEET Deliverable 6, Technische Universität Graz, Graz, Austria, August 1998.

[183] H. Suzuki and T. Sugie. MPC for LPV systems with bounded parameter variation using ellipsoidal set prediction. In *Proceedings of the 2006 American Control Conference*, pages 5251–5256, Minneapolis, Minnesota, USA, June 2006.

[184] S. Takahashi. Fundamental study of low fuel consumption control scheme based on combination of direct fuel injection engine and continuously variable transmission. In *Proceedings of the 37$^{\text{th}}$ IEEE Conference on Decision and Control*, pages 1522–1529, Tampa, Florida, USA, December 1998.

[185] *METANET – A simulation program for motorway networks*. Technical University of Crete, Greece, Dynamic Systems and Simulation Laboratory and A. Messmer, July 2000.

[186] M. Treiber, A. Hennecke, and D. Helbing. Congested traffic states in empirical observations and microscopic simulations. *Physical Review E*, 62(2):1805–1824, August 2000.

[187] G. H. Tzeng and C. H. Chen. Multi-objective decision making for traffic assignment. *IEEE Transactions on Engineering Management*, 40(2):180–187, May 1993.

[188] M. van den Berg, A. Hegyi, B. De Schutter, and J. Hellendoorn. A macroscopic traffic flow model for integrated control of freeway and urban traffic networks. In *Proceedings of the 42$^{\text{nd}}$ IEEE Conference on Decision and Control*, pages 2774–2779, Maui, Hawaii, USA, December 2003.

[189] D. H. van Hessem and O. H. Bosgra. A full solution to the constrained stochastic closed-loop MPC problem via state and innovations feedback and its receding horizon implementation. In *Proceedings of the 42$^{\text{nd}}$ IEEE Conference on Decision and Control*, pages 929–934, Haui, Hawaii, USA, December 2003.

[190] S. Vardoulakis, B. E. A. Fisher, K. Pericleous, and N. G. Flesca. Modelling air quality in street canyons: a review. *Atmospheric Environment*, 37(2):155–182, January 2003.

[191] S. Vedal. Ambient particle and health: lines that divide. *Journal of Air and Waste Management Association*, 47(5):551–581, May 1997.

[192] R. G. M. M. Vermijs, H. J. Papendrecht, L. R. F. Spelberg, and W. J. Toetenel. Short term forecasting of the level of service on a motorway network, by using a microscopic simulation model. In *Proceedings of the 2$^{\text{nd}}$ Erasmus-Network Conference on Transportation and Traffic Engineering*, Kerkrade, The Netherlands, 1995.

[193] S. Vordoulakis, B. E. A. Fisher, K. Pericleous, and N. Gonzalez-Flesca. Modelling air quality in street canyons: a review. *Atmospheric Environment*, 37(2):155–182, January 2003.

[194] P. Wåhlin, F. Palmgren, and R. Van Dingenen. Experimental studies of ultrafine particles in streets and the relationship to traffic. *Atmospheric Environment*, 35(1): 63–69, 2001.

[195] Y. Wang and S. Boyd. Fast model predictive control using online optimization. *IEEE Transactions on Control Systems Technology*, 18(2):267–278, March 2010.

[196] H. C. Watson, E. E. Milkins, and G. Marshall. A simplified method for quantifying fuel consumption of vehicles in urban traffic. Technical Report A.R.R.B. Project 312, Department of Mechanical Engineering, University of Melbourne, Melbourne, Australia, 1980.

[197] WHO. Health aspects of air pollution, *Results from the WHO projects "Systematic review of health aspects of air pollution in Europe"*. Technical report, World Health Organization, June 2004.

[198] B. Wie, R. L. Tobin, D. Bernstein, and T. L. Friesz. A comparison of system optimum and user equilibrium dynamic traffic assignments with schedule delays. *Transportation Research Part C*, 3(6):389–411, December 1995.

[199] B. Wie, R. L. Tobin, T. L. Friesz, and D. Bernstein. A discrete time, nested cost operator approach to the dynamic network user equilibrium problem. *Transportation Science*, 29(1):79–92, February 1995.

[200] Y. Xiaolong, Y. Jing, and L. Tieping. The effect of an SI engine using butanol-gasoline blended fuel on performance and environment. In *Proceedings of the International Conference on Energy and Environment Technology*, pages 402–405, Guilin, China, October 2009.

[201] T. Yamada. Merging CFD and atmospheric airflows and dispersion in urban areas. *Computational Fluid Dynamics*, 13(2):323–335, July 2004.

[202] R. J. Yamartino and G. Wiegand. Development and evaluation of simple models for the flow, turbulence and pollutant concentration fields within an urban street canyon. *Atmospheric Environment*, 20(11):2137–2156, 1986.

[203] Q. I. Yang and H. N. Koutsopoulos. A microscopic traffic simulator for evaluation of dynamic traffic management systems. *Transportation Research Part C*, 4(3):113–129, June 1996.

[204] J. Yi, H. Lin, L. Alvarezt, and R. Horowitz. Stability of macroscopic traffic flow modeling through wavefront expansion. In *Proceedings of the 2002 American Control Conference*, pages 1484–1490, Anchorage, Alaska, USA, November 2002.

[205] L. Yu. Remote vehicle exhaust emission sensing for traffic simulation and optimization models. *Transportation Research Part D*, 3(5):337–347, September 1998.

[206] H. Yue. *Mesoscopic Fuel Consumption and Emission Modeling*. PhD thesis, Virginia Polytechnic Institute and State University, Blacksburg, Virigina, USA, March 2008.

[207] S. K. Zegeye, B. De Schutter, J. Hellendoorn, and E. A. Breunesse. A model-based predictive traffic control approach for the reduction of emissions. In *Proceedings of the 10$^{\text{th}}$ TRAIL Congress*, pages 283–297, Rotterdam, The Netherlands, October 2008.

[208] S. K. Zegeye, B. De Schutter, J. Hellendoorn, and E. A. Breunesse. Model-based traffic control for balanced reduction of fuel consumption, emissions, and travel time. In *Proceedings of the 12$^{\text{th}}$ IFAC Symposium on Transportation Systems*, pages 149–154, Redondo Beach, California, USA, September 2009.

[209] S. K. Zegeye, B. De Schutter, J. Hellendoorn, and E. A. Breunesse. Model-based traffic control for the reduction of fuel consumption and emissions, and travel time. In *mobil.TUM 2009 - International Scientific Conference on Mobility and Transport - ITS for larger Cities*, Munich, Germany, May 2009. CD ROM.

[210] S. K. Zegeye, B. De Schutter, J. Hellendoorn, and E.A. Breunesse. Reduction of travel times and traffic emissions using model predictive control. In *Proceedings of the 2009 American Control Conference*, pages 5392–5397, St. Louis, Missouri, USA, June 2009.

[211] S. K. Zegeye, B. De Schutter, and J. Hellendoorn. Model predictive traffic control to reduce vehicular emissions – An LPV-based approach. In *Proceedings of the 2010 American Control Conference*, pages 2284–2289, Baltimore, Maryland, June–July 2010.

[212] S. K. Zegeye, B. De Schutter, J. Hellendoorn, and E. A. Breunesse. Integrated macroscopic traffic flow and emission model based on METANET and VT-micro. In G. Fusco, editor, *Models and Technologies for Intelligent Transportation Systems* (Proceedings of the International Conference on Models and Technologies for Intelligent Transportation Systems, Rome, Italy, June 2009), pages 86–89. Aracne Editrice, Rome, Italy, 2010.

[213] S. K. Zegeye, B. De Schutter, J. Hellendoorn, and E. A. Breunesse. Variable speed limits for area-wide reduction of emissions. In *Proceedings of the* 13^{th} *International IEEE Conference on Intelligent Transportation Systems*, pages 507–512, Madeira Island, Portugal, September 2010.

[214] S. K. Zegeye, B. De Schutter, J. Hellendoorn, and E. A. Breunesse. Variable speed limits for green mobility. In *Proceedings of the* 14^{th} *International IEEE Conference on Intelligent Transportation Systems*, Washington, DC, USA, October 2011.

[215] S. K. Zegeye, B. De Schutter, J. Hellendoorn, and E. A. Breunesse. Nonlinear MPC for the improvement of dispersion of freeway traffic emissions. In *Proceedings of the* 8^{th} *IFAC World Congress*, Milan, Italy, August–September 2011.

[216] S. K. Zegeye, B. De Schutter, J. Hellendoorn, and E. A. Breunesse. Parametrized MPC to reduce dispersion of road traffic emissions. In *Proceedings of The 2011 American Control Conference*, pages 4428–4433, San Francisco, California, USA, June–July 2011.

[217] S. K. Zegeye, B. De Schutter, J. Hellendoorn, and E. A. Breunesse. Reduction of area-wide emissions using an efficient model-based traffic control strategy. In *Proceedings of the* 1^{st} *IEEE Forum on Integrated and Sustainable Transportation Systems*, Vienna, Austria, June–July 2011.

[218] S. K. Zegeye, B. De Schutter, J. Hellendoorn, E. A. Breunesse, and A. Hegyi. Integrated macroscopic traffic flow, emission, and fuel consumption model for control purposes. *Transportation Research Part C*, To appear, 2011.

[219] H. Zhang, S. G. Ritchie, and W. W. Recker. Some general results on the optimal ramp control problem. *Transportation Research Part C*, 4(2):51–69, April 1996.

[220] J. Zhang, A. Boiter, and P. Ioannou. Design and evaluation of a roadway controller for freeway traffic. In *Proceedings of the 8$^{\text{th}}$ International IEEE Conference on Intelligent Transportation Systems*, pages 543–548, Vienna, Austria, September 2005.

[221] X. Zhao and Z. Gao. Controlling traffic jams by a feedback signal. *The European Physical Journal B*, 43(4):565–572, 2005.

Glossary

Conventions

The following conventions are used in this thesis for notation and symbols:

- $\mathbb{N}$ represents the set of natural numbers.
- $\mathbb{R}$ denotes the set of all real numbers.
- $\hat{x}(k_2|k_1)$ designates the predicted value of x at a time step k_2 using the information at time step k_1.
- An operator $\mathcal{A}$ is defined such that $\mathcal{A}(x)$ provides the value of the area of a region defined by x.
- The $\#$ in $\#(x)$ is defined as the set cardinality of x.
- The intersection between two or more regions is described using $\bigcap$, e.g., $A \bigcap B$ denotes the intersection of region A and region B.
- The superscript $\top$ denotes the transpose of a matrix (or vector).
- The $\tilde{}$ operator is defined in such a way that $\tilde{x}$ results in a vector $[1\ x\ x^2\ x^3]^\top$.

List of symbols and notations

Below follows a list of symbols and notations used in this thesis.

Latin symbols

A_{i_c,j_c}	area of cell C_{i_c,j_c}
$A_{\mathrm{int},m,i}$	area of an intersection between $A_{m,i}$ and a target zone t
$A_{m,i}$	area of a dispersion tetragon of the emissions released from segment i of link m
A_{tg,i_c,j_c}	area of dispersion tetragon C_{tg,i_c,j_c} of a cell C_{i_c,j_c}
a	average acceleration
a	instantaneous acceleration
$\bar{a}$	average acceleration of a number of vehicles
$a_{2+i_c-u_c}$	part of a horizontal dimension of an expanded cell

$a_{\mathrm{cross},m,i,i+1}$	acceleration of vehicles crossing segment i to $i+1$ of link m
$a_{\mathrm{cross},m,m+1}$	acceleration of vehicles crossing link m to link $m+1$
$a_{\mathrm{cross,off},o}$	acceleration of vehicles leaving an off-ramp
$a_{\mathrm{cross,on},o}$	acceleration of vehicles entering an on-ramp
$a_{\max,\alpha}$	maximum acceleration of vehicle α
$a_{\mathrm{seg},m,i}$	acceleration of vehicles within segment i of link m
a_α	acceleration of vehicle α
$\tilde{a}_\alpha$	a vector $[1\ a_\alpha\ a_\alpha^2\ a_\alpha^3]^\top$
$b_{2+j_\mathrm{c}-v_\mathrm{c}}$	part of a vertical dimension of an expanded cell
b_m	parameter of the fundamental diagram of link m
$b_{\max,\alpha}$	maximum comfortable deceleration of vehicle α
b_μ	parameter of the fundamental diagram of link μ
$\mathcal{C}_\mathrm{all}$	the set of all pairs of consecutive traffic control measures
$C(x,y,z)$	contamination concentration at the point (x,y,z)
$C_{i_\mathrm{c},j_\mathrm{c}}$	a cell in a grid with its bottom-left coordinate at $(i_\mathrm{c},j_\mathrm{c})$
C_o	capacity flow of origin o
$C_{\mathrm{target},t}$	a polytope of target zone t
$C_{\mathrm{tg},i_\mathrm{c},j_\mathrm{c}}$	a dispersion tetragon of cell $C_{i_\mathrm{c},j_\mathrm{c}}$
$C_{u_\mathrm{c},v_\mathrm{c}}$	a cell in a grid with its bottom-left coordinate at $(u_\mathrm{c},v_\mathrm{c})$
c	controller performance criteria
$c_o,\ c_1,\ c_2$	coefficients of COPERT model
c_cMPC	values of the performance criteria c of cMPC controller
c_RHPC	values of the performance criteria c of RHPC controller
c_α	GHR model parameter for vehicle α
$D_{\bar{y},t}$	dispersion level of emission $\bar{y}$ at a target zone t
$d_1,\ d_2,\ d_{3,\mathrm{cal}},\ d_4$	traffic demands of cases 1, 2, 3, and 4
d_o	traffic demand of origin o
E	a diagonal matrix with 0, 1, 2, and 3 as its diagonal entries
$e_{\mathrm{av},\bar{y}}$	average of absolute relative-estimation error of emission $\bar{y}$
f	state vector function
f_m	a vector of nonlinear control law functions
$f_{m,1},\ f_{m,2},\ f_{m,3}$	nonlinear control law functions
$f_{\bar{y}}$	microscopic emission and fuel consumption function
f_α	stimulus response function
$\mathcal{G}$	nonlinear constraint
g	gravitational acceleration
g	inequality constraint function
g	input state vector function
$h(x)$	equality constraint function
$h(x)$	output vector function
h_s	mirror emission source distance beneath the ground

$\mathcal{I}_n$	the set of links that enter node n
I	identity matrix
I_p	relative performance indicator of a controller
i	segment index
i_c	horizontal grid-cell index
$\imath$	GHR model parameter
J	objective function
$\bar{J}_{\mathrm{cross},\bar{y},m,i,i+1}$	total $\bar{y}$ of vehicles crossing from segment i to $i+1$ of link m
$\bar{J}_{\mathrm{cross},\bar{y},m_i,\mu_j}$	total $\bar{y}$ of vehicles crossing from link m_i to link μ_j
$J_{\mathrm{ext},\bar{y},i_\mathrm{c},j_\mathrm{c}}$	emission contributed to cell $C_{i_\mathrm{c},j_\mathrm{c}}$ by an external source
$\bar{J}_{\mathrm{seg},\bar{y},m,i}$	total $\bar{y}$ of vehicles within segment i of link m
$J_{\mathrm{src},\bar{y},i_\mathrm{c},j_\mathrm{c}}$	emissions released in the cell $C_{i_\mathrm{c},j_\mathrm{c}}$
$J_{\mathrm{tot},\bar{y},t,m,i}$	total emission rate of segment i of link m of emission $\bar{y}$ generated in the past time and that intersects a target zone during the time period $[kT,(k+1)T)$
$\bar{J}_{\mathrm{total},\bar{y}}$	total emission $\bar{y}$ generated by vehicles in a network
J_vector	a vector of objective functions
$J_{\mathrm{vector},i}$	i^th objective function of vector J_vector
$J_{\bar{y}}$	emission or fuel consumption rate
$J_{\bar{y},i_\mathrm{c},j_\mathrm{c}}$	the emission level of $\bar{y}$ at $C_{i_\mathrm{c},j_\mathrm{c}}$
$J_{\bar{y},m,i}$	the emission rate of a wavefront of segment i of link m
$J_{\bar{y},t,m,i}$	emission rate $J_{\bar{y},m,i}$ that arrives the target zone t
$J_{\bar{y},\alpha}$	emission $\bar{y}$ generated by vehicle α
j	positive integer counter
j'	positive integer counter
j_c	vertical grid-cell index
$\jmath$	GHR model parameter
k	macroscopic simulation time step counter
k_c	cMPC and RHPC optimization layer control time step counter
$k_{\mathrm{c},i}$	RHPC feedback layer control time step counter
k_m	microscopic simulation time step counter
k_s	sampling time step counter
L	length (or width) of a grid cell
L_e	length (or width) of a expanded cell
L_m	length of segments of link m
l_α	length of vehicle α
ℓ	time step at which an emission is released
$\mathcal{M}$	the set of links in a network
$\mathcal{M}_\mathrm{all}$	the set of all pairs of indices of segments and links
$M_1,\ M_2,\ M_3,\ M_4$	positive integer multipliers
m	index of a link
$m_1,\ m_2,\ \ldots, m_{n_1}$	indices of merging links
$\mathcal{N}$	the set of nodes in a network

$\mathcal{N}$	the set of neighborhood cells of a cell and the cell it self
N_{s}	number of total simulation time steps
N_m	number of segments of link m
N_{c}	control horizon
N_{p}	prediction horizon
n	number of vehicles, a node
$n_{\mathrm{cross},m,i,i+1}$	number of vehicles crossing segment i to $i+1$ of link m
$n_{\mathrm{cross},m,m+1}$	number of vehicles crossing link m to link $m+1$
$n_{\mathrm{cross,off},o}$	number of vehicles leaving an off-ramp
$n_{\mathrm{cross,on},o}$	number of vehicles entering an on-ramp
$n_{\mathrm{seg},m,i}$	number of vehicles within a segment
$n_u,\ n_x,\ n_y$	dimensions of control input, state, and output of a system
n_{vsl}	number of variable speed limits
$\mathcal{O}_{\mathrm{all}}$	the set of all origins
$\mathcal{O}_n$	the set of links that leave node n
o	origin index
$\mathcal{P}(\rho, v, t)$	traffic pressure
$\mathcal{P}_{\mathrm{all}}$	the set of all pairs of consecutive speed limits
$P_{\bar{y}}$	parameter matrix of emission or fuel consumption $\bar{y}$
p	traffic performance criteria
$p_{\mathrm{controlled}}$	the value of a performance criteria of a controlled scenario
$p_{\mathrm{l},m,i}$	left most point of an emission dispersion wavefront
$p_{\mathrm{r},m,i}$	right most point of an emission dispersion wavefront
$p_{\mathrm{uncontrolled}}$	the value of a performance criteria of uncontrolled scenario
$\mathcal{Q}$	nonlinear equality constraint
Q	source strength (mass of released material per unit time)
$Q_n(k)$	total flow entering node n
q	flow
$q(x,t)$	instantaneous flow
$q_{\mathrm{max},\mu,1}$	maximum outflow of the first segment of link μ
$q_{m,i}$	outflow of segment i of link m
q_o	the outflow of origin o
$q_{\mathrm{off},o}$	off-ramp flow of origin o
$q_{\mathrm{on},o}$	on-ramp flow of origin o
$q_{\mu_i,0}(k)$	flow leaving node n via link μ_i
$\mathcal{R}_{\mathrm{all}}$	the set of all controlled on-ramps
R_c	relative controller performance
r	index of on-ramp
r_o	ramp metering rate of origin o
$\mathcal{S}_{\mathrm{all}}$	the set of all speed limits
$S_1,\ S_2,\ S_3,\ S_4,\ S_5$	simulation scenarios
s	speed limit index of segment s
$s_1,\ s_2$	speed limit indies of segments s_1 and s_2

$s_{0,\alpha}$	minimum stand-still headway distance of vehicle α
s_α	actual headway distance of vehicle α from vehicle $\alpha - 1$
s^*	minimum desired headway distance of a vehicle
$\mathcal{T}_{\text{all}}$	the set of all target zones
$\mathcal{T}_{\text{int},t}$	the set of all cells that intersect a target zone t
T	macroscopic simulation time step size
$\text{TTS}_\text{n},\ \text{TE}_\text{n},\ \text{TFC}_\text{n}$	normalized values of TTS, TE, and TFC
$\text{MDL}_\text{n},\ \text{TDL}_\text{n}$	normalized values of MDL and TDL
T_c	computation time step size of RHPC optimization layer or cMPC
$T_{\text{c},i}$	RHPC feedback layer control time step size
$T_{\text{d},\alpha}$	overall driver reaction time
T_m	microscopic simulation time step size
T_s	sampling time step size
t_h	headway time of a vehicle
$t_{\text{arrival,managed}}$	destination arrival time of managed vehicle
$t_{\text{arrival,unmanaged}}$	destination arrival time of unmanaged vehicle
$t_{\text{jam,dissolved}}$	jam dissolving time
$t_{\text{jam,managed}}$	arrival time of managed vehicle to a downstream jam
$t_{\text{jam,unmanaged}}$	arrival time of unmanaged vehicle to a downstream jam
t	continuous time
t	target zone
$\mathcal{U}_{\text{all}}$	the set of all traffic control measures
U_Δ	weighted sum of control input variation over time and space
$U_{\Delta,\text{n}}$	normalized value of U_Δ
$U_{\text{vsl,cMPC},m}$	a vector of $[u_{\text{vsl,cMPC},m,i}(k_\text{c})\ \ldots\ u_{\text{vsl,cMPC},m,n_\text{vsl}}(k_\text{c})]^\top$
$\boldsymbol{U}_{\text{vsl,cMPC},m}$	a sequence of predicted $U_{\text{vsl,cMPC},m}$
$\boldsymbol{U}^*_{\text{vsl,cMPC},m}$	the optimal value of $\boldsymbol{U}_{\text{vsl,cMPC},m}$
$U_{\text{vsl,RHPC},m}$	a vector of $[u_{\text{vsl,RHPC},m,i}(k_\text{c})\ \ldots\ u_{\text{vsl,RHPC},m,n_\text{vsl}}(k_\text{c})]^\top$
$\boldsymbol{U}_{\text{vsl,RHPC},m}$	a sequence of predicted $U_{\text{vsl,RHPC},m}$
$\boldsymbol{U}^*_{\text{vsl,RHPC},m}$	the optimal value of $\boldsymbol{U}_{\text{vsl,RHPC},m}$
$\boldsymbol{u}$	control input sequence over a prediction horizon
$\boldsymbol{u}^*$	optimal value of $\boldsymbol{u}$
u_c	a control input
u_r	a ramp metering of on-ramp r
$u_{\text{r},m}$	ramp metering rate of an on-ramp r of link m
$u_{\text{r,ref},m}$	reference ramp metering rate of an on-ramp r of link m
$u_s,\ u_{s_1},\ u_{s_2}$	speed limit control of segments s, s_1, and s_2
$\bar{u}_s,\ \bar{u}_{s_1},\ \bar{u}_{s_2}$	traffic control measure of segments s, s_1, and s_3
$u_{\text{vsl,cMPC},m,i}$	variable speed limit of cMPC controlled segment i of link m
$u_{\text{vsl},m,i}$	variable speed limit of segment i of link m
$u_{\text{vsl,ref},m}$	reference variable speed limit of link m
$u_{\text{vsl,RHPC},m,i}$	variable speed limit of RHPC controlled segment i of link m
$\mathcal{V}(k_\text{m})$	the set of vehicles present in a network at time step k_m
$V(\rho, t)$	generalized equilibrium speed, desired speed
V	a description of the cost function

$V_{\mathrm{l},m}$	lower boundary of variable speed limit
$V_{\mathrm{u},m}$	upper boundary of variable speed limit
V_{w}	wind speed
v	instantaneous speed
v	space-mean speed
v	time-average wind speed
$\bar{v}$	the average speed of a number of vehicles
$v_{0,\alpha}$	desired speed of vehicle α
v_{av}	trip-based average speed
v_{c}	measured or estimated space-mean speed at control time step
$v_{\mathrm{c},m,i},\ v_{\mathrm{c},m,i+1}$	v_{c} of segment i and $i+1$ of link m
$v_{\mathrm{free},m}$	free-flow speed
$v_{\mathrm{lim},\mu,1}$	limiting speed of the first segment of link μ
$v_{m,i}$	space-mean speed of segment i of link m
$v_{m_i,N_{m_i}}$	space-mean speed of segment N_{m_i} of link m_i
$v_{\min}$	minimum space-mean speed
$v_{\mathrm{on},o}$	on-ramp space-mean speed of origin o
$v_{\mathrm{off},o}$	off-ramp space-mean speed
v_{step}	the maximum speed limit step change allowed
$v_{\mathrm{vsl},\alpha}$	speed limit of vehicle α
$v_\alpha,\ v_{\alpha-1}$	speed of vehicle α and $\alpha-1$
$\tilde{v}_\alpha$	a vector $[1\ v_\alpha\ v_\alpha^2\ v_\alpha^3]^\top$
$v_{\mu_i,0}(k)$	virtual upstream space-mean speed of link μ_i
w_o	queue length of origin o
$\boldsymbol{x}$	a vector of predicted values of state x
x	coordinate
x	state variable
x	vehicle position
$\hat{x}$	predicted value of the variable x
x_0	origin of the $x-$axis
x_{c}	the state x at a control time step
$\hat{x}_{\mathrm{c}}$	predicted value of the state x_{c}
$x_{\mathrm{l}},\ x_{\mathrm{r}}$	left and right $x-$axis coordinate values of a line
$x_{\mathrm{l},i_{\mathrm{c}}},\ x_{\mathrm{r},i_{\mathrm{c}}}$	left and right side $x-$axis coordinate values of a cell $C_{i_{\mathrm{c}},\cdot}$
$x_{\mathrm{l},m,i}$	value of x coordinate of $p_{\mathrm{l},m,i}$
$x_{\mathrm{r},m,i}$	value of x coordinate of $p_{\mathrm{r},m,i}$
$x_\alpha,\ x_{\alpha-1}$	position of vehicle α and $\alpha-1$
$\bar{\mathcal{Y}}$	the set {CO, HC, NO_x, CO_2, fuel}
$\boldsymbol{y}$	a vector of predicted values of output y
y	coordinate, output vector
y_0	origin of the $y-$axis
y_{c}	the output y at a control time step
$\hat{y}_{\mathrm{c}}$	predicted value of the state y_{c}
$y_{\mathrm{l}},\ y_{\mathrm{r}}$	left and right $y-$axis coordinate values of a line
$y_{\mathrm{l},j_{\mathrm{c}}},\ y_{\mathrm{r},jc}$	left and right side y-axis coordinate values of cell $C_{\cdot,j_{\mathrm{c}}}$

$y_{\mathrm{l},m,i}$	value of y coordinate of $p_{\mathrm{l},m,i}$
$y_{\mathrm{r},m,i}$	value of y coordinate of $p_{\mathrm{r},m,i}$
$\bar{y}$	emissions CO, HC, NO_x, and CO_2 or fuel consumption
$\bar{y}_{\mathrm{model}}$	the value of $\bar{y}$ computed using a given model
$\bar{y}_{\mathrm{VT-micro}}$	the value of $\bar{y}$ computed using VT-micro model
Z_m	a vector of $z_{m,i}$ of all segments
$\boldsymbol{Z}_m$	a diagonal matrix with Z_m as its diagonal entries
z	coordinate
$z_{m,i}$	a vector $[v_{\mathrm{free},m}\ f_{1,m,i}(\cdot)\ f_{2,m,i}(\cdot)]^\top$

Greek symbols

α	an index of a vehicle
$\alpha_{i_\mathrm{c},j_\mathrm{c}}^{u_\mathrm{c},v_\mathrm{c}}$	an area of the intersection between cell $C_{i_\mathrm{c},j_\mathrm{c}}$ and the dispersion tetragon of cell $C_{u_\mathrm{c},v_\mathrm{c}}$
β	half of the emission divergence angle
β_0	temperature dependent emission dispersion model parameter
$\beta_{\max}$	half of the maximum emission divergence angle
β_{m_i,n,μ_j}	fraction of vehicles that leave link m_i to link μ_j through node n
β_{n,μ_i}	fraction of vehicles leaving node n to link μ_i
γ	vertical emission dispersion ("evaporation") factor
Δt	a small time span
Δv	a small fraction of speed v
Δv_α	an approach rate of vehicle α to vehicle $\alpha - 1$
Δx	a small section of x
δ	free-flow acceleration exponent of IDM model
δ	METANET on-ramp model parameter
$\delta_1,\ \delta_2$	model parameters relating fuel consumption and CO_2
$\delta_{\mathrm{a},\alpha}$	relative acceleration deviation of vehicle α from the average acceleration $\bar{a}$
$\delta_{\mathrm{v},\alpha}$	relative speed deviation of vehicle α from the average speed $\bar{v}$
$\epsilon_{\mathrm{approx},\alpha,\bar{y}}$	approximate relative estimation error of emission or fuel consumption $\bar{y}$ of vehicle α
ζ_i	weight of traffic performance criterion
$\zeta_{4,\mathrm{MDL}},\ \zeta_{4,\mathrm{TDL}}$	weights of emission dispersion for the MDL and TDL
η_h	high anticipation constant
η_l	low anticipation constant
$\eta_{m,i}$	anticipation constant of segment i of link m
Θ_m	a vector of $\theta_m^\top(\cdot)$ over a prediction horizon
Θ_m^*	optimal value of Θ_m
$\boldsymbol{\theta}$	the sequence of parameter θ over a prediction horizon

θ	control law parameter of RHPC controller
θ_m	control law parameter vector $[\theta_{m,0}\ \theta_{m,1}\ \theta_{m,2}\ \theta_{m,3}]^\top$ of link m
$\theta_{m,0},\ \theta_{m,1},\ \theta_{m,2}$	variable speed limit control law parameter of link m
$\theta_{m,3}$	ramp metering control law parameter of link m
κ	non-zero constant parameter of METANET model
λ_m	number of lanes of link m
$\mu_1, \ldots, \mu_j, \ldots, \mu_{n_2}$	indices of diverging links
μ_{cs}	weight of the variation of variable speed limits over space
$\mu_{\mathrm{d},\bar{y}}$	weight of dispersion of emissions $\bar{y}$
$\mu_{f,\alpha}$	friction coefficient of vehicle α
μ_{r}	weight of the variation of ramp metering
μ_{s}	weight of the variation of variable speed limits over time
$\mu_{\mathrm{u},1}$	weight of the variation of control input over time
$\mu_{\mathrm{u},2}$	weight of the variation of control input over space
$\mu_{\bar{y}}$	weight of emission or fuel consumption $\bar{y}$
ν	a source term denoting rate of vehicles entering an on-ramp or leaving an off-ramp
π	a constant of value 3.14159
ϖ	grid-cell emission expansion factor
ρ	density
$\rho_{\mathrm{c},m,i},\ \rho_{\mathrm{c},m,i+1}$	measured or estimated density of segments i and $i+1$ of link m at control time step k_{c}
$\rho_{\mathrm{cr},m}$	critical density of link m
ρ_{d}	user defined downstream density
$\rho_{\mathrm{jam},m}$	jam density of link m
$\rho_{m,i}$	density of segment i of link m
$\rho_{m_i,N_{m_i}+1}$	density of segment $N_{m_i}+1$ of link m_i
$\rho_{\mu_i,1}$	density of the first segment of link μ_i
$\hat{\rho}$	phase-space density
ϱ	drivers non-compliance factor
σ_y	standard deviation of $C(x,y,z)$ along the $y-$axis direction
σ_z	standard deviation of $C(x,y,z)$ along the $z-$axis direction
σ_α	free-flow sensitivity of vehicle α
τ	relaxation time
ϕ	lane-drop/increase model parameter of METANET
φ	wind direction

List of abbreviations

The following are list of frequently used abbreviations in this thesis:

ALINEA	Asservissement LINéaire d' Entré Autoroutière
CFD	Computational Fluid Dynamics
cMPC	conventional Model Predictive Control
CPU	Central Processing Unit
GHR	Gazis-Herman-Rothery
IDM	Intelligent Driver Model
LPV	Linear Parameter Varying
MDL	Maximum Dispersion Level
METANET	Modèle d'Ecoulement du Traffic Autoroutier NETwork
MPC	Model Predictive Control
MPT	Multi-Parametric Toolbox
RHPC	Receding Horizon Parametrized Control
Seg. (or seg.)	Segment
SQP	Sequential Quadratic Programing
TDL	Total Dispersion Level
TE	Total Emissions
TFC	Total Fuel Consumption
TTS	Total Time Spent

TRAIL Thesis Series

The following list contains the most recent dissertations in the TRAIL Thesis Series. For a complete overview of more than 100 titles see the TRAIL website: www.rsTRAIL.nl.

The TRAIL Thesis Series is a series of the Netherlands TRAIL Research School on transport, infrastructure and logistics.

Zegeye, S.K., *Model-Based Traffic Control for Sustainable Mobility*, T2011/12, October 2011, TRAIL Thesis Series, the Netherlands

Máhr, T., *Vehicle Routing under Uncertainty*, T2011/11, September 2011, TRAIL Thesis Series, the Netherlands

Pel, A.J., *Transportation Modelling for Large-scale Evacuations*, T2011/10, July 2011, TRAIL Thesis Series, the Netherlands

Zheng, F., *Modelling Urban Travel Times*, T2011/9, July 2011, TRAIL Thesis Series, the Netherlands

Vlassenroot, S.H.M., *The Acceptability of In-vehicle Intelligent Speed Assistance (ISA) Systems: from trial support to public support*, T2011/8, June 2011, TRAIL Thesis Series, the Netherlands

Kroesen, M., *Human Response to Aircraft Noise*, T2011/7, June 2011, TRAIL Thesis Series, the Netherlands

Nielsen, L.K., *Rolling Stock Rescheduling in Passenger Railways: applications in short-term planning and in disruption management*, T2011/6, May 2011, TRAIL Thesis Series, the Netherlands

Qing, O., *New Approach to Fusion of Heterogeneous Traffic Data*, T2011/5, May 2011, TRAIL Thesis Series, the Netherlands

Walta, L., *Getting ADAS on the Road: actors interactions in Advanced Driver Assistance Systems deployment*, T2011/4, April 2011, TRAIL Thesis Series, the Netherlands

Lin, S., *Efficient Model Predictive Control for Large-Scale Urban Traffic Networks*, T2011/3, April 2011, TRAIL Thesis Series, the Netherlands

Oort, N. van, *Service Reliability and Urban Public Transport Design*, T2011/2, April 2011, TRAIL Thesis Series, the Netherlands

Mahmod, M.K.M., *Using Co-Operative Vehicle-Infrastructure Systems to Reduce Traffic Emissions and Improve Air Quality at Signalized Urban Intersections*, T2011/1, March 2011, TRAIL Thesis Series, the Netherlands

Corman, F., *Real-Time Railway Traffic Management: dispatching in complex, large and busy railway networks*, T2010/14, December 2010, TRAIL Thesis Series, the Netherlands

Kwakkel, J., The *Treatment of Uncertainty in Airport Strategic Planning*, T2010/13, December 2010, TRAIL Thesis Series, the Netherlands

Pang, Y., *Intelligent Belt Conveyor Monitoring and Control*, T2010/12, December 2010, TRAIL Thesis Series, the Netherlands

Kim, N.S., *Intermodal Freight Transport on the Right Track? Environmental and economic performances and their trade-off*, T2010/11, December 2010, TRAIL Thesis Series, the Netherlands

Snelder, M., *Designing Robust Road Networks: a general design method applied to the Netherlands*, T2010/10, December 2010, TRAIL Thesis Series, the Netherlands

Hinsbergen, C.P.IJ. van, *Bayesian Data Assimilation for Improved Modeling of Road Traffic*, T2010/9, November 2010, TRAIL Thesis Series, the Netherlands

Zuurbier, F.S., *Intelligent Route Guidance*, T2010/8, November 2010, TRAIL Thesis Series, the Netherlands

Larco Martinelli, J.A., *Incorporating Worker-Specific Factors in Operations Management Models*, T2010/7, November 2010, TRAIL Thesis Series, the Netherlands

Ham, J.C. van, *Zeehavenontwikkeling in Nederland: naar een beter beleidsvormingsproces*, T2010/6, August 2010, TRAIL Thesis Series, the Netherlands

Boer, E. de, *School Concentration and School Travel*, T2010/5, June 2010, TRAIL Thesis Series, the Netherlands

Berg, M. van den, *Integrated Control of Mixed Traffic Networks using Model Predictive Control*, T2010/4, April 2010, TRAIL Thesis Series, the Netherlands

Top, J. van den, *Modelling Risk Control Measures in Railways*, T2010/3, April 2010, TRAIL Thesis Series, the Netherlands

Craen, S. de, *The X-factor: a longitudinal study of calibration in young novice drivers*, T2010/2, March 2010, TRAIL Thesis Series, the Netherlands

Tarau, A.N., *Model-based Control for Postal Automation and Baggage Handling*, T2010/1, January 2010, TRAIL Thesis Series, the Netherlands

Knoop, V.L., *Road Incidents and Network Dynamics: effects on driving behaviour and traffic congestion*, T2009/13, December 2009, TRAIL Thesis Series, the Netherlands

Baskar, L.D., *Traffic Control and Management with Intelligent Vehicle Highway Systems*, T2009/12, November 2009, TRAIL Thesis Series, the Netherlands

Konings, J.W., *Intermodal Barge Transport: network design, nodes and competitiveness*, T2009/11, November 2009, TRAIL Thesis Series, the Netherlands

Summary

Model-Based Traffic Control for Sustainable Mobility

Faster and more reliable transportation systems are necessary for sustained and faster economic growth of a country. Freeway traffic networks are one of the main economic blood vessels that link cities, towns, and villages with each other and with other economic hubs (such as ports and industrial zones). However, due to the increasing demand for mobility and hence the increasing number of vehicles, traffic networks are jammed more and more frequently, impairing the traffic flow, increasing fuel consumption, increasing emissions and the dispersion of the emissions to sensitive areas.

Freeway traffic systems often operate below capacity during the rush hours due to high traffic demand and due to inefficient driving behavior of drivers and non-optimal traffic management systems. It is recognized that the low efficiency of freeway traffic flow can be improved either by shifting the mode of transport, by introducing incentives to shift the departure and arrival time of commuters, or by improving the traffic control and management systems such that the traffic networks are operated more optimally.

However, improving the traffic flow may have a negative impact on the emissions, fuel consumption, and safety. Traffic management and control strategies that focus on the reduction of emissions and fuel consumption are neither favorable for the traffic flow, because emissions and fuel consumption are minimal at low vehicular speeds (between 30 km/h and 70 km/h), which can severely hinder the traffic flow and thereby increase the travel times. This means that traffic control and management strategies that resolve or avoid traffic jams can be beneficial for both the travel times and the environment when the traffic speed is optimized within a limited range (e.g., up to 80 km/h).

So, policy makers and traffic managers have to provide balanced solutions to the concern of traffic congestion and environmental issues depending on the traffic conditions. However, this is not a simple task, because the dynamic nature of the traffic flow (both in time and space) and the effect of other weather factors (such as wind on the dispersion of emissions and rain on the flow of the traffic and dispersion of emissions) have to be taken into account.

As the literature suggests, there are several possible approaches to improve the day-to-day traffic jams, the increased traffic emissions and fuel consumption, and the increased number of traffic accidents. The span of possible traffic solutions ranges from the extension of existing infrastructures and construction of new infrastructures, over large-scale substitution of fossil oil by alternative environmentally safe fuels and enhancing vehicle technology, to the utilization of efficient traffic control and management strategies (e.g., the introduction of intelligent transportation systems).

For several reasons, Intelligent Transportation Systems (ITS) offer promising solutions

to the multi-dimensional traffic problems. One of the fundamental reasons is that with the use of ITS, traffic operators and managers can increase the efficiency of the operation of the traffic network such that during high-demand periods the traffic network can be operated close to their designed operational capacity. To this end, this thesis presents an ITS-based state-of-the-art freeway traffic control approach, a model-based traffic control solution that takes the need to optimize both economic criteria (such as travel times and fuel consumption) and environmental criteria (such as emissions and their dispersion) into account.

The model-based control approach adopted in this thesis, viz. Model Predictive Control (MPC) makes use of two basic concepts: on-line prediction and rolling horizon. In order to make predictions of the traffic variables and to make decisions on the traffic control measures depending on the intended control objectives, the control approach requires models of traffic flow, traffic emissions, traffic fuel consumption, and dispersion of the traffic emissions to a given target zone. Based on the evolution of predicted variables over a certain prediction horizon and using on-line optimization, the controller determines traffic control inputs that can optimize a desired traffic performance criterion. To avoid possible model mismatch and unpredicted uncertainties, the proposed controller applies the second concept—rolling horizon, where after the computation of a sequence of optimal control inputs, only the first control input is implemented and next, the horizon is shifted one sample and the optimization is restarted with new information about the traffic states.

However, due the high computation time required by the on-line optimization process, the conventional MPC controller is often not tractable in practice, i.e., the computation time required by the optimization process of the conventional MPC controller is often larger than one control time step. In order to reduce the computation time, this thesis presents an alternative for the conventional MPC control strategy, viz. a Receding Horizon Parametrized Control (RHPC). In this newly proposed RHPC control approach, the control inputs (such as variable speed limits and ramp metering rates) are described by parametrized state-dependent control laws. The RHPC controller then optimizes the parameters of the control laws, different from the conventional MPC controller, where the traffic control inputs are optimized directly. As a result, the optimization process of the RHPC controller is in general faster than the optimization process of the conventional MPC controller.

The conventional MPC and the RHPC approaches are illustrated using macroscopic models for traffic flow, traffic emissions, traffic fuel consumption, and dispersion of traffic emissions. In most of the simulations in this thesis the macroscopic METANET model is used as traffic flow model. However, as there are no emission, fuel consumption, and emission dispersion models that are suitable for real-time on-line prediction-based control applications, while still providing estimates with considerable accuracy, this thesis first presents fast emission, fuel consumption, and emission dispersion models. These models are developed in such a way that they can be integrated seamlessly with the macroscopic traffic flow model METANET.

As emission and fuel consumption model, the macroscopic VT-macro model is developed. The VT-macro model is obtained by integrating the macroscopic METANET traffic flow model and the microscopic VT-micro emission and fuel consumption model. The VT-macro model uses the macroscopic traffic variables (average speed, density, and flow) to generate the acceleration and corresponding number of the vehicles subject to the given average speed and acceleration in the traffic flow. The values of the average speed, average acceleration, and corresponding number of vehicles are used to estimate the emissions and fuel consumption of the traffic flow.

Furthermore, this thesis investigates the possible errors that can be introduced due to the integration of the macroscopic traffic flow model METANET and the microscopic emission and fuel consumption model VT-micro. The results of the specific case studies considered show that the errors introduced are small. Moreover, the comparison of the emissions and fuel consumption estimates of the VT-macro model and the COPERT model with respect to the VT-micro model (which is claimed to be accurate but slow) show that the VT-macro model tracks the evolution of the emissions generated by the VT-micro model with better accuracy than the COPERT model does. The simulations also show that the VT-macro model has the same computation speed as the COPERT model, while at the same time it is faster than the VT-micro model.

In order to predict the dispersion of emissions to the neighborhoods of freeway traffic networks, dispersion models are required. As literature suggest, the existing dispersion models are computationally very slow and are not suitable for on-line control applications. So, this thesis also develops new dispersion models that are computationally efficient. First the basic point-source dispersion model is presented. Next, these point-source dispersion model is extended to grid-based dispersion models that are computationally efficient. Two of such models are developed, viz. extended grid-based and expanding grid-based dispersion. These models can consider the effects of variable wind speeds, wind directions, and temperatures and can be used with both microscopic and macroscopic traffic emission models. As the main focus of this thesis has been on the dispersion of the emissions at the ground level, the dispersion of the emissions into the vertical direction is modeled via an "evaporation" factor. Note, however, that these models are not yet compared to the already existing dispersion models and are neither calibrated to real-life data, which is one of the topics of the thesis that is recommended for future work.

The conventional MPC controller and the RHPC controller use the aforementioned models in the extensive simulation-based case studies of the thesis to illustrate the potential of the control approaches. Using the proposed models and the control approaches, this thesis assesses the potential benefits of the existing infrastructure-based traffic control measures, in particular variable speed limits and ramp meters. In the simulations the control law of the variable speed limits is described using three parameters and the control law of the ramp metering is described using one parameter. However, the RHPC approach is so general that the control laws can be defined in any way suitable one opts to. Moreover, the conventional MPC and the RHPC controllers proposed in this thesis can also be used with other more complex and computationally fast models.

Moreover, a multi-objective performance criterion that considers the total time spent by vehicles in the traffic network, the total emissions, total fuel consumption, and the dispersion of the emissions to a given target zone is considered for both the conventional MPC and RHPC controllers, so that the controllers can optimize the control measures to provide a balanced trade-off between the mobility and the environmental performance indicators. Moreover, the trade-offs involved between these conflicting (and sometimes concurring) traffic performance indicators are discussed.

As the simulation results of the thesis indicate, both the conventional MPC and the RHPC controllers are able to provide a balanced trade-off between travel time, emissions, fuel consumption, and dispersion of emissions. Moreover, the simulations show that the conventional MPC controller suffers from high computation time requirements, which makes it infeasible in practice. On the contrary, the RHPC controller requires a very low computation time and it is shown to be applicable in practice. Moreover, the simulations show that

the performance of the RHPC controller is similar to the performance of the conventional MPC controller, which is considered to be more optimal within the given context. Furthermore, the extensive case studies show that depending on the traffic conditions and weather factors, it is possible to reduce—with a balanced trade-off—the travel times, emissions, fuel consumption, and the dispersion of emissions to a given target zone using the control approaches and control measures investigated in this thesis. Moreover, although reduction of the total emissions from a freeway has a positive impact on the global emissions levels, it does not always reduce the emission levels in a specific target zone (protected area) where emissions levels are required to be as low as possible. Instead, if the focus of the controllers is on reducing the emission levels in a specific target zone, the controllers can reduce the emission levels at the target zone while allowing the total emissions from a freeway to be higher than when the focus of the controllers is on reducing the total emissions of the freeway. This is because of the following. When the focus of the controllers is on reducing the travel time and the dispersion level in a target zone, the controller dynamically—based on the wind speed and wind direction—affects the part of the freeway that releases the emissions that will be dispersed to the target zone, while improving the traffic flow on the part of the freeway the emissions of which do not have effect on the emission levels of the target zone.

Finally, the thesis also indicates some recommendations regarding the open issues that are not investigated in the thesis and that can be considered as topic for future work. These topics include extensive validation of models, simulation and practical test of the control approaches, and investigation of different control measures and different performance indicators for the traffic controllers.

Solomon Kidane Zegeye

Samenvatting

Modelgebaseerde Verkeersregeling voor Duurzame Mobiliteit

Voor een duurzame en snelle economische groei van een land is een snel en betrouwbaar transportsysteem noodzakelijk. Snelwegnetwerken zijn vitale economische slagaders die steden en dorpen met elkaar en met economische centra (zoals havens en industrieterreinen) verbinden. De toenemende vraag naar mobiliteit en daarmee het toenemende aantal voertuigen zorgt er echter voor dat verkeersnetwerken steeds vaker verstopt raken. Dit doet afbreuk aan de verkeersdoorstroming, zorgt voor toenemend brandstofverbruik, meer uitstoot en de verspreiding van schadelijke stoffen naar kwetsbare plaatsen.

Door de hoge verkeersvraag, het inefficiënte gedrag van bestuurders en niet-optimale verkeersregelsystemen functioneren snelwegen tijdens het spitsuur vaak onder hun capaciteitsgrens. Het is bekend dat de lage efficiëntie van snelwegverkeer verhoogd kan worden door andere vormen van transport aan te bieden, door alternatieve aankomst- en vertrektijden te belonen, en door het verkeersregeling- en -managementsysteem te verbeteren zodat het verkeersnetwerk optimaler functioneert.

Het bevorderen van de verkeersdoorstroming kan echter een negatieve invloed hebben op de uitstoot, het brandstofverbruik en de veiligheid. Verkeersmanagement- en -regelstrategieën die gericht zijn op het verminderen van de uitstoot en het brandstofverbruik, kunnen juist nadelig zijn voor de verkeersdoorstroming, omdat de uitstoot en het brandstofverbruik minimaal zijn bij lage voertuigsnelheden (tussen 30 km/h en 70 km/h), wat een sterk nadelig effect kan hebben op de verkeersdoorstroming en daarmee op de reistijden. Dit betekent dat verkeersregel- en -managementstrategieën die files oplossen of vermijden slechts dan een positief effect hebben op reistijden en het milieu als de verkeerssnelheid wordt geoptimaliseerd binnen een beperkt interval (bv. tot 80 km/h).

Politici en verkeersmanagers moeten dus een evenwichtige oplossing zoeken die rekening houdt met het probleem van de files en met de milieuaspecten die afhankelijk van de verkeersituatie ontstaan. Dit is geen eenvoudige opgave omdat het dynamische karakter van de verkeersstroom (zowel in tijd als in ruimte) en de invloed van weersfactoren (zoals wind bij de verspreiding van emissies en regen bij de verkeersdoorstroming en de verspreiding van emissies) meegenomen moeten worden.

In de literatuur worden verschillende mogelijke methoden beschreven voor het aanpakken van dagelijkse files, de toenemende verkeersuitstoot, het toenemende brandstofverbruik en het toenemend aantal verkeersongelukken. De reikwijdte van de mogelijke verkeersoplossingen loopt van het uitbreiden van de bestaande infrastructuur en de bouw van nieuwe

infrastructuur, via grootschalige vervanging van fossiele brandstoffen door alternatieve, milieuvriendelijke brandstoffen en verbetering van de voertuigtechnologie, naar het gebruik van efficiënte verkeersregel- en -managementstrategieën (bv. de invoering van intelligente transportsystemen).

Intelligente Transportsystemen (ITS) bieden om diverse redenen interessante, veelbelovende oplossingen voor de veelzijdige verkeersproblemen. De belangrijkste reden is dat verkeersoperatoren en -managers door het invoeren van ITS de efficiëntie van het regelen van het verkeersnetwerk kunnen verhogen zodat tijdens spitstijden het verkeersnetwerk tot zijn uiterste capaciteit kan worden gebruikt. Dit proefschrift stelt daarom een ITS-gebaseerde, geavanceerde, modelgebaseerde snelwegregeling voor, die rekening houdt met de noodzaak van zowel het optimaliseren van economische criteria (zoals reistijden en brandstofverbruik) en met milieucriteria (zoals uitstoot en de verspreiding daarvan).

De modelgebaseerde regelmethode die in dit proefschrift beschreven wordt, *Model Predictive Control* (MPC), maakt gebruik van twee basisconcepten: online voorspelling en een schuivende horizon. De regelmethode heeft modellen van de verkeersstroom, de uitstoot, het brandstofverbruik en de verspreiding van de uitstoot nodig om voorspellingen te maken van de verkeersvariabelen en om afhankelijk van de regeldoelen beslissingen te nemen over de verkeersmaatregelen. Op basis van de evolutie van de voorspelde waardes over een afgesproken voorspellingshorizon en met gebruik van online optimalisering, bepaalt de regelaar regelingangen voor verkeersmaatregelen die de gewenste criteria voor de verkeersprestatie optimaliseren. De methode maakt daarnaast gebruik van een schuivende horizon om mogelijke modelfouten en onvoorziene onzekerheden te voorkomen. Hierbij worden na het bepalen van een reeks optimale regelingangen enkel de regelingangen voor de eerste regelstap geïmplementeerd, waarna de voorspellingshorizon één regelstap opgeschoven wordt en het optimalisatieproces opnieuw gestart wordt met nieuw verkregen informatie over de situatie van het verkeersnetwerk.

De conventionele MPC-regelaar is in de praktijk vaak niet realiseerbaar, doordat het online optimalisatieproces teveel rekentijd nodig heeft. Dat wil zeggen dat de rekentijd die nodig is voor de conventionele MPC-regelaar meestal langer is dan de duur van een regelstap. Om de rekentijd te reduceren introduceert dit proefschrift een alternatief voor de conventionele MPC-regelstrategie, namelijk *Receding Horizon Parametrized Control* (RHPC). In deze nieuwe RHPC-methode worden de regelingangen (zoals variabele snelheidslimieten en doseringsfracties voor toeritdoseringen) beschreven met behulp van geparameteriseerde, toestandsafhankelijke regelwetten. In tegenstelling tot de conventionele MPC-regelaar, waar de verkeersregelingangen direct worden geoptimaliseerd, optimaliseert de RHPC-regelaar de parameters van de regelwetten. Hierdoor is het optimaliseringsproces van de RHPC-regelaar in het algemeen sneller dan het optimaliseringsproces van de conventionele MPC-regelaar.

De conventionele MPC-aanpak en de RHPC-aanpak worden geïllustreerd met behulp van macroscopische modellen voor de verkeersstroom, de uitstoot, het brandstofverbruik en de verspreiding van de uitstoot. In de meeste simulaties in dit proefschrift is het macroscopische METANET-model als verkeersstroommodel gebruikt. Aangezien er echter geen modellen voor de uitstoot, het brandstofverbruik en de verspreiding van de uitstoot bestaan die geschikt zijn voor *real-time* online modelgebaseerde regeling en die nog steeds voldoende nauwkeurige schattingen geven, introduceert dit proefschrift snelle modellen voor de uitstoot, het brandstofverbruik en de verspreiding van de uitstoot. Deze modellen zijn zo ontworpen dat ze naadloos kunnen worden geïntegreerd met het macroscopische verkeers-

stroommodel METANET.

Een macroscopisch VT-macro model is ontwikkeld als uitstoot- en brandstofverbruikmodel. Het VT-macro model is verkregen door de integratie van het macroscopische verkeersstroommodel METANET en het microscopische uitstoot- en brandstofverbruikmodel VT-micro. Het VT-macro model maakt gebruik van macroscopische verkeersvariabelen (gemiddelde snelheid, dichtheid en doorstroming) om de versnelling van de verkeersstroom en het corresponderende aantal voertuigen te berekenen die de gegeven gemiddelde snelheid en versnelling hebben. De waardes van de gemiddelde snelheid, gemiddelde versnelling en het corresponderende aantal voertuigen worden gebruikt om de uitstoot en het brandstofverbruik van de verkeersstroom in te schatten.

Verder onderzoekt dit proefschrift de mogelijke fouten die kunnen ontstaan door de integratie van het macroscopische verkeersstroommodel METANET en het microscopische uitstoot- en brandstofverbruikmodel VT-micro. De resultaten van verschillende casestudies die onderzocht zijn, tonen aan dat de ontstane fouten klein zijn. Verder toont de vergelijking van schattingen van de uitstoot en het brandstofverbruik van het VT-macro model en het COPERT-model ten opzichte van het VT-micro model (waarvan men stelt dat het precies maar langzaam is) aan dat het VT-macro model de ontwikkeling van uitstoot gegenereerd door het VT-micro model preciezer volgt dan het COPERT-model. De simulaties tonen ook dat het VT-macro model even snel is als het COPERT-model, terwijl het sneller is dan het VT-micro model.

Om de verspreiding van de uitstoot in de omgeving van snelwegnetwerken te voorspellen, zijn verspreidingsmodellen nodig. De literatuur stelt dat de bestaande verspreidingsmodellen erg langzaam zijn en ongeschikt voor online regeltoepassingen. Daarom zijn in dit proefschrift nieuwe verspreidingsmodellen ontwikkeld die efficiënt werken. Eerst wordt als basis het puntbron-verspreidingsmodel gepresenteerd. Daarna wordt dit puntbron-verspreidingsmodel uitgebreid naar rastergebaseerde modellen die zeer efficiënt werken. Er worden twee rastergebaseerde modellen ontwikkeld, namelijk het uitgebreide rastergebaseerde model en het uitdijende rastergebaseerde model. Deze modellen kunnen omgaan met de gevolgen van een variabele windsnelheid, windrichting en temperatuur en ze kunnen worden gebruikt in combinatie met zowel microscopische als macroscopische verkeersuitstootmodellen. Omdat de focus van dit proefschrift ligt op de verspreiding van de uitstoot dicht bij de grond, wordt de verspreiding van de uitstoot in de verticale richting gemodelleerd met behulp van een “verdampings”-factor. Merk op dat deze modellen nog niet worden vergeleken met bestaande verspreidingsmodellen en dat ze ook niet worden geijkt met echte data. Dit is één van de open onderwerpen die in dit proefschrift worden aanbevolen voor toekomstig onderzoek.

Om de mogelijkheden van de regelmethoden te illustreren gebruiken de conventionele MPC-regelaar en de RHPC-regelaar de bovengenoemde modellen in de uitgebreide simulatiegebaseerde casestudies van dit proefschrift. Met behulp van de voorgestelde modellen en regelmethoden bepaalt dit proefschrift de mogelijke voordelen van bestaande infrastructuurgebaseerde verkeersmaatregelen, met name variabele snelheidslimieten en toeritdoseringen. In de simulaties wordt de regelwet van de variabele snelheidslimieten beschreven door middel van drie parameters en de regelwet van de toeritdosering wordt beschreven met behulp van één parameter. De RHPC-aanpak is echter zo algemeen dat de regelwetten op elke geschikte en gewenste manier kunnen worden gedefinieerd. Verder kunnen de conventionele MPC-regelaars en de RHPC-regelaars die in dit proefschrift zijn voorgesteld, ook gebruikt worden in combinatie met andere complexere en snellere modellen.

Verder is er een *multi-objective* prestatiecriterium onderzocht dat van alle voertuigen in het verkeersnetwerk de totale reistijd, de gezamenlijke uitstoot, het gezamenlijke brandstofverbruik en de verspreiding van de uitstoot naar een bepaald gebied beschouwt; dit voor zowel de conventionele MPC-regelaars als voor de RHPC-regelaars, zodat de regelaars de maatregelen kunnen optimaliseren en een evenwichtig compromis kunnen vinden dat zowel de mobiliteits- als de milieukwaliteitscriteria recht doet. Ook worden de afwegingen die samenhangen met deze tegenstrijdige (en soms parallel lopende) indicatoren van de verkeersprestatie besproken.

Zoals de simulatieresultaten van dit proefschrift aantonen, zijn zowel de conventionele MPC-regelaars als de RHPC-regelaars in staat een evenwichtig compromis tussen reistijd, uitstoot, brandstofverbruik en verspreiding van schadelijke stoffen te bereiken. Tevens tonen de simulaties aan dat de conventionele MPC-regelaar gebukt gaat onder een hoge rekentijd, wat hem in de praktijk onbruikbaar maakt. Daarentegen heeft de RHPC-regelaar slechts weinig rekentijd nodig en blijkt hij in de praktijk goed bruikbaar te zijn. Verder tonen de simulaties aan dat de prestaties van de RHPC-regelaar vergelijkbaar zijn met de prestaties van de conventionele MPC-regelaar, die in principe meer optimale resultaten oplevert in de gegeven context. Verder tonen uitgebreide casestudies aan dat het afhankelijk van de verkeerstoestand en de weersfactoren mogelijk is om met behulp van de regelmethoden uit dit proefschrift de reistijden, van de uitstoot, het brandstofverbruik en de verspreiding de uitstoot — met een evenwichtig compromis — te reduceren. Hoewel de reductie van de totale uitstoot van een snelweg een positief effect heeft op de gebiedsbrede emissieniveaus, zal het niet altijd de emissieniveaus in een specifiek gebied (een beschermde zone, waarvoor vereist wordt dat de emissieniveaus juist zo laag mogelijk moeten zijn) verlagen. Omgekeerd, als de focus van de regelaars op het reduceren van de emissieniveaus in een bepaald gebied ligt, kan dat tot lokaal lagere emissieniveaus leiden, terwijl de totale uitstoot van de snelweg hoger is dan wanneer de focus van de regelaars op de totale uitstoot ligt. Dit kan als volgt uitgelegd worden. Als de focus van de regelaar ligt op het reduceren van reistijden en het emissieniveau in een specifiek gebied, dan zal de regelaar — afhankelijk van de windsnelheid en de windrichting — dynamisch de verkeersstroom vertragen op dat deel van de snelweg dat verantwoordelijk is voor de uitstoot, terwijl de verkeersstroom in het overige deel van de snelweg waarvandaan uitstoot geen effect op het specifieke gebied heeft, verhoogd zal worden.

Tenslotte geeft dit proefschrift enkele aanbevelingen voor open problemen die in dit proefschrift niet behandeld zijn en die in aanmerking komen voor toekomstig onderzoek. Hiertoe horen onder meer een uitgebreide validatie van de modellen, simulatie en praktijktests van de regelmethoden en onderzoek naar bijkomende regelmaatregelen en andere prestatie-indicatoren voor de verkeersregelaars.

(Dutch translation provided by Prof. dr. ir. J. Hellendoorn)

Curriculum Vitae

Solomon Kidane Zegeye was born in Tigray province, Ethiopia in 1979. In 2003 he got his B.Tech. in Control and Optimization Technology from Defense Engineering College, Debre Zeit, Ethiopia and received gold medal of the 2003 graduates. He then worked as assistant lecturer in the same department for a year and a half.

In 2005, Solomon got a scholarship from Netherlands Fellowship Program (NFP) for his M.Sc. study. He studied his M.Sc. in Systems and Control in the period of 2005-2007 at the Delft Center for Systems and Control, Delft University of Technology, Delft, the Netherlands. The concluding thesis work was on quasi-LPV modeling of variable speed wind turbine.

Since October 2007 Solomon has been working on his PhD research project at the Delft Center for Systems and Control of Delft University of Technology, Delft, the Netherlands. His project was supported by the Shell/TU Delft Sustainability program. The research of his PhD project has been on the use of model-based traffic control approaches for a balanced reduction of travel times, emissions, fuel consumption, and dispersion of emissions to a protected area. He has been working under the supervision of Prof. dr. ir. Bart De Schutter and Prof. dr. ir. Hans Hellendoorn.

During his PhD project, Solomon obtained the DISC certificate for fulfilling the course program requirements of the Dutch Institute for Systems and Control. Since 2007, he has been a member of the DISC and of the Netherlands Research School for Transport, Infrastructure, and Logistics (TRAIL). He is also awarded Best Session Presentation Award of the 2010 American Control Conference. He has supervised four master students and they have successfully defended their theses. He has also tutored and assisted courses within the Delft Center for Systems and Control.